

Dynamics of vortices in the two-dimensional anisotropic Heisenberg model with magnetic fields

Von der Universität Bayreuth
zur Erlangung des Grades eines
Doktors der Naturwissenschaften (Dr. rer. nat.)
genehmigte Abhandlung

vorgelegt von

Juan Pablo Zagorodny

geboren in La Plata, Argentinien

1. Gutachter: Prof. Dr. F. G. Mertens
2. Gutachter: Prof. L. Kramer, Ph.D.

Tag der Einreichung: 23.12.2003

Tag des Kolloquiums: 10.04.2004

Contents

1	Introduction	1
2	Classical many-spin systems	7
2.1	Energy terms	7
2.1.1	Anisotropy terms	9
2.2	Heisenberg model with uniaxial anisotropy	11
2.3	Dynamics of classical spins	15
2.4	Variation of non-conserved quantities	17
3	Vortices and static magnetic fields	21
3.1	Continuum limit and topological excitations	22
3.1.1	In-plane (IP) vortices	27
3.1.2	Out-of-plane (OP) vortices	30
3.2	Dynamics of OP vortices at zero field	33
3.2.1	The Thiele equation	36
3.2.2	Force exerted by the image vortex	38
3.2.3	The Thiele equations in polar coordinates at zero field	40
3.2.4	Results of simulations at zero field	42
3.3	Dynamics of vortices with static fields	44
3.3.1	In-plane field	44
3.3.2	Perpendicular field	49
4	Vortices and time-dependent fields 1: out-of-plane dynamics	57
4.1	Basic effects of the rotating field	58
4.1.1	The uniformly rotating ground state	59
4.1.2	Energy dissipation	61
4.1.3	A discrete symmetry: classification of vortex dynamics	62

4.2	Switching phenomenology	64
4.2.1	Review of previous results	64
4.2.2	Results of new series of simulations	67
4.2.3	Coupling between IP and OP oscillations	74
4.2.4	Simulations with static fields	75
4.3	Discrete core models	76
4.3.1	Full core model	77
4.3.2	Reduced core model	78
4.4	Summary	83
5	Vortices and time-dependent fields 2: in-plane dynamics	85
5.1	Trajectories of OP vortices driven by in-plane rotating fields	85
5.1.1	Circular limit cycles	91
5.2	The Thiele approach with a time-dependent magnetic force	95
5.3	A new collective coordinate approach	97
6	Summary	103
A	Some calculations	105
A.1	Classical spins from quantum spins	105
A.2	Landau-Lifshitz equations from quantum spins	106
A.2.1	The coefficients in the Landau-Lifshitz equations.	108
A.3	Rate of change of the total energy	109
A.4	The energy of an IP vortex in a circular domain	117
A.5	Dynamics with the original LLG equations	120
B	Total momenta and Thiele equation: discrete <i>vs.</i> continuum	123
C	Vorticity & winding number: 2D vs. 3D	127
D	Numerical procedures	131
D.1	Integration in time in the simulations	131
D.2	Boundary conditions, image vortices	131
D.3	Numerical relaxation of an initial condition	132
D.4	Measurement/definition of the center of the vortex in the simulations .	133
D.5	Gyrodensity and its momenta	134
D.6	Results of simulations	136

E Force due to the rotating field	143
E.1 The energy of a vortex in the AC magnetic field	146
E.2 Equations of motion for collective coordinates	147
Bibliography	149
Acknowledgements	155

Chapter 1

Introduction

Vortices are a usual phenomenon in Nature: everyone who has seen a tornado, or the water flow pattern in the bathtub drain, may have an idea of what a vortex is. These are examples of a vortex in a fluid (air or water) and they have in common a characteristic flow, which forms a “curling” pattern in the velocities field. Vortices can appear as a particular curling pattern in other continuous media (*e.g.* the gravitational field in the case of a spiral galaxy, the electromagnetic field in the case of an optical vortex, the density field in a superfluid like Helium, etc). Vortices can move with respect to the medium, or (as is usually the case in fluids) they can be “pinned” or “frozen” into the medium, moving only together with the medium when the latter moves (*e.g.* the wind carrying the tornado along with it). There exist vortices deep into the solid matter too, where no flux or transport of matter takes place. Magnetic vortices are formed by the spins of the atoms of a magnetic material, and enjoy of an astonishing persistence. They exhibit mobility, interaction, and other intrinsic particle-like properties, which distinguish them from vortices in fluid media. A magnetic vortex can appear as an “antivortex” as well, with the opposite “circulation”. Vortices and antivortices can form bound pairs (“molecules”) where the constituent vortices undergo a parallel “Kelvin” motion, and these pairs scatter at right angles under collisions with other pairs.

The last feature induces some people to associate magnetic vortices, from a more mathematical viewpoint, with “non-linear excitations” of a magnet, like solitary waves and solitons, as opposite to “linear excitations” or spin waves. We distinguish between “linear” and “non-linear” excitations of a medium, in the sense that the first ones are solutions of the *linearized* underlying field equations, usually non-linear, describing the continuous medium, while the latter are more complicated structures, whose existence and stability is usually observed first in computer simulations, whenever the complete non-linear field equations are too complicated to be solved exactly.

In the case of magnetic materials, the underlying equations are often posed as the classical limits of the quantum equations of *discrete* spins systems on lattices. The

resulting models, like the Classical Heisenberg model to be studied in this work, are in principle discrete, but some of its features can also be cast in the so-called “long-wave approximation” or, in short, the continuum limit. Not all of its features, however, can be described in the frame of the continuum limit, and thus an interesting subject –at least for me– is to observe the relationships between discrete and continuous dynamical descriptions. In particular, a vortex is often linked to a singularity or a discontinuity at some point of a phase-like field, which represents a problem for the continuum descriptions (think of doing integrals of a function which diverges at some point), but is naturally regularized for discrete systems or lattices.

Another source for infinities appearing in the continuous descriptions of vortices in magnetic media is the size, which usually was let to tend to infinity for bulk samples. In this respect it appears to me very interesting the study of the crossovers between the bulk and the systems where finite size effects start to play a role. The latter is actually the case in much of today’s research about vortices in small magnetic systems, with dimensions so reduced (5-50nm) that they can not be considered a bulk (more details below).

The stability and the dynamics of spin vortices in ferromagnetic materials have been subject of study since at least three decades [75, 44, 74, 28], but nowadays this field is receiving even more attention, from the pure scientist viewpoint, as well as from the applied science perspective.

Very recently, direct experimental observation of vortices or “curling” states, as stable micromagnetic states of small (submicron) magnetic particles (dots), has been attained thanks to novel magnetic microscopy techniques, -magnetic force microscopy (MFM) and Lorentz transmission electron microscopy (LTEM), which enhanced the resolution of traditional methods for observing magnetic structures.

Notable MFM experiments on circular nanoscale dots of Permalloy ($\text{Ni}_{80}\text{Fe}_{20}$) [72, 65], and Co [65, 14] disposed in arrays over nanopatterned films, reported images of vortex cores, where the magnetization was found to point out of the plane of the film. LTEM imaging also showed vortices to be favorable configurations in permalloy nanodisks [65, 68]. High sensitivity magneto-optical methods have been used [12] to measure the hysteresis loops of Supermalloy ($\text{Ni}_{80}\text{Fe}_{14}\text{Mo}_5$) nanodisks, and it was found that the shape of the loops agrees very well with that of loops calculated by means of micromagnetic simulations [29, 9] of thin disks with vortex states.

These experiments have provided us with the possibility of directly checking theories of vortices in ferromagnetic materials, making feasible a better understanding of the interplay between mesoscopic nonlinear collective excitations and geometrical constraints, such as shape, size and boundary conditions at the interfaces (see Ref. [33]).

Concerning dynamical properties, it is important to investigate the response of systems

with vortex states to applied bias fields, which are control variables in experiments and potential applications. The dynamical effects of nonlinear excitations in finite two-dimensional (2D) and quasi-2D spin systems are especially relevant for read-heads in storage devices, because of the high speeds of transfer reached by today's hard disks. Still, experiments are lacking which can resolve in space and time simultaneously, and hence numerical simulations of Landau-Lifshitz equations have been the traditional source of data regarding vortex dynamics. Simulation of 2D systems is important because there are many 2D and quasi-2D magnetic materials, in the form of monolayers, layered and intercalated-layered compounds (for a review see Ref. [13, 56]), which are known to support nonlinear excitations.

On the other hand, vortices have been shown to be relevant for many 2D systems of theoretical physics, including 2D electron plasmas, 2D superfluid and superconducting systems, and 2D Josephson junction arrays, because it is well established that vortices drive, in all these 2D systems, a “topological” phase transition, called the Berezinskii-Kosterlitz-Thouless (BKT) transition [8, 44], at a certain temperature T_{BKT} . For $T < T_{\text{BKT}}$ vortex-antivortex pairs are thermally excited and destroyed, and for $T > T_{\text{BKT}}$ the pairs dissociate and the density of free vortices increases with the temperature. Let us recall that according to the Mermin-Wagner theorem [53, 54], long-range order is not possible in 1D and 2D models with a continuously degenerated ground state. In magnetic materials T_{BKT} can depend (only weakly) on material parameters like anisotropy [25] (to be introduced in Chap. 2) and on the applied external fields [36]. To study the vortex dynamics one usually assumes, and we will do so in our work, that the density of free vortices above T_{BKT} is so small, that one can isolate individual vortices to follow their dynamics. We will also neglect thermal effects, which lead to diffusive vortex motion and have been treated usually by means of stochastic terms in the dynamical equations (see *e.g.* [40, 19]).

In the continuum approach, exact static solutions for the 2D isotropic Heisenberg model are known, in the form of topological metastable states [7], but as soon as a weak XY-type anisotropy or a magnetic field are included, the topologically non-trivial solutions are not known in a closed analytical form, but only through numerically obtained vortex-like profiles. For the 2D anisotropic easy-plane case, already in the 1980s two kinds of vortices were identified [28]: in-plane (IP) or planar vortices, which are solutions with the magnetization always parallel to the XY-plane, and out-of-plane (OP) vortices, with OP components of the magnetization in the vortex center region or “core”, from which only asymptotic behavior was known [28, 58]. In numerical simulations, each type of vortex was found to be stable in different regimes of the anisotropy parameter λ (see Hamiltonian (2.12) in Section 2.2), and their asymptotic behavior and deformations due to movement were calculated for each regime [22].

In the context of a phenomenology of a dilute gas of vortices, their contributions to low-frequency “central peaks” in dynamical form factors were studied [55, 22]. The crossover from IP vortices (for $\lambda < \lambda_c$, see Section 2.2) to OP vortices (for $\lambda > \lambda_c$) was also established by analytical arguments [22, 83].

Most of the above work was done mainly at zero magnetic fields which complicate even more the scenario. Although some work has been done on the XY-model ($\lambda = 0$) with static IP magnetic fields [24], little is known about the properties of easy-plane models with magnetic fields for general λ . A field applied in the XY-plane lifts the degeneracy of the ground state and selects a preferential direction. In the presence of a vortex this kind of field can lead to formation of domain walls connecting the vortex core with the boundary of the system.

A magnetic field perpendicular to the easy plane tilts the ferromagnetic IP ground state into the so-called “cone state”, in which the z-component of magnetization results from a competition between the OP field and the effective anisotropy field [36]. The IP component of magnetization still points to an arbitrary direction of the plane, since the isotropy in the XY plane is not broken by the perpendicular applied field. The shape of an OP vortex in the presence of such a perpendicular field was calculated in Ref. [36], and a study of the magnon modes in this system was carried out in Ref. [38]. To my knowledge, the dynamics of OP vortices in easy-plane magnets in an external static field with both IP and OP components has not been investigated before, due to the complications which arise mainly from the IP component of the field, which deforms the well known “arctan” distribution of the spin field in the simplest vortex state.

In addition, I believe that very little is known about the behavior of OP vortices in the presence of time-dependent IP magnetic fields. Apart from the work of our group in Refs. [18, 87], where one aspect of the dynamics of OP vortices under the action of a uniform rotating IP field has been investigated, namely the switching phenomenon (See Chapter 4), I am aware of only one work (Ref. [64]) about vortex pairs in a uniform oscillating IP field.

In this Thesis, I am concerned with the *dynamics* of OP vortices, driven by either an IP rotating magnetic field or a static field with both IP and OP components, in the Heisenberg model with easy-plane anisotropy.

I investigate mostly in numerical simulations the phenomenological facts, and propose some possible explanations for these facts, by means of analytical models which qualitatively account for the features observed in the simulations.

I will present a general introduction to the Heisenberg-like models, with different terms of energy, as paradigmatic examples of classical spin systems, and to the non-linear excitations called vortices, that these models support, in the Chapters 2 and 3. In

the latter, I will also show some basic known results about the dynamics of vortices under the action of static fields, both IP and OP, for the easy-plane system. Together with this, some new results which I have observed in numerical simulations will be presented.

In Chapter 4, the phenomenon of switching of the OP components of the magnetization of the vortex, under the action of the rotating field, will be studied in detail (Sec. 4.2). Based on the results of an earlier work [18], we carry out an extensive set of numerical simulations to complete the phenomenological picture of the switching, and we formulate a discrete model of the vortex core, which can account qualitatively for the features of the process. This model is described in Sec. 4.3.

By transforming variables to a rotating reference frame in the spin space, we have found that the dynamics of our original model, where the IP rotating field is applied, is equivalent to the dynamics of a system in the rotating frame where only a static field with both IP and OP components is applied. In both cases, a coupling between the OP oscillation modes of the vortex structure and the IP movement of the vortex center, while it moves around in the lattice, is observed in the simulations. In the context of our model of the vortex core, a formal connection is found between one of its equations, governing the antisymmetric oscillation modes, and an equation in collective coordinates, that is similar to the Thiele equation but with a mass term [84, 86] and is believed to give a low-order approximation to the movement of the vortex center. Part of the results of this Chapter were published in Ref. [87].

In Chapter 5, we turn the attention to the movement of the vortex in the XY plane, under the combined action of the rotating field and the damping. I first describe the variety of trajectories that arise, and then I direct the attention to the study of certain trajectories which form a circular limit cycle. These are especially relevant since the vortex stays inside the system in a stationary movement, conditioned by the simultaneous action of damping and driving.

In order to describe analytically this equilibrium trajectories, the inconvenience of applying the Thiele approach to this problem is discussed, and based on these results a new Collective Variable Theory is formulated. This theory starts from a generalization of the steady-movement Ansatz, which introduces, in addition to the usual collective variables $(X(t), Y(t)) = (R(t) \cos \Phi(t), R(t) \sin \Phi(t))$ for the coordinates of the vortex center, a variable “width” $l(t)$ of the vortex core, or equivalently a variable $M(t)$, the total z-component of the spins, strongly localized in the vortex core, either of them accounting for oscillations of the shape of the vortex core, and a variable “phase” $\Psi(t)$ describing collective oscillation modes in the IP structure of the vortex, excited by the rotating field. We derive the equations of motion for these 4 collective variables $\{R, \Phi, M, \Psi\}$ and we show that those equations produce circular limit-cycles in the

expected regime of parameters, leading to a qualitative agreement with the results of the simulations.

The new Collective Variable Theory gives us, thus, a better understanding of the vortex movement in the presence of the rotating magnetic field. However, this theory, being based on a continuum approach, is unsuitable for explaining the switching phenomenon of Chapter 4, because in a continuum model the polarization of the vortex should be a conserved. The discrete models of Chapter 4 remain thus as a good physical picture of the switching phenomenon.

Finally, in Chapter 6, I briefly summarize the conclusions and perspectives of possible future work.

Chapter 2

Classical many-spin systems

In this chapter I present a basic introduction to the classical Heisenberg model with different anisotropy terms, which gives a fair description of ferromagnetic materials, and represents an archetypical example of classical spin systems. I review many features of the discrete system, some of which are known and some of which are not easily found in the literature. In particular, I show the dissipation relations in the discrete system or lattice, when damping and driving are considered, for quantities like energy and magnetization, and I derive these relations showing how one can perform calculations directly at the level of discrete systems. These results are useful, whenever we want to understand the behavior of the discrete system, which, on the other hand, is appropriated to be simulated in computers. I introduce as well the dynamical equations of classical many-spin systems. After this short introduction, in the next Chapter I will present the basics of the topological collective excitation named vortex, and give a review of some known facts, in the frame of a continuum approach. This will serve as a sufficient basis for the next Chapters¹.

2.1 Energy terms

Consider a piece of ferromagnetic material, like Fe or Ni, composed by an ensemble of atoms, each of one is assumed to have a magnetic moment \vec{m} . We adopt the quantum-mechanical result [4] that this magnetic moment is proportional to the total angular momentum of the atom or ion,

$$\vec{m} = \frac{g \mu_B}{\hbar} \vec{J} \quad ,$$

¹ The presentation is based on material spread over some recent books about ferromagnetism [2, 33], and spin dynamics in confined systems [29], review articles about non-linear excitations in magnets [73, 5, 43, 56], as well as the Ph.D. thesis of my predecessors [78, 69, 39], and, finally, my own calculations for discrete spin systems.

where

$$g = 1 + \frac{J(J+1) + S(S+1) - L(L+1)}{2J(J+1)} ,$$

the so-called Landé factor, takes into account contributions from the spin and orbital part, and $\mu_B = -|e|\hbar/(2m_e c)$ is known as Bohr magneton. Usually the orbital part is neglected², as for a pure spin ($L = 0, J = S$), the value of $g = 2$ is twice as large as for a pure orbit case ($S = 0, J = L$). In this case, the angular momentum \vec{J} is just the total spin \vec{S} of the atoms or ions and we write

$$\vec{m} = \gamma \vec{S} \quad , \quad \gamma = -|e|\hbar/(m_e c) < 0 \quad , \quad (2.1)$$

When placed in an external magnetic induction \vec{B} , these atomic momenta will experience a torque which, in absence of other interactions, would be sufficient to align them in the direction of the field. The interaction energy of a dipole moment \vec{m} with a field induction \vec{B} is known to be

$$\mathcal{V} = -\vec{m} \cdot \vec{B} = -\gamma \vec{S} \cdot \vec{B} \quad (2.2)$$

This field would determine, thus, a preferred direction, say \hat{z} , along which the corresponding components of the spins would take the $2S + 1$ integer or half-integer values $\{-S, -S + 1, \dots, S - 1, S\}$. But the atomic spins in a ferromagnet, unlike the paramagnetic substances, do interact with each other, each of them trying to align the other in its own direction. The interaction between them originates from a quantum mechanical property of the atoms, namely the fact that the wave functions of the electrons bound to different ions overlap. In quantum mechanics one can calculate the intensity of this coupling (see, *e.g.* [2]) usually using a mean-field theory, such as in the method of Hartree-Fock. The calculation of the total energy of N atomic spins, combining the Coulomb electrostatic interaction between pairs of electrons and the Pauli Exclusion Principle, gives rise to an effective interaction, which is a sum of interactions between pairs of spins, described by the Hamiltonian

$$\mathcal{H}_{\text{eff}} = -\frac{1}{2} \sum_{i,j=1}^N J_{ij} \vec{S}_i \cdot \vec{S}_j \quad , \quad (2.3)$$

²Some materials, like the rare earths, have a strong orbit contribution, and some others exhibit contributions from itinerant electrons. These materials will not be considered here, having in mind the simplest ferromagnetic materials, where the magnetic momenta are basically the total spin of the electrons bound to the ions. For metals, only the electrons in the inner shell are counted, which typically means for metals like Ni, Co and Fe, the d electrons.

proposed by Heisenberg [27] in 1928, where \vec{S}_i is the total spin of all electrons bound to the atom or ion at the lattice site i and the coefficients J_{ij} , known as the “exchange integrals”, are integrals over the real space which involve the overlap of single-electron wave functions. From this fact is clear that (a) they must be symmetric, $J_{ij} = J_{ji}$, and (b) their values must decrease very rapidly with increasing distance between ions. In particular, J must be negligible for farther atoms. Therefore, it is usually sufficient to consider exchange interactions between nearest neighbors only. It is customary also to keep the minus sign in front of (2.3) so that a positive J_{ij} means a ferromagnetic coupling that tends to align spins parallel to each other, while a negative J_{ij} means an antiferromagnetic coupling.

The Heisenberg Hamiltonian (2.3) is isotropic in spin space, i.e., the coupling between \hat{x} -components has the same intensity as the coupling between \hat{y} - and \hat{z} -components. Therefore, its extreme value is reached when all the spins are parallel in the ferromagnetic case, or antiparallel in the antiferromagnetic case, the direction of the total spin vector being arbitrary, at zero applied field. Actually, real magnetic materials are not isotropic, and there are several theorems, and arguments based on Statistical Mechanics, which show that *if* there were no other energy term besides the isotropic Heisenberg Hamiltonian (with the spins treated as classical variables), magnetism at zero field would not exist [2].

2.1.1 Anisotropy terms

In a crystal, the spin orbit interaction causes the most common form of anisotropy, called *magnetocrystalline* anisotropy. The electron orbits are coupled to the crystallographic structure, which makes the spins prefer to align along well-defined crystallographic axes. There are therefore directions in space along which it is easier to magnetize a given crystal than along others. This fact is described by means of a direction-dependent energy term, which is usually small compared with the exchange energy. The *magnitude* of the total magnetization (in the present context, mainly the vectorial sum of spins, $\vec{M} = \gamma \sum_i \vec{S}_i$, for a unity volume), at some temperature T , is determined almost only by the exchange, but its *direction* is determined by the direction of the “anisotropy field”, derived from the anisotropy energy terms. Since a quantitative evaluation of the spin-orbit interaction from basic principles is not accurate, as is the case with exchange integrals, anisotropy energies are often introduced as phenomenological terms, which are power expansions of the unit vector

$$\hat{m} = \frac{\vec{M}}{|\vec{M}|} \quad (2.4)$$

parallel to the total magnetization.

Among the *magnetocrystalline* anisotropies we can mention the *uniaxial* anisotropy

$$\mathcal{W}_u = -K_1 m_z^2 + K_2 m_z^4 \quad , \quad (2.5)$$

which appears, for instance, in hexagonal lattices where the \hat{z} direction is the c-axis, and usually $|K_2| \ll |K_1|$ are dependent on T . When $K_1 > 0$ the c-axis is an *easy-axis*, and \vec{m} in that direction gives the minimum energy. When $K_1 < 0$, the c-axis is a *hard-axis*, with an *easy-plane* perpendicular to it. The odd powers of \vec{m} are excluded by the experimental observation that the energy is symmetric with respect to the ab-plane.

For cubic crystals, there exists the *cubic* anisotropy: the previous expansion should be unchanged if x is replaced by y , etc., and again odd powers are excluded, so the lowest-order combination would be $(m_x^2 + m_y^2 + m_z^2)$, but this is a constant. Therefore, four is the lowest order, and the expansion starts with

$$\mathcal{W}_c = K_1 (m_x^2 m_y^2 + m_y^2 m_z^2 + m_z^2 m_x^2) + K_2 m_x^2 m_y^2 m_z^2 \quad . \quad (2.6)$$

For instance, $K_1 > 0$ in Fe, so that the easy axes are along (100), while $K_1 < 0$ for Ni, and the easy axes are along the body diagonals, (111).

There are other situations in which the presence of interfaces of different media, or deformations in the crystalline structure itself, give rise to *anisotropic exchange*, where the different components of the neighbor spins are coupled with different intensities. In a thin film, for instance, realized by depositing few layers of magnetic atoms over a non-magnetic substrate, or in compounds which contain intercalated planes of magnetic and non-magnetic substances, the planar structures give rise to *anisotropic exchange* which can be modeled in terms of the spins in the form

$$-\frac{1}{2} \sum_{i,j=1}^N \left(J_x S_i^x S_j^x + J_y S_i^y S_j^y + J_z S_i^z S_j^z \right) \quad , \quad (2.7)$$

This form is what we will use in most of this work, since we are interested in small 2D ferromagnets, particularly with a circular shape.

There are also situations in which the geometry itself, through the magnetostatic dipole-dipole interaction \mathcal{U}_M which solves the magnetic Poisson equation

$$\nabla^2 \mathcal{U}_M = -\vec{\nabla} \cdot \vec{M} \quad , \quad (2.8)$$

where \vec{M} is the total magnetization, causes the appearance of *shape* anisotropy terms. The use of magnetostatic instead of the complete Maxwell equations is justified here, whenever the time variations of typical magnetic structures are slow. Only for a few

simple cases, like a uniformly magnetized ellipsoid, this problem is exactly solved, and leads to an effective energy term in the form

$$\mathcal{U}_M = \frac{1}{2} \left(N_x M_x^2 + N_y M_y^2 + N_z M_z^2 \right) , \quad (2.9)$$

with N_i constants, which is very similar to the above mentioned crystalline anisotropies. This kind of result can be obtained only for *uniformly* magnetized bodies, and not for other spatial distributions of the magnetization. Note that in applying magnetostatics, we have passed to a continuum description of matter, which was not necessary for the previously discussed anisotropy terms. Alternatively, one could include in the energy a dipole-dipole interaction, as the formal integral of (2.8). A discrete version of it, namely

$$\mathcal{U}_M = -\frac{D}{2} \sum_{i,j} \left(\frac{\vec{S}_i \cdot \vec{S}_j}{|\vec{r}_{ij}|^3} - 3 \frac{(\vec{S}_i \cdot \vec{r}_{ij})(\vec{S}_j \cdot \vec{r}_{ij})}{|\vec{r}_{ij}|^5} \right) , \quad (2.10)$$

can be used for numerical calculations [20]. However, this term is a long-range interaction which makes very difficult the theory and very time-consuming the numerical calculations. For the 2D systems that we consider here in many cases (depending on the relative intensities D/J or D/K), this term is usually neglected.

We are interested exclusively in the Hamiltonian (2.7) with easy-plane anisotropy. For typical quasi-2D materials with an easy-plane (for instance, the compound K_2CuF_4 , a layered magnet with a ratio of interplane-to-intraplane exchange constants $J'/J \approx 10^{-4}$, see Ref. [30]), at low temperatures ($T_{BKT} \approx 6.2\text{K}$), the exchange constants are in the order $J \approx 10\text{K}$, and the anisotropies range from 1 to 10%.

2.2 Heisenberg model with uniaxial anisotropy

So far the spins involved in the energy terms (except the magnetostatic term which is derived from Classical Electromagnetism), are a quantum concept. The quantum many-body problem is so complex that it is tractable only in a few very restricted cases. Therefore, a usual practice is to consider *classical* spins variables, as the classical limit

$$S \rightarrow \infty , \quad \hbar \rightarrow 0 , \quad \hbar S \rightarrow S_c \equiv \text{const} \quad (2.11)$$

of the (non-commuting) spin operators, and justify this procedure a posteriori, by contrasting the results with the experiments. We will investigate, thus, the dynamics of a classical spin system, whose equations of motion arise, in the case of a Hamiltonian system, as the classical limit of the corresponding quantum equations of motion (see Appendix A).

Throughout this work, we will be interested in the dynamics of a strictly 2D ferromagnet, say a monolayer, forming a square lattice of spins $\vec{S}_{\vec{n}}$ indexed by a vector of integers $\vec{n} = (n_x, n_y)$. The system in our numerical simulations and in some analytical considerations, has a finite size, often with a circular border, although for some calculations (particularly in discrete form) a rectangular border ($1 \leq n_x \leq N_x$, $1 \leq n_y \leq N_y$) is assumed for simplicity.

Our model system is chosen to have anisotropic exchange in the form (2.7), although in some of the next calculations and in some parts of the numerical work, for the sake of comparisons, I will use on-site or self-interaction terms of the form of (2.5) as well. All together with a rescaled static field $\vec{h} := \gamma \vec{B}$, we will use the Hamiltonian

$$\mathcal{H} = \mathcal{H}_0 + \mathcal{H}_1 + \mathcal{V} = -\frac{1}{2} \sum_{\vec{n}, \vec{a}} \vec{S}_{\vec{n}} \cdot \hat{J} \vec{S}_{\vec{n}+\vec{a}} - \frac{1}{2} \sum_{\vec{n}} \vec{S}_{\vec{n}} \cdot \hat{D} \vec{S}_{\vec{n}} - \vec{h} \cdot \sum_{\vec{n}} \vec{S}_{\vec{n}} \quad (2.12)$$

where $\vec{n} = (n_x, n_y)$ is a lattice site, and $\vec{a} = \{(0, -a), (0, a), (-a, 0), (a, 0)\}$ are the elemental displacements to its 4 neighbors, with $a > 0$ the lattice constant, $\hat{J} = \text{diag}(J_x, J_y, J_z)$ is a diagonal matrix which includes the exchange constants with anisotropy in the 3 axes of the spin space, and the on-site anisotropy is included in $\hat{D} = \text{diag}(D_x, D_y, D_z)$. The spin lengths are fixed to its classical value $|\vec{S}| = S_c$.

The models included in (2.12) are classified by their state of minimum energy at zero field. In the *easy-axis* as well as in the *easy-plane* models, both extremes of *uni-axial* anisotropy, the coupling constants for 2 of the main directions, say in the XY plane, are equal to each other, and different to the corresponding constants for the remaining axis, say the \hat{z} -axis³, so it proves convenient to write

$$\text{Easy-Plane or Easy-Axis : } \quad \hat{J} = J \text{diag}(1, 1, \lambda) \quad , \quad \hat{D} = D \text{diag}(1, 1, \mu) \quad , \quad (2.13)$$

where usually $|\lambda| \approx 1$ and $|\mu| \approx 1$. Whether the spins in a uniform configuration prefer to align in some arbitrary direction in the XY plane, or perpendicular to it, at zero field, depends on the competition between the two anisotropies. We can evaluate the Hamiltonian (2.12) for *any* uniform state ($\vec{S}_{\vec{n}} = \vec{S}_{\vec{n}+\vec{a}} \equiv \vec{S}, \forall \vec{n}$): at zero field, assuming (2.13) and because of $(S^x)^2 + (S^y)^2 = S_c^2 - (S^z)^2$ we have

$$\mathcal{H}(S^z) = -\frac{4J+D}{2} S_c^2 N + \frac{4J(1-\lambda)+D(1-\mu)}{2} (S^z)^2 N \quad (2.14)$$

where $N = \sum_{\vec{n}} 1$ is the number of spins. The first term is a constant, the energy of the in-plane (IP) uniform state E_{\parallel} , when $S^z = 0$. On the other hand, the energy of

³The case of 2 different axes for exchange anisotropy and on-site anisotropy, respectively, would correspond, for instance, to a monolayer of a rectangular lattice, and will not be treated here.

the perpendicular (\perp) state, when $S^z = S_c$, is $E_{\perp} = -(4J\lambda + D\mu) S_c^2 N/2$, so which state has the lowest energy depends on the quantity

$$K \equiv 4J(1 - \lambda) + D(1 - \mu) \begin{cases} < 0 & , E_{\parallel} > E_{\perp} \rightsquigarrow \text{Easy-Axis} \\ > 0 & , E_{\parallel} < E_{\perp} \rightsquigarrow \text{Easy-Plane} \end{cases} \quad (2.15)$$

From here it is clear that when all the constants are positive the system exhibits an easy plane, which is the case of interest in this work.

When there is a static magnetic field present, the uniform state with minimum energy results from the competition between the anisotropies and the field. For a perpendicular field $\vec{h}_{\perp} = h_{\perp} \hat{z}$, which does not break the $O(2)$ symmetry in the XY plane, we can simply add the energy $-h_{\perp} S_c N$ to E_{\perp} , while E_{\parallel} remains unchanged, which amounts to add the term $+h_{\perp}/S_c$ to the l.h.s. of the inequalities (2.15), to determine which state will have the lowest energy.

However, the uniform state with the lowest energy in this case may be none of (2.15), but a sort of compromise [36, 38], where the IP components of the spins point in an arbitrary direction of the plane, while the out-of-plane (OP) components result from minimizing

$$\frac{\mathcal{H}(S^z)}{N} = \frac{E_{\parallel}}{N} + \frac{K}{2} (S^z)^2 - h_{\perp} S^z \quad (2.16)$$

with respect to S^z , which gives

$$\tilde{S}^z = \frac{h_{\perp}}{K} := \frac{h_{\perp}}{h_a} S_c \quad (2.17)$$

where we defined the anisotropy field intensity $h_a = K S_c$. Together with the constraint $|S^z| \leq S_c$, which means $|h_{\perp}| \leq |h_a|$, this formula says that the minimum of the energy is shifted to the right with increasing $h_{\perp} > 0$, for $K > 0$, until the field takes the critical value $h_{\perp} = h_a$, when the magnet has an easy-axis with $\tilde{S}^z = S_c$. When $h_{\perp} < 0$, for $K > 0$, the minimum of S^z in the interval $|S^z| \leq S_c$ is reached at $\tilde{S}^z < 0$, until eventually $h_{\perp} = h_a$, and the ferromagnet is again an easy-axis, but with $-\hat{z}$ as easy direction. The situation is depicted in **Fig. 2.1**, where I plot (2.16) divided by $(K S_c^2)$, *i.e.* the function

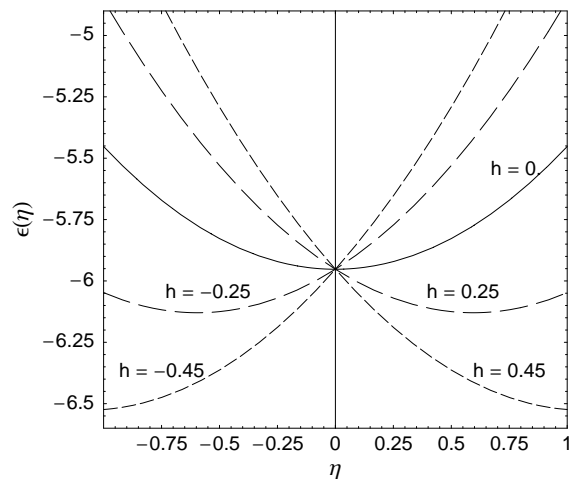


Fig. 2.1: The energy (2.18) for typical settings (see the text) and various field intensities h .

$$\epsilon(\eta) = E_0 + \frac{1}{2} \eta^2 - h \eta \quad (2.18)$$

of the reduced variables $\eta = S^z/S_c$ and $h = h_\perp/h_a$, with $E_0 = E_\parallel/(N K S_c^2)$, for typical settings $J = D = 1$, $\lambda = 0.9$, and $\mu = 0.98$, and for different reduced fields h . Here $K = 0.42$, and $E_0 \approx -5.95$. Thus, at very low fields the magnet has an easy-plane, while at high fields the magnet has an easy-axis.

For an applied field with an additional IP component, we can choose the \hat{x} -axis in that direction and write $\vec{h} = (h_x, 0, h_z)$. It is convenient to parameterize the spin vectors in terms of their z-component $S_{\vec{n}}^z$ and of the IP angle $\phi_{\vec{n}} = \arctan(S_{\vec{n}}^y/S_{\vec{n}}^x)$ as

$$\vec{S}_{\vec{n}} = (P_{\vec{n}} \cos \phi_{\vec{n}}, P_{\vec{n}} \sin \phi_{\vec{n}}, S_{\vec{n}}^z) , \quad (2.19)$$

where $P_{\vec{n}} = \sqrt{S_c^2 - (S_{\vec{n}}^z)^2}$. In these variables the Hamiltonian (2.12) plus the IP magnetic field contribution is

$$\begin{aligned} \mathcal{H} = & -\frac{J}{2} \sum_{\vec{n}, \vec{a}} \left\{ P_{\vec{n}} P_{\vec{n}+\vec{a}} \cos(\phi_{\vec{n}} - \phi_{\vec{n}+\vec{a}}) + \lambda S_{\vec{n}}^z S_{\vec{n}+\vec{a}}^z \right\} - \frac{D}{2} \sum_{\vec{n}} \left(P_{\vec{n}}^2 + \mu (S_{\vec{n}}^z)^2 \right) \\ & - h_x \sum_{\vec{n}} P_{\vec{n}} \cos \phi_{\vec{n}} - h_z \sum_{\vec{n}} S_{\vec{n}}^z . \end{aligned} \quad (2.20)$$

In the uniform state, with $S_{\vec{n}}^z \equiv S_z$, $P_{\vec{n}} \equiv P = \sqrt{S_c^2 - S_z^2}$, $\phi_{\vec{n}} \equiv \phi$, $\forall \vec{n}$, we have

$$\frac{\mathcal{H}}{N} = -\frac{J}{2} \left(4P^2 + 4\lambda S_z^2 \right) - \frac{D}{2} \left(P^2 + \mu S_z^2 \right) - h_x P \cos \phi - h_z S_z . \quad (2.21)$$

Minimizing with respect to (ϕ, S_z) gives $\phi = 0$, and, therefore, $S_x = P$, so that the IP components of the spins are aligned with the IP component of the field, while the value of S_z results from the quartic equation

$$K S_z + h_x \frac{S_z}{P} - h_z = 0 ,$$

recalling that $K = 4J(1 - \lambda) + D(1 - \mu)$. In terms of S_z we have the relation

$$(K S_z - h_z) \sqrt{S_c^2 - S_z^2} + h_x S_z = 0 , \quad (2.22)$$

where the constraint $|S_z| \leq S_c$ assures a physical result. We note, first, that the solution $S_z = S_c$ is proscribed unless $h_x = 0$, and secondly, for $h_x = 0$ we recover also the solution (2.17) for a pure \perp field.

Finally, for a pure IP field, as long as it is weak enough, $|h_x| < K S_c$, we obtain

$$S_z = \pm \sqrt{S_c^2 - h_x^2/K^2} , \quad S_x = h_x/K , \quad (2.23)$$

and, otherwise, saturation in the \hat{x} direction.

2.3 Dynamics of classical spins

The equations of motion for the system (2.12) can be obtained, either by taking the classical limit (2.11) of the quantum-mechanical Heisenberg equations (see Appendix A.2), or directly from the Euler-Lagrange equations of Classical Mechanics. By the first method, the equations are usually obtained just for the anisotropic Heisenberg model, while the second method allows for more general forms of the energy, including contributions coming, for instance, from Classical Electromagnetism. Both methods give the same conservative terms, but only in the classical formalism a dissipative term can be introduced⁴ in a phenomenological way, which formally corresponds to the introduction of the simplest dissipation function [66, 21], proportional to the square of the generalized velocities, into the Euler-Lagrange equations.

The classical description can also be extended, more easily than the quantum one, to a field theory of a continuous medium. As we will drive the system in later chapters with time dependent forces, we need to include also dissipative terms to keep a balance in the total energy and to damp out the non-desired spin waves.

We start, thus, by posing the classical formalism, for the $2N$ degrees of freedom (ϕ_n, S_n^z) , where n is a site index on the lattice, $\phi_n := \arctan(S_n^y/S_n^x)$ as before. If we *impose* them to be canonically conjugated variables by defining the Poisson brackets of two functions $F(\phi_n, S_n^z)$ and $G(\phi_n, S_n^z)$ in the form

$$\{F, G\} := \sum_n \left(\frac{\partial F}{\partial \phi_n} \frac{\partial G}{\partial S_n^z} - \frac{\partial F}{\partial S_n^z} \frac{\partial G}{\partial \phi_n} \right) , \quad (2.24)$$

then we get the obvious relations $\{\phi_n, S_m^z\} = \delta_{nm}$, and the more interesting relations

$$\{S_n^\alpha, S_m^\beta\} = \delta_{nm} \varepsilon^{\alpha\beta\gamma} S_m^\gamma , \quad (2.25)$$

where δ_{nm} is the Kronecker-symbol, $\varepsilon^{\alpha\beta\gamma}$ is the totally antisymmetric tensor, and a sum is implied over any repeated Greek index ($= x, y, z$). Equation (2.25) is then compatible with the quantum commutation relations (A.1) (see Appendix A.1). In the sense of (2.25), the variables (ϕ_n, S_n^z) are then canonically conjugated. In this case, the

⁴At present, there is no agreed way of introducing dissipative terms in Quantum Mechanics in general, and in particular for the case of spins, there are attempts which deal with a magnon bath, coming either from spin-orbit interactions, or from interactions with the nuclear spins.

Euler-Lagrange equations with dissipative forces take the form

$$\frac{d}{dt} \left(\frac{\partial \mathcal{L}}{\partial \dot{\phi}_n} \right) - \frac{\partial \mathcal{L}}{\partial \phi_n} + \frac{\partial \mathcal{F}}{\partial \dot{\phi}_n} = 0 \quad , \quad (2.26a)$$

$$\frac{1}{P_n} \frac{d}{dt} \left(P_n \frac{\partial \mathcal{L}}{\partial \dot{S}_n^z} \right) - \frac{\partial \mathcal{L}}{\partial S_n^z} + \frac{\partial \mathcal{F}}{\partial \dot{S}_n^z} = 0 \quad , \quad (2.26b)$$

where the dot over a variable means total time derivative, for the Lagrangian

$$\mathcal{L} = \sum_n \dot{\phi}_n S_n^z - \mathcal{H}(\phi_n, S_n^z) \quad , \quad (2.27)$$

where $\mathcal{H}(\phi_n, S_n^z)$ is the Hamiltonian, and the above mentioned dissipation function

$$\mathcal{F} = \frac{\varepsilon S_c}{2} \sum_n \left\{ \frac{1}{P_n^2} (\dot{S}_n^z)^2 + \frac{P_n^2}{S_c^2} (\dot{\phi}_n)^2 \right\} = \frac{\varepsilon}{2 S_c} \sum_n (\dot{S}_n^z)^2 \quad , \quad (2.28)$$

where again $P_n^2 = S_c^2 - (S_n^z)^2$ and ε is to be identified later as a damping constant. Explicitly, from (2.26) we get the equations of motion

$$\dot{\phi}_n = \frac{\partial \mathcal{H}}{\partial S_n^z} + \frac{\varepsilon S_c}{P_n^2} \dot{S}_n^z \quad , \quad (2.29a)$$

$$\dot{S}_n^z = - \frac{\partial \mathcal{H}}{\partial \phi_n} - \frac{\varepsilon}{S_c} P_n^2 \dot{\phi}_n \quad . \quad (2.29b)$$

These are the Landau-Lifshitz-Gilbert (LLG) equations⁵, in one of their many forms, with a damping term in the form first given by Gilbert. We note that these equations, at zero damping, coincide with the Hamilton equations for a Hamiltonian depending on the $2N$ variables (ϕ_n, S_n^z) , canonically conjugated in the Hamiltonian sense, since the momentum conjugated to ϕ_n is $\Pi_n := \partial \mathcal{L} / \partial \dot{\phi}_n = S_n^z$. By using the relations

$$\dot{\phi}_n = \frac{1}{P_n^2} \left(S_n^x \dot{S}_n^y - S_n^y \dot{S}_n^x \right) \quad , \quad \dot{S}_n^x = - S_n^y \dot{\phi}_n - \frac{S_n^x}{P_n^2} S_n^z \dot{S}_n^z \quad (2.30)$$

$$\dot{S}_n^z = - \frac{1}{S_n^z} \left(S_n^x \dot{S}_n^x + S_n^y \dot{S}_n^y \right) \quad , \quad \dot{S}_n^y = + S_n^x \dot{\phi}_n - \frac{S_n^y}{P_n^2} S_n^z \dot{S}_n^z \quad (2.31)$$

$$\frac{\partial \mathcal{H}}{\partial \phi_n} = \frac{P_n^2}{S_n^x} \frac{\partial \mathcal{H}}{\partial S_n^y} = - \frac{P_n^2}{S_n^y} \frac{\partial \mathcal{H}}{\partial S_n^x} \quad . \quad (2.32)$$

⁵Actually, the original LLG equations are written in terms of magnetic momenta \vec{m} of Eqs. (2.1), and a coefficient γ appears in front of $\partial \mathcal{H} / \partial \vec{S}$, fixing dimensions. In the present context, we work with $\gamma = 1$, and therefore $\varepsilon \rightarrow -\varepsilon$ with respect to the original LLG equations (where $\gamma < 0$) to get decreasing energy in (2.38). For further details, see the discussion in Appendices A.2.1 and A.5.

it is easy to show that (2.29) are equivalent to

$$\dot{\vec{S}}_n = -\vec{S}_n \times \frac{\partial \mathcal{H}}{\partial \vec{S}_n} - \frac{\varepsilon}{S_c} \vec{S}_n \times \dot{\vec{S}}_n \quad , \quad (2.33)$$

which is a more familiar form of the LLG equations. For the purpose of numerical simulations we would like to have still another form, where the time derivative of the spins does not appear on the r.h.s.. One easy way to solve (2.33) for $\dot{\vec{S}}_n$, is replacing $\dot{\vec{S}}_n$ on the r.h.s. by its value, *i.e.* by the whole r.h.s. of the equation, and then using $\vec{S}_n \times \vec{S}_n \times \dot{\vec{S}}_n = -S_c^2 \dot{\vec{S}}_n$ (because $2\vec{S}_n \cdot \dot{\vec{S}}_n = d(\vec{S}_n^2)/dt = 0$). In this way we obtain

$$(1 + \varepsilon^2) \dot{\vec{S}}_n = -\vec{S}_n \times \frac{\partial \mathcal{H}}{\partial \vec{S}_n} + \frac{\varepsilon}{S_c} \vec{S}_n \times \vec{S}_n \times \frac{\partial \mathcal{H}}{\partial \vec{S}_n} \quad (2.34)$$

This is the form of the LL equations that we integrate in time in our numerical simulations. Notice that all these equations are dimensionally correct.

Of course, the last procedure is consistent with the result of replacing successively \dot{S}_n^z and $\dot{\phi}_n$ on the r.h.s. of eqs. (2.29), which gives

$$(1 + \varepsilon^2) \dot{\phi}_n = \frac{\partial \mathcal{H}}{\partial S_n^z} - \frac{\varepsilon S_c}{P_n^2} \frac{\partial \mathcal{H}}{\partial \phi_n} \quad (2.35a)$$

$$(1 + \varepsilon^2) \dot{S}_n^z = -\frac{\partial \mathcal{H}}{\partial \phi_n} - \frac{\varepsilon P_n^2}{S_c} \frac{\partial \mathcal{H}}{\partial S_n^z} \quad (2.35b)$$

2.4 Variation of non-conserved quantities

To specify which quantities (and under which circumstances) are conserved we need to specify the model. Quite generally, within the uni-axial models (2.12) and (2.13), where the distinguished axis was chosen to be \hat{z} , the dynamical equations (2.34) or (2.29), at zero damping and zero field, preserve at least the energy and the total magnetization in the \hat{z} direction. Indeed, as calculated in the Appendix A.3, for the rate of change of the Hamiltonian (2.12), under the dynamics (2.34), *i.e.*

$$(1 + \varepsilon^2) \dot{\vec{S}}_n = \vec{S}_n \times \vec{B}_n - \frac{\varepsilon}{S_c} \vec{S}_n \times \vec{S}_n \times \vec{B}_n \quad , \quad (2.36)$$

where the local effective “field” is defined⁶ as

$$\vec{B}_n := -\frac{\partial \mathcal{H}}{\partial \vec{S}_n} = \hat{J} \sum_a \vec{S}_{n+a} + \hat{D} \vec{S}_n + \vec{h}_n(t) \quad , \quad (2.37)$$

⁶Actually, it has units of frequency.

including possibly a non-uniform and time-dependent magnetic field $\vec{h}_n(t)$, we get the result

$$\frac{d\mathcal{H}}{dt} = -\frac{\varepsilon}{(1+\varepsilon^2)S_c} \sum_n \left(\vec{S}_n \times \vec{B}_n \right)^2 - \sum_n \vec{S}_n \cdot \frac{d}{dt} \vec{h}_n(t) \quad , \quad (2.38)$$

from which it is seen that even in presence of a static field the energy *decreases* as a consequence of damping, and otherwise it is conserved if the damping is zero. When the field is time-dependent, the second term of (2.38) comes into play and depending on the intensity (and frequency, in case of an AC field) of the field, this term can be dominant, giving rise to oscillations and even blowing up of the energy along the time.

Magnetization

From the structure of the equations (2.34) we see that the conservation of each component of the total magnetization, $\vec{M} := \sum_n \vec{S}_n$, implies more symmetry requirements. In general, under the dynamics (2.36), we have trivially

$$(1+\varepsilon^2) \frac{d\vec{M}}{dt} := (1+\varepsilon^2) \sum_n \dot{\vec{S}}_n = - \sum_n \vec{S}_n \times \vec{B}_n + \frac{\varepsilon}{S_c} \sum_n \vec{S}_n \times \vec{S}_n \times \vec{B}_n \quad . \quad (2.39)$$

At zero damping, in view of the equality

$$\sum_{na} \left(S_n^\alpha S_{n+a}^\beta - S_n^\beta S_{n+a}^\alpha \right) = 0 \quad , \quad \forall \alpha, \beta = x, y, z \quad ,$$

we obtain conservation of a component (say M^z) of the total magnetization, provided that (a) the magnetic field points in the same direction (\hat{z}), and (b) the effective field contains the same exchange and anisotropy constants in the remaining two directions (\hat{x} and \hat{y}), respectively. This is the case of M^z in the uniaxial model (2.12)–(2.13) with a perpendicular field $\vec{h}_n(t) = h_n(t) \hat{z}$ (even time-dependent, in which case there is an irregular precession of \vec{M} around \hat{z} , *i.e.* with the angle $\phi_M(t) = \arctan(M_y/M_x)$ being a non-monotonous function of time, but preserving M^z).

Naturally, in the isotropic model, at zero field and zero damping, all the 3 components of \vec{M} are conserved.

Linear and angular momenta, etc.

So far we demonstrated the conservation/variation of two quantities for the discrete system. The analogous results for a continuum system (see the next Chapter) arise simply as a limiting case of the discrete ones. There are other quantities which can be shown to be conserved (at zero damping and field), like the total linear and angular

momenta of the lattice, and some “topological” quantities, all of which arise more naturally in the continuum approach, as will be discussed in the next Chapter. By now it suffices to mention that the question of the conservation (and even the definition) of the total linear momentum for the continuum system is plagued with difficulties, whenever the fields involved exhibit singularities or discontinuities, and the whole subject remains since a long time a matter of controversy [26, 81, 60, 62] (see also [3]). We also note that, since all these quantities involve spatial derivatives (in all the various proposed definitions), their simplest discrete versions –among several possibilities– are generally not conserved even for zero damping (see Appendix B).

Chapter 3

Vortices and static magnetic fields

In Chapter 2, I presented some basics of the Heisenberg model, and some details of calculations that can be done in a discrete manner. We turn now to topological excitations, which may be better understood if we consider, simultaneously with the discrete system, the so-called called *long-wave approximation*, or *continuum limit*. The uniform state of Sec.(2.2) is not the most interesting state a magnet can exhibit. Actually, if some other terms are included in the energy besides exchange and anisotropy, like the dipolar interaction (2.10), in a finite system the presence of surfaces and borders will produce non-uniform configurations, through the “pole avoidance principle” [2], which will try as much as possible to put all the spins parallel to the surfaces. This gives rise to magnetic domains inside the magnet. In small dots of Permalloy, for instance, the dipolar interaction, dominating the exchange, provides the mechanism for the nucleation of a “vortex” state, from the surface (border) towards the center, where a singularity or flux line is then trapped. This vortex has, thus, lower energy than that of a uniform state, and, therefore, is spontaneously generated. In our work we do not consider the dipolar interaction, which, however, does not prevent us from studying vortices in our simulations: once a vortex is generated by some relaxation procedure starting from an approximate vortex configuration, it can be stable inside the system, as far as the energy has to be conserved. Damping can make the system expel the vortex. But we can also drive the system with a periodic force which pushes the vortex back towards the center, and this is what we do in the Chapters 4 and 5. To prepare for that, we first present the concept of a vortex in the frame of a continuum theory, and try to understand how this vortex interacts with external static fields.

3.1 Continuum limit and topological excitations

From now on we will work with a 2D square lattice, i.e., the site index n has two components (n_x, n_y) , and the border of the system is assumed to form a circle of radius R_s : $-R_s \leq n_x \leq R_s$, $-N_y(n_x) \leq n_y \leq N_y(n_x)$, where $N_y(n_x) := \sqrt{R_s^2 - n_x^2}$. The four elemental lattice displacements are

$$\vec{a} = \{(-a, 0), (+a, 0), (0, -a), (0, +a)\} := \{-\vec{a}_x, \vec{a}_x, -\vec{a}_y, \vec{a}_y\}$$

where a is the lattice constant. The continuum approximation to the model (2.12) starts by assuming that the change in the spin vector $\vec{S}_{\vec{n}}$ from one lattice site to a neighbor site is rather smooth, so the spins can be considered a *continuous* function of the coordinates $\vec{r} = (x, y)$, and we can expand $\vec{S}_{\vec{n}+\vec{a}}$ in the exchange part \mathcal{H}_0 of (2.12) in a series around $\vec{S}_{\vec{n}}$. Up to second order we have

$$\vec{S}_{\vec{n}+\vec{a}} = \vec{S}_{\vec{n}} + (\vec{a} \cdot \vec{\nabla}) \vec{S}_{\vec{n}} + \frac{1}{2} (\vec{a} \cdot \vec{\nabla})^2 \vec{S}_{\vec{n}} ,$$

where $(\vec{a} \cdot \vec{\nabla})^j = (a^x \partial_x + a^y \partial_y)^j$ is applied formally j times to $\vec{S}_{\vec{n}}$, and $\vec{\nabla} := (\partial_x, \partial_y)$. The linear terms will drop out of the sum¹ because $\sum_{\vec{a}} (\vec{a} \cdot \vec{\nabla}) \vec{S}_{\vec{n}} = 0$, as well as the cross derivative terms, because, for every \vec{a} , the product $a_x a_y = 0$. Thus, it remains

$$\begin{aligned} H_0 &= -\frac{1}{2} \sum_{\vec{n}, \vec{a}} \vec{S}_{\vec{n}} \cdot \hat{J} \left[\vec{S}_{\vec{n}} + \frac{1}{2} (\vec{a} \cdot \vec{\nabla})^2 \vec{S}_{\vec{n}} \right] \\ &= -\frac{1}{2} \sum_{\vec{n}} 4 \vec{S}_{\vec{n}} \cdot \hat{J} \vec{S}_{\vec{n}} - \frac{1}{4} \sum_{\vec{n}} \vec{S}_{\vec{n}} \cdot \hat{J} \left[2 a^2 (\partial_x^2 + \partial_y^2) \right] \vec{S}_{\vec{n}} \\ &= -\frac{1}{2} \sum_{\vec{n}} \vec{S}_{\vec{n}} \cdot \hat{J} \left(4 \hat{I} + a^2 \Delta \right) \vec{S}_{\vec{n}} \end{aligned} \quad (3.1)$$

where \hat{I} is the 3×3 identity matrix and Δ the 2D Laplacian. In particular, for the uniaxial model (2.13) with $\hat{J} = J \text{diag}(1, 1, \lambda) = J \hat{I} - J \text{diag}(0, 0, \delta)$, with $\delta = 1 - \lambda$, we have for the exchange term

$$H_0 = -2JNS_c^2 - \frac{J}{2} \sum_{\vec{n}} a^2 \left\{ \vec{S}_{\vec{n}} \cdot \Delta \vec{S}_{\vec{n}} - \frac{4\delta}{a^2} (S_{\vec{n}}^z)^2 - \delta S_{\vec{n}}^z \Delta S_{\vec{n}}^z \right\}$$

The first term, a constant, can be dropped. For the rest, the continuum limit gives

$$H_0 = -\frac{J}{2} \int dx dy \left\{ \vec{S} \cdot \Delta \vec{S} - \frac{4\delta}{a^2} (S^z)^2 - \delta S^z \Delta S^z \right\} \quad (3.2)$$

¹In fact, all further odd- j powers disappear, so the result (3.1) is actually $\mathcal{O}(a^4)$.

Obtaining the analogous expressions for the on-site anisotropy term H_1 and the Zeeman energy V in (2.12) is straightforward. Note that the expression (3.2) for H_0 contains in its second term essentially the same as the analogue for the on-site anisotropy term

$$H_1 = -\frac{1}{2} D N S_c^2 + \frac{D(1-\mu)}{2a^2} \int d^2x (S^z)^2$$

upon a rescaling of δ . All together, the continuum version of (2.12) is

$$H = -\frac{J}{2} \int d^2x \left\{ \vec{S} \cdot \Delta \vec{S} - \frac{K}{a^2} (S^z)^2 - \delta S^z \Delta S^z + \frac{2}{Ja^2} \vec{S} \cdot \vec{h} \right\} := \int d^2x \mathcal{E}_0 \quad (3.3)$$

where we defined an effective anisotropy constant

$$K := 4(1-\lambda) + D(1-\mu)/J \quad (3.4)$$

and the energy density \mathcal{E}_0 . The dropped constant is the energy of an IP uniform state $E_{\parallel} = -(4J + D) S_c^2 N/2$, at zero field. The third term is often neglected for $\delta \ll 1$, showing that, for small anisotropies, the continuum limits for each type of anisotropy terms are approximately the same. However, it is not difficult to keep this term in our equations, and, since δ and K appear in separate terms, it is easy to let $\delta \rightarrow 0$ at the end, keeping K , to obtain that further approximation. The canonical variables $\{\phi_{\vec{n}}, S_{\vec{n}}^z\}$ of Sec. (2.3) become now fields $\{\phi(\vec{x}, t), \Pi(\vec{x}, t)\}$, the Poisson brackets (2.24) are written in terms of functional derivatives,

$$\{F, G\} := \int d^2x \left(\frac{\delta F}{\delta \phi} \frac{\delta G}{\delta \Pi} - \frac{\delta F}{\delta \Pi} \frac{\delta G}{\delta \phi} \right), \quad (3.5)$$

such that the relations $\{\phi(\vec{x}), \Pi(\vec{x}')\} = \delta(\vec{x} - \vec{x}')$ are fulfilled. From the requirement that $\dot{\phi} \Pi$ had units of energy density, now the momentum conjugated to ϕ is $\Pi := \delta \mathcal{L} / \delta \dot{\phi} = S^z / a^2$, where the Lagrangian from (2.27) becomes the functional

$$\mathcal{L} = \int d^2x \left\{ \dot{\phi} \frac{S^z}{a^2} - \mathcal{E}_T(\phi, \partial_\alpha \phi, S^z, \partial_\alpha S^z, \partial_{\alpha\alpha}^2 S^z) \right\} := \int d^2x \mathcal{L}, \quad (3.6)$$

where we defined the lagrangian density \mathcal{L} , the total energy density $\mathcal{E}_T = \mathcal{E}_0 + \mathcal{E}_h$ (including magnetic fields), $(\dot{\phi}) := \partial_t \phi$ (the dot is partial derivation with respect to time), and we use the notations $\partial_\alpha := (\vec{\nabla})_\alpha$ and $\partial_{\alpha\alpha}^2 := \vec{\nabla} \cdot \vec{\nabla} := \Delta$, for $\alpha = x, y$ (repeated indices are summed). In terms of $m(\vec{x}, t) = S^z(\vec{x}, t)/S_c$, and using the fact that²

²In the continuum case, $\vec{S} \cdot \Delta \vec{S} = \vec{S} \partial_\alpha \partial^\alpha \vec{S} = \partial_\alpha (\vec{S} \cdot \partial^\alpha \vec{S}) - (\partial_\alpha \vec{S})^2 = -(\partial_\alpha \vec{S})^2$, since $\vec{S} \cdot \partial^\alpha \vec{S} = \partial^\alpha S^2 / 2 = 0$. It is interesting to compare this with the discrete case, where spatial deriva-

$$-\vec{S} \cdot \Delta \vec{S} = (\vec{\nabla} \vec{S})^2 = S_c^2 \left\{ \frac{(\vec{\nabla} m)^2}{1-m^2} + (1-m^2) (\vec{\nabla} \phi)^2 \right\} , \quad (3.7)$$

the energy density from (3.3) is

$$\mathcal{E}_0 = \frac{JS_c^2}{2} \left\{ \frac{(\vec{\nabla} m)^2}{1-m^2} + (1-m^2) (\vec{\nabla} \phi)^2 + \frac{K}{a^2} m^2 + \delta m \Delta m \right\} . \quad (3.8)$$

The last term can also be replaced by $-\delta(\vec{\nabla} m)^2$, which has identical effects in the equations below. With a general magnetic field

$$\vec{h} = (h_{\parallel} \cos \beta_0 , h_{\parallel} \sin \beta_0 , h_{\perp}) , \quad (3.9)$$

the magnetic energy density is

$$\mathcal{E}_h = -\frac{S_c}{a^2} \left\{ h_{\parallel} \sqrt{1-m^2} \cos(\phi - \beta_0) + h_{\perp} m \right\} . \quad (3.10)$$

The dissipation function from (2.28) becomes the functional

$$\mathcal{F} = \frac{\varepsilon}{2S_c a^2} \int d^2x \left(\frac{\partial \vec{S}}{\partial t} \right)^2 = \frac{\varepsilon S_c}{2a^2} \int d^2x \left\{ \frac{(\dot{m})^2}{1-m^2} + (1-m^2) (\dot{\phi})^2 \right\} := \int d^2x \mathcal{F} , \quad (3.11)$$

where we defined the corresponding density \mathcal{F} . The motion equations are then derived from the Langrange equations for the generalized coordinates $q_1 = \phi$ and $q_2 = m$, including dissipation,

$$\frac{\delta \mathcal{L}}{\delta q_i} = \frac{\partial \mathcal{L}}{\partial q_i} - \frac{\partial}{\partial t} \left(\frac{\partial \mathcal{L}}{\partial \dot{q}_i} \right) - \partial_{\alpha} \left(\frac{\partial \mathcal{L}}{\partial (\partial_{\alpha} q_i)} \right) + \partial_{\alpha\alpha}^2 \left(\frac{\partial \mathcal{L}}{\partial (\partial_{\alpha\alpha}^2 q_i)} \right) = \frac{\partial \mathcal{F}}{\partial \dot{q}_i}$$

However, for the purpose of discussing some static properties, we will content ourselves with the equations of motion without damping, so we can use the Hamilton equations

$$\frac{\partial \phi}{\partial t} = \frac{\delta \mathcal{E}_T}{\delta \Pi} = \frac{a^2}{S_c} \frac{\delta \mathcal{E}_T}{\delta m} = \frac{a^2}{S_c} \left\{ \frac{\partial \mathcal{E}_T}{\partial m} - \partial_{\alpha} \frac{\partial \mathcal{E}_T}{\partial (\partial_{\alpha} m)} + \partial_{\alpha\alpha}^2 \frac{\partial \mathcal{E}_T}{\partial (\partial_{\alpha\alpha}^2 m)} \right\} \quad (3.12a)$$

$$\frac{\partial \Pi}{\partial t} = \frac{S_c}{a^2} \dot{m} = -\frac{\delta \mathcal{E}_T}{\delta \phi} = -\frac{\partial \mathcal{E}_T}{\partial \phi} + \partial_{\alpha} \frac{\partial \mathcal{E}_T}{\partial (\partial_{\alpha} \phi)} \quad (3.12b)$$

which give

tives are approximated by finite differences (see Appendix B)

$$\frac{\partial \phi}{\partial t} = JS_c a^2 \left\{ -\frac{m(\vec{\nabla} m)^2}{P^4} + m \left(\frac{K}{a^2} - (\vec{\nabla} \phi)^2 \right) + \left(\delta - \frac{S_c^2}{P^2} \right) \Delta m + \frac{b_{\parallel} m \cos(\phi - \beta_0)}{a^2 P} - \frac{b_{\perp}}{a^2} \right\} , \quad (3.13a)$$

$$\frac{\partial m}{\partial t} = JS_c a^2 \left\{ \vec{\nabla} \cdot \left(P^2 \vec{\nabla} \phi \right) + \frac{b_{\parallel}}{a^2} P^2 \sin(\phi - \beta_0) \right\} , \quad (3.13b)$$

where $P^2 = 1 - m^2$, and we defined a rescaled magnetic field $\vec{b} := \vec{h}/(JS_c)$.

Naturally, we will not face such nonlinear PDEs, but only some particular *static*, or at most *stationary*, solutions are to be discussed³. Notice that the anisotropy does not explicitly enter (3.13b), but through the effect on the coupled variable ϕ .

Let us take first the **isotropic** case ($\delta = K = 0$), at **zero field** ($\vec{b} = 0$). Then, defining the field $\theta(\vec{x}, t)$ such that $\cos \theta := m(\vec{x}, t)$ and $P := \sin \theta$, the static sector of (3.13) reduces to

$$(\dot{\phi} = 0) : \quad \sin \theta \cos \theta (\vec{\nabla} \phi)^2 - \Delta \theta = 0 \quad (3.14a)$$

$$(\dot{m} = 0) : \quad 2 \cos \theta \vec{\nabla} \theta \cdot \vec{\nabla} \phi + \sin \theta \Delta \phi = 0 \quad (3.14b)$$

Non-trivial solutions of these equations were found by Belavin and Polyakov (1975) [7] and Trimper (1979) [77], for an infinite medium, satisfying the asymptotic condition

$$\vec{S}(x, y) \rightarrow S_c \hat{z} \quad , \quad \text{for } |\vec{x}| \rightarrow \infty \quad , \quad (3.15)$$

which comes from requiring the energy (in the present case, the first term of (3.3)) to be finite in the infinite system, relative to the energy of the uniform state.

The first set of solutions was expressed in terms of a complex variable $\omega = \cot(\theta/2) \exp(i\phi)$, which is required by eqs. (3.14) and continuity of the fields to be a function of the dependent variable $z = x + iy$ with, at most, single poles,

$$\omega(z) = \cot(\theta/2) \exp(i\phi) = \prod_j \left(\frac{z - z_j}{\beta} \right)^{m_j} \prod_k \left(\frac{\beta}{z - z_k} \right)^{n_k} , \quad (3.16)$$

where β is an arbitrary constant and $\sum_j m_j > \sum_k n_k$. The authors of [7] called these solutions “metastable states”, because they have the property that they can not be continuously deformed one into each other, *i.e.* they can not decay into each other. This fact is explained in terms of topological concepts in the following way. The values of the spin field $\vec{S}(x, y)$ are associated with points on the surface of a 3-D sphere S^2 . The condition (3.15) means that the plane XY is in turn equivalent⁴ to another

³Only in the 1-D (“Heisenberg chain”) and effective 1-D (e.g. radially symmetric) cases, even with anisotropy $K > 0$, eqs. (3.13) are proven to be integrable, and its time-dependent soliton solutions are known (see, for instance, [15, 49, 50, 43, 1] and ref. therein).

⁴For a 3-D magnet, the equivalence is natural, without need of the constraint (3.15).

sphere \tilde{S}^2 , and, thus, each field $\vec{S}(x, y)$ of (3.16) carries out a *mapping* $\tilde{S}^2 \rightarrow S^2$. Such mappings are classified into “homotopical classes”, each of them characterized by an integer number Γ , called “degree of mapping” or “winding number”, given by

$$\Gamma = \frac{1}{4\pi} \int \gamma(x, y) d^2x \quad , \quad \gamma(x, y) = -\frac{1}{2} \epsilon_{\mu\nu} \left(\partial_\mu \vec{S} \times \partial_\nu \vec{S} \right) \cdot \vec{S} \quad , \quad (3.17)$$

where $\epsilon_{\mu\nu}$ is the antisymmetric tensor in 2-D, the indices $\mu, \nu = x, y$, and $\gamma(x, y)$ is called “topological density” [60, 41, 43]. Γ counts the number of times that the sphere S^2 is covered in the course of the mapping, as can be seen from

$$\Gamma = \frac{S_c^2}{4\pi} \int d^2x (\vec{\nabla}\psi \times \vec{\nabla}\phi) \cdot \hat{z} = -\frac{S_c^3}{4\pi} \int \sin\theta d\theta d\phi \quad , \quad (3.18)$$

where, in the last expression, the integrand is the solid angle element. For the solutions (3.16), the eq. (3.17) gives indeed an integer: $\Gamma = \sum_j m_j$. A non-null degree of mapping Γ is a key feature which affects the dynamics of excitations in ferromagnets, as we will see in deeper detail below.

The second set of solutions of (3.14), found by Trimper and called by him “pseudoparticles” [77], contains solutions whose azimuthal angle has the form

$$\phi(x, y) = \sum_j q_j \arctan \left(\frac{y - Y_j}{x - X_j} \right) + \varphi_0 \quad , \quad (3.19)$$

with q_j integer. This is a solution of the Laplace equation $\Delta\phi = 0$ forming *vortices* at the points (X_j, Y_j) , in the sense that the circulation of its gradient, around any closed path c which contains these points is an integer,

$$Q = \frac{1}{2\pi} \oint_c \vec{\nabla}\phi \cdot d\vec{l} = \sum_j q_j \quad (3.20)$$

called “vorticity”. This is a second topological property, related to the IP structure of a magnetic configuration, independent of Γ , although the inverse is not true (see Appendix C). The corresponding polar angle is found in [77] to have the form

$$\theta(x, y) = 2 \arctan \left(\prod_j (r_j)^{-q_j} \right) \quad , \quad (3.21)$$

where $r_j = \sqrt{(x - X_j)^2 + (y - Y_j)^2}$, and (X_j, Y_j) are the positions of the pseudoparticles. These solutions fulfill also the conditions (3.15), and one can check that some of them are in fact included in the first set (3.16). In both sets, the components of the spins are quotients of polynomials of x and y . The fact that these solutions approach

the uniform state (3.15) at infinity, motivated that they were known also under the name “semitopological solitons”. However, Eq. (3.20) is strictly valid for any path, even at infinity.

3.1.1 In-plane (IP) vortices

So far we have seen the isotropic case at zero field, which is the only case in which static solutions with non trivial IP *and* OP components have been found. Apart from making easier the introduction of topological concepts, this is not the case of our interest.

As soon as we allow for anisotropy of the **easy-plane** type, the simplest case being $K > 0$, $\delta = 0$, in (3.13a), the equation for the OP structure get too complicate. The most important difference is that now the uniform state with minimum energy lies on the plane, and, therefore, the conditions (3.15) at spacial infinity are changed to

$$S^z(x, y) \rightarrow 0 \quad , \quad \text{for } |\vec{x}| \rightarrow \infty \quad , \quad (3.22)$$

while the angle ϕ remains arbitrary. It is immediately seen that *planar* solutions (this is, $\dot{\phi} = 0$ and $\dot{\psi} = \psi = 0$) do exist, with the non-trivial angular distribution (3.19). We refer to them as “IP vortices”. For them it is clear that $\Gamma = 0$, while $Q \neq 0$.

The condition (3.22) has a drastic consequence: the energy of a single IP vortex, which from (3.8) with $\psi = 0$ is simply

$$E_{\text{IP}} = \frac{JS_c^2}{2} \int dx dy (\vec{\nabla}\phi)^2 \quad , \quad (3.23)$$

scales with the logarithm of the size of the system, and becomes infinite in an infinite medium⁵. This prevents its existence as a solitary excitation, which would extend over the whole system, but not their appearance in pairs of opposite vorticity. In **Fig. 3.1** we see how the 2-D fields of (3.19) look for $Q = 1$, called a “vortex” (left), $Q = -1$, called “antivortex” (center). It is enough to look at the diagonals to see the opposite arrows in opposite directions.

The pair formed by linear superposition of these two fields in the right panel shows, instead, that the field far from the vortex “dipole” tends to be uniform. Therefore, a vortex-antivortex pair has a finite energy (relative to the energy of the uniform state) and is in this sense “localized”, in contrast to single vortices, in an infinite medium.

It is interesting to note that a *stationary* solution where the IP vortex structure (3.19) rotates as a rigid whole, can be obtained by changing to a reference frame (in the spin

⁵In addition, (3.23) must be regularized by some means, since the integrand is singular at the center of a vortex. This is not necessary for the OP vortices to be studied in Sec. 3.1.2.

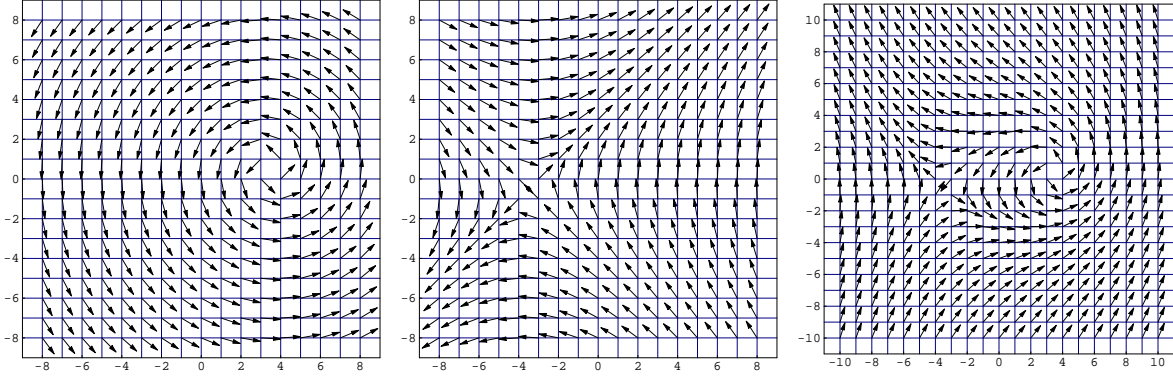


Fig. 3.1: (left) A vortex with $Q = 1$ and $\varphi_0 = -\pi/2$ at $\vec{X} = (3.5, 0.5)$, (center) an antivortex with $Q = -1$ and $\varphi_0 = \pi/2$ at $\vec{X} = (-3.5, -0.5)$, (right) a vortex-antivortex pair, linear superposition of the last two cases.

space) which rotates with a constant angular velocity, say ω , i.e.,

$$\tilde{\phi} = \phi - \omega t \quad (3.24)$$

While eq. (3.13a) in terms of $\tilde{\phi}$ is modified only by the constant term ω on the l.h.s. (recall that by now $\vec{b} = 0$), the eq. (3.13b) remains unchanged. Thus, adding a term ωt to ϕ in (3.19) results in a constant precession of the IP vortex, which still satisfies the Laplace equation for each instant.

Correspondingly, there exists an underlying $O(2)$ -symmetry of the Hamiltonian upon rotations in the spin space which let S^z invariant. Note that the vortex (3.19) is a solution which has broken the $O(2)$ -symmetry in the spin space, i.e., it is *less symmetric* than the Hamiltonian.

Rotations in the spacial plane XY, instead, let the Hamiltonian invariant only for an infinite system, or for a finite system with a border which is circular. And, of course, it is a symmetry operation only for the continuum system, not for the discrete one.

Precisely a finite, circular system is what we are interested in.

A border will break the translational invariance of the infinite system, and the associated total momentum conservation⁶. The rotational invariance, instead, will be preserved, for a circular border, under proper boundary conditions.

The usual boundary conditions (BC) for the Laplace equation which are satisfied by (3.19), are the Dirichlet-BC and the Neumann-BC. The Dirichlet-BC fix the phase of the spin field at the border to some definite function, for instance, through the requirement

$$\phi(x, y) \Big|_{r=L} = q\varphi + \phi_0 \implies \frac{\partial\phi}{\partial\varphi} \Big|_{r=L} = q \quad (3.25)$$

⁶A vortex in an infinite system experiences no force and cannot move [58].

where $\varphi = \arctan(y/x)$ is the polar angle in the plane, and L denotes the radius of the system. The Neumann-BC simply require a null derivative of the field in direction normal to the border,

$$\left. \frac{\partial \phi}{\partial r} \right|_{r=L} = 0 \quad (3.26)$$

The effect of these two types of borders can be described, in analogy with a 2-D electrostatic potential problem, by introducing an “image” vortex outside the system, whose field superpose to the vortex inside the system, to assure either of the above conditions. I would like to emphasize that an “image vortex” is a pictorial way to speak about the effect of a border on the only vortex which is present inside the system (perhaps it would not be a bad idea to call the outer one “imaginary” vortex). The effect of the border is, precisely, to deform the field (3.19) such that the conditions (3.25) or (3.26) are fulfilled. This also produces an effective “force” and a consequent movement of the vortex. A minute of algebra shows that, for a vortex at $\vec{X} = (X, Y)$ with vorticity q , the necessary deformation has the form

$$\Phi(x, y) = q \arctan\left(\frac{y - Y}{x - X}\right) \pm q \arctan\left(\frac{y - Y_1}{x - X_1}\right) \quad (3.27)$$

where the (+) corresponds to Dirichlet-BC and the (−) to Neumann-BC, $R^2 = X^2 + Y^2$, and

$$\vec{X}_1 = (X_1, Y_1) = \frac{L^2}{R^2} \vec{X} \quad (3.28)$$

is interpreted as the position of the image (outside the system), since (3.27) has the form of a superposition (the Laplace equation is linear!). Later on, after giving the form of the interaction between vortices, we will describe the “force” that the border produces over the vortex in the system, as the force exerted over it by the image vortex. We will see that the results of numerical simulations completely support this identification.

To conclude about IP vortices, let us show the result for the energy (3.23) in a circular system with a field distribution (3.27). There are a couple of tricks to calculate this integral as a line integral, which I do not reproduce here, but refer the reader to [46, 45]. In the Appendix A.4 we calculate the integral in the (mobil) frame which is fix to the coordinates of the vortex center. The energy of a single IP vortex, *without* the image term in (3.27), at a distance R from the center of a circular system of radius L , is (its self-energy, in units of JS_c^2)

$$E_0 = \pi \ln\left(\frac{L}{r_v}\right) + \frac{\pi}{2} \ln\left(1 - \frac{R^2}{L^2}\right) \quad (3.29)$$

while the *total* energy, *with* the image contribution, is (see App. A.4)

$$E_{\text{IP}} = \pi \ln \left(\frac{L}{r_v} \right) + \pi \ln \left(1 - \frac{R^2}{L^2} \right) , \quad (3.30)$$

Here r_v is a small cut-off parameter, to be identified in the next Section with the characteristic size of vortex excitations which have a non-trivial out-of-plane structure. The excess energy of a single vortex

$$\Delta E = -\frac{\pi}{2} \ln \left(1 - \frac{R^2}{L^2} \right) \approx \frac{\pi}{2} \frac{R^2}{L^2} , \quad (3.31)$$

as initial condition for simulations, over an initial condition including the image vortex, appears in the form of spin waves generated during the vortex movement, and the interaction between these waves and the vortex plays a role in the observed dynamics, as will be seen later. Finally, a simple inspection of (3.13a) shows that in order that an IP vortex can move, so that the position of its center translates, it must develop an OP structure [22], because otherwise $\dot{m} = \dot{\phi} = 0$ and the IP structure would not change in time (letting aside a possible precession of all the spins with the same frequency, produced by a perpendicular field b_{\perp}).

3.1.2 Out-of-plane (OP) vortices

The main interest of our work lies on vortices which have a non-trivial OP structure. Their existence can be proven mathematically, although the proof is not a constructive one. One simply inserts the IP structure (3.19) into (3.13a), and assumes further that the field $m(\vec{x}, t)$ depends only on the radial coordinate $r = |\vec{x}|$ on the plane. One obtains in this way an ordinary differential equation for S , of second order in r . For one vortex with $(\vec{\nabla}\phi)^2 = q^2/r^2$, in terms of $m(r) := S^z(r)/S_c$, the equation is

$$-\frac{m}{(1-m^2)^2} \left(\frac{dm}{dr} \right)^2 + m \left(\frac{K}{a^2} - \frac{q^2}{r^2} \right) + \frac{1}{r} \left(\delta - \frac{1}{1-m^2} \right) \frac{d}{dr} \left(r \frac{dm}{dr} \right) = 0 . \quad (3.32)$$

Smooth solutions of this non-linear equation are obtained numerically for the conditions

$$\begin{aligned} m(r) &\rightarrow \pm 1 , & r &\rightarrow 0 \\ m(r) &\rightarrow 0 , & r &\rightarrow \infty . \end{aligned} \quad (3.33)$$

Consistently, the asymptotic form of the solution of (3.32) is known [22, 28, 58] to be exponentially decaying. For instance for $D = 0$ (exchange anisotropy only), it is

$$m(r) \equiv m(r/r_v) = \begin{cases} \pm \left(1 - \frac{b}{2} \frac{r^2}{r_v^2}\right) , & \text{for } r \rightarrow 0 , \\ \pm c \sqrt{r_v/r} \exp(-r/r_v) , & \text{for } r \rightarrow \infty , \end{cases} \quad (3.34)$$

where

$$r_v = \frac{a}{2} \sqrt{\frac{1-\delta}{\delta}} = \frac{a}{2} \sqrt{\frac{\lambda}{1-\lambda}} \quad (3.35)$$

is interpreted as the radius of the vortex “core” (the region near the vortex center, where the OP structure is very pronounced), and b and c are constants whose values are determined by matching the two expressions and its derivatives at $r = r_v$, which gives $b = \frac{6}{7}$ and $c = \frac{4}{7} e$, where $e = \exp(1)$. The expression (3.34) looks like in **Fig. 3.2**, for a lattice constant $a = 1$ and two typical values of λ . In numerical simulations [82, 22]

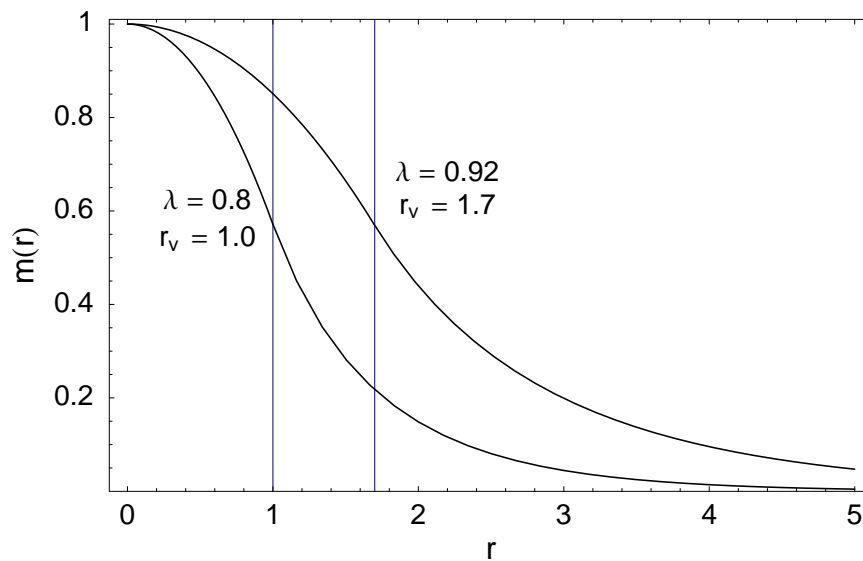


Fig. 3.2: OP structure of a vortex, from asymptotics (3.34).

it was observed that there is a critical value λ_c which depends on the type of the lattice and determines whether an IP vortex or an OP vortex is stable. For hexagonal lattices $\lambda_c \approx 0.86$, for square lattices $\lambda_c \approx 0.72$, and for triangular lattices $\lambda_c \approx 0.62$, such that in each case, for $0 < \lambda < \lambda_c$ the IP vortex and for $\lambda_c < \lambda < 1$ the OP vortex is stable. This observation was later confirmed analytically by Wysin [83], who used a reduced model of the vortex core. Taking into account only a few spins in the region near the vortex center, he was able to explain what we now may call “out-of-plane instability” of vortices in the easy-plane Heisenberg model, for $\lambda \rightarrow \lambda_c$, and he got values of λ_c very close to those observed in the simulations. For instance, for a square lattice he

obtained $\lambda_c \approx 0.716$. This gives us confidence in this kind of discrete models, which are able to capture the essential dynamical aspects of the OP vortex structure, *i.e.* oscillations and switching, and similar models will be applied in Chapter 4.

For OP vortices, the topological charge Γ can be easily calculated from (3.18) using only the asymptotic values (3.33). We have to assume also that in the (moving) reference frame whose origin is fixed at the vortex center, the IP structure is like in (3.19),

$$\phi := \Phi_0(\vec{x}) = q \arctan\left(\frac{y}{x}\right) + \varphi_0 \quad , \quad \vec{\nabla}\Phi_0 = \frac{q}{r} \hat{\varphi} \quad , \quad (3.36)$$

which is a very good approximation (to the static solution of (3.13b), far from the vortex core where $m \rightarrow 0$), and the OP structure is azimuthally symmetric,

$$\theta \equiv \theta(r) \quad , \quad \vec{\nabla}\theta(r) = \theta'(r) \hat{r} \quad , \quad (3.37)$$

where polar coordinates ($x = r \cos \varphi$, $y = r \sin \varphi$) are used, \hat{r} and $\hat{\varphi}$ are unit vectors in the radial and azimuthal directions, respectively. Recalling that $\hat{\varphi} \times \hat{r} = \hat{z}$, for an infinite domain we have

$$\Gamma = \frac{S_c^3}{4\pi} \int_0^{2\pi} d\varphi \int_0^\infty r dr \left(\frac{q}{r} \sin \theta \theta'(r) \right) = \frac{q S_c^2}{2} \left[S_z(r \rightarrow \infty) - S_z(r = 0) \right] \quad (3.38)$$

and from (3.33), $S_z(r \rightarrow \infty) \rightarrow 0$, so we obtain $\Gamma = -\frac{1}{2} q S_c^2 S_z(r = 0)$. The sign of S_z at the center of the vortex is usually called ‘‘polarization’’ of the vortex, $p = S_z(r = 0)/S_c = \pm 1$, and it is usual to write

$$\Gamma = -\frac{1}{2} S_c^3 q p \quad . \quad (3.39)$$

Since Γ is conserved⁷ during the time evolution at zero damping, we might conclude that the polarization itself must be another conserved quantity. However, we observe that the result (3.39) depends strongly on the *shape* assumption (3.36), and will not hold in general under the time evolution. For example, when an IP field is present, it deforms the field (3.36) in all the plane, such that the gradient is not longer $\mathcal{O}(r^{-1})$ at infinity.

At zero field, it is correct to say that the time evolution of OP vortices in an infinite domain preserves p , and so it does not allow oscillations (nor switchings) of the z -component of the spin field at the center of the vortex, in this order of the continuum approach⁸. However, as shown by Nikiforov and Sonin [58], a vortex without any

⁷ in general for any configuration, see App. C. The vorticity q defined as the result of (3.20) is also a conserved quantity (App. C).

⁸ but it does allow changes of p , if we include derivatives of a higher order, as shown in [38].

driving force in an infinite medium is spontaneously pinned, and it does not move.

The situation changes when a time-dependent field is present, even at zero damping, as we will see later. Both quantities, vorticity q and polarization p , are to be taken into account for classifying the possible dynamics of OP vortices. The result (3.39) is related with the work of Thiele on the dynamics of vortices in stationary movement, which will be explained in the next Section.

All along this work we adopt the following convention: we refer to a “vortex” for $q = 1$ and “up” for $p = 1$, if not otherwise explicitly said.

3.2 Dynamics of OP vortices at zero field

Let us present first the basic facts of the phenomenology, as observed in numerical simulations. To fix ideas we take the discrete model Hamiltonian (2.12)-(2.13), where we choose exchange anisotropy only ($D = 0, \vec{h} = 0$). Typical settings are $J = S_c = 1$ and λ in the range $0.9 - 0.99$. We integrated numerically the evolution equations (2.34) in a Runge-Kutta scheme (see details of numerical procedures in Appendix D), with a damping constant ε in the range 0.002 to 0.01 , for a system with a circular border over a square lattice with lattice constant $a = 1$.

We start the simulations with a vortex ($q = 1$) configuration whose IP structure is given by (3.27), with or without the image (2nd term), and its OP structure (“up”, $p = 1$) is given by a trial function⁹ which fits very well the numerical solution of (3.32). We apply, before the integration in time, a static relaxation procedure, which adapts the mentioned functions to the discrete lattice, by turning the spins iteratively towards the direction of the effective field, without affecting the vortex position. The result of this procedure (see details in the Appendix D) is still a static distribution, a solution of the static sector of the discrete LL equations (2.34).

If we start the simulation with the vortex at the center of the system, at zero field, it will not move. For this special case, the image position lies at infinity, and, therefore, we initialize the IP field of the vortex (3.27) without the second term. The center of the system is a comfortable option as initial vortex position in simulations with magnetic fields, which push the vortex out of it, as will be discussed later.

In order to observe a movement at zero field, we launch the vortex from a position shifted out of the system center. Due to the interaction with its image, the vortex starts to move, and generates some spin waves, which in turn affect the movement of the vortex. This is seen in the **Fig. 3.3**, where we launched a vortex, *without* the

⁹ details of this function are given in [69, 39], but it is basically similar to the second branch of (3.34), for $r \rightarrow \infty$.

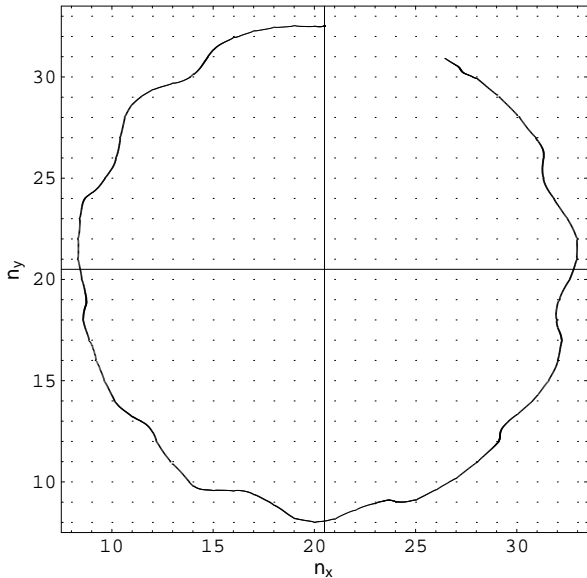


Fig. 3.3: Single vortex trajectory, initially *without* image vortex, at zero damping and zero field, up to $t = 2300$.

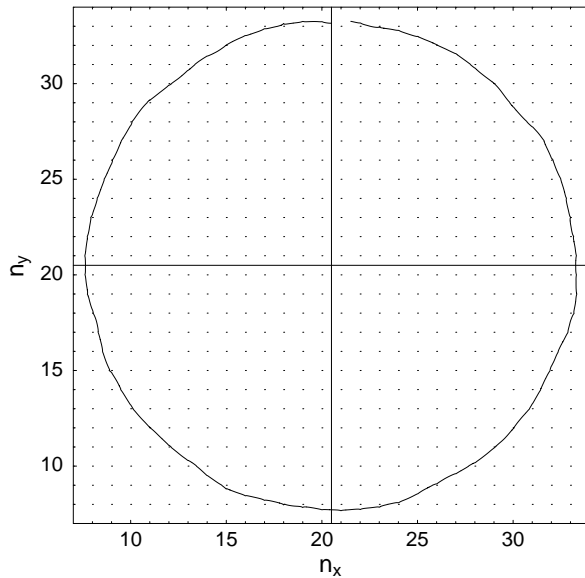


Fig. 3.4: Same as in **Fig. 3.3**, but initially *with* image vortex. Up to the same time, it covered a little more of the circle.

image term, from the position $\vec{X} = (20.5, 32.5)$ of a system of radius $L = 20$ (only the inner part of the system is shown, the center of the system is the point $(20.5, 20.5)$, the locations of the spins are indicated by points at integer values n_x, n_y).

The observed oscillations around the main (circular) trajectory have been subject of several papers [80, 57], and particularly in a recent work by Kovalev et al. [45], they have been explained in terms of the excess of energy (3.31) and the conservation of angular momentum. For our purposes we will discuss below only the main trajectories, and let aside the phenomenon of oscillations, and the related problem of eigenmodes of the system. On the other hand, these oscillations can be avoided in the simulations by including the image term in the initial condition, and a damping term in the dynamical equations during some time interval after the start.

In fact, we already get trajectories very close to a circle if we initialize the spin field including explicitly the image vortex, the 2nd term of (3.27), which is shown in the **Fig. 3.4**: for the same initial position as in **Fig. 3.3** we placed an image anti-vortex¹⁰ at $\vec{X}_I = (20.5, 53.83)$ and we see that the deviation from the circular trajectory is very small, though still not zero. This is due to the fact that even when we have provided a spin distribution more “appropriate” to the present BC, it is still a static one, and it generates waves as it starts to move.

If damping is present, the amplitude of the waves will decrease in time, but the trajectories will be spirals, as can be seen in the **Fig. 3.5**. One idea to get a *moving* vortex

¹⁰ we summarized in **Table D.1** the values of vorticity and polarization carried by image vortices.

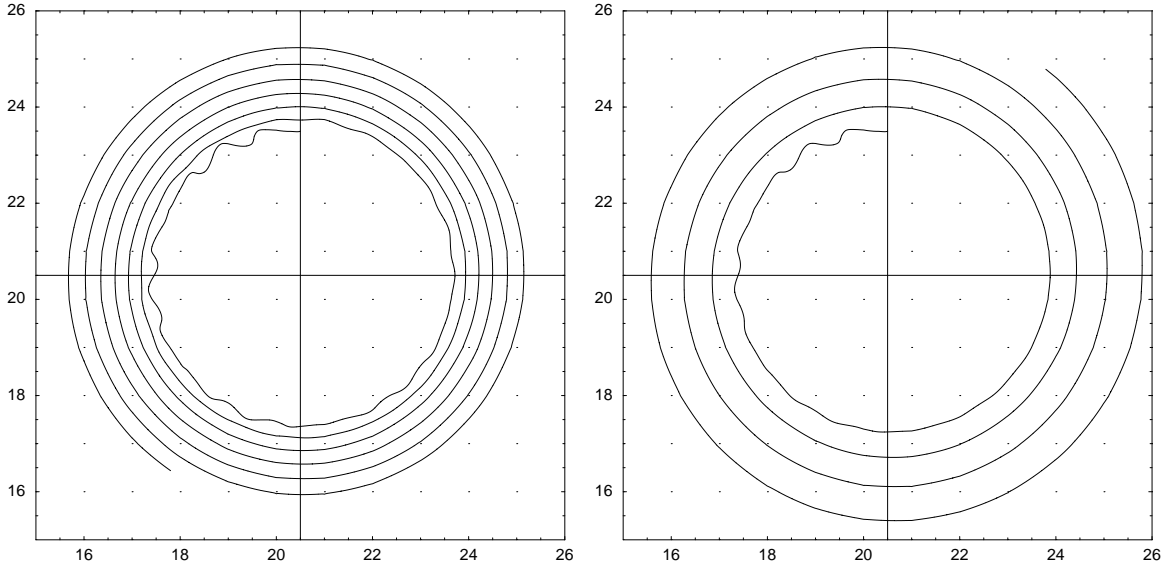


Fig. 3.5: Single vortex trajectories, initially *without* image vortex, at zero field, in a system of radius $L = 20$: At the left, with damping $\varepsilon = 0.005$, up to a time $t = 15200$. At the right, with damping $\varepsilon = 0.01$, up to the time $t = 9200$.

describing a fairly good circular trajectory (with spin waves of negligible amplitude), is to apply damping only *initially*, and switch it off after some time. Although damping is a material property (It cannot be switched off in real experiments), this is just a numerical trick to generate a “clean” moving initial condition. By letting different values of damping act during different times, one gets, after the switching-off, circular trajectories with different radii. Measuring then the frequency of the vortex rotation for each radius, allows to compare the results of the simulations with the theoretical predictions.

We will build in the following a theory for explaining the basic trajectories, by searching for an equation of motion of a collective property of the system, in the context of the continuum limit. In our case the center of the vortex $\vec{X} = (X, Y)$ can be taken as a pair of “collective variables” and the assumption of a stationary movement, which keeps the shape of the vortex fixed or rigid, has to be adopted, at least as an approximation. Early in the 70’s this approach appeared in the context of ferromagnets, in connection with the movement of domain walls, in a fundamental work by Thiele [75, 76]. In 1982 Huber applied this idea to the case of vortices in 2D systems [31, 32]. The use of collective variables for the case of vortices in 2D has a long history now [57, 80, 79, 86] and it was put into a formal context by Schnitzer [70, 69].

We remark that Thiele-like approaches always rely on some kind of travelling wave Ansatz, for an excitation which moves on a *continuous* medium. Therefore, they are expected to give better results for large lattices, and in the case of small anisotropies, where the size of the excitations is large compared with the lattice constant. Never-

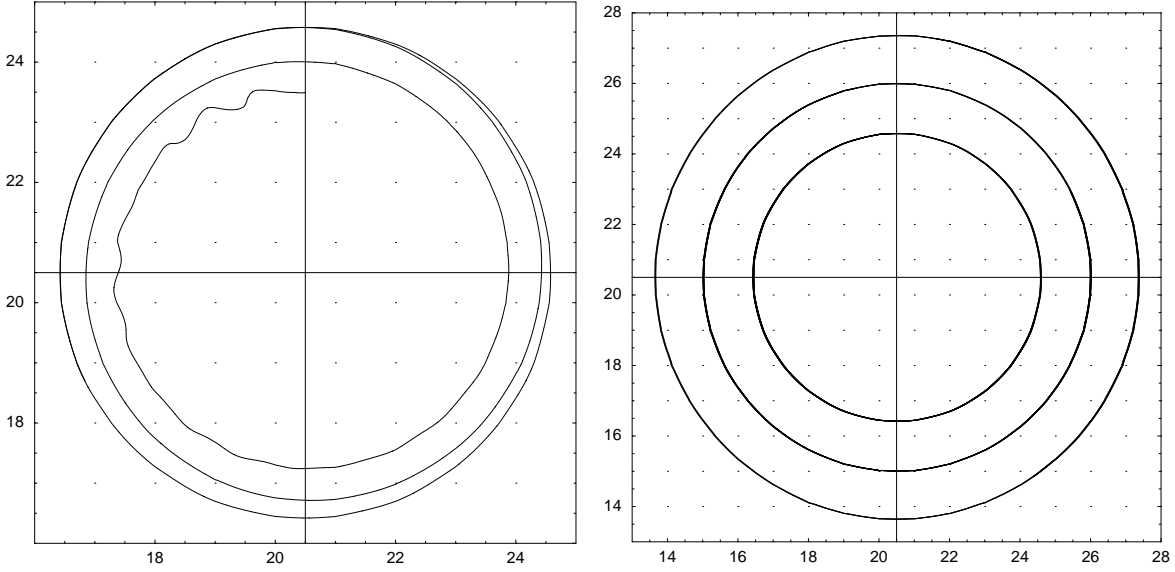


Fig. 3.6: (Left) Single vortex trajectory, like in **Fig. 3.5** (right), initially with damping $\varepsilon = 0.01$, which is switched off at time $t = 4800$, and continued without damping up to $t=7800$. (Right) Three circular trajectories obtained by this method.

theless, we will see that this kind of description works well even down to anisotropies of 10%, and on lattices with a lateral size of few tens of sites.

3.2.1 The Thiele equation

Let us suppose that the vortex is already in a stationary movement and its shape does not change in time, i.e., the vortex performs a rigid movement. Then it is reasonable to make a “travelling wave” Ansatz for the (continuous) spin field of the vortex, namely

$$\vec{S}(\vec{x}, t) \equiv \vec{S}(\vec{x} - \vec{X}(t)) ,$$

From this we can write

$$\vec{\nabla}_{\vec{x}} \equiv -\vec{\nabla}_{\vec{X}} \quad , \quad \frac{\partial \vec{S}}{\partial t} = \sum_{\beta} \frac{\partial \vec{S}}{\partial X_{\beta}} \frac{dX_{\beta}}{dt} \quad , \quad X_1 := X \quad , \quad X_2 := Y \quad . \quad (3.40)$$

To get an equation for the collective coordinates, we start from the Landau-Lifshitz equation with Gilbert damping, in the continuum form

$$\frac{\partial \vec{S}}{\partial t} + \frac{\varepsilon}{S_c} \vec{S} \times \frac{\partial \vec{S}}{\partial t} = -\vec{S} \times \frac{\delta H}{\delta \vec{S}} \quad , \quad (3.41)$$

and form the cross product of $\vec{S} \cdot \frac{\partial \vec{S}}{\partial X_\alpha}$ with it,

$$\vec{S} \cdot \left(\frac{\partial \vec{S}}{\partial X_\alpha} \times \dot{\vec{S}} \right) + \frac{\varepsilon}{S_c} \vec{S} \cdot \left(\frac{\partial \vec{S}}{\partial X_\alpha} \times \vec{S} \times \dot{\vec{S}} \right) = -\vec{S} \cdot \left(\frac{\partial \vec{S}}{\partial X_\alpha} \times \vec{S} \times \frac{\delta H}{\delta \vec{S}} \right) . \quad (3.42)$$

The second term is $\frac{\varepsilon}{S_c} \vec{S} \cdot \left[\vec{S} \left(\frac{\partial \vec{S}}{\partial X_\alpha} \cdot \dot{\vec{S}} \right) - \dot{\vec{S}} \left(\vec{S} \cdot \frac{\partial \vec{S}}{\partial X_\alpha} \right) \right]$ and recalling that $\vec{S} \cdot \dot{\vec{S}} = 0$, and $\vec{S} \cdot \vec{S} = S_c^2$, only the first term of it contributes. The same is valid for the r.h.s. of (3.42), recalling also¹¹ that $\vec{S} \cdot \frac{\partial \vec{S}}{\partial X_\alpha} = 0$. Inserting now our Ansatz (3.40),

$$\sum_\beta \vec{S} \cdot \left(\frac{\partial \vec{S}}{\partial X_\alpha} \times \frac{\partial \vec{S}}{\partial X_\beta} \right) \dot{X}_\beta + \varepsilon S_c \sum_\beta \left(\frac{\partial \vec{S}}{\partial X_\alpha} \cdot \frac{\partial \vec{S}}{\partial X_\beta} \right) \dot{X}_\beta = -S_c^2 \left(\frac{\partial \vec{S}}{\partial X_\alpha} \cdot \frac{\delta H}{\delta \vec{S}} \right) ,$$

and integrating over the domain, we finally obtain the Thiele equation,

$$(\hat{\mathbf{G}} + \hat{\mathbf{g}}) \dot{\vec{X}} = \vec{F} , \quad (3.43)$$

which contains: a so-called ‘‘gyromagnetic’’ tensor

$$G_{\alpha\beta} = \int d^2r \vec{S} \cdot \left(\frac{\partial \vec{S}}{\partial X_\alpha} \times \frac{\partial \vec{S}}{\partial X_\beta} \right) , \quad (3.44)$$

a ‘‘dissipation’’ tensor

$$g_{\alpha\beta} = \varepsilon S_c \int d^2r \frac{\partial \vec{S}}{\partial X_\alpha} \cdot \frac{\partial \vec{S}}{\partial X_\beta} , \quad (3.45)$$

and, on the r.h.s., an effective force acting on the vortex,

$$F_\alpha = -S_c^2 \int d^2r \frac{\partial H}{\partial X_\alpha} = -S_c^2 \frac{\partial \mathcal{U}(\vec{X})}{\partial X_\alpha} . \quad (3.46)$$

Here $\mathcal{U}(\vec{X})$ is the total energy (Hamiltonian) in terms of the collective variables \vec{X} . Note that the gyromagnetic tensor (3.44) is essentially our previous definition of the topological charge (3.17), times 4π . Therefore, it is a conserved quantity at zero damping¹², and we see that it is antisymmetric, its components (calculated in Eq.(3.39)), are given by

$$G_{\alpha\beta} = G \epsilon_{\alpha\beta} \quad , \quad G = 2\pi p q \quad , \quad (\text{for } S_c = 1) \quad , \quad (3.47)$$

where $\epsilon_{\alpha\beta}$ is the 2D antisymmetric tensor.

¹¹ In the discrete case we have problems precisely with this statement, see the Appendix B.

¹² And of course within the continuum limit, but not in the discrete case.

The quantity G can be thought as the modulus of a vector $\vec{G} := G \hat{z}$, called ‘‘gyrovector’’, in terms of which the (3.43) is written as

$$\vec{G} \times \dot{\vec{X}} + \hat{\mathbf{g}} \dot{\vec{X}} = \vec{F} \quad , \quad (3.48)$$

which shows that the first term is analogous to the Lorentz force on a charged particle, where \vec{G} plays the role of a (self-induced) magnetic induction. Thus, as soon as an OP vortex ($G \neq 0$) gains speed it appears this force which is perpendicular to the direction of movement. For an IP vortex ($G = 0$) this force is absent.

For the damping term, however, we observe that the trace of the tensor (3.45) is proportional to the exchange energy (with $J = 1$), which is a constant of motion only if the exchange is the only term present in the Hamiltonian (the total energy). Therefore, the elements of g_{ij} can not be considered in general as constants. Nevertheless, we will take as a reasonable approximation the often used [76, 31, 39] results¹³,

$$g_{\alpha\beta} = g \delta_{\alpha\beta} \quad , \quad g = \pi \varepsilon \left(\ln L + C(\lambda) \right) \quad , \quad (3.49)$$

where $\delta_{\alpha\beta}$ is the 2D unit matrix, L is the radius of the system, and the constant $C(\lambda)$ is the contribution from the OP structure in the innermost region of the vortex. The latter depends only on the anisotropy, and in any case $C(\lambda) \ll \ln L$.

As forces on the r.h.s. of (3.43) we can include the Coulomb-like force \vec{F}_I exerted by the image vortex in a finite domain (see next Section), and, later on (Chap. 5), we will be interested in the force \vec{F}_h exerted on the vortex by a magnetic field $\vec{h}(t)$.

3.2.2 Force exerted by the image vortex

The first of the forces mentioned above, exerted on a vortex with charge q at the position \vec{X} , by its image vortex with charge q_I at the position $\vec{X}_I = (L^2/R^2) \vec{X}$ (in a circular system), providing that they are not too close to each other, $|\vec{X} - \vec{X}_I| \gg r_v$, is (usually) derived from the well known expression for the interaction energy

$$E_I(|\vec{X}|) = -2\pi q q_I \log \left| \frac{\vec{X} - \vec{X}_I}{a_c} \right| = -2\pi q q_I \log \left(\frac{L^2 - R^2}{R} \right) + \text{const.} \quad , \quad (3.50)$$

where $R = |\vec{X}| = \sqrt{X^2 + Y^2}$ is the distance from the vortex center to the center of the system, and a_c is a small cut-off of the order of r_v which gives a constant contribution.

¹³ I have found no reason why the non-diagonal elements of (3.45) should vanish, as often quoted, but in our simulations we have measured all the elements of the tensor (3.45), and it turns out that its diagonal terms are negligible compared with the corresponding contribution of $G_{\alpha\beta}$, which is much larger for not very large systems. The diagonal elements (3.49), instead, scale as $\ln L$, as calculated in [76, 31], in good agreement with our simulations results.

By taking the gradient in cartesian components we get the force

$$\vec{F}_I(\vec{X}) = -\vec{\nabla}_{\vec{X}} E_I(|\vec{X}|) = 2\pi q q_I \frac{(\vec{X} - \vec{X}_I)}{|\vec{X} - \vec{X}_I|^2} = -\frac{2\pi q q_I}{L^2 - R^2} \vec{X}, \quad (3.51)$$

For free boundary conditions (BC) we have $q q_I = -1$ and the force is attractive, while for Dirichlet BC, $q q_I = 1$ and the force is repulsive. This force gives an essentially nonlinear character to the equation (3.43). However, the problem is completely solvable when only this force is present, as we will see in the following.

Discussion

It is to be observed that (minus) the gradient of the first expression in (3.50), in cartesian components, $-\vec{\nabla}_{\vec{X}} E_I(|\vec{X}|)$, gives the right result (by “right result” I mean: the one which agrees with the results of simulations), while if we take the gradient of the second expression in (3.50), in polar coordinates ($X = R \cos \Phi$, $Y = R \sin \Phi$), observing that the energy does not depend on the angle Φ , we would get

$$-\frac{d}{dR} E_I(R) = \frac{d}{dR} \left[2\pi q q_I \log \left(\frac{L^2 - R^2}{R} \right) \right] = -2\pi q q_I \frac{L^2 + R^2}{R(L^2 - R^2)}, \quad (3.52)$$

which is clearly not the radial component of the force, since from (3.51),

$$\vec{F}_I = -2\pi q q_I \frac{R}{L^2 - R^2} \hat{R} \quad (3.53)$$

is the right result. The energy (3.50) is actually not the correct interaction energy inside the *finite* domain. The usual error consists in a naive inserting of X_I in the formula (3.50) which has been used since Kosterlitz and Thouless [44] in the 70’s used it for an *infinite* domain. It is clear also that the formula refers to IP vortices, but this is not important here, since the OP structure gives a small contribution which does not depend on the coordinates of the vortex nor on the size of the system, but just on the anisotropy. On the other hand, if we calculate more carefully the total energy

$$E_{0-I} = \int d^2x \{ (\vec{\nabla}\Phi_0)^2 + (\vec{\nabla}\Phi_I)^2 + \vec{\nabla}\Phi_0 \cdot \vec{\nabla}\Phi_I \} \quad (3.54)$$

between the IP vortex (say, for simplicity, at $X = (R, 0)$, since the energy does not depend on Φ),

$$\Phi_0 = q \arctan \frac{y}{(x - R)} \quad (3.55)$$

and its image

$$\Phi_I = q_I \arctan \frac{y}{(x - L^2/R)} \quad (3.56)$$

inside a *finite*, circular domain, we know (see App. A.4) that the result is (Eq. 3.30)

$$E_{0-I} = -\pi q q_I \log\left(\frac{L^2 - R^2}{Lr_v}\right) \quad (3.57)$$

and it turns out that

$$-\frac{d}{dR} E_{0-I} = -2\pi q q_I \frac{R}{L^2 - R^2} \quad (3.58)$$

is again the correct result.

3.2.3 The Thiele equations in polar coordinates at zero field

The Thiele equations (3.43)

$$g \dot{X} + G \dot{Y} + \frac{\partial \mathcal{U}}{\partial X} = 0 \quad (3.59a)$$

$$-G \dot{X} + g \dot{Y} + \frac{\partial \mathcal{U}}{\partial Y} = 0 \quad (3.59b)$$

can be put into polar coordinates of the vortex, by using

$$\begin{aligned} X = R \cos \Phi & \quad , \quad \dot{X} = \frac{X}{R} \dot{R} - Y \dot{\Phi} \quad , \quad \frac{\partial \mathcal{U}}{\partial X} = \frac{X}{R} \frac{\partial \mathcal{U}}{\partial R} - \frac{Y}{R^2} \frac{\partial \mathcal{U}}{\partial \Phi} \\ Y = R \sin \Phi & \quad , \quad \dot{Y} = \frac{Y}{R} \dot{R} + X \dot{\Phi} \quad , \quad \frac{\partial \mathcal{U}}{\partial Y} = \frac{Y}{R} \frac{\partial \mathcal{U}}{\partial R} + \frac{X}{R^2} \frac{\partial \mathcal{U}}{\partial \Phi} \end{aligned} \quad (3.60)$$

Then multiplying both eqs. (3.59a)-(3.59b) by R , and carrying out the operations:

(3.59a) $\times X$ + (3.59b) $\times Y$, and (3.59a) $\times Y$ - (3.59b) $\times X$, we get

$$g \dot{R} + G R \dot{\Phi} + \frac{\partial \mathcal{U}}{\partial R} = 0 \quad (3.61a)$$

$$-G \dot{R} + g R \dot{\Phi} + \frac{1}{R} \frac{\partial \mathcal{U}}{\partial \Phi} = 0 \quad (3.61b)$$

There is a particular case which represents a wide class of interesting situations, namely when the total energy is independent of the angle Φ . This is the case, for instance, for the interaction (3.50) or (3.57) between a vortex and its image. In general, from (3.61b) we have

$$\frac{\partial \mathcal{U}}{\partial \Phi} = 0 \quad \implies \quad \dot{\Phi} = \frac{G}{g} \frac{\dot{R}}{R} = \frac{G}{g} \frac{d \log R}{dt} \quad , \quad (3.62)$$

which gives

$$\Phi(t) = \Phi(t_0) + \frac{G}{g} \log \frac{R(t)}{R_0} \quad , \quad R_0 = R(t_0) \quad (3.63)$$

and for $R(t)$, after inserting (3.62) into (3.61a), we have the equation

$$g \dot{R} + \frac{G^2}{g} \dot{R} + \frac{d\mathcal{U}}{dR} \equiv \beta \dot{R} + \frac{d\mathcal{U}}{dR} = 0 \quad , \quad \beta = \frac{g^2 + G^2}{g} \quad (3.64)$$

which can be integrated in some particular cases. For example, with the force (3.51), using the relations (3.60) –or directly from (3.58)–,

$$-\frac{d\mathcal{U}}{dR} = -\frac{R}{X} \frac{\partial E_I(|\vec{X}|)}{\partial X} = -\frac{R}{Y} \frac{\partial E_I(|\vec{X}|)}{\partial Y} = -2\pi q q_I \frac{R}{L^2 - R^2} \quad (3.65)$$

we have

$$\dot{R} = -\frac{1}{\beta} \frac{d\mathcal{U}}{dR} = -\frac{2\pi q q_I}{\beta} \frac{R}{L^2 - R^2} \geq 0 \quad \text{for } q q_I = \mp 1 \quad , \quad (3.66)$$

$$\dot{\Phi} = \frac{G}{g} \frac{\dot{R}}{R} = -\frac{2\pi q q_I G}{g^2 + G^2} \frac{1}{L^2 - R^2} \geq 0 \quad \text{for } q q_I G \leq 0 \quad , \quad (3.67)$$

where $0 < R < L$. The solution of eq. (3.66), again with $R(t_0) = R_0$, gives an implicit relation,

$$L^2 \log R(t) - \frac{R(t)^2}{2} = L^2 \log R_0 - \frac{R_0^2}{2} - \frac{2\pi q q_I}{\beta} (t - t_0) \quad , \quad (3.68)$$

which together with (3.63) solves completely the problem. From the solution (3.68), we see that $R(t)$ is increasing with time for free BC ($q q_I = -1$), and decreasing for Dirichlet BC ($q q_I = 1$). From (3.63) we see that the vortex moves along a spiral parameterized by $R > 0$, counter-clockwise for $G > 0$ and clockwise for $G < 0$.

In fact, we easily calculate the accelerations \ddot{R} and $\ddot{\Phi}$ by derivating (3.66) and (3.67) again with respect to time, and we get definite sign expressions:

$$\ddot{R} = -\frac{2\pi q q_I}{\beta} \frac{(L^2 + R^2) \dot{R}}{(L^2 - R^2)^2} = \left(\frac{2\pi}{\beta}\right)^2 \frac{(L^2 + R^2) R}{(L^2 - R^2)^3} > 0 \quad , \quad (3.69)$$

$$\ddot{\Phi} = -\frac{4\pi q q_I G}{g^2 + G^2} \frac{R \dot{R}}{(L^2 - R^2)^2} = \frac{8\pi^2 G g}{(g^2 + G^2)^2} \frac{R^2}{(L^2 - R^2)^3} \geq 0 \quad , \quad \text{for } G \geq 0 \quad (3.70)$$

All these expressions show that, for free BC ($q q_I = -1$) the vortex covers a divergent (outwards) spiral, the sense of the movement is counter-clockwise if $G = 2\pi p q > 0$ and clockwise if $G < 0$, and the speed on the spiral is increasing towards the boundary. If the vortex starts at $R_0 = 0$, we see that $\dot{R}(t)|_{t_0} = \ddot{R}(t)|_{t_0} = 0$, and it does not move. For Dirichlet BC ($q q_I = +1$) the vortex covers a convergent (inwards) spiral ($\dot{R} < 0$), clockwise if $G > 0$ and counter-clockwise if $G < 0$, accelerating towards the center of the lattice.

Furthermore, for zero damping ($g = 0$), eqs. (3.61) give trivially a circular trajectory

($\dot{R} = 0$, $R(t) \equiv R_0$) with the frequency

$$\Omega_0 = -\frac{2\pi q q_I}{G} \frac{1}{L^2 - R_0^2} \quad (3.71)$$

whose sign depends again on the sign of the product $q q_I G$.

3.2.4 Results of simulations at zero field

The predictions of the Thiele equation of the previous section, at zero field, are in excellent agreement with the results of simulations. Let us see some examples. The trajectories are predicted to be a circle at zero damping and a spiral when the damping is not zero. As explained at the beginning of Sec. 3.2, in the simulations we have “prepared” circular trajectories by applying damping initially, so that all spin waves, appearing as consequence of a “non-perfect” *static* initial condition, are damped out. In **Figs. 3.5** and **3.6** we show some examples, for an up-vortex $q = p = 1$ under free BC. For our purposes, it was sufficient to take a small system of radius $L = 20$. The **Table 3.1** shows the frequencies measured and predicted for the 3 circular trajectories shown in the right panel of **Fig. 3.6**. The agreement with the formula (3.71) is excellent.

$\langle R \rangle$	Ω (fit)	Ω_0 , eq. (3.71)
4.07890	0.002659	0.002608
5.49234	0.002752	0.002704
6.84918	0.002885	0.002832

Table 3.1: Radius and frequency of rotation measured in simulations (corresponding to the right panel of **Fig. 3.6** with $L = 20$), and the prediction of Eq. (3.71).

We now analyze some spiral trajectories when damping is present. In the **Fig. 3.7** we plot the measured angle of rotation Φ (in radians) as a function of the logarithm of the measured radius $R(t)$, for four values of the damping, launching every time the vortex from the same place ($R_0 = 3, \Phi(0) = \pi/2$). We observe here the linear relation predicted by eq. (3.63). The **Table 3.2** resumes some results of fitting the function

$$\Phi = A + B \log R \quad (3.72)$$

to the simulation data, for different damping values ε and the same system size $L = 20$. The equation (3.63) gives then the relation between the coefficients A and B of (3.72), the damping matrix element g , and the initial values $R_0 = 3.0$ and $\Phi(0) = \pi/2$,

$$B = \frac{2}{\varepsilon(\log L + C(\lambda))} \quad , \quad A = \Phi(0) - B \log R_0 \quad . \quad (3.73)$$

The last 2 columns in **Table 3.2** are calculated from (3.73), by using the values of B from the 2nd column in the table.

Table 3.2: Simulation data and predictions of eq. (3.63)-(3.73), at fixed $L = 20$ and $\lambda = 0.92$, for different damping values ε .

ε	A (fit)	B (fit)	$C(\lambda)$	A , eq. (3.73)
0.0025	-182.9952	167.1566	1.7902	-182.0693
0.0050	-90.9581	83.7432	1.7808	-90.4303
0.0075	-60.2715	55.9318	1.7720	-59.8764
0.0100	-44.9992	42.0714	1.7581	-44.6491

The eq. (3.68) is also confirmed in these simulations, as can be seen in the **Table 3.3**, where we show the results of fitting the function

$$L^2 \log R(t) - \frac{R(t)^2}{2} := f(t) = k_1 + k_2 t \quad , \quad (3.74)$$

where, following eq. (3.68), $k_1 = L^2 \log R_0 - \frac{R_0^2}{2} - k_2 t_0$. This relation, with $L = 20$, $R_0 = 3.0$ and $t_0 = 0$, gives $k_1 = 434.945$, which is very close to the values in the 1st column of the table (within 0.5%). The l.h.s. of (3.74) is taken from the measured values of R for each time.

ε	k_1 (fit)	k_2 (fit)	$B/(1+B^2)$
0.0025	437.294	0.00606	0.00598
0.0050	437.025	0.01221	0.01194
0.0075	437.760	0.01820	0.01787
0.0100	437.811	0.02427	0.02376

Table 3.3: Simulation data and predictions of eq. (3.68), at fixed size $L = 20$ and anisotropy $\lambda = 0.92$, for different damping values ε .

We also have calculated, in the last column of **Table 3.3**, $k_2 = \frac{2\pi}{\beta} = \frac{B}{1+B^2}$, where B is taken from **Table 3.2**, and we can observe a very good agreement.

In **Table 3.4**, instead, we fix the damping to $\varepsilon = 0.01$ and repeat the simulation for different sizes L . From the table we calculate $2/(\varepsilon B)$ for each B , which should be equal to $\log L + C(\lambda)$, for each L . We then fit to those values the function $k_3 + k_4 \log L$, which gives $k_3 = 1.481$ ($\approx C(\lambda)$) and $k_4 = 1.07$, values that are very close to the expected results.

All these simulation results show that at zero field the Thiele approach describes fairly

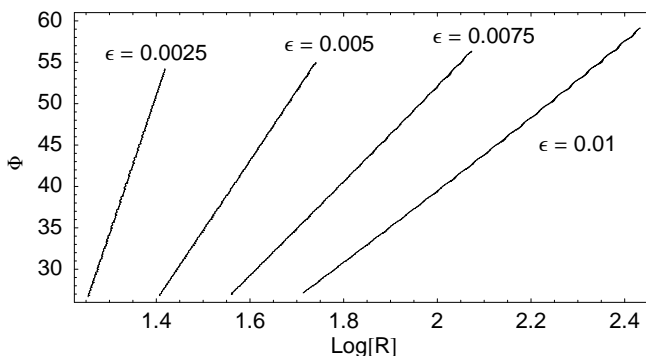


Fig. 3.7: Azimuthal angle Φ of the vortex center *vs.* logarithm of the distance $R(t)$ to the system center, for different values of damping ε . All the vortices launched from $\vec{X} = (20.5, 23.5)$ on a lattice of radius $L = 20$ with anisotropy $\lambda = 0.92$.

Table 3.4: Simulation data and predictions of eq. (3.63), at fixed $\varepsilon = 0.01$ and anisotropy $\lambda = 0.92$, for different system sizes L .

L	A (fit)	B (fit)	$C(\lambda)$	A (pred.)
24	-55.6489	40.9669	1.7039	-55.2212
30	-61.3229	38.9064	1.7393	-61.0465
36	-65.6230	37.4155	1.7618	-65.4686
42	-69.2574	36.3259	1.7680	-69.1160
48	-72.0515	35.3579	1.7852	-71.9539
54	-74.7075	34.6721	1.7793	-74.6114
60	-77.0753	34.1182	1.7676	-76.9891

well the dynamics of the OP vortex, even for the small system radius and relatively high anisotropy of the examples shown here.

3.3 Dynamics of vortices with static fields

The reaction of vortices to applied fields, the main topic of this work, gives rise to a very rich phenomenology. This response depends in general on the kind of vortex, whether it is an IP or an OP one, and on the direction and intensity of the applied field. It is a topic with many open questions, which attracts the interest of theoreticians and experimentalists as well, due to the possibility of applying fields as control variables in the experiments. Some recent experiments [72, 65, 14, 12, 68] deal already with the control of vortex states in small magnetic dots by means of applied magnetic fields. (for recent reviews see also Refs. [33, 29]). The dynamical problems in this context are also relevant to techniques of high-density magnetic recording [63]. We will try to give in the following a brief picture of the wide phenomenology of vortices in presence of static fields, and leave for the next Chapters the case of a time-dependent field.

3.3.1 In-plane field

IP vortices

If we look for *static* and *planar* solutions ($\dot{\phi} = 0$ and $\dot{m} = m = 0$) of eqs. (3.13), then eq. (3.13a) requires $b_{\perp} = 0$ (*i.e.* there are no static planar solutions when a perpendicular field is applied), and eq. (3.13b) becomes a static sine-Gordon equation

$$\Delta\phi = \frac{b_{\parallel}}{a^2} \sin(\phi - \beta_0) \quad (3.75)$$

which is probably the most studied equation of nonlinear physics. It has been shown to admit vortex solutions by Hudák [34], but with the vorticity $Q = \pm 4$, a case which is not very relevant to dynamics, since vortices with $Q = \pm 4$ are seen in the simulations to decay rapidly to several vortices with $Q = \pm 1$, which are then at least in simulations

observed to be stable. Eq. (3.75) was also studied in connection with IP vortices of the XY-model ($D = 0, \lambda = 0$) by Gouvêa et al. [23, 24].

It was found in [23] by numerical simulations that the main effect of the IP applied field, while forcing the spins to align towards its direction, is to deform the vortex shape, so that a region where the spin distribution is homogeneous (and pointing in the direction of the field) grows, pushing the vortex into the other region towards the border of the system. In other words, the system with an IP static field wants to be homogeneous and, for a field strong enough, it manages to expel out the inhomogeneities.

The trajectories observed in the simulations are in general a quite irregular “drift” movement, determined by several factors. First, there are two driving forces: the force exerted by the image vortex (or the effect of the boundary) and the (effective) force exerted by the applied field.

Secondly, the vortex suffers accelerations and decelerations in the background of the potential produced by the discrete lattice. It is known that IP vortices are much more sensitive to the discreteness than OP vortices. Discreteness is the first factor which breaks the rotational symmetry in the XY plane (in the 2D case, it defines two “cristallographic” special directions). Thus, the trajectory towards the border will be a straight line only in a case of extreme symmetry¹⁴. Eventually, the effect of discreteness may be so strong that the vortex can get pinned in a fixed position during the course of its trajectory.

The direction of the movement is, theoretically, affected by the relative phases of the vortex and the applied field. We note that the constant β_0 is easily removed from the equation (3.75) by rotating the XY plane such that $\phi \rightarrow \phi' = \phi - \beta_0$, but in any case the final solution will contain this constant, which corresponds to the fact that the applied IP field additionally breaks the rotational symmetry in the XY plane, in the discrete as well as in the continuum system. Since the applied IP field (4.5) couples directly to the ϕ field, with the interaction density

$$-\vec{S}(x, y) \cdot \vec{h} = -h S_c \cos(\phi - \beta_0) \quad , \quad (m = 0) \quad , \quad (3.76)$$

the initial phase of the vortex φ_0 (providing that the form (3.36) is used as initial condition), will contribute to determine the initial direction of the vortex trajectory. In the simulations, however, strong effects of discreteness turn the trajectory to be practically unpredictable after few time steps (see below).

¹⁴ Providing, for instance, that the vortex is initially at the center of the lattice, a “valley” of the Peierls-Nabarro potential, and the field is applied either in \hat{x} or in \hat{y} direction, the vortex moves perpendicularly to the field, always between two lines of spins. If the initial position is shifted from the center of the system, the trajectory is more complicated.

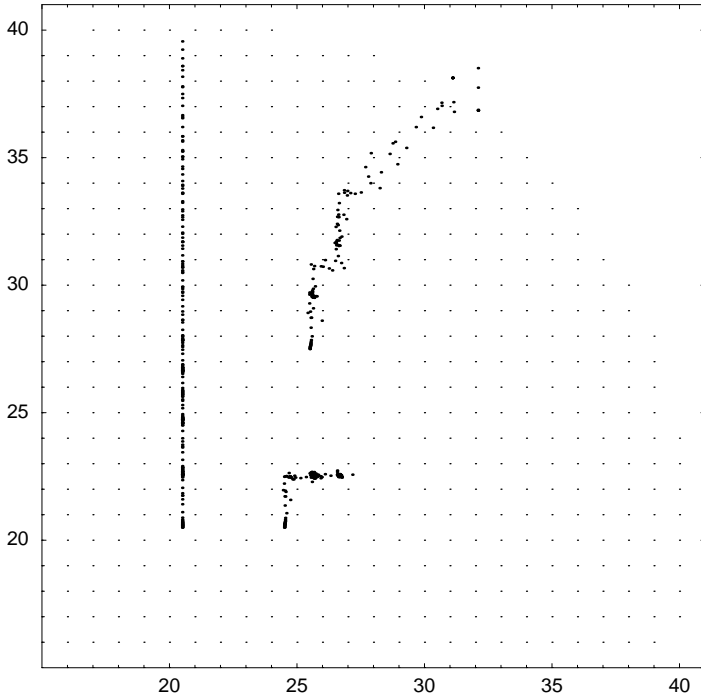


Fig. 3.8: Trajectories of an IP vortex under the action of a static field in \hat{x} direction, $h_x = 0.007$, starting from 3 different points, in a system of radius $L = 20$ with anisotropy $\lambda = 0$. The vortex launched from $\vec{X} = (20.5, 20.5)$ (the center of the system) approaches the border vertically, the vortex starting at $\vec{X} = (20.5, 24.5)$ gets pinned at $\vec{X} \approx (27.2, 22.5)$, and the vortex starting at $\vec{X} = (25.5, 27.5)$, gets to the border on a very irregular path. The grid of points represents the spin sites, only a section of the circular system is shown.

The numerical work in [23] was carried out on square systems. We have confirmed this scenario for circular systems in our simulations, and next we illustrate it with some examples.

The **Fig. 3.8** shows some trajectories in a small system of radius $L = 20$, obtained with an applied field $\vec{h} = h_x \hat{x}$, with intensity $h_x = 0.007$. For this field intensity, the discreteness can cause the pinning of the vortex in some point of the lattice, an effect which depends on the initial conditions (IC): for the same value of the magnetic field, some IC result in trajectories which end up in a pinned state, and some other IC result in trajectories which get up to the border.

The method for determining the position of the vortex center (more details in Appendix D) relies on fitting the form (3.36) for the four innermost spins, after having found in which plaquette of 4 spins in the lattice the circulation (the integral (3.20) in discrete version) is non-zero. This is clearly just an approximation, for the innermost plaquette in the vortex, in the case that this is deformed by the applied field. In any case, it is enough to show us the main tendency of the movement. In order to complete the picture, in the **Fig. 3.9** we depict the spin field for two points of the trajectory of **Fig. 3.8** which starts at $\vec{X} = (25.5, 27.5)$ and goes to the boundary, at the instants $t = 0$ (left) and $t = 40$ (right), where we can see that an increasing portion of the lattice is turning into an almost homogeneous state pointing in the direction of the magnetic field. The final state looks like the bottom part of the figure at the right panel, when the vortex has left the system.

If we want to get some information about this dynamics from the Thiele eq. (3.43), the

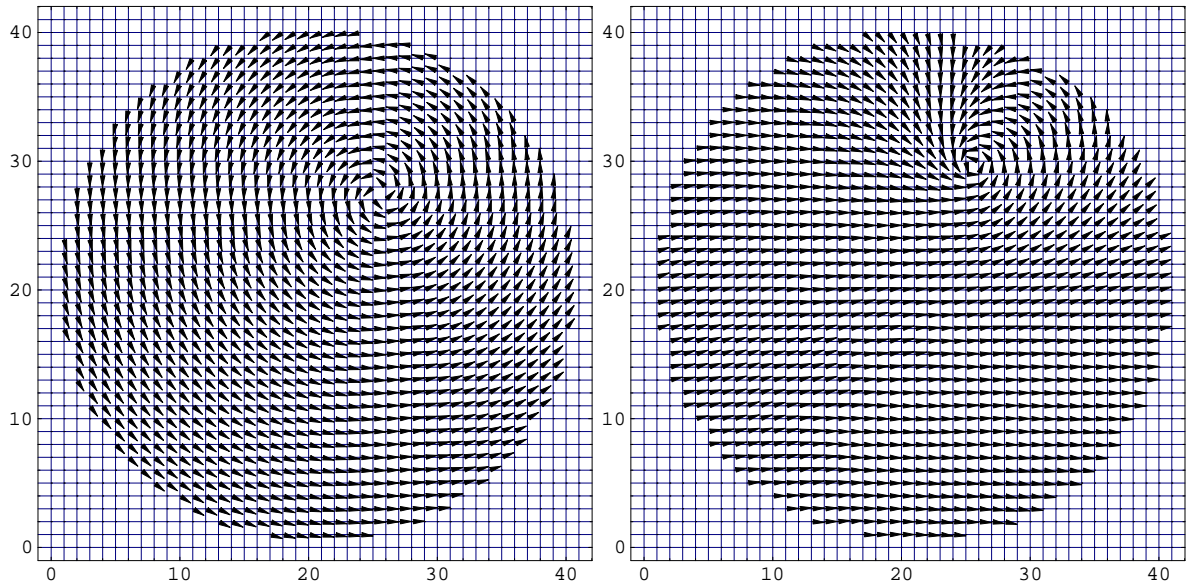


Fig. 3.9: Two snapshots of the IP field, corresponding to the trajectory of **Fig. 3.8** which starts at $\vec{X} = (25.5, 27.5)$, taken at times $t = 0$ (left) and $t = 40$. (right).

first thing we should do is to try to estimate from eq. (3.46) the effective force made by the applied field, which for the magnetic interaction density (3.76), can be written as:

$$\vec{F}_h = S_c^2 \int d^2r \left[\vec{\nabla}\theta \frac{\partial}{\partial\theta} + \vec{\nabla}\phi \frac{\partial}{\partial\phi} \right] \left(-h \sin\theta \cos(\phi - \beta_0) \right), \quad (3.77)$$

where, for IP vortices, $\sin\theta = 1$, and the first term vanishes. Already Huber in 1982 saw the trouble to do so in the fact that, unfortunately, we do not know the mathematical expression for the spin distribution ϕ of the **Fig. 3.9**. In the words of Huber [32],

“The response to in-plane applied fields is less certain. If the vortex moves without distortion (which is probably a reasonable approximation only at very low fields, *if at all*) then the corresponding static force takes the form [... of eq. (3.77) ...]”.

Here I have emphasized “*if at all*”, because the integral in eq. (3.77), and the Thiele equation itself, assume already a stationary movement. Therefore, we restrict us here to show just the basic facts of the phenomenology as seen in the simulations.

OP vortices

Naturally, in the case of OP vortices in the circular system, in addition to this applied field, there is always the action of the gyrotropic force and the force exerted by the image vortex. But, in contrast, the OP vortex, in a range of anisotropies of 0.9–0.99, is

much less sensitive to the discreteness, and therefore the trajectories are much smoother than those of the IP vortex. The resultant of the magnetic force caused by the applied field, the gyrotropic force, and the force of the image vortex, gives a complex drift movement for strong enough fields, but a “damping dominated” spiral-like movement for weak fields. The damping can cause a large difference in the movement of the vortex.

To illustrate this effect, we show some simulation results for an OP vortex in presence of an IP field applied in \hat{x} direction. The rest of parameters are chosen to be $L = 20$, $\lambda = 0.95$ and $\varepsilon = 0.005$.

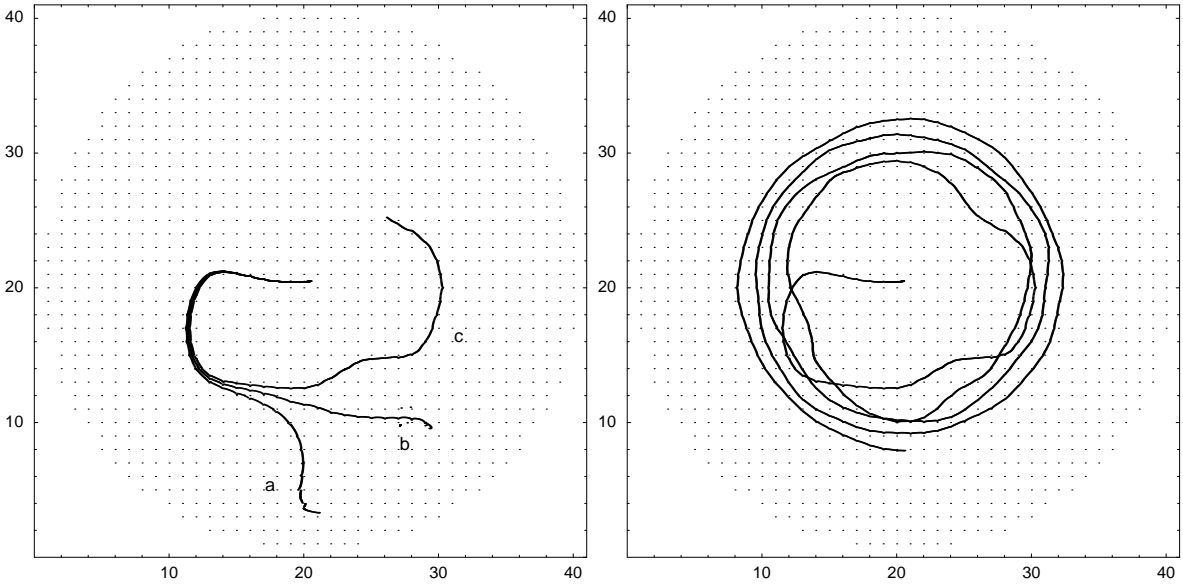


Fig. 3.10: Trajectories of an OP vortex, starting from the center of the system, (Left Panel) corresponding to three values of an applied field (a) $h_x = 0.0055$, (b) $h_x = 0.0054$ and (c) $h_x = 0.0053$. (Right Panel) The trajectory (c) up to time $t = 3490$. Other parameters are: $L = 20$, $\lambda = 0.95$, $\varepsilon = 0.005$.

We see in **Fig. 3.10** that for slightly different intensities of the field, we have the vortex approaching the border in different ways. For $h_x = 0.0053$ the trajectory develops into the spiral typical for the damping-dominated regime, but for $h_x = 0.0054$ and larger intensities, the drift towards the border is more direct. This picture is changed in absence of the damping. Damping provides a way to decrease the energy, which otherwise is constant, also in presence of the static field. At zero damping, the extra energy left in the system when the vortex abandons it, is transferred continuously into spin waves, which are thus more pronounced than in the case with damping.

3.3.2 Perpendicular field

The same equation (3.75) is obtained, also searching for *planar* solutions ($m = 0$), when we allow the precession of the spin field as a whole around the \hat{z} direction, *i.e.* we can allow a non-zero OP component of the magnetic field $b_{\perp} \neq 0$ if we simultaneously remove the *static* character of the azimuthal angle ($\dot{\phi} = 0$). In this case still $\dot{m} = m = 0$ while, from (3.13a), $\dot{\phi} = Ja^2 b_{\perp}$, which shows that the precession frequency is fixed by the perpendicular field b_{\perp} . Thus, this IP vortex can rotate as a rigid body, with an angular speed which depends on b_{\perp} . However, we will see next that applying a perpendicular magnetic field has the effect of shifting up or down the z -components of all the spins, giving rise to the so-called “cone state” [36, 38], where all the spins (and not only those of the vortex core) are tilted in an angle outside the XY plane (see **Fig. 3.11**) and, thus, a solution with $m = 0$ is not realized in this case. The extent of this deviation from the XY plane depends on the relative values of the anisotropy and the applied field, and it turns out that, for this effect to be observable, the applied field must be rather strong (in the following $h_z \approx 0.05$, compare with the IP field of the last Section, and with the time-dependent fields to be used in the next Chapters, with intensities $h \approx 10^{-3}$).

IP vortices

For an IP vortex, we observed in simulations that if the applied OP field is weak compared with the (effective) anisotropy field, whose intensity in our case is defined as $h_a = 4JS_c(1 - \lambda)$, see Ref. [36, 38], then nothing relevant happens: an IP vortex at rest at the center of the system stays in-plane. We can consider this as the solution at vanishing field. We have checked this fact, for $\lambda \approx 0$ (close to XY-model) and an applied field of $h_z = \pm 0.05$.

In contrast, if the anisotropy decreases to, say, $\lambda \approx 0.5$ (still in the region where, at zero field, the IP vortex is stable), the application of the above mentioned field gives rise to an interesting effect: the IP vortex develops an OP structure, consisting of a small¹⁵ vortex core, in the background of the cone state.

In **Fig. 3.11** and **Fig. 3.12** we show the effects of an applied perpendicular field of intensity $h_z = \pm 0.05$ on the structure of an IP vortex, which stays at rest at the center of the system of radius is $L = 20$, and the anisotropy is $\lambda = 0.55$ ($J = S_c = 1$). The field is applied (“turned on”) at $t = 0$, to the planar vortex structure, which was previously relaxed at zero field. We then integrate in time the LL eqs. (2.34), and all the spins relax again, in presence of the field and the damping, in around thousand

¹⁵ *small* in height (deepness), compared with height (deepness) of the OP vortex core (see next subsection).

time units (with a typical damping $\varepsilon = 0.005$), to a new equilibrium position, which does no longer change. It is interesting to note the formation of the small core, in the background of the cone state, and pointing in the same direction as the field.

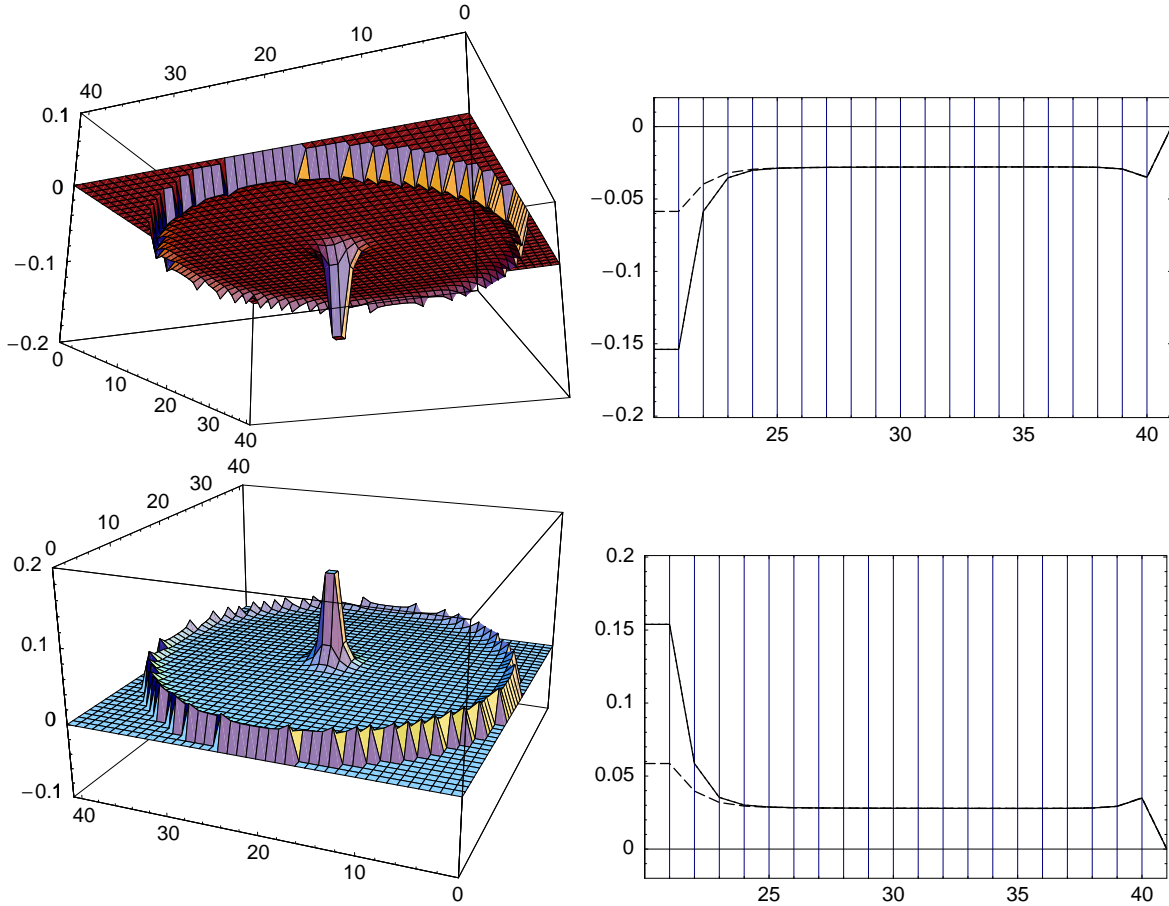


Fig. 3.11: S_z components of the spins of an initially IP vortex state, in presence of an applied field (above) $h_z = -0.05$, and (below) $h_z = +0.05$, at time $t = 5000$. At the right, two cross sections passing through the vortex core in the \hat{x} -direction are shown.

The time evolution of S_z and ϕ of some individual spins is shown in **Fig. 3.12**. The signals recorded correspond to spins lying on a line from the center of the vortex (and of the system) to the periphery, every two sites: concretely, at the sites $(n_x, n_y) = (21, 21)$, $(23, 21)$ and $(25, 21)$ –recall that the center of the system is at $(20.5, 20.5)$. The formation of the core is observed at the left panels, where S_z of the central innermost spin (solid line) separates more from the signals of the other spins. It is clearly seen from the right panels that, as the field is applied, the vortex starts to rotate rigidly around the \hat{z} -axis until it gets a new equilibrium angle (saturation of the signals), except that the central spin (solid line), in the just-formed core of the vortex, ends up in a slightly different angle, showing a different response to the field. It is as if the vortex suffered a torsion around the \hat{z} direction, to reach the new equilibrium state

while it develops the small core. Note that this effect is not symmetric with respect to the direction of the field, because in both cases the vortex had the same initial angular distribution, but opposite directions of the field make the spins rotate in opposite sense.

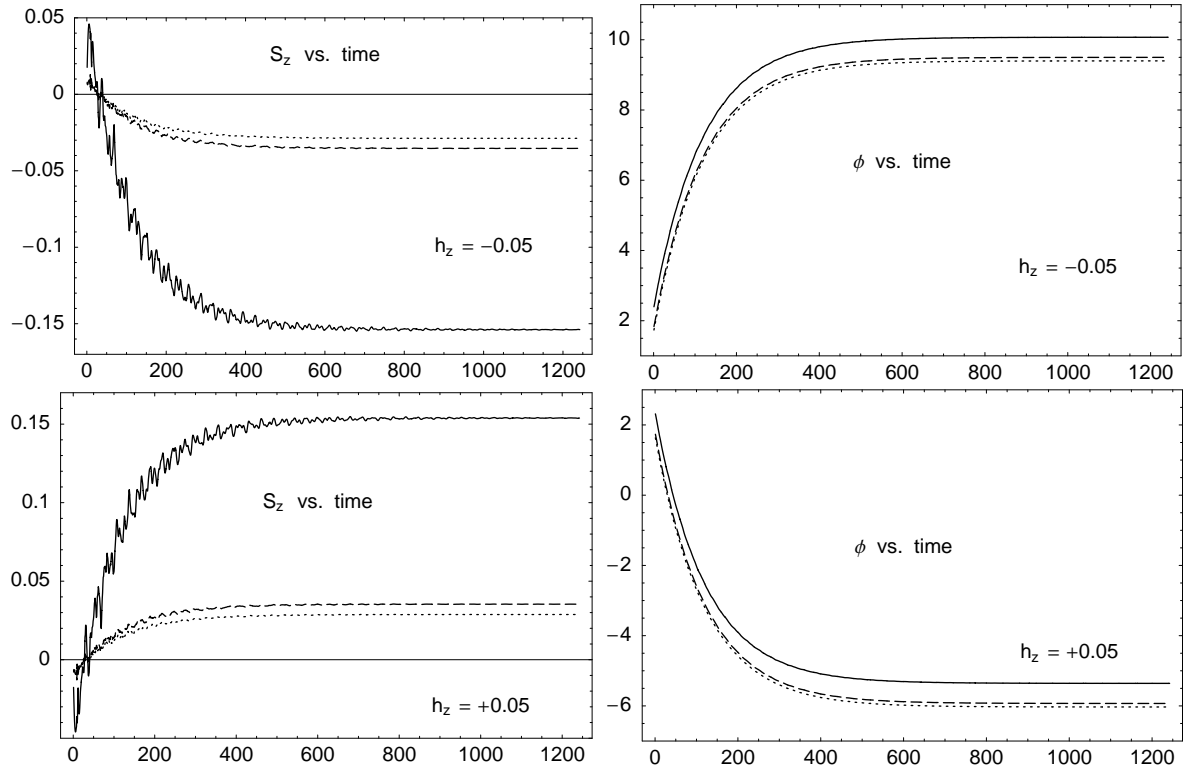


Fig. 3.12: Time evolution of S_z component (Left) and ϕ angle (Right) of some individual spins of an initially IP vortex state, in presence of an applied field (Above) $h_z = -0.05$, and (Below) $h_z = +0.05$, under a damping $\varepsilon = 0.005$, in a system with $L = 20.5a$ and $\lambda = 0.55$. The signals correspond to spins lying on a system radius, from the center of the vortex (solid line) towards the border (dashed and dotted lines), along the \hat{x} axis.

Zero-damping case

We note that none of these relaxation effects is observed at zero damping. In this case there is no mechanism to change the total energy, and the energy of the magnetic perturbation transfers itself into spin waves and a regular rotation of all the spins. The signals of S_z stay oscillating with small amplitude and always the same sign. As expected, the signals of ϕ are in a linear relation with time, with *the same slope* (i.e., frequency) for *all* the spins. In other words, the vortex at zero damping rotates around \hat{z} as a rigid whole, with a frequency which depends on the anisotropy and the intensity of the OP field (see **Fig. 3.13**). This frequency is clearly proportional to the applied field, but the dependence on λ is less clear. Particularly, there is a small difference between “up” or “down” vortices concerning this frequency, above the critical zone

where OP vortices (see next subsection) are stable for strong fields. This effect can be seen in the **Fig. 3.14**, for two values of the anisotropy λ .

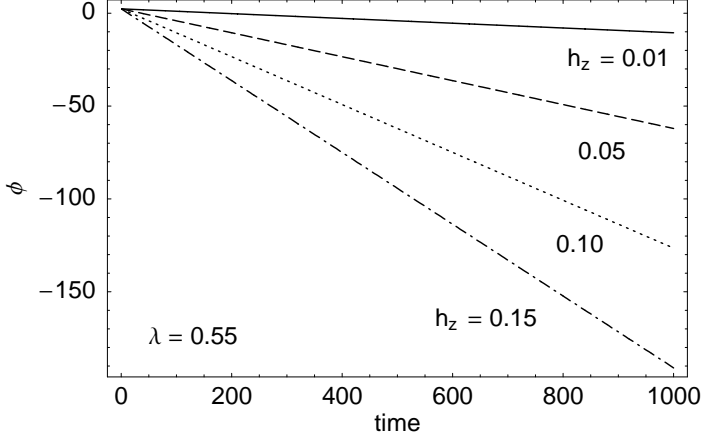
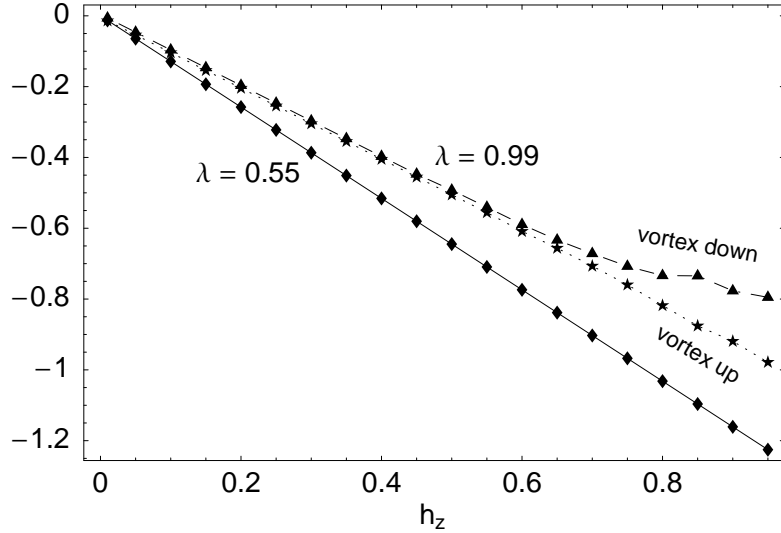


Fig. 3.13: Time evolution of the azimuthal angle ϕ of the spins, at zero damping, for various applied perpendicular fields h_z . The frequency is the same for all the spins in the system (here only the signal ϕ of the innermost spin is shown).

Fig. 3.14: The frequency of rotation of the spins, in the XY plane, is the same for all of them, and increases linearly with the applied field h_z , for not too small anisotropy and not too strong fields.



OP vortices

An OP vortex can still exist in the presence of an applied perpendicular field, as was shown by Ivanov et al. in [36, 38], in the background of a cone state, provided that the applied field is not too strong to turn the spins parallel to the \hat{z} axis. In those papers the authors classify the OP vortices according to the relative orientation of the polarization and the magnetic field: vortices whose gyrovector is parallel to the magnetic field are called “light” vortices, while those with antiparallel gyrovector are called “heavy” vortices.

In [38] the authors studied the spectrum of linear excitations in the presence of the vortex, and the change of the vortex shape, both as a function of the applied field h_z . They fix the polarization “up” and try both signs of h_z . It was shown that the field

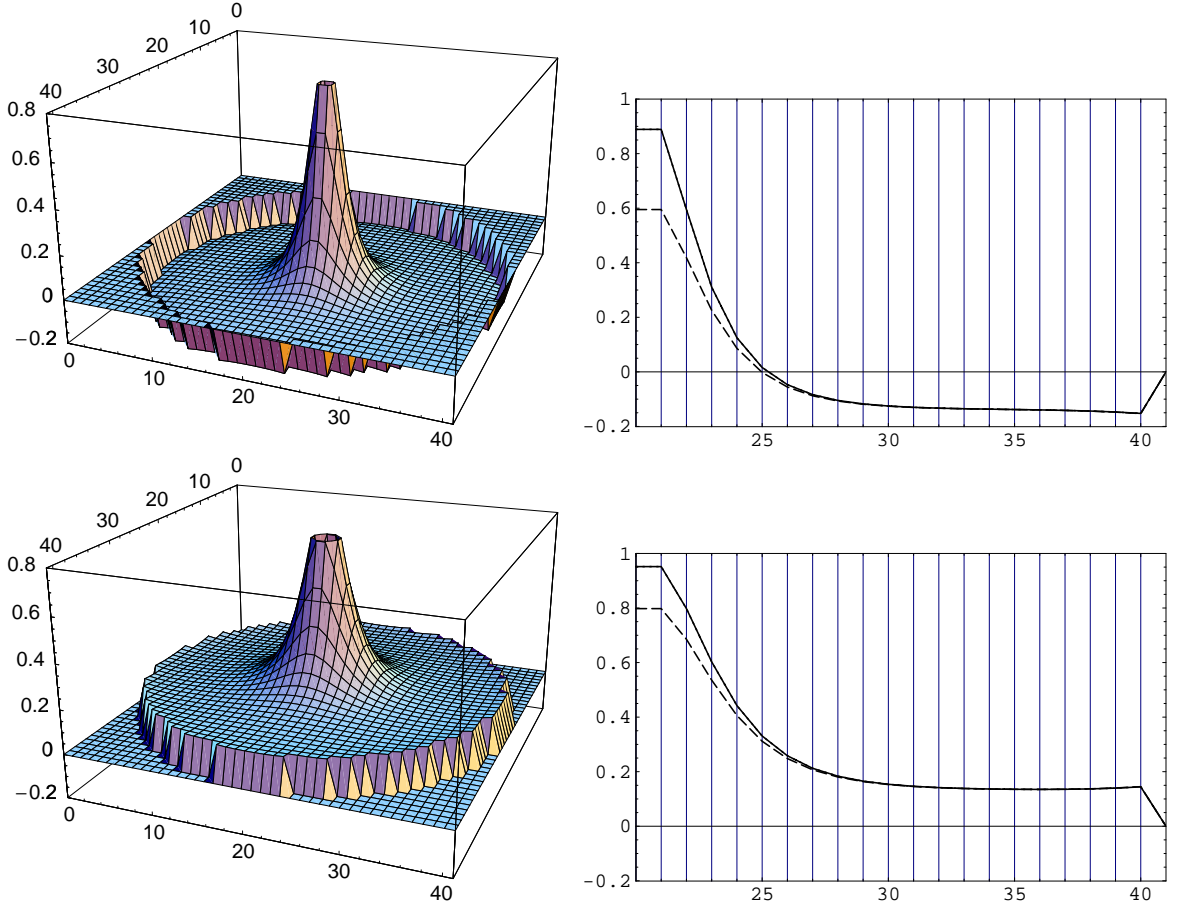


Fig. 3.15: S_z components of the spins of an OP vortex state, in presence of an applied field $h_z = -0.05$ (above), and $h_z = +0.05$ (below), after 840 time units under a damping $\varepsilon = 0.005$, in a system with $L = 20$ and $\lambda = 0.95$. The lattice sites lie at integer numbers.

increases the size of the vortex core for light vortices, while decreases this size for heavy vortices. Light vortices are stable for field intensities which fulfill $0 < h_z < h_a$, while if $h_z > h_a$ the vortex becomes a uniform state pointing towards \hat{z} . In contrast, for $h_z < 0$ there exists a critical field $h_c < 0$ which determines the stability of heavy vortices, such that for $h_c < h_z < 0$ the heavy vortex is stable, for $-h_a < h_z < h_c$ the heavy vortex converts to a light vortex (in our language, it flips or switches the polarization) and finally for $h_z < -h_a$ the vortex becomes again a uniform state but pointing towards $-\hat{z}$. The radius of the vortex was estimated to change with the field intensity following

$$r_v(h) = \frac{a}{2} \sqrt{\frac{(1-\lambda)h^2 + \lambda}{(1-\lambda)(1-h^2)}} \approx \frac{r_v}{\sqrt{1-h^2}}, \quad (3.78)$$

where $h = h_z/h_a$ and $r_v = r_v(h = 0)$ is given by (3.35). The asymptotic behavior of S_z and its value at the border of the system change also due to the field, since the vortex

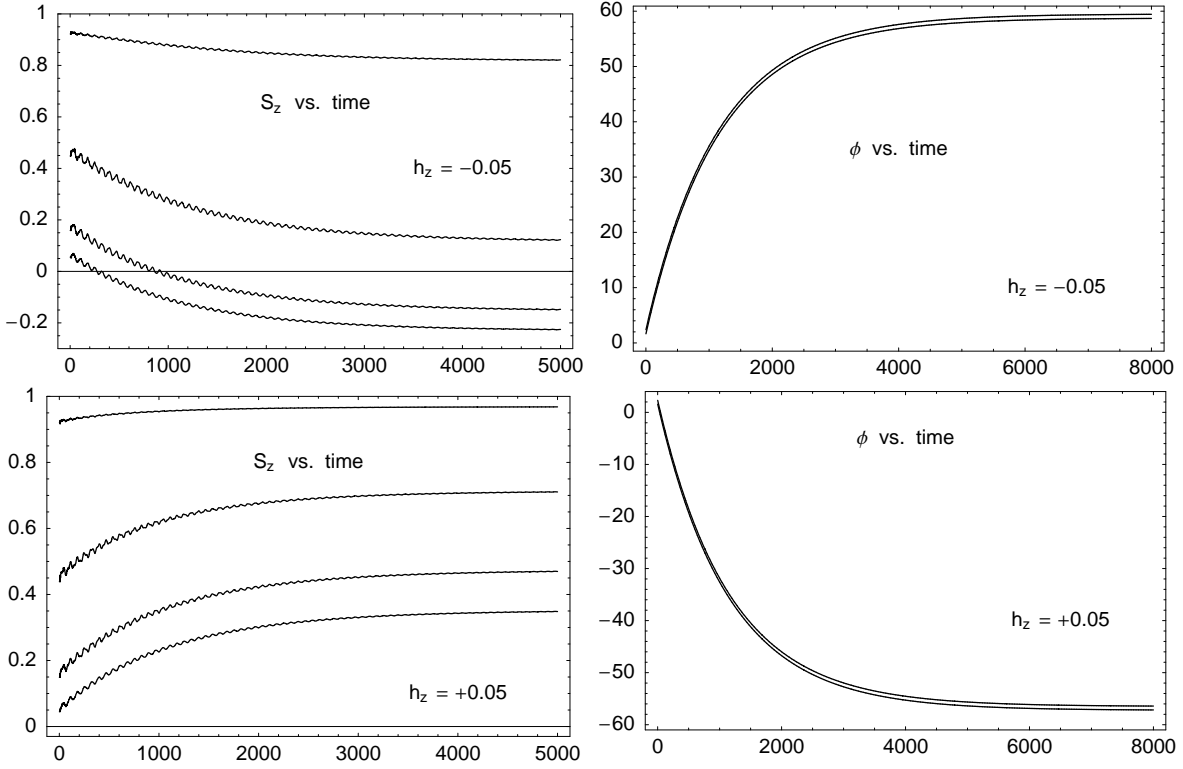


Fig. 3.16: Time evolution of S_z component (Left) and ϕ angle (Right) of some individual spins of an OP vortex state, in presence of an applied field (Above) $h_z = -0.05$, and (Below) $h_z = +0.05$, under a damping $\varepsilon = 0.005$, in a system with $L = 20$ and $\lambda = 0.95$. The lines from up to down correspond to spins lying on a system radius, from the center of the vortex towards the border, along the \hat{x} axis.

is superposed to a cone state, *i.e.* the ground state fulfills now

$$\cos \theta(r) \rightarrow h \quad \text{for } r \rightarrow L \quad . \quad (3.79)$$

It is also mentioned in [38] that the asymptotic behavior follows now a power law, instead of the exponential decay (3.34). At the origin the behavior of $\cos \theta(r)$ is still like the first branch of (3.34), but with a constant b which depends strongly on the field intensity h . Far from the vortex core, the OP structure follows the power law $\cos \theta(r) \approx h + h/x^2$, with $x = r/r_v$, for both light and heavy vortices, at the values $x \gg \max\{1, h/\sqrt{1-h^2}\}$.

We now discuss some other aspects, based on results of our simulations. In **Fig. 3.15** and **Fig. 3.16** we show the effects of an applied perpendicular field over the structure of an OP vortex, which stays at rest at the center of the system. Like in the case of the IP vortex, the field is turned on at $t = 0$. Starting from the initial OP vortex configuration, which was previously relaxed at zero field, we integrate the LL equations **Fig. 2.34** in presence of the field and the damping. Again, in some thousand time units

(with a typical damping $\varepsilon = 0.005$), a new equilibrium configuration is reached, which does no longer change. The torsion of the IP angular distribution as seen in the right panels of **Fig. 3.16** is less pronounced than in the IP vortex case (compare **Fig. 3.12**). Also, the vortex has rotated as a whole around \hat{z} at much higher speed, giving much more turns than in the IP vortex case, before the new static configuration is reached. We want to discuss also a dynamical effect which was not covered in the work of Ref. [38], namely a shift in the orbit frequency of an OP vortex in circular stationary motion, due to the action of the OP applied field. As described in Sections 3.2.3 and 3.2.4, at zero field the orbit frequency Ω_0 is given by (3.71). Here there is very good agreement between the theory and the simulations. A natural question is how the OP field modifies this result.

The same kind of Thiele approach should still be reasonably valid, since the OP field does not destroy the circular symmetry of the vortex, but affects essentially the z-components of the spins.

It is easy to check that the modulus of the gyrovectector is changed in the same proportion as the S_z components at the border of the system, *i.e.*

$$\text{since } \cos\theta(r) \rightarrow h \text{ then } G = 2\pi q(p - h) \text{ , } h = h_z/h_a \text{ .} \quad (3.80)$$

Motivated by these remarks I have started to perform simulations where I choose as initial condition a vortex at some position shifted from the center of the lattice, and I apply at $t = 0$ perpendicular fields with different intensities h_z , together with the damping. While the vortex describes a spiral outwards, the system relax to the configurations which are consistent with the field h_z . Once the vortex reaches a desired orbit radius, I switch off the damping, and the vortex remains in a stationary circular motion in the background of the cone-state.

Here I will briefly comment a preliminary result. I have observed that the the presence of the OP field does not destroy the shape of the vortex trajectories at zero field, but indeed a shift in the velocities occurs, which for weak fields is consistent with the change (3.80). On the circular orbit, the heavy vortex is observed to be slower, and the light vortex faster, than the vortex at zero field.

By the time of writing this Thesis the work on this area is still in progress, to answer the question whether, in addition to the change (3.80), an effective force appears also on the r.h.s. of the Thiele equation, due to the action of the OP field in the finite system¹⁶, which would then contribute to the shift of the orbit frequencies with respect to the frequency Ω_0 without the field.

¹⁶ It is clear that the OP field will not exert any effective force on the vortex in an infinite system.

Chapter 4

Vortices and time-dependent fields

1: out-of-plane dynamics

In the last Chapter, we have reviewed the basic results about dynamics of vortices in the 2D Heisenberg model with anisotropy, and investigated the effects of including static fields. In this and the next Chapter, we turn to the dynamical response of an OP vortex to a time dependent applied field. The purpose of this Chapter is to investigate the process of switching of the polarization of a vortex, *i.e.* the sudden change of sign of the z-components of the spins, particularly –but not exclusively– in the region of the vortex core, as a result of application of a circularly polarized AC magnetic field, a homogeneous field which rotates in the XY plane. Specifically, we apply a time-dependent field in the form

$$\vec{h}(t) = h \left(\cos(\omega t + \beta_0), \sin(\omega t + \beta_0), 0 \right), \quad (4.1)$$

where h is the amplitude, ω the frequency and β_0 an initial phase, usually set to zero. Given the OP vortex structure pointing in one of the $\pm\hat{z}$ directions, this phenomenon occurs mainly for a definite sense of the rotation of the field, *i.e.* for one sign of the frequency and not for the other¹. This means that for one sense of rotation, the field exerts a definite force over the spins in the \hat{z} direction, which is reversed for the opposite sense of rotation. This is very similar to the case of a static OP field, and actually this “pressure” down or up on the spins can also be observed for the spins in the lattice without the vortex. However, in the present case, also a movement of the vortex is caused by the IP rotating field. As a result of this movement, as we will see, the switching is favored. The process starts from the center of the vortex and propagates outwards in all radial directions. Some preliminary results about the effects of the field

¹Provided the anisotropy is not close to the critical value λ_c , as will be seen later.

(4.1) on the switching-dynamics of OP vortices were given in the Ref. [18], and some of the new results described in this Chapter were published in [87]. In this Chapter we will concentrate on some aspects of the switching phenomenon in the presence of the rotating field (4.1), and we will leave for the next Chapter the study of the movement of the vortex in the XY plane caused by this field.

A note on the order of magnitude of the field parameters

For typical quasi-2D ferromagnetic materials with easy-plane symmetry (for instance the layered magnet K_2CuF_4 , which was mentioned at the end of Sec. 2.1.1, with an exchange interaction $J \approx 10$ K and anisotropies ranging from 1 to 10 % ($\lambda \approx 0.99$ to 0.9 resp.), at low temperature ($T_c \approx 6.25$ K), the anisotropy field, given by $\gamma H_a = 4JS_c(1 - \lambda)$, is in the range $H_a \approx 3$ to 30 kOe [30, 38]. Corresponding resonances are in the range $\omega_a \equiv \gamma H_a \approx 50$ to 500 GHz, resp. The intensities of the field (4.1) that we use in the simulations of Sec. 4.2 are in the order $h \approx 10^{-3}J$, which for the above value of J represent a field intensity $H \approx 74.4$ Oe $\ll H_a$. For an estimation of the frequencies, we restore the value of \hbar . Our dimensionless time variable has then a scaling factor $\omega_0 = J/\hbar \approx 1.3$ THz, so the typical frequencies in our simulations are in the range $\omega \approx 10^{-3}\omega_0$ to $10^{-2}\omega_0 \approx 1$ GHz to 10 GHz $\ll \omega_a$, in most of our simulations ($\lambda = 0.9$).

4.1 Basic effects of the rotating field

In the continuum approach, the total energy density including the field (4.1) is

$$\mathcal{E}_T = \frac{JS_c^2}{2} \left\{ \frac{(\vec{\nabla}m)^2}{1-m^2} + (1-m^2)(\vec{\nabla}\phi)^2 + \frac{K}{a^2}m^2 + \delta m\Delta m \right\} - \frac{hS_c\sqrt{1-m^2}}{a^2} \cos(\phi - \omega t - \beta_0) \quad (4.2)$$

and the Landau-Lifshitz equations (3.13) in completely normalized form result

$$\begin{aligned} \frac{\partial\phi}{\partial\tau} &= -\frac{m(\vec{\nabla}'m)^2}{(1-m^2)^2} + m[1 - (\vec{\nabla}'\phi)^2] - \frac{\Delta'm}{1-m^2} + \frac{bm\cos(\phi - \nu\tau - \beta_0)}{\sqrt{1-m^2}} + \frac{\varepsilon}{(1-m^2)}\frac{\partial m}{\partial\tau}, \\ \frac{\partial m}{\partial\tau} &= \vec{\nabla}'[(1-m^2)\vec{\nabla}'\phi] - b\sqrt{1-m^2}\sin(\phi - \nu\tau - \beta_0) - \varepsilon(1-m^2)\frac{\partial\phi}{\partial\tau}, \end{aligned} \quad (4.3)$$

where $\tau = JS_cKt \equiv \omega_0 t$ is a dimensionless time, all the gradients are taken with respect to a dimensionless coordinate $\vec{x}' = \sqrt{K}\vec{x}/a = \vec{x}/l_0$, and $\vec{b} \equiv \hbar/(JS_cK) = \hbar/\omega_0$ and $\nu = \omega/\omega_0$ are the renormalized field intensity and frequency, resp. A term $\delta\Delta'm$, coming from the 4th term of (4.2), which gives a small contribution for $\delta = 1 - \lambda \ll 1$, was neglected in the first of eqs. (4.3). In the following we omit the prime over the

gradients. Note that we have renormalized the space and time variables, at the level of the differential equations, using only l_0 and ω_0 , respectively. We can also express these equations in the rotating frame (in the spin space) by changing the dependent variable ϕ to

$$\psi \equiv \phi - \omega t = \phi - \nu \tau \quad , \quad (4.4)$$

and in this frame we have

$$\begin{aligned} \frac{\partial \psi}{\partial \tau} &= -\frac{m(\vec{\nabla} m)^2}{(1-m^2)^2} + m[1 - (\vec{\nabla} \psi)^2] - \frac{\Delta m}{1-m^2} + \frac{b m \cos(\psi - \beta_0)}{\sqrt{1-m^2}} + \frac{\varepsilon}{(1-m^2)} \frac{\partial m}{\partial \tau} - \nu \\ \frac{\partial m}{\partial \tau} &= \vec{\nabla}[(1-m^2)\vec{\nabla} \psi] - b\sqrt{1-m^2} \sin(\psi - \beta_0) - \varepsilon(1-m^2) \frac{\partial \psi}{\partial \tau} - \varepsilon(1-m^2)\nu \end{aligned}$$

At zero damping, these equations are exactly the same as the equations which one obtains for the case of an applied *static* field with both IP and OP components given by

$$\vec{b}_{\text{stat}} = (b \cos \beta_0, b \sin \beta_0, \nu). \quad (4.5)$$

However, in the case of non-zero but small damping the above equivalence is only approximate, since in the 2nd of these equations we observe an additional term, which contains the damping and is present even in the static sector of them,

$$0 = -\frac{m(\vec{\nabla} m)^2}{(1-m^2)^2} + m[1 - (\vec{\nabla} \psi)^2] - \frac{\Delta m}{1-m^2} + \frac{b m \cos(\psi - \beta_0)}{\sqrt{1-m^2}} - \nu \quad , \quad (4.6a)$$

$$0 = \vec{\nabla}[(1-m^2)\vec{\nabla} \psi] - b\sqrt{1-m^2} \sin(\psi - \beta_0) - \varepsilon \nu (1-m^2) \quad . \quad (4.6b)$$

We could try to solve numerically the static eqs. (4.6), for the shape of the vortex. Here, the term containing $\varepsilon \nu$ gives definitely a very small contribution, but the presence of the IP applied field b prevents us to insert the usual Ansatz for the IP spin distribution of a vortex, $\psi = q \varphi$, into (4.6b), and so we do not have easy access to an ODE for $m(r)$. We observe in the simulations that the vortex shape is *rigid* only when a circular limit-cycle is reached (Chap. 5), and is *static* only in a frame which rotates synchronically with the vortex at a frequency Ω . To change to this frame, the *coordinates* of the *real* space must be transformed, such that the origin is translated to $(X(t), Y(t))$ and the axes are rotating with frequency Ω . In other words, for this circular trajectory of a vortex, the spin distribution is a rigid, the OP structure of the vortex rotating as a whole around the center of the system with the orbit frequency Ω .

4.1.1 The uniformly rotating ground state

Without magnetic field the ground state of the system is a uniform state in which all the spins are lying in the XY plane, with $m_0 = 0$ and $\phi = \varphi_0 = \text{const}$. The field

λ	ν	b	m_0 (data)	m_0 (eq. 4.7)
0.90	0.0750	0.0150	0.073883	0.073890
0.92	0.0937	0.0187	0.092042	0.092019
0.94	0.1250	0.0250	0.121931	0.121933
0.96	0.1875	0.0375	0.180819	0.180622
0.98	0.3750	0.0750	0.348752	0.347258
0.99	0.7500	0.1500	0.629995	0.628793

Table 4.1: Simulation data and predictions of eq. (4.7), for the uniform state (initially pointing towards \hat{x}) in a system with $L = 24$, after relaxation under damping $\varepsilon = 0.01$, and a rotating field (4.1) with $\omega = 0.03$ and $h = 0.006$. In the last line, the initial state was chosen out of the XY plane for a better convergence.

changes essentially the picture: if we pass to the rotating frame (4.4), there appears an effective static field along the hard axes, which leads to the cone state with nonzero z -magnetization. Inserting into eqs. (4.6a)-(4.6b) the Ansatz $m = m_0 = \text{const}$ and $\psi = \psi_0 = \text{const}$, we find that the equilibrium values m_0 and ψ_0 must satisfy the equations

$$(\nu - m_0)^2 + (\varepsilon \nu m_0)^2 = \frac{(b m_0)^2}{1 - m_0^2}, \quad (4.7)$$

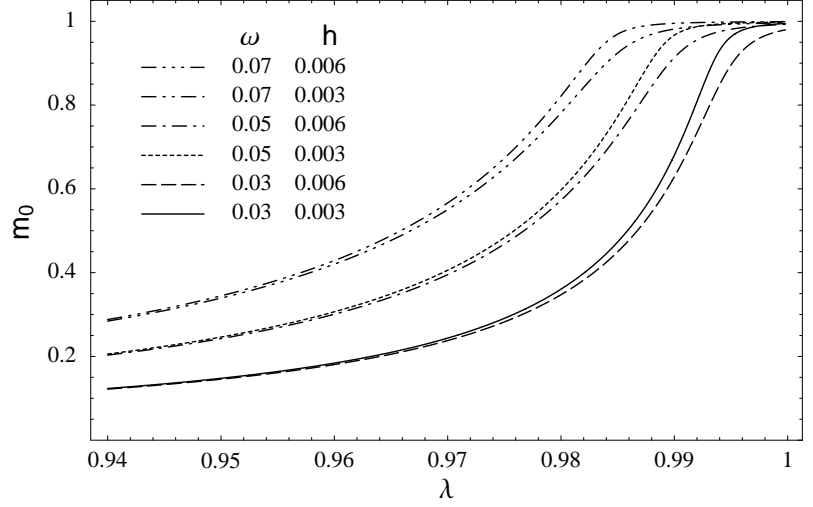
$$\tan(\psi_0 - \beta_0) = -\frac{\varepsilon \nu m_0}{\nu - m_0}. \quad (4.8)$$

We note that ψ_0 does not enter in the equation for m_0 , but ψ_0 depends on the value of m_0 . The numerical solution of (4.7) gives results which are in excellent agreement with the simulations. In the **Table 4.1** we show as an example the results of simulations where we initialized a small circular system ($L = 24$) on lattice, with a uniform state pointing in the \hat{x} direction, and afterwards we integrated in time the LL equations (2.34), fixing the damping at $\varepsilon = 0.01$ and the field at $\omega = 0.03$ and $h = 0.006$, and for various values of the anisotropy.

Of course, only one of the 4 roots of (4.7) matches the simulation data, and providing that the parameters (ν, b, ε) fulfill some solvability conditions for (4.7), which are too lengthy to be written here. For instance, for $\lambda \gtrsim 0.988$ and the mentioned values of the field, we observe in the simulations that, starting with the uniform state on the XY-plane, in the final state m_0 is oscillating around zero at all times. In the eq. (4.7) one starts to observe complex roots at $\lambda \gtrsim 0.988$, while for $\lambda \leq 0.988$ all the four roots of (4.7) are real. However, there is still a real solution, which we plot in the **Fig. 4.1**. This solution matches the simulation data, if we initialize the latter with a uniform state out of the plane. For some finite initial value of m_0 , closer to the corresponding root of (4.7), the value of m_0 in the simulations converges to this root.

On the other hand, for $\lambda \leq 0.96$ (which is the case for most of our simulations in the

Fig. 4.1: Numerical solutions of eq. (4.7), as a function of the anisotropy for different field parameters.



next Sections), the numerical solution of (4.7) shows that for the range of the field parameters that we will use, *i.e.* $h < 0.01$ ($b < 0.05$) and $\omega < 0.1$ ($\nu < 0.5$), all the four roots are real.

We can see in the **Fig. 4.1** that approaching the small anisotropy region, the system is much more sensitive to changes in the anisotropy, than to the parameters of the field. In the simulation data there is actually a very small upwards deviation of the “surface” $m(x, y)$ from m_0 , for the spins approaching the border, due to the fact that the spins at the border have less neighbors, and therefore a reduced exchange interaction. This is, however, a small border effect, and the data of **Table 4.1** correspond to several spins between the center and the border, all of them showing the same value of m_0 .

4.1.2 Energy dissipation

We derive the continuum analogue for the power-dissipation relation (2.38). In terms of $\vec{m} = \vec{S}/S_c$, the dissipation function is

$$\mathcal{F} = \int d^2x \mathcal{F} \quad , \quad \mathcal{F} = \frac{\varepsilon S_c}{2a^2} \left(\frac{d\vec{m}}{dt} \right)^2 > 0 \quad , \quad (4.9)$$

and the LLG equations are

$$\frac{\partial \vec{m}}{\partial t} = -\frac{a^2}{S_c} \vec{m} \times \frac{\delta \mathcal{E}_T}{\delta \vec{m}} - \varepsilon \vec{m} \times \frac{\partial \vec{m}}{\partial t} \quad . \quad (4.10)$$

For the time derivative of the total energy we have

$$\frac{dE_T}{dt} = \int d^2x \left\{ \frac{\delta \mathcal{E}_T}{\delta \vec{m}} \cdot \frac{\partial \vec{m}}{\partial t} + \frac{\delta \mathcal{E}_T}{\delta \vec{h}(t)} \cdot \frac{d\vec{h}(t)}{dt} \right\} \quad . \quad (4.11)$$

Now,

$$\begin{aligned}
\frac{\delta \mathcal{E}_T}{\delta \vec{m}} \cdot \frac{\partial \vec{m}}{\partial t} &= \frac{\delta \mathcal{E}_T}{\delta \vec{m}} \cdot \left(-\varepsilon \vec{m} \times \frac{\partial \vec{m}}{\partial t} \right) = \varepsilon \frac{\partial \vec{m}}{\partial t} \cdot \left(\vec{m} \times \frac{\delta \mathcal{E}_T}{\delta \vec{m}} \right) \\
&= \varepsilon \frac{\partial \vec{m}}{\partial t} \cdot \left(-\frac{S_c}{a^2} \right) \left(\frac{\partial \vec{m}}{\partial t} + \varepsilon \vec{m} \times \frac{\partial \vec{m}}{\partial t} \right) \\
&= -\frac{\varepsilon S_c}{a^2} \left(\frac{\partial \vec{m}}{\partial t} \right)^2 = -2 \mathcal{F} \quad , \tag{4.12}
\end{aligned}$$

and, on the other hand,

$$\frac{\delta \mathcal{E}_T}{\delta \vec{h}(t)} = -\frac{S_c}{a^2} \vec{m} \quad . \tag{4.13}$$

Thus,

$$\frac{dE_T}{dt} = - \int d^2x \left\{ 2 \mathcal{F} + \vec{m} \cdot \frac{d\vec{h}(t)}{dt} \right\} \quad , \tag{4.14}$$

or, in normalized units,

$$\frac{dE_T}{d\tau} = -J S_c^2 \int d^2x' \left\{ \left(\frac{\partial \vec{m}}{\partial \tau} \right)^2 + \vec{m} \cdot \frac{d\vec{b}}{d\tau} \right\} \quad . \tag{4.15}$$

It is rather easy to check that $\frac{dE_T}{d\tau} = 0$ holds in the uniformly rotating equilibrium state (4.7)-(4.8), and so the dissipation balances perfectly the work done by the rotating field.

4.1.3 A discrete symmetry: classification of vortex dynamics

We have seen in the Chapter 2 that a vortex is characterized by its vorticity q and polarization p . Now we can observe that the energy density (4.2) and the eqs. (4.3) are left invariant by the changes

$$m \rightarrow -m \quad , \quad \phi \rightarrow -\phi \quad , \quad \omega \rightarrow -\omega \quad , \quad \beta_0 \rightarrow -\beta_0 \tag{4.16}$$

or in cartesian components

$$\begin{aligned}
S^x &\rightarrow S^x \quad , \quad b^x \rightarrow b^x \\
S^y &\rightarrow -S^y \quad , \quad b^y \rightarrow -b^y \\
S^z &\rightarrow -S^z \quad , \quad b^z \rightarrow -b^z
\end{aligned} \tag{4.17}$$

i.e., a parity operation in the YZ plane of the spin space, accompanied by the same operation on the components of the field.

An analogous statement is valid for the discrete eqs. (2.29) or (2.33) and (2.34), affecting all the spin variables of a subindex \vec{n} .

Table 4.2: Combinations of charges of a single vortex and signs of the field parameters: (β_0, ω) refer to the rotating field (4.1), while (b^y, b^z) refer to a static field (4.5). The numbers in the left and right columns of the table denote systems with indistinguishable dynamics.

	q	p	β_0 or b^y	ω or b^z	$q\beta_0$	$p\omega$	
1	+1	+1	+1	+1	+1	+1	16
2	+1	+1	+1	-1	+1	-1	15
3	+1	+1	-1	+1	-1	+1	14
4	+1	+1	-1	-1	-1	-1	13
5	+1	-1	+1	+1	+1	-1	12
6	+1	-1	+1	-1	+1	+1	11
7	+1	-1	-1	+1	-1	-1	10
8	+1	-1	-1	-1	-1	+1	9
9	-1	+1	+1	+1	-1	+1	8
10	-1	+1	+1	-1	-1	-1	7
11	-1	+1	-1	+1	+1	+1	6
12	-1	+1	-1	-1	+1	-1	5
13	-1	-1	+1	+1	-1	-1	4
14	-1	-1	+1	-1	-1	+1	3
15	-1	-1	-1	+1	+1	-1	2
16	-1	-1	-1	-1	+1	+1	1

Let us use the label “up” for the \hat{z} direction. It is easy to see that the two first changes in (4.16) transform a vortex configuration pointing up ($q = 1, p = 1$) into an antivortex pointing down ($q = -1, p = -1$). Thus, according to (4.16) the dynamics of an up-vortex with an anti-clockwise rotating field ($\vec{\omega} = \omega\hat{z}$, with $\omega > 0$) initially pointing towards, say, the positive \hat{y} direction ($\beta_0 = \pi/2$), is indistinguishable from the dynamics of a down-antivortex in a clockwise “down” field ($\omega < 0$), initially pointing in the $-\hat{y}$ direction ($\beta_0 = -\pi/2$).

In this way, out of the 16 combinations of charges (q, p) and signs of the field parameters (ω, β_0) , only 8 have a different dynamics, as can be seen in the **Table 4.2**, which allows us to consider a reduced number of cases.

Within the 8 independent combinations, we have 2 scenarios: the 4 systems for which the angular velocity $\vec{\omega} = \omega\hat{z}$ of the field is antiparallel to the initial vortex polarization ($p\omega < 0$) are seen to produce during the dynamics (given the proper material and field parameters $(\lambda, \varepsilon, \omega, b)$, to be quantified later) a switch in the sign of the whole OP vortex structure (referred to as “flip” or “switching”), in particular $p \rightarrow -p$, while those 4 systems whose $\vec{\omega}$ is parallel to the initial polarization ($p\omega > 0$) do not show a flip. In the language of the static field (4.5), following [38], we call a vortex with $pb^z > 0$ a “light” vortex, while a vortex with $pb^z < 0$ is called a “heavy” vortex, the latter having a tendency to flip its polarization, given the proper parameters $(\lambda, \varepsilon, b^z, b)$. We will study this process in detail in the next Sections.

4.2 Switching phenomenology

In order to investigate the dynamics of an OP vortex in the presence of the rotating field (4.1), we have carried out extensive computer simulations, where we have integrated in time the full set of discrete Landau-Lifshitz equations (2.34), on square lattices of several sizes (with $N^2 = 48^2, 72^2, 96^2$, and 120^2 spins), taking care of separating the cases when the vortex dynamics has a stronger influence from the external field, from those cases in which the influence from the image-vortex field is stronger. On each lattice the system is limited by a circular border with radius $L = N/2$, the same geometry as in the simulations of Chapter 3. We set free boundary conditions using the image method in analogy with electrostatics in 2D. For a vortex ($q = 1$) with polarization up ($p = 1$) at the position $\vec{X} = (X, Y)$, only one image anti-vortex ($q = -1$) with polarization up at the position $\vec{X}_I = L^2\vec{X}/R^2$, where $R = |\vec{X}|$, is set initially. For a vortex initially at the center of the system, $\vec{X}_I \rightarrow \infty$, so we do not need to set any image-vortex.

For most of the simulations, unless otherwise stated, the values of anisotropy ($\lambda = 0.90$) and damping ($\varepsilon = 0.002$) were set as in Ref. [18]. At this λ , the typical radius (3.35) of the OP structure of the vortex, given by the continuum limit is around 1.5 lattice constants, although, as can be seen in the **Fig. 4.12a**, non-negligible z-components of the spins extend in fact well up to 2.5 lattice sites in each direction.

We have studied mainly the system of radius $L = 36$ with free boundary conditions, for which we present (in Sec. 4.2.2) a diagram of flip events in the space of the parameters (ω, h) of the field. We used relatively weak amplitude fields so as neither to change the ground state significantly, nor to destroy the vortex. The integration time for this diagram was set to a maximum of 25,000 time units, in a 4th order Runge-Kutta integration method with time step 0.01, although we performed some special simulations until much longer times. Further details of the numerical procedures employed, such as the generation of the initial vortex configuration and the way to calculate the vortex core position at each time, are described in the Appendix D.

4.2.1 Review of previous results

It was first shown in Ref. [18] that due to the action of an IP rotating magnetic field the z-components of all spins in the core of an OP vortex, and therefore the vortex polarization p (the value of M_z at the vortex center), can abruptly change sign, so that the whole vortex OP structure is reversed from one side of the lattice plane to the other (we refer to this event as a “flip” or “switch”, see the **Fig. 4.2**) provided that the amplitude of the field is higher than a certain critical value h_{cr} which depends on the frequency and the initial vortex polarization, but not on the vorticity. The

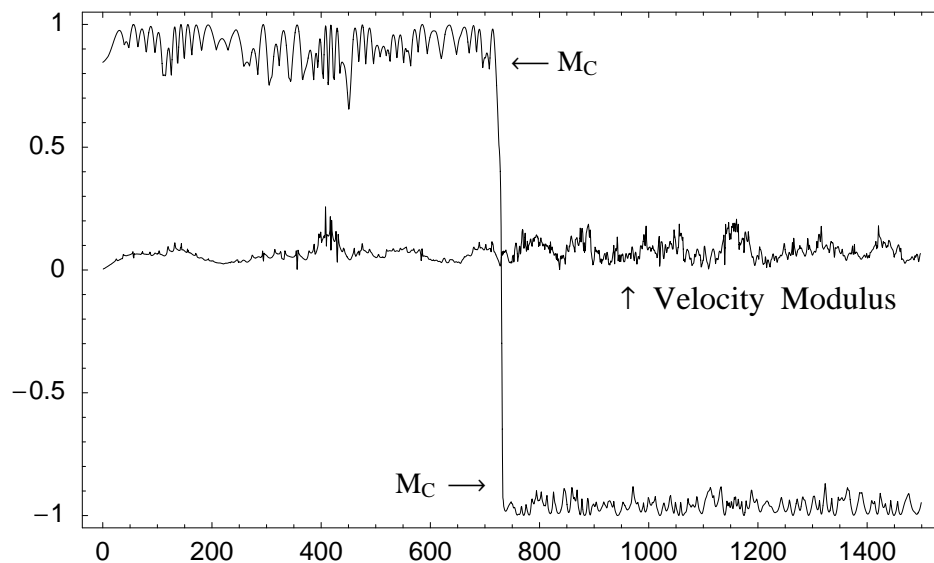


Fig. 4.2: Typical time evolution of the core magnetization M_c (average of $M_{\vec{n}}$ over the 4 inner spins) of a vortex ($q = 1$), initially pointing up ($p = 1$), showing a flip at $t \sim 730$ in a rotating field with $\omega = -0.04$, $h = 0.0032$. The time evolution of the velocity modulus of the vortex center is also shown. Data from numerical simulations on a system of radius $L = 36$, with anisotropy $\lambda = 0.90$ and damping $\varepsilon = 0.002$.

authors of that work used a square lattice with circular boundary of radius $L=24$, and presented for this system a curve of the critical amplitude as a function of ω . Starting with a vortex with polarization $p = 1$ it was found that the threshold value $h_{cr}(\omega)$ for a clockwise rotating field ($\omega < 0$) was much smaller than that for a counter-clockwise ($\omega > 0$) field. In the latter case the final structure of the vortex was often destroyed by spin waves. Exactly the inverse situation occurred when they used a vortex with $p = -1$ as initial condition: this time the switch to $p = 1$ was favored for a counter-clockwise rotating field.

The switch of the magnetization was then found to be a unidirectional event: a vortex state with a determined polarization and not the opposite one is favored by the rotating field, so that only when the product $\omega p < 0$ does the final state of the vortex have a well defined structure.

The basic reason for the switching was argued in [18] to be easily understood by using the frame of reference (in the spin space) which rotates uniformly at the frequency of the magnetic field: $\psi_n := \phi_n - \omega t$.

As we explained in the Sec. 4.1, the vortex feels in this frame approximately an effective static field with both IP and OP components. To make this point more clear, also in the discrete case, we used in Ref. [87] (like the authors of Ref. [18]) a set of slightly

modified Landau-Lifshitz equations,

$$(1 + \varepsilon^2) \dot{\vec{S}}_n = \vec{S}_n \times \vec{B}_n - \frac{\varepsilon}{S_c} \vec{S}_n \times \vec{S}_n \times \vec{F}_n \quad , \quad (4.18)$$

where

$$\vec{B}_n := - \frac{\partial}{\partial \vec{S}_n} [\mathcal{H}_0 + \mathcal{V}(t)] = \hat{J} \sum_a \vec{S}_{n+a} + \vec{h}(t) \equiv \vec{F}_n + \vec{h}(t) \quad . \quad (4.19)$$

(Only exchange-anisotropy was used). The difference with the LL equations (2.36) is that in the damping term of (4.18) the magnetic field is absent. In the variables (ϕ_n, S_n^z) these equations give

$$(1 + \varepsilon^2) \dot{\phi}_n = \frac{\partial}{\partial S_n^z} [\mathcal{H}_0 + \mathcal{V}(t)] - \frac{\varepsilon}{(S_c^2 - (S_n^z)^2)} \frac{\partial \mathcal{H}_0}{\partial \phi_n} \quad (4.20a)$$

$$(1 + \varepsilon^2) \dot{S}_n^z = - \frac{\partial}{\partial \phi_n} [\mathcal{H}_0 + \mathcal{V}(t)] - \varepsilon (S_c^2 - (S_n^z)^2) \frac{\partial \mathcal{H}_0}{\partial S_n^z} \quad (4.20b)$$

Since the usual amplitudes h are of $\mathcal{O}(10^{-3})$ and the usual damping ε is of $\mathcal{O}(10^{-2})$, the omitted term is usually $\mathcal{O}(10^{-5})$ and does not produce visible effects². On the other hand, for this set of equations, the mentioned approximate equivalence becomes exact. Indeed, in the rotating frame,

$$(1 + \varepsilon^2) \dot{\psi}_n = \frac{\partial}{\partial S_n^z} [\mathcal{H}_0 + \mathcal{W}] - \frac{\varepsilon}{(S_c^2 - (S_n^z)^2)} \frac{\partial \mathcal{H}_0}{\partial \psi_n} - (1 + \varepsilon^2) \omega \quad (4.21a)$$

$$(1 + \varepsilon^2) \dot{S}_n^z = - \frac{\partial}{\partial \psi_n} [\mathcal{H}_0 + \mathcal{W}] - \varepsilon (S_c^2 - (S_n^z)^2) \frac{\partial \mathcal{H}_0}{\partial S_n^z} \quad (4.21b)$$

with

$$\mathcal{H}_0 = - \frac{J S_c^2}{2} \sum_{n,a} \left\{ \sqrt{1 - m_n^2} \sqrt{1 - m_{n+a}^2} \cos(\psi_n - \psi_{n+a}) + \lambda m_n m_{n+a} \right\} \quad , \quad (4.22)$$

$$\mathcal{W} = - h S_c \sum_n \sqrt{1 - m_n^2} \cos(\psi_n - \beta_0) \quad . \quad (4.23)$$

The last term of (4.21a) can be absorbed into the first term of the r.h.s., if we add to \mathcal{W} the potential of an effective OP field $\vec{h}_\perp = (0, 0, (1 + \varepsilon^2) \omega)$, *i.e.*

$$\mathcal{W}_\perp = - (1 + \varepsilon^2) \omega S_c \sum_n m_n \quad , \quad (4.24)$$

which does not modify (4.21b). From this we can see why up-vortices will tend to flip when $\omega < 0$. It is this perpendicular component of the effective field, which selects a preferential direction along \hat{z} , and thus the vortex states with different polarizations are

²This was checked in our simulations (see discussion in Appendix A of [87]).

no longer equivalent, the switching process becoming energetically favored for heavy vortices.

It was noticed, however, that this argument does not explain why the threshold amplitude for the switching, as well as the flipping time, are not monotonic functions of the frequency ω (see next Section). In our further work [87], we have found that the concept of “critical field” itself has a loose meaning here, since the system shows instability regions or “windows”, where the response of the vortex (whether it will flip or not) to the field is, in the practice, unpredictable, as is typical for many-body and finite-size systems. Explanations of this behavior seem to be difficult, considering the set of parameters $(L, \lambda, \varepsilon, h, \omega)$ which are playing a role.

We will work out in the next sections, however, a reduced model which, though it can not account quantitatively for the flip times, it can capture qualitatively many features of the flip process.

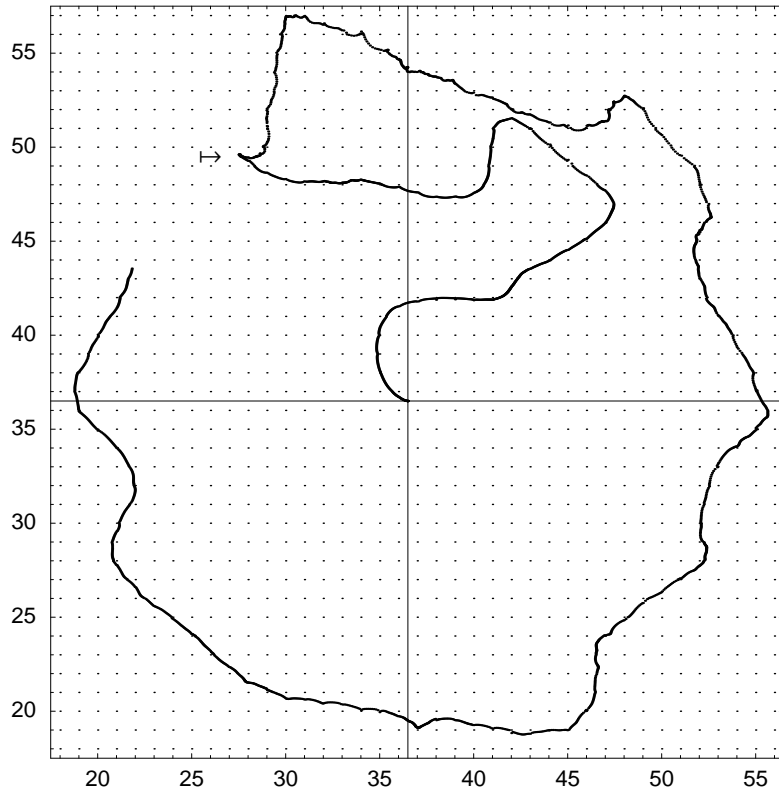
4.2.2 Results of new series of simulations

The results of Ref. [18] were substantially confirmed by the simulations of our further work [87]. We first noted, however, that some main conclusions in [18] were drawn from simulations at $|\omega| = 0.1$, which was found to be close to the frequency of the lowest radially symmetric eigenmode in the presence of a vortex [83, 85, 37]. We realized meanwhile that $|\omega| = 0.1$ is already a rather high frequency (corresponds to $|\Omega| = 0.25$ at $\lambda = 0.9$), as can be seen from the considerations of the ground state in Sec. 4.1.1, for $J = S = 1$ and $\lambda = 0.9$. For the same reason, when we present the size-dependence of the flipping time, and a phase diagram of flip events in the space of the field parameters (ω, h) , we do so for values $|\omega| < 0.1$.

Secondly we noted that the argument of Sec. 4.2.1 can not be applied to the limiting case $\omega \rightarrow 0$, *i.e.* of an OP vortex driven by a constant IP field. The transformation to the rotating frame has no meaning here. It is clear that in this case the perturbation does not select any preferential direction along \hat{z} . In some sets of our simulations with $\omega = 0$ (static IP field) we also found switching behavior. In this case, however, back-flips can occur, as expected, provided that the system is large enough, so that these successive flips can be observed before the vortex leaves the lattice at the boundary. Concerning this case, we believe that the magnon emission produced by the static field interacting with the moving vortex is responsible for a flip to occur, as is the case when the perturbation is thermal noise [17]. We will not study this case of $\omega = 0$ any further here.

In the **Figs. 4.2 – 4.5** we show some typical results of the simulations for a system of radius $L = 36$ in a rotating field ($\omega = -0.04$, $h = 0.0032$). In **Fig. 4.2** we plotted

Fig. 4.3: Typical vortex trajectory, corresponding to the time evolution shown in **Fig. 4.2**, until a time $t = 2240$. Starting from the center $(36.5, 36.5)$ of the system, it develops rather irregularly. The flip occurs in the part of the trajectory signaled by a symbol “ \mapsto ”. A few thousand time units after the flip the trajectory converges to a circle (not shown here, see Chap. 5) turning clockwise. The grid of points are the lattice sites.



the core magnetization M_c , *i.e.* the average of $M_{\vec{n}}$ over the 4 innermost spins of the vortex. Note that, by the definition of the vortex center position with usual methods (see Appendix D) this signal exhibits strong discreteness effects. These are, however, unavoidable (this means, they are physical effects), since the center of a vortex is always inside one plaquette of 4 spins, which then will be the spins with the highest value of S_z , except in the rare cases when the vortex crosses exactly over a lattice site (like the event marked “3” in **Figs. 4.4** and **4.5**), and so the z-component of this spin reaches the highest value $S_z = 1$. A more detailed discussion of what is inherent to which numerical method for determining the vortex positions is presented in Appendix D, but already this comment should be enough to convince the reader that the “polarization” p , defined as the value of S_z at the “center of the vortex”, and therefore its gyrovector \vec{G} , in the discrete system will show always oscillations while the vortex moves through the lattice.

The velocity modulus is also plotted in **Fig. 4.2**, in order to observe (a) the correlations between these two signals, and (b) the increasing velocity fluctuations immediately following the flip. The latter is a clear finite size effect: the flip process produces a circular spin wave propagating outwards, which is reflected at the boundary in a non-symmetric way because the vortex is not at the center of the system at the moment of flipping. After some time these waves are damped out due to the damping term we added in the equations (2.34). The fluctuations in the core magnetization are, in

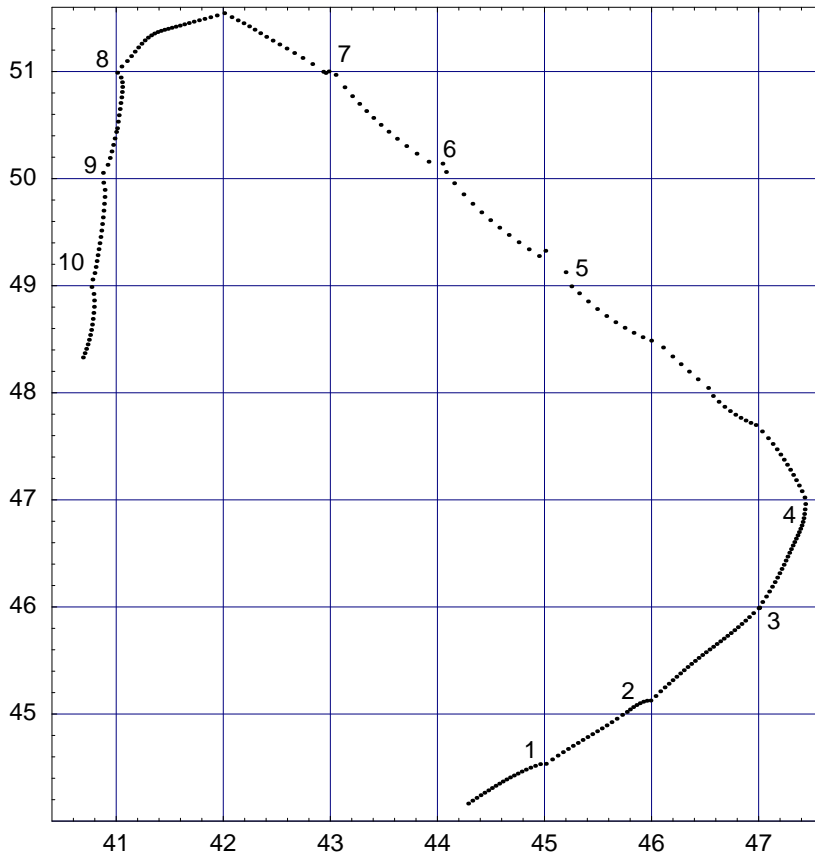


Fig. 4.4: Enhancement of a sector of the trajectory from the **Fig. 4.3**, between $t = 300$ and $t = 500$.

contrast, smaller in amplitude after the flip than before, showing the larger stability of the vortex whose grovector is parallel to the angular velocity $\vec{\omega}$ of the field.

We also plotted in **Fig. 4.3** a section of the trajectory, traced by the successive positions of the vortex center. Since the main goal of this Chapter is to study the vortex flip process, a more complete analysis of the trajectories will be given in the next Chapter. Here we only show a small trajectory section as a reference, to illustrate a) how the sense of the main rotation changes after the flip, and b) how the movement of the vortex in the XY plane, over the discrete lattice, which is usually modeled by a periodic potential (“Peierls-Nabarro potential”), is coupled to the oscillations of the vortex core magnetization in the z-direction (see the enhancements of **Fig. 4.4**), which will be discussed later.

We have also noticed that when the anisotropy approaches the instability region close to λ_c [83] back-flips can occur, as can be seen in **Fig. 4.6**, but the prior result about uni-directionality of flips is strictly correct at the value $\lambda = 0.9$, at which most of the simulations in Ref. [18] and ours were carried out. It is interesting to note that there is no monotonous dependence of the tendency to flip (quantified approximately by the flip times) on the anisotropy λ , as can be seen in the **Fig. 4.7**, where for $\lambda > 0.8$ there was only one flip, and for $\lambda \leq 0.8$ only the first flip was taken into account.

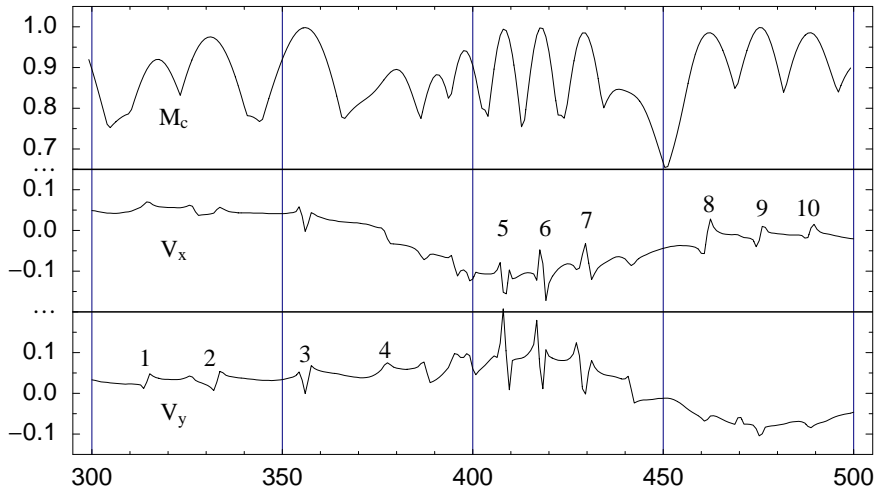


Fig. 4.5: Signals of the core magnetization M_c and the velocity components (like in **Fig. 4.2**) vs. time, for the trajectory section shown in **Fig. 4.4**.

Among the questions left open by the work of Ref. [18] is the relative importance of the boundary (size effects) and the magnetic field on the switching of vortex polarization. We have extended in our work [87] the numerical simulations to include the sizes mentioned at the beginning of this section. An illustration of the size effects can be seen in **Fig. 4.8**, where the flip time vs. field amplitude h , for the frequency $\omega = -0.05$, is shown for several sizes. We can see from this figure, first that the flip times increase mainly with decreasing amplitudes (up to some non-monotonic jumps), which gives confidence to speak reasonably about a critical amplitude, or a threshold field, for the flipping process to occur, within the time considered. We emphasize that all the simulations are carried out in a finite observation time, so a “critical curve” to be drawn using the data of **Fig. 4.9** is determined as that curve which separates fast events of flips from very late or impossible ones, at the considered size.

Except for the critical region at very low amplitudes, the flip process is in general a relatively rapid event, of some hundreds of time units, in all the simulations. Very long simulations ($t \gtrsim 30,000$) in an unstable configuration will start to meet accuracy problems. This number is about the limit when the energy of the system at zero damping and zero field stops being constant due to the presence of accumulative numerical errors. In the work [18], the simulations were stopped immediately after a flip was detected, with a maximum time of 12,000 time units. We have continued all our simulations after the flips, to see in more detail the final states, and we have set a maximum time of 25,000 time units.

The **Fig. 4.8** also gives insight into the relative effects of the size of the system on the flip time. It tells us that the prior results of Ref. [18] were obtained for a rather small lattice. We can see that the present system with radius $L = 36$ is already much closer to what we can expect as bulk behavior, minimizing thus the size effects. We can expect relatively small size effects whenever we consider amplitudes $h \gtrsim 0.004$ (for

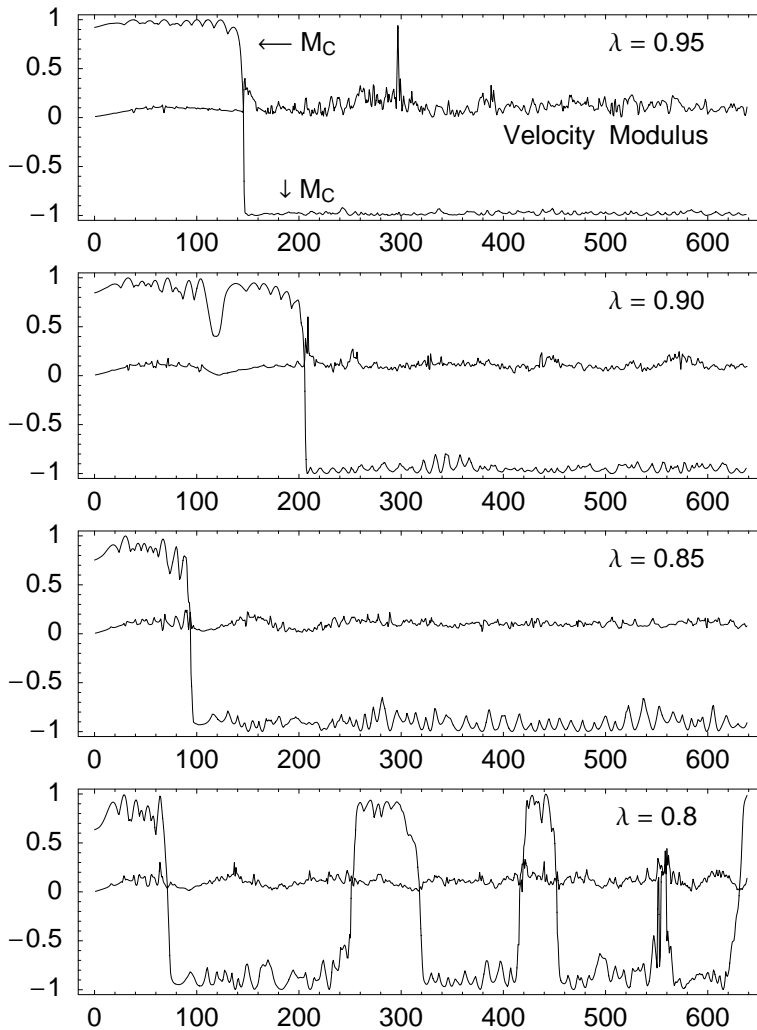


Fig. 4.6: Core magnetization M_c and velocity modulus *vs.* time, in a field with $\omega = -0.025$ and $h = 0.006$. The flips of M_c show a strong non-monotonous dependence on the anisotropy λ . Fluctuations of M_c are larger for $\lambda \approx \lambda_c$, as can be seen in the lower panels.

frequency $\omega = -0.05$), over a wide range of sizes from $L = 36$ up to the bulk, as is seen in **Fig. 4.8**. The time evolution of the core magnetization M_c and the velocity modulus for a field with $\omega = -0.05$ and $h = 0.0022$ is plotted in **Fig. 4.10** for 3 sizes. We can see that the velocity fluctuations after the flip are the larger the smaller the system is, showing the size effect mentioned above. The velocities here, in contrast to the corresponding figure of our work [87], have been calculated with centered differences over the positions signals.

In **Fig. 4.9** we show a diagram of the flip and non-flip events in the space of the field parameters (ω, h) resulting from numerical simulations of a system of radius $L = 36$, concentrated in the region of low frequency and low amplitude of a clockwise ($\omega < 0$) applied field. We have observed almost the same behavior as in the Fig. 2 of Ref. [18], with a relatively small shift of the threshold values, but, in contrast, here appeared “windows”: flip events in regions where no flip was expected, and vice versa, non-flip events in regions where flips were expected. Interestingly, a zoom-in of these

Fig. 4.7: Flip times *vs.* anisotropy λ : non-monotonous effects.

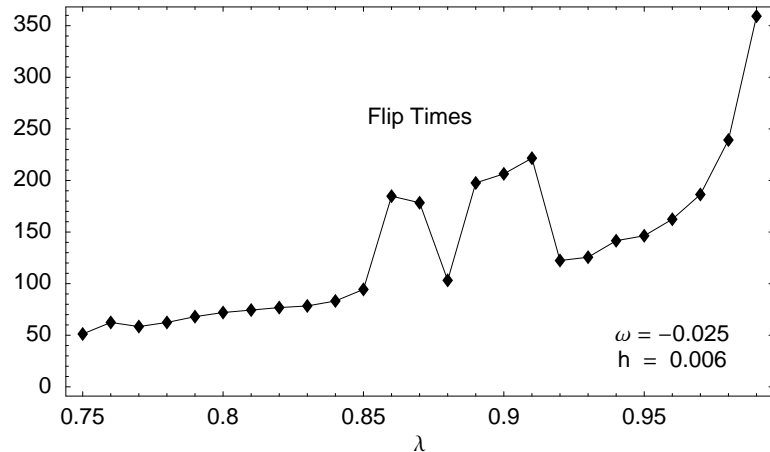
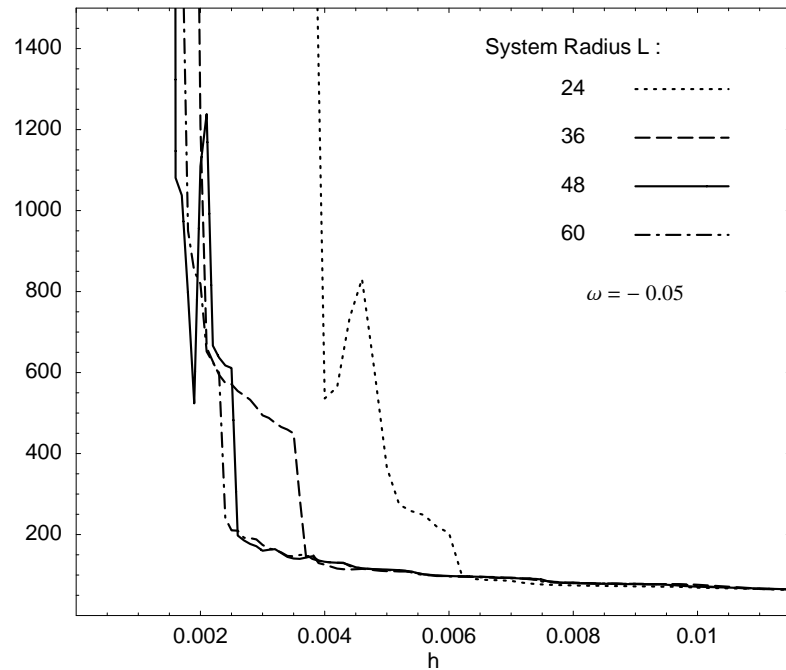


Fig. 4.8: Flip times *vs.* field amplitude h for several system radii L : non-monotonous size effects are small at high amplitudes.



windows shows again the same effect, as is typical of a self-similarity phenomenon. We can at present only account, with the model calculations of the next sections, for the qualitative mean behavior of the system, including discreteness, finite size and anisotropy only in an approximate way, which does not allow for an explanation of these windows. We consider them as most likely effects of tuning of all the parameters of the system $(h, \omega, \lambda, \varepsilon, N)$, because changing slightly any of them changes considerably the position, extension and even the existence of these windows in the diagram³.

In addition, for some cases a further effect must be considered: in many simulations, particularly in the longest ones, we have observed destruction of vortices. This was

³ This, together with the self-similar behavior of the windows, is a strong hint for the appearance of chaos in this many-body system. We did not go, however, deeper in this sense with the tools of the chaos theory.

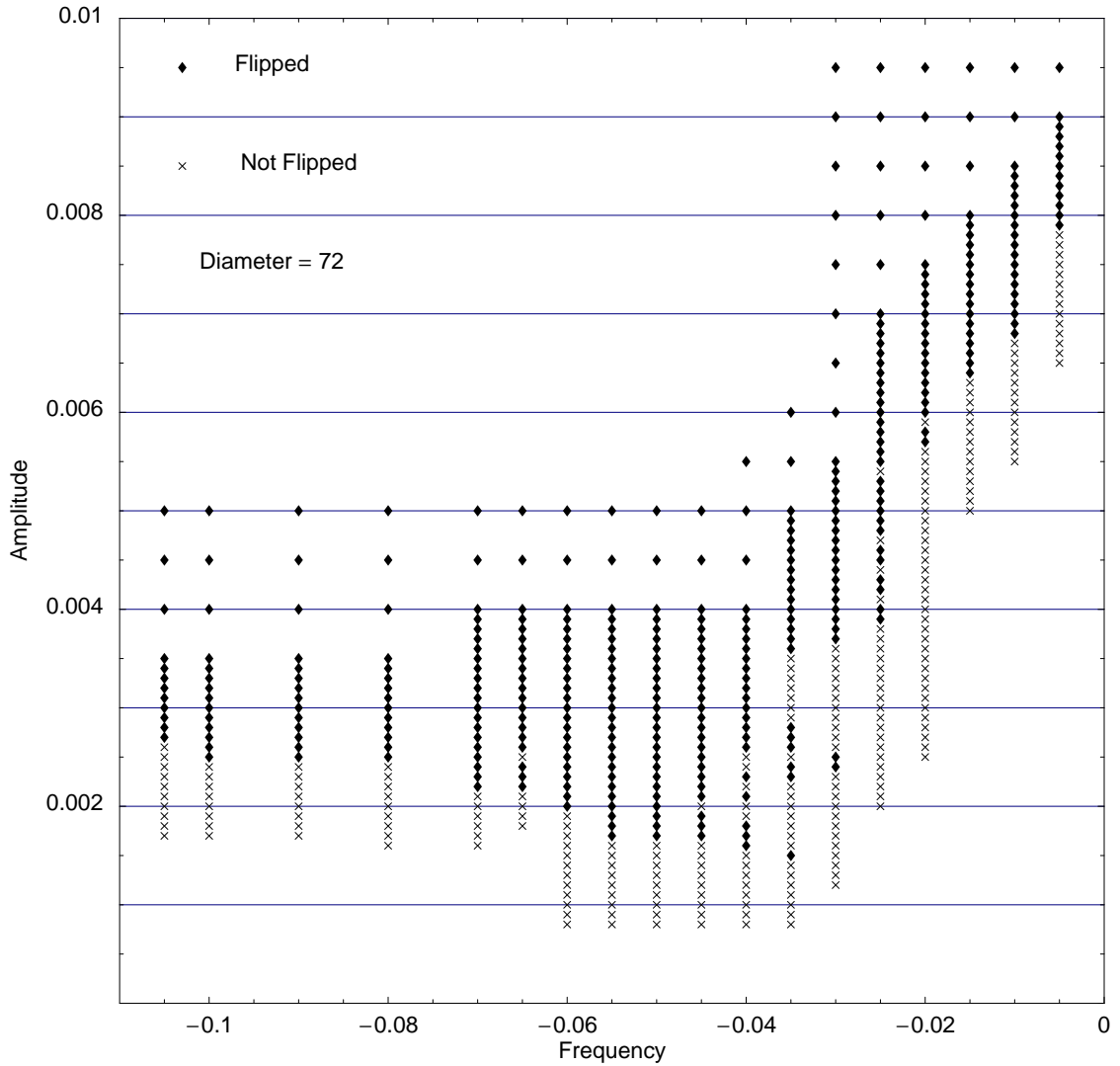


Fig. 4.9: Diagram of flip events in the frequency-amplitude space (ω, h) , for the system of radius $L = 36$, with damping $\varepsilon = 0.002$ and anisotropy $\lambda = 0.9$.

seen to be caused by

- new additional vortices forming at the boundaries due to the magnetic field, diffusing into the lattice. There they annihilate with the vortices already present, or escape again towards the boundary, annihilating there with the new corresponding images.
- the original vortex simply annihilates at the boundary with its image, with no additional vortices created during the time of the simulation.

We do not deal with these cases here, because our main concern is studying the flipping process as a rather rapid and clean event with only one vortex. These destruction processes are taken into account only when they occur before the flip of $p \rightarrow -p$, giving therefore a finished simulation without flip.

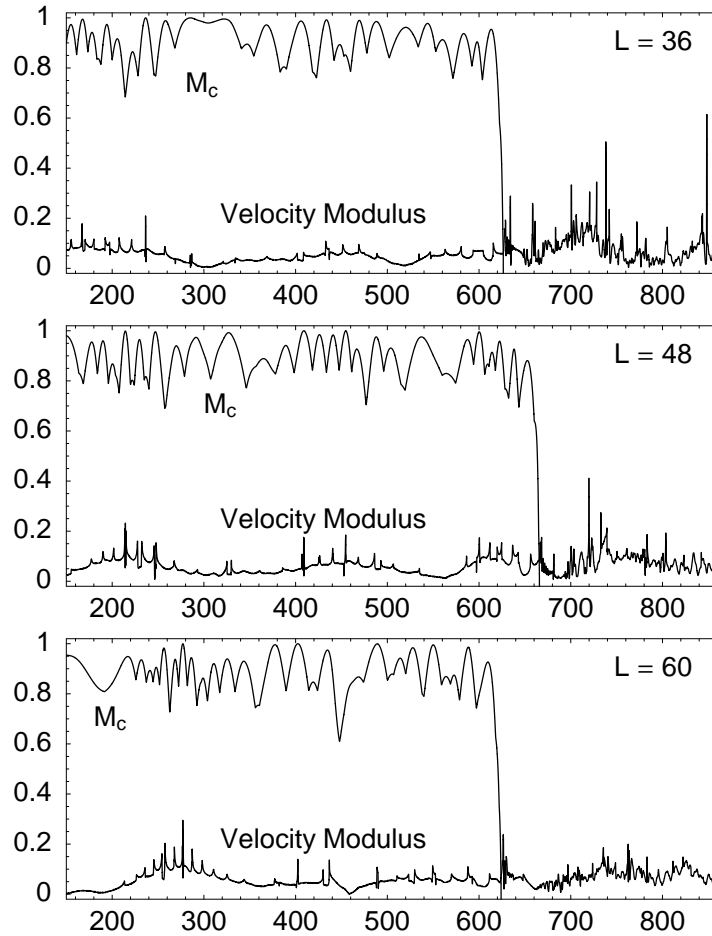


Fig. 4.10: Time evolution of the core magnetization M_c and the velocity modulus, in a field with $\omega = -0.05$ and $h = 0.0022$, in systems with different radii $L = 36, 48, 60$, with damping $\varepsilon = 0.002$ and anisotropy $\lambda = 0.9$. After the flip, the fluctuations of the velocity are more pronounced for the smaller systems.

4.2.3 Coupling between IP and OP oscillations

One of the main results of our work was to show that the IP movement of the center of the vortex (“center of mass motion”) is, to some extent⁴, correlated with the OP oscillations of the vortex magnetization, supporting the idea already mentioned in Ref. [18] that the flipping process is helped by a finite velocity and the perturbation due to the discrete lattice potential.

The time evolution of both the magnetization of the vortex core M_c and the components of the velocity of its center were shown enhanced in **Fig. 4.5**, together with the corresponding trajectory sector in the **Fig. 4.4**, for some typical intensity of the magnetic field and for a system of radius $L = 36$, with a single vortex pointing up ($p = 1$) and sitting in the center of the lattice as initial condition. The correlation between both signals was evident in that each maximum and minimum in the magnetization, or maximum in the velocity modulus, in **Fig. 4.5**, can be identified with a single crossing

⁴ up to long wavelength spin waves and non-localized modes of the whole lattice excited by the rotating field.

of a ridge or a saddle of the Peierls-Nabarro potential of the lattice, in **Fig. 4.4**. The vertices of the grid represent the lattice sites. The correlation is most evident before and for some time after the flip. In the immediate time after the flip there are larger fluctuations because the flip itself creates an azimuthally symmetric spin wave which propagates radially towards the boundary and is reflected there in a non-symmetric way, so that at those moments many spin waves are present. After this transient, the correlation is evident again.

Under the action of the AC field, there appear many kinds of possible trajectories, depending on the frequency ω and amplitude h , which will be the subject of the next Chapter. For our present purposes it is enough to know that, independently on whether there will be a final “limit cycle” and the vortex will stay inside the system, or the vortex at some time will leave the system through the boundary, in all the cases there is a correlation between out-of-plane oscillations and center of mass movement, like that shown in the **Fig. 4.5**, which suggests a first hint for understanding the flipping process: the same instability which makes a moving IP vortex develop out-of-plane components for $\lambda > \lambda_c$ [22], should give some contribution to the flipping process of a moving OP vortex. Since all the peaks and minima in the velocity are correlated with the crossing of some ridge or saddle of the Peierls-Nabarro potential, we ascribe them to the discreteness of the lattice (see also Appendix D). This is also supported by the **Fig. 4.7**, where larger fluctuations -even back-flip events- occur for values of λ closer to the critical value $\lambda_c \sim 0.72$. This out-of-plane instability in the presence of anisotropy (discussed in Ref. [83]), will be taken into account in the models of Sec. 4.3.

4.2.4 Simulations with static fields

Another result of this work is that we have confirmed, in our numerical simulations with static fields containing both an IP component \vec{h}_{\parallel} and an OP component \vec{h}_{\perp} , as mentioned above, the predicted switching behavior. As an example, the **Fig. 4.11** shows a comparison of flipping times for both systems under discussion here.

We do not expect the flipping times to be exactly the same, since the equivalence holds strictly in the bulk limit only at very small damping. However, in the cases when the flip occurs relatively close to the center of the lattice, we get better agreement, as the boundary effects are less important. As shown in Ref. [36, 38], when a static magnetic field is applied along the hard axis there exist two types of OP vortices in the easy-plane ferromagnets: “light” and “heavy” vortices with the gyrovectore being parallel and antiparallel to the applied magnetic field, respectively. The energy of the heavy vortex is always higher than that of the light one. The physical reason for switching is then obvious: the system transfers from the high energy state (heavy vortex) to the

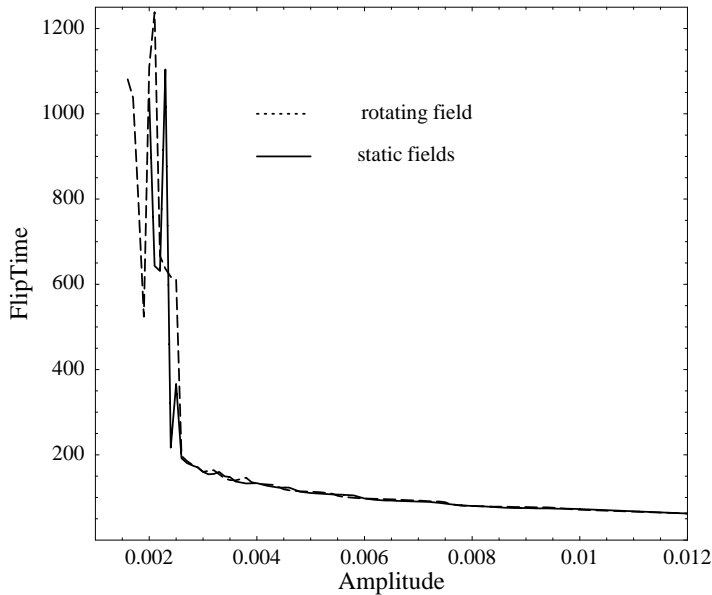


Fig. 4.11: Flipping times of 2 different systems: (dashed line) with IP rotating field $\omega = -0.05$, *vs.* amplitude h , and (solid line) with a static field $\vec{h} = (0, h_y, h_z)$, with $h_z = -0.05$, *vs.* h_y . The 2nd system is approx. equivalent, in the rotating frame, to the 1st one in the static frame, under the dynamics of eqs. (4.18) at small damping $\varepsilon = 0.002$. Trajectories are coincident only once we rotate the spins of one system at each time, according to $\psi_n := \phi_n - \omega t$, but this does not affect the flip times. Here $L = 48$ and $\lambda = 0.9$.

low energy state (light vortex). However, it is worth mentioning that the presence of an out-of-plane magnetic field is a necessary but not sufficient condition for switching, if we want to apply a relatively weak OP field, so that the vortex structure and the easy-plane character of the system are not destroyed. In this case, the heavy vortex exists as a metastable state of the system, and the presence of an additional IP component of the static field makes the flipping process much easier, by means of the movement described here. This IP component must be weak too, in order to keep the vortex confined to the finite system, for a time long enough to observe the flip.

4.3 Discrete core models

As was mentioned in the work [18], the totally symmetric core mode which describes the dynamics of the vortex polarization does not interact directly with a spatially uniform external magnetic field when the vortex is at the center of the system. Two possibilities were proposed to remove this restriction:

1. In finite systems the vortex moves away from the center due to the interaction with its image, in this way the totally symmetric core mode may be excited.
2. Switching may occur as a result of nonlinear mixing between the totally symmetric mode and non-symmetric vortex modes, which do interact with the spatially uniform external magnetic field.

Considering relatively small systems, the work of Ref. [18] assumed that the first mechanism is more important. However, our further numerical simulations showed that

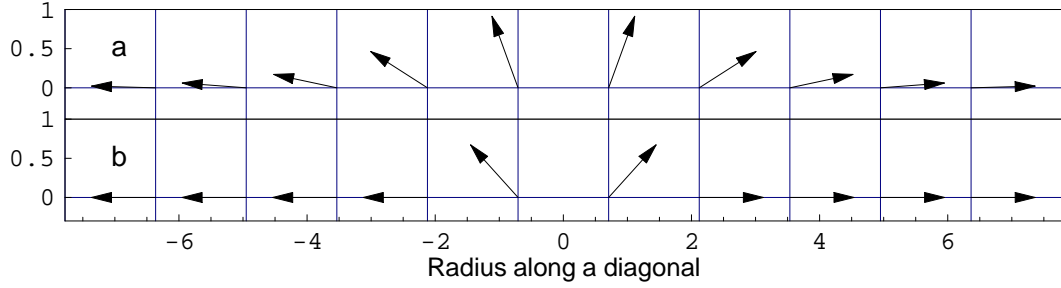


Fig. 4.12: Section of the OP structure (z-components) of static vortices *vs.* distance along a lattice diagonal (spins separated by $\sqrt{2}$ for $a = 1$), with initial phase $\varphi_0 = 0$. In **(a)**: data from the full many-spin system with $\lambda = 0.9$, a vortex at the center after relaxation under the dynamics (4.18). In **(b)**: the vortex used as initial condition in the full core model (4.28) with $\lambda = 0.95$.

the switching process does not depend crucially on the size of the system provided it is large enough (**Fig. 4.10**). Therefore, in this Section we discuss the second mechanism for the switching of the vortex polarization.

4.3.1 Full core model

To gain an insight into how the external magnetic field affects the vortex dynamics we need a reduced form of the Hamiltonian (4.22) and the interaction (4.23) which can take into account effectively both in-plane (IP) and out-of-plane (OP) vortices. We will use a core approach which is a generalization of the approach used in Ref. [83] for studying the transition from IP to OP vortices at $\lambda \approx \lambda_c$. In the present case we will assume that

i) the IP angles $\Phi_{\vec{n}}^0$ for static IP and OP vortices are given by Eq. (3.27), for $X = Y = 0$ without the image contribution.

ii) the deviations of the IP angles from their static values $\psi_{\vec{n}} = \Phi_{\vec{n}} - \Phi_{\vec{n}}^0$ and the OP moments $m_{\vec{n}}$ rapidly decay with the distance $r_{\vec{n}} = \sqrt{n_x^2 + n_y^2}$ from the center of the vortex:

$$(\psi_{\vec{n}}, m_{\vec{n}}) = \begin{cases} (\psi_1, m_1) & , \text{ for } \vec{n} = (1/2, 1/2) , \\ (\psi_2, m_2) & , \text{ for } \vec{n} = (-1/2, 1/2) , \\ (\psi_3, m_3) & , \text{ for } \vec{n} = (-1/2, -1/2) , \\ (\psi_4, m_4) & , \text{ for } \vec{n} = (1/2, -1/2) , \\ (0, 0) & , \text{ otherwise.} \end{cases} \quad (4.25)$$

Thus, only the first four spins nearest to the vortex center have non-zero z-components, and appreciable IP deviations from the IP static vortex structure. All other spins lie in the x-y plane, and follow the IP distribution (3.27). A sketch of this vortex structure can be seen in **Fig. 4.12(b)**. Under these assumptions the dynamics of the vortex core

is described by the following Hamiltonian

$$H_c = -J \sum_{i=1}^4 \{ \lambda m_i m_{i+1} + p_i p_{i+1} \sin(\psi_i - \psi_{i+1}) + 2\lambda_c p_i \cos \psi_i \} , \quad (4.26)$$

where $p_i = \sqrt{1 - m_i^2}$ and $m_5 \equiv m_1, \psi_5 \equiv \psi_1$. Here $\lambda_c = 2/\sqrt{5} \approx 0.894$, as in the lowest order, “1st-shell” approach for square lattices of Ref. [83], but in the present approach the four spins are allowed to have different (m_i, ψ_i) values, and the model automatically includes the interaction of this shell with the second (inactive) one. The interaction with the external field (4.23) takes the form

$$V_c(t) = -h \sum_{i=1}^4 \sqrt{1 - m_i^2} \cos(\psi_i - \omega t - i \frac{\pi}{2}) \quad (4.27)$$

and the equations of motion for the core variables m_i and ψ_i now read

$$\begin{aligned} \frac{d\psi_i}{dt} &= \frac{\partial(H_c + V_c)}{\partial m_i} - \frac{\varepsilon}{1 - m_i^2} \frac{\partial H_c}{\partial \psi_i} , \\ \frac{dm_i}{dt} &= -\frac{\partial(H_c + V_c)}{\partial \psi_i} - \varepsilon (1 - m_i^2) \frac{\partial H}{\partial m_i} . \end{aligned} \quad (4.28)$$

To check the applicability of the core model (4.26)-(4.27), we solved numerically the set of equations (4.28) and found (see **Fig. 4.13**) a qualitative agreement with the vortex behavior obtained in the simulations of the full many-spin system⁵. The core model gives a rather good global description of the switching process. However, the details of the process are very sensitive to the particular choice of parameters. Changing, for instance, the amplitude or frequency of the field in a fraction smaller than 10^{-4} can give rise to the existence of precursors for the flip, But eventually the switching occurs and the system is locked in the new vortex state.

4.3.2 Reduced core model

The core model presented in the previous subsection is still rather complicated and to gain deeper insight a further reduction is needed. This can be achieved by considering the behavior of the system near the threshold of IP–OP vortex instability: $(\lambda - \lambda_c)/\lambda_c \ll 1$. It is convenient to introduce instead of m_i and ψ_i the linear combinations which correspond to the four irreducible representations of the site symmetry

⁵Note that eqs. (4.28) give results very different from the eqs. (4.3) reduced for the case of a uniform state (neglecting all gradients), whose numerical solution does not show flips, but smooth relaxation to equilibrium.

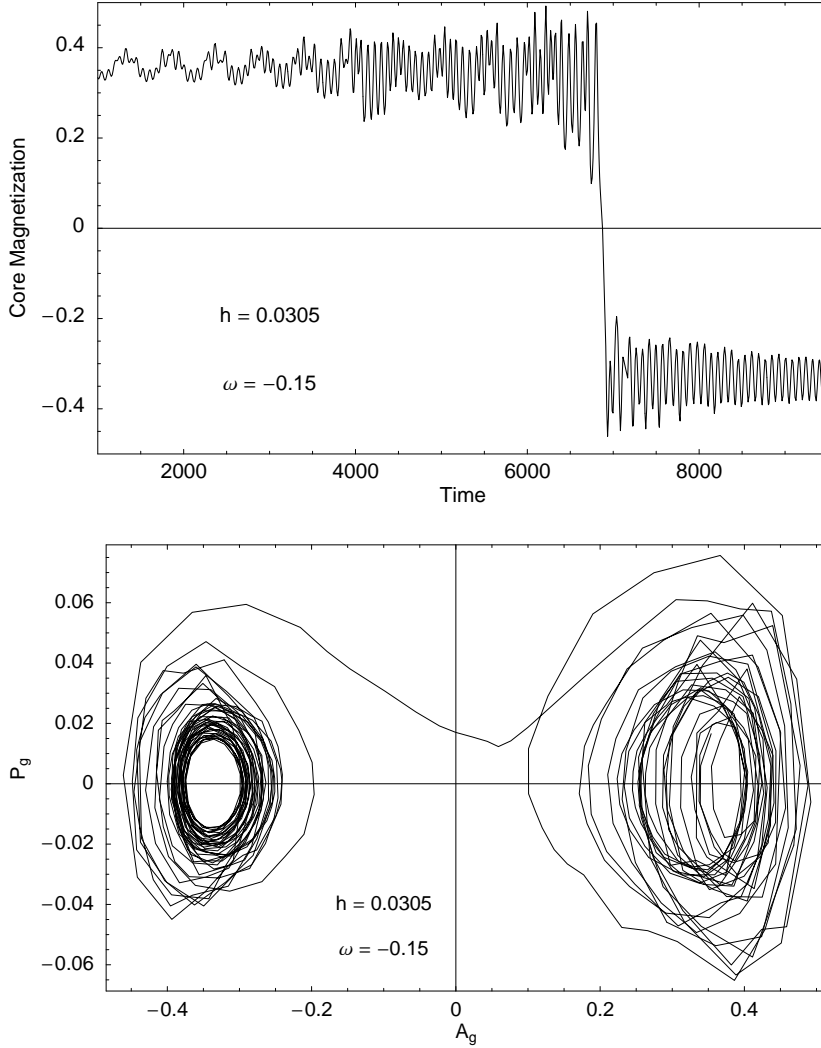


Fig. 4.13: (Top) Time evolution of the core magnetization (average of the m_i) from the numerical solution of the core model (4.28), in a field with $\omega = -0.15$ and $h = 0.0305$. Here $J = 1/8$, $\lambda = 0.95$ and $\varepsilon = 0.002$. (Bottom) Projection of the phase trajectory onto the plane of the totally symmetric modes (A_g, P_g), calculated as averages of the m_i and ψ_i , resp., (eq. 4.29).

group of the square (2 inversions, 2 reflections):

$$\begin{aligned}
 A_g &= (m_1 + m_2 + m_3 + m_4) / 4, & P_g &= (\psi_1 + \psi_2 + \psi_3 + \psi_4) / 4, \\
 B_g &= (m_1 - m_2 + m_3 - m_4) / 4, & Q_g &= (\psi_1 - \psi_2 + \psi_3 - \psi_4) / 4, \\
 A_u &= (m_1 + m_2 - m_3 - m_4) / 4, & P_u &= (\psi_1 + \psi_2 - \psi_3 - \psi_4) / 4, \\
 B_u &= (m_1 - m_2 - m_3 + m_4) / 4, & Q_u &= (\psi_1 - \psi_2 - \psi_3 + \psi_4) / 4.
 \end{aligned} \tag{4.29}$$

where the A 's and B 's are conjugate momenta of the P 's and Q 's. For instance, the A_g, P_g -mode is totally symmetric under reflections ($1 \leftrightarrow 2$ and $3 \leftrightarrow 4$, or $1 \leftrightarrow 4$ and $2 \leftrightarrow 3$) and inversions ($1 \leftrightarrow 3$ or $2 \leftrightarrow 4$), the B_g, Q_g -mode is inversion-symmetric and reflection-antisymmetric, and so on. It was shown in Ref. [83] and [85] that the totally symmetric mode, when all core spins move in phase, is responsible for the instability of IP vortices in easy-plane ferromagnets with weak anisotropy. Therefore, to take into account the soft character of this mode, we will consider the totally sym-

metric A_g, P_g -mode as a nonlinear one, while all other modes will be considered in the harmonic approximation. By inserting Eqs (4.29) into Eq. (4.26) and expanding the corresponding Hamiltonian we get

$$H_c = -16J\lambda_c + H_s + H_{ns} + H_u, \quad (4.30)$$

where

$$H_s = 8J \left\{ \frac{1}{2}(\lambda_c - \lambda)A_g^2 + \frac{1}{8}\lambda_c A_g^4 + \frac{1}{2}\lambda_c P_g^2 \right\} \quad (4.31)$$

is the Hamiltonian of the totally symmetric mode,

$$H_{ns} = 8J \left\{ \frac{1}{2}\lambda_c Q_g^2 + \frac{1}{2}(\lambda + \lambda_c)B_g^2 \right\} \quad (4.32)$$

is the Hamiltonian of the non-symmetric g-mode, and

$$H_u = 8J \left\{ \frac{1}{2}\lambda_c (A_u^2 + B_u^2 + P_u^2 + Q_u^2) + A_g (A_u Q_u - P_u B_u) \right\} \quad (4.33)$$

is the part of the core Hamiltonian which describes the antisymmetric u-modes. In the same approximation the interaction Hamiltonian (4.27) is expressed as follows

$$\begin{aligned} V_c(t) = & -2h [Q_u - P_u + A_g(A_u + B_u) + P_g(P_u + Q_u)] \sin(\omega t) \\ & -2h [Q_u + P_u + A_g(A_u - B_u) + P_g(P_u - Q_u)] \cos(\omega t) . \end{aligned} \quad (4.34)$$

In terms of the new variables (4.29) the equations of motion (4.28) read

$$\frac{dA_\nu}{dt} = -\frac{\partial}{\partial P_\nu} [H + V_c(t)] - \varepsilon \frac{\partial H}{\partial A_\nu}, \quad (4.35a)$$

$$\frac{dP_\nu}{dt} = \frac{\partial}{\partial A_\nu} [H + V_c(t)] - \varepsilon \frac{\partial H}{\partial P_\nu}, \quad (4.35b)$$

$$\frac{dB_\nu}{dt} = -\frac{\partial}{\partial Q_\nu} [H + V_c(t)] - \varepsilon \frac{\partial H}{\partial B_\nu}, \quad (4.35c)$$

$$\frac{dQ_\nu}{dt} = \frac{\partial}{\partial B_\nu} [H + V_c(t)] - \varepsilon \frac{\partial H}{\partial Q_\nu}, \quad (4.35d)$$

where $\nu = u, g$ and it was taken into account that for $(\lambda - \lambda_c)/\lambda_c \ll 1$ the out-of-plane components m_i are small and therefore in Eqs (4.35) small terms εA_ν^2 and B_ν^2 were neglected.

Let us first consider the eigenmodes of the Hamiltonian (4.30). For the no-driving case

($h = 0$) the equations of motion for the modes (4.29) read

$$\begin{aligned}\dot{A}_g &= -8J\lambda_c P_g, \quad \dot{P}_g = 8J\{(\lambda_c - \lambda)A_g + \frac{1}{2}\lambda_c A_g^3 + A_u Q_u - P_u B_u\}, \\ \dot{B}_g &= -8J\lambda_c Q_g, \quad \dot{Q}_g = 8J(\lambda + \lambda_c)B_g,\end{aligned}\tag{4.36}$$

$$\begin{aligned}\dot{A}_u &= 8J(-\lambda_c P_u + A_g B_u), \quad \dot{P}_u = 8J(\lambda_c A_u + A_g Q_u), \\ \dot{B}_u &= 8J(-\lambda_c Q_u - A_g A_u), \quad \dot{Q}_u = 8J(\lambda_c B_u - A_g P_u),\end{aligned}\tag{4.37}$$

where $\dot{x} \equiv \frac{dx}{dt}$. When $\lambda < \lambda_c$ (IP vortex is stable) the equilibrium state of the Hamiltonian (4.31) is achieved for $A_g = 0, P_g = 0$. Near this state the second term on the r.h.s. of the second of Eqs. (4.36), as well as the last terms on the r.h.s of Eqs. (4.37), are small and may be omitted in the harmonic approximation. Under these conditions the totally symmetric A_g, P_g -mode is characterized by the eigenfrequency $\omega_{in} = 8J\sqrt{\lambda_c(\lambda_c - \lambda)}$. The B_g, Q_g -mode is decoupled and oscillates with the eigenfrequency $8J\sqrt{\lambda_c(\lambda_c + \lambda)}$. The A_u, P_u - and B_u, Q_u -modes also result in decoupled eigenmodes of the system, both with the same frequency $8J\lambda_c$. Note that the totally symmetric A_g, P_g -mode is the only one which requires $\lambda < \lambda_c$.

When $\lambda > \lambda_c$ (OP vortex is stable) the Hamiltonian (4.31) possesses two minima $P_g = 0, A_g = \pm\sqrt{2(\lambda - \lambda_c)/\lambda} := \pm m_0$ (m_0 has the meaning of core magnetization). For the OP vortex the frequency of the totally symmetric eigenmode is given by $\omega_{out} = 8J\sqrt{2\lambda_c(\lambda - \lambda_c)}$. It follows from Eqs. (4.37) that in this case the antisymmetric eigenmodes are

$$\begin{aligned}\chi_+ &= \frac{1}{2}(A_u + Q_u - i(B_u - P_u)), \\ \chi_- &= \frac{1}{2}(A_u - Q_u + i(B_u + P_u)),\end{aligned}\tag{4.38}$$

and χ_+^*, χ_-^* , with the corresponding eigenfrequencies $\omega_{\pm} = 8J(\lambda_c \pm m_0)$.

In the driving case when $h \neq 0$, inserting eqs. (4.38) into eqs. (4.33) and (4.34) we get

$$H_u = 8J[(\lambda_c + A_g)|\chi_+|^2 + (\lambda_c - A_g)|\chi_-|^2],\tag{4.39}$$

$$V_c(t) = h(i - 1)[(-1 + A_g - iP_g)\chi_- + (1 + A_g + iP_g)\chi_+^*]e^{i\omega t} + c.c.\tag{4.40}$$

Note that χ_μ and χ_μ^* ($\mu = \pm$) are now canonically conjugated variables with the equations of motion in the form

$$\dot{\chi}_\mu = i\frac{\partial(H + V_c(t))}{\partial\chi_\mu^*} - \varepsilon\frac{\partial H}{\partial\chi_\mu^*},\tag{4.41}$$

where the Hamiltonian is given by $H = H_s + H_u$. As can be seen from Eqs (4.40) and (4.29) the interaction $V_c(t)$ vanishes in the case of the totally symmetric A_g, P_g -mode.

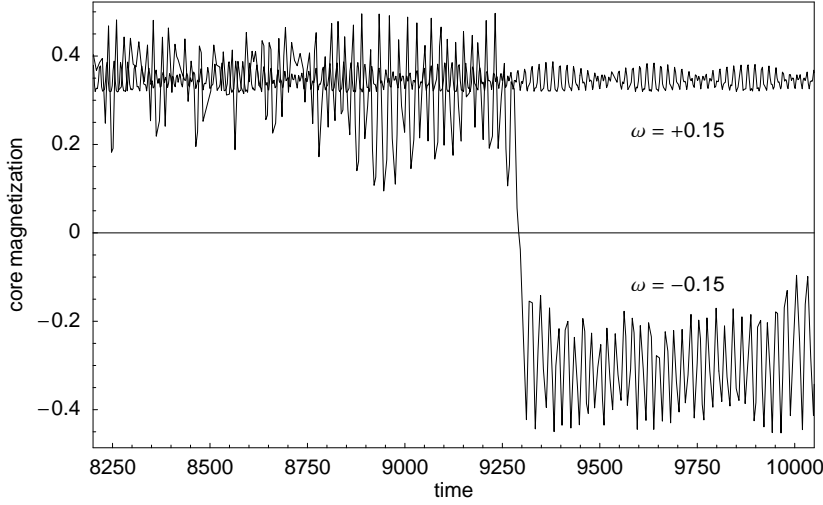


Fig. 4.14: Time evolution of the core magnetization A_g , for amplitude $h = 0.05$ and two opposite frequencies $\omega = \pm 0.05$, from the numerical solution of the reduced core model of eqs. (4.30)-(4.35). Here $J = 1/8$, $\lambda = 0.95$ and $\varepsilon = 10^{-4}$.

Therefore, *switching processes under the action of the spatially uniform magnetic field can occur only as a result of nonlinear mixing between the totally symmetric mode and antisymmetric core modes, where the latter ones do interact with the spatially uniform alternating field.* It is worth noting that the antisymmetric χ_{\pm} modes may be identified with the two lowest modes T_{\pm} of Ref. [86] that produce the cycloidal orbital motion of the vortex center [86, 45]. The equations of motion for the χ_{\pm} modes,

$$\dot{\chi}_+ = i8J(\lambda_c + A_g)\chi_+ - 8J\varepsilon\chi_+ + h(1-i)(1 + A_g + iP_g)e^{i\omega t} \quad , \quad (4.42)$$

$$\dot{\chi}_- = i8J(\lambda_c - A_g)\chi_- - 8J\varepsilon\chi_- + h(i+1)(1 - A_g - iP_g)e^{i\omega t} \quad , \quad (4.43)$$

can be thought of as a microscopic version of the Thiele equations with mass [87], where the gyrovector modulus $G \sim A_g$ is a time dependent quantity which is governed by the equations

$$\dot{A}_g = -8J(\lambda_c P_g + \varepsilon A_g) + h(i+1)(\chi_-^* - \chi_+)e^{i\omega t} + h(1-i)(\chi_- - \chi_+^*)e^{-i\omega t} \quad , \quad (4.44)$$

$$\begin{aligned} \dot{P}_g = & 8J \left[(\lambda_c - \lambda)A_g + \frac{A_g^3}{2} + |\chi_+|^2 - |\chi_-|^2 - \varepsilon P_g \right] \\ & + h(i-1)(\chi_-^* + \chi_+)e^{i\omega t} - h(1+i)(\chi_- + \chi_+^*)e^{-i\omega t} \quad . \end{aligned} \quad (4.45)$$

Thus the modes χ_{μ} (the orbital motion) are excited by the external field (4.1) and they in turn act as drivers giving impetus to the switching dynamics of the vortex.

In the **Fig. 4.14** we show an example of the time evolution of the core mode A_g for two opposite frequencies of the field, based on numerical integration of the reduced core model (4.30)-(4.35). The distinction between the action of clockwise- and counterclockwise-rotating fields can be seen. It should be mentioned also that in the framework of the reduced model the unidirectional character of flipping events is not so well pronounced. As a rule, a significant part of time the system is in a state when

back and forth flips take place. This is, however, in agreement with our full simulations of the LL eqs. (2.34) which show the same behavior in the near-critical case $\lambda \approx \lambda_c$ for which the reduced model was derived (see **Fig. 4.6**).

4.4 Summary

The results presented in this Chapter may be summarized as follows:

- Flipping times do not depend essentially on the size of the system, provided that the lattice is large enough (radius $L \gtrsim 36$). In other words, the switching of the vortex polarization is not much affected by the presence of boundaries.
- A clear correlation exists between the core magnetization dynamics (the oscillations of the core spins in the perpendicular-to-plane direction) and the velocity of the vortex center in the plane of the lattice.
- We found that in the (ω, h) parameters space there is no well-defined curve which separates the region where the flips do not occur from the region where they do. For a given frequency ω and increasing amplitude h we found intervals (“windows”) of intermittent flip and non-flip events.
- The switching process is unidirectional only if the anisotropy parameter λ is not too close to the critical value λ_c . The closer λ to λ_c is, the larger fluctuations of the vortex core magnetization are observed and the more unstable the system is against flips of the vortex polarization in weak fields.
- Switching of the vortex polarization can be achieved also by applying a static magnetic field with both in-plane and out-of-plane components.
- The switching dynamics can be described in terms of a generalized Thiele equation which takes into account a coupling between the vortex polarization dynamics and the motion of the vortex center.

After flipping a heavy “vortex” ($p\omega < 0$) becomes a “light” vortex ($p\omega > 0$), which is a more stable configuration in the presence of the IP rotating field. For the light vortex we will study in the next Chapter the trajectories in the XY plane under the combined action of the field and the damping.

Chapter 5

Vortices and time-dependent fields

2: in-plane dynamics

In the last Chapter we studied the movement of spins in the presence of a rotating IP field, and we were interested in the switching phenomenon of “heavy” vortices, *i.e.* in the dynamics of the spins and the vortex structure in the \hat{z} direction when the gyrovector of the vortex and the angular velocity of the field were antiparallel ($p > 0$ and $\omega < 0$). In this Chapter we turn to the movement of the spins and the vortex structure in the XY plane. Attention is directed to the observation of stable orbits of a “light” vortex ($p > 0$ and $\omega > 0$), in a range of values of the field parameters (ω, h) for which the vortex stays inside the system in a circular stationary movement or limit-cycle. We discuss the failure of the conventional Thiele approach to explain the circular orbits observed in the simulations, and we propose a new collective variable approach, which allows for oscillations of the total magnetization $M(t)$ and describes the in-plane movement of the vortex, by introducing a variable $\Psi(t)$ as a uniform mode of the ϕ field, coupled to the polar coordinates $R(t)$ and $\Phi(t)$ of the vortex. The numerical solutions of this collective variables model show several of the features observed in the simulations of the many-spin system, like the circular limit-cycle and a linear dependence of the orbit radius R_v with the radius L of the system.

5.1 Trajectories of OP vortices driven by in-plane rotating fields

Under the combined action of the driving field (4.1) and the gyrotropic and the damping terms in the LL eqs. (2.34), a rich variety of trajectories arises. In the simplest cases, when the amplitude h of the field is too high or too low, for a particular frequency, the vortex will go towards the border and abandon the system, but in different ways and

for different reasons. From the knowledge that we already have about the response of the vortex under the action of the IP field alone (quasi-static) or the action of the damping alone (almost zero field) we can guess the response of the vortex in these two limiting cases. In the first case, the amplitude of the field is too high and the field at low frequency points almost all the time in the same direction, so the vortex goes towards the boundary of the system in a “drift” movement (distorted only by its own gyrotropic force and the image force, recall the **Fig. 3.10**). In the second case, at very low amplitudes and not too high frequencies, the damping dominates and the vortex goes again outwards, but in a spiral movement (recall the **Fig. 3.5**). If the frequency is relatively high, this spiral can also contain very pronounced cycloidal oscillations, which are damped out while the vortex approaches the border (we show this case for $\omega = 0.045$ and $h = 0.001$ later below). On the other hand, in a middle range of amplitudes and frequencies, the trajectories are mostly “confined”, this is, the vortex stays inside the system for all times. As we will see below, these confined trajectories can be, according to the particular combinations of h and ω , either very irregular paths (where discreteness effects are visible), or converging in time to some limit cycle, most likely circular around the center of the system (though we have also observed cycles switching between two different orbits).

In summary, we can classify the trajectories into three main types: “escaping”, “confined” (where it is meant that no limit cycle is reached) and “limit cycle”.

We will illustrate the different types of trajectories showing results of simulations in a system of radius $L = 36$. Qualitatively, most of the features of these trajectories appear already in smaller systems. A diagram of the types of trajectories as a function of the parameters h and ω , together with some sets of numerical data for the circular limit cycles, will be presented later for $L = 36$.

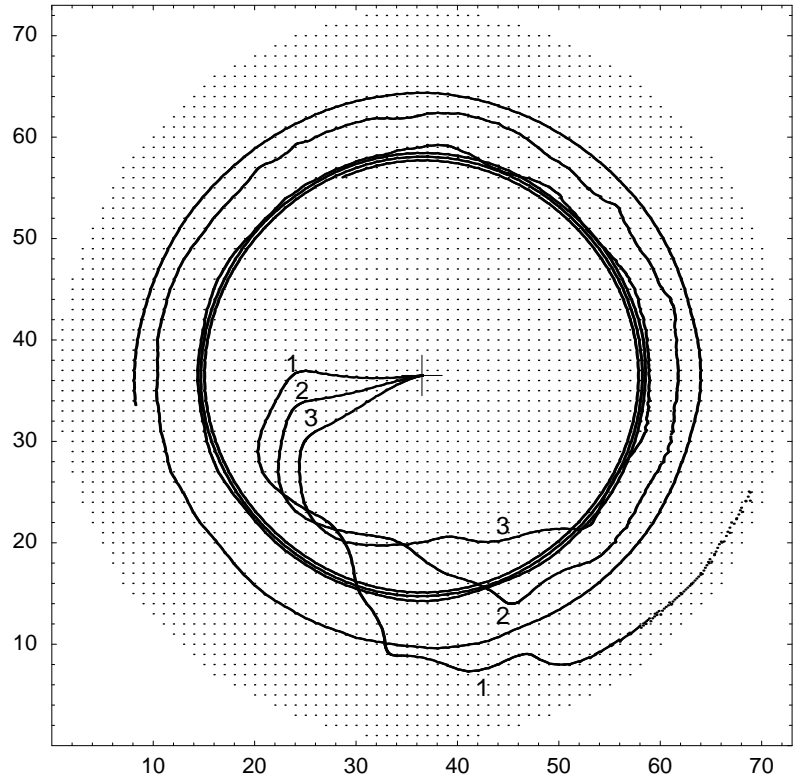
The **Fig. 5.1** shows trajectories of a vortex in a field of rather high amplitude $h = 0.008$, for three different frequencies. At the smallest frequency $\omega = 0.01$, the field can be considered quasi-static (at this amplitude), and the vortex leaves the system rather soon (in about 300 time units, for $\varepsilon = 0.01$). At the next higher frequency $\omega = 0.02$, the vortex also leaves the system, but turning several times on an spiral outwards, as is typical for a damping-dominated regime.

At the highest frequency shown, $\omega = 0.03$, in contrast to the two previous cases, the trajectory gets confined, and it actually orders itself into a spiral inwards, converging slowly to a limit cycle, which is a circle around the center of the system. Much faster is the convergence for $\omega = 0.04$, to a circular limit cycle with another orbit radius R_v ; the trajectory of this case is shown in **Fig. 5.2**. Note that the vortex travels first outwards, and then approaches the circular limit cycle from outside.

The way to approach the circular trajectory can be different, depending on the initial

Fig. 5.1: Trajectories of a vortex in a system of radius $L = 36$, with anisotropy $\lambda = 0.92$ and damping $\varepsilon = 0.01$, at a fixed (rather high) amplitude $h = 0.008$ and three frequencies:

- (1) $\omega = 0.01$
- (2) $\omega = 0.02$
- (3) $\omega = 0.03$



position of the vortex, but the final orbit radius R_v is in all the cases the same, for fixed system size and field parameters (provided that the initial position is not too close to the boundary, such that the vortex does not get more attracted to the image vortex than to the limit cycle “attractor”). An example of this effect, for a system with radius $L = 24$, is shown in **Fig. 5.5**. We verify, thus, that the system keeps no memory of the initial position of the vortex, and, therefore, it is justified to denote these circular trajectories with the name of “limit cycles”. A remarkable fact of the simulations is that the orbit radius R_v and frequency Ω depend essentially on the field parameters (ω, h) and the system radius L , but not on the damping constant ε . The effect of changing the damping is to accelerate or retard (and even to facilitate or prevent) the process of reaching the circular orbit –providing the appropriate field parameters– but it does not affect the size of this circular orbit, if the latter is established¹. We note, however, that the reaching of this stationary state needs both the field *and* the damping, because we verify that, once the equilibrium is established, the switching-off of any of these terms in the equations of motion immediately destroys the circular movement.

Concerning the way to escape out of the system, as mentioned above, the trajectories are also different depending on the field parameters. We notice that in all the cases

¹We have changed the damping value ε up to a factor 6, from $\varepsilon = 0.002$ to $\varepsilon = 0.012$, obtaining changes in R_v and Ω after the fifth decimal.

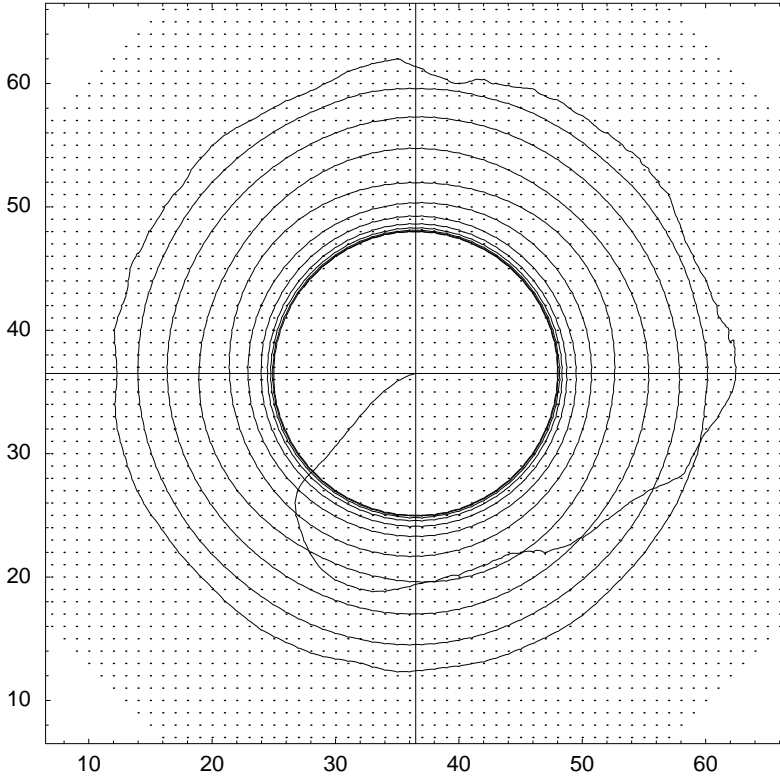


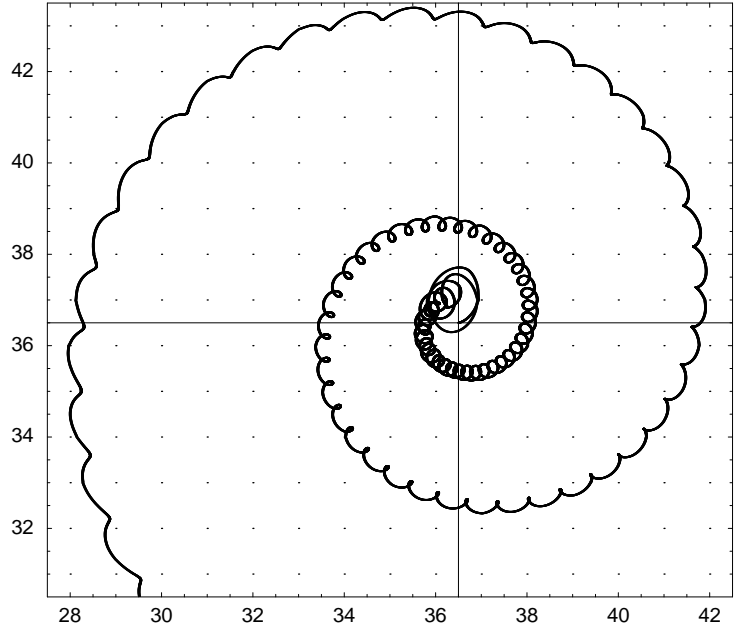
Fig. 5.2: Trajectory of a vortex, in a system like in **Fig. 5.1** with $\omega = 0.04$ and $h = 0.008$, showing the convergence to a circular orbit.

when an outwards spiral is developed, no convergence to any cycle is observed, but all outwards spirals end up in the border. In the process of escaping the vortex can also be subject to large oscillations, like the cases observed for $\omega = 0.0045$ and $\omega = 0.005$, with $h = 0.001$, the former shown in **Fig. 5.3** (in this figure there is an initial phase $\beta_0 = \pi$ –different from all other simulations in this Chapter, with $\beta_0 = 0-$, whose only effect was to rotate the whole picture in the XY plane).

As a guide to see where each trajectory appears, in **Fig. 5.4** we show a diagram of the three main types of trajectories, as they appear in the system of radius $L = 36$, with anisotropy $\lambda = 0.92$ and damping $\varepsilon = 0.01$, as a function of the field parameters (ω, h) . Similarly to what we found in the Chapter 4, in the diagram of switching events (see **Fig. 4.9**), which was drawn for heavy vortices ($\omega < 0$), in the present case of light vortices we also find “windows”, *i.e.* events which are not expected in a particular region (for instance, the point $(0.03, 0.006)$ in the diagram). The zoom-in of any region of the diagram containing windows shows again a similar behavior. We can also observe that the response of the light vortex shows a high sensitivity to small variations of the field parameters, and that this behavior is not monotonous (follow, for example, the line of $h = 0.008$ for increasing frequencies). All this features are again, like in the case of the flips studied in Chapter 4, hints for the appearance of chaos in this system.

Although most of the trajectories which converge to limit cycles end up in a circular orbit around the center of the system, we have observed a few cases of a limit cycle

Fig. 5.3: Escaping vortex trajectory with large oscillations, in a system like in **Fig. 5.1** with $\omega = 0.045$ and $h = 0.001$, and with initial phase of the field $\beta_0 = \pi$.



which switches between an elliptical and an almost circular orbit in each turn, as shown in the top left panel of **Fig. 5.6**. In the same figure are also shown, as examples, some other cases of confined trajectories which are not observed to converge to limit cycles, as well as a trajectory which converges to a circular movement in a diminutive scale

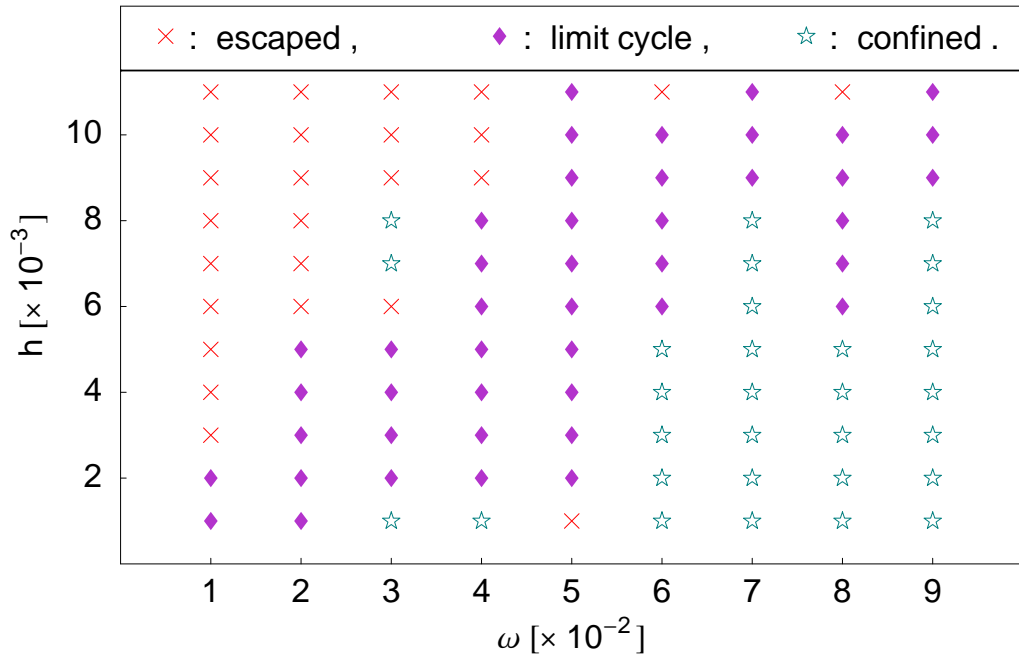


Fig. 5.4: Diagram of types of trajectories in the (ω, h) field parameters space –the rest of parameters like in **Fig. 5.1**. “confined” means that no limit cycle was reached, though the vortex stayed inside the system, during the time of observation ($t \lesssim 20000$).

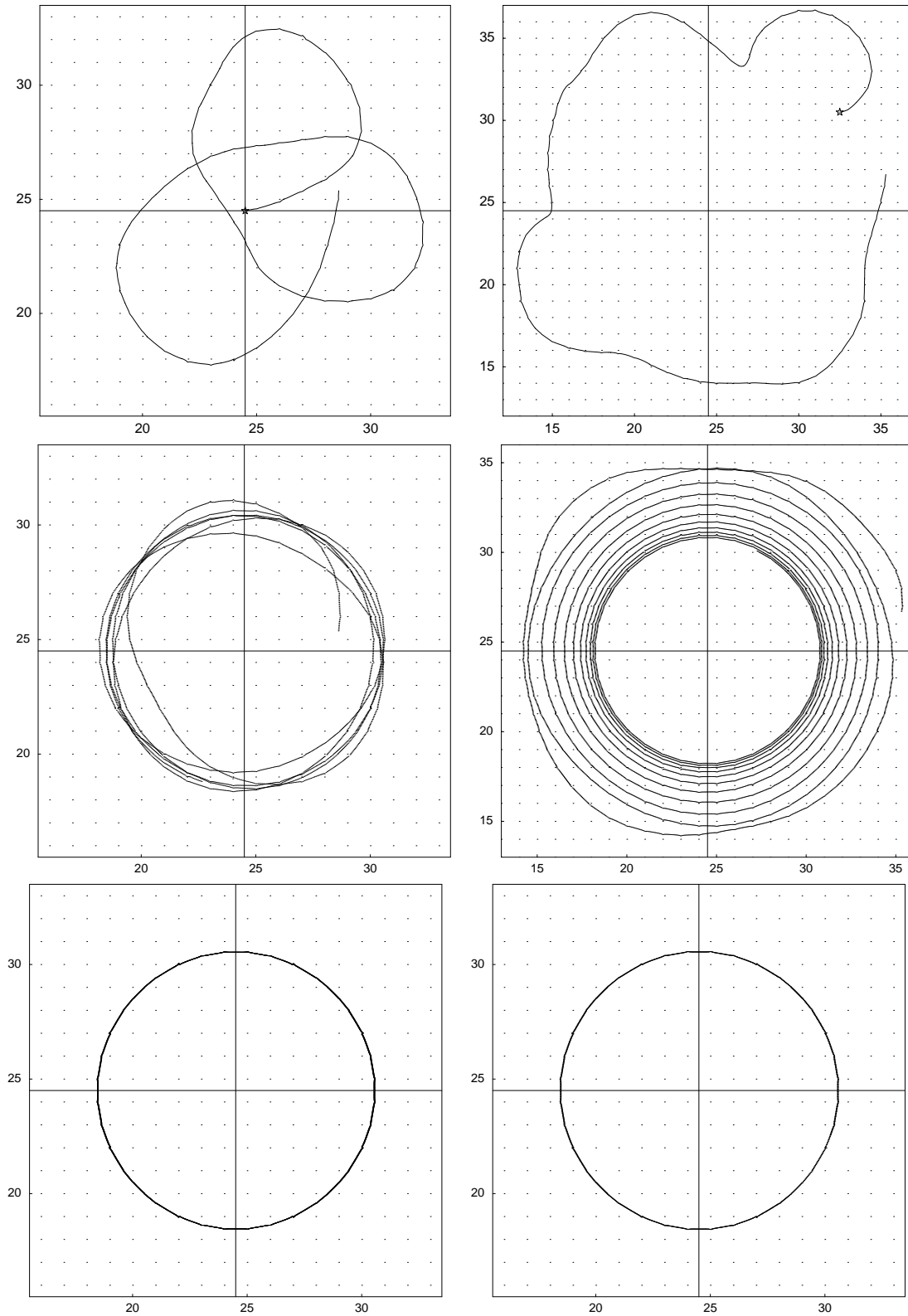


Fig. 5.5: Trajectories in a system of radius $L = 24$, in a field with $h = 0.004$ and $\omega = 0.02$, with $\varepsilon = 0.01$ and $\lambda = 0.92$. Time runs from up to bottom. Left panels: the vortex is launched from the center of the lattice $\vec{X}_c = (24.5, 24.5)$ (upper-left panel) and converges to a circle (bottom-left panel). The same circle is reached on a different path in the panels on the right, where the vortex is launched from $\vec{X} = (32.5, 30.5)$.

(top right panel, compare with **Fig. 5.3**), and a trajectory which escapes at extremely long times due to a large number of oscillations around a mean spiral (middle left panel), all of them at relatively high frequencies. The two bottom panels and the middle-right panel of **Fig. 5.6** show also some irregular confined trajectories, where strong discreteness effects are visible, the last trajectory even looking rather chaotic.

The purpose of the next Sections will be to study the simplest circular limit cycles, assuming that the conditions to its formation are given, and we will discuss and formulate possible models for understanding this phenomenon.

5.1.1 Circular limit cycles

In the rest of this Chapter, we will concentrate the attention on the simplest case of a circular limit cycle. In this section we give some results of simulations concerning the dependences of the orbit radius R_v and frequency Ω on the size of the system and the field parameters, once the circular orbit is completely established. In this stationary movement, the signals of the total energy and total magnetization (sum of S_z over all the spins) *vs.* time show sinusoidal oscillations of small amplitude, both signals with the same frequency ω_E (which is different from the orbit frequency Ω).

In **Fig. 5.7** we show the radius R_v of the vortex orbit in the circular limit cycle, as a function of the radius L of the system, for fixed field frequency and several field amplitudes. The lines drawn through the points are linear fits of the form $R_v = a + bL$. The linear dependence of R_v on the size of the system is very clear.

In **Fig. 5.8** we plot the frequency Ω of the vortex orbit, again *vs.* the system radius L , for fixed frequency and several amplitudes of the field. The lines drawn are fits of the form $\Omega = d + eL^{-1}$, which seem to represent very well the numerical data.

In **Table 5.1** we show the results of these two fits to the data of the simulations. These two figures together suggest that, whenever we can neglect the product bd , which

ω	h	a	b	$d [\times 10^{-3}]$	e
0.02	0.002	-1.28377	0.15369	2.11766	0.36042
0.02	0.003	-1.30196	0.21992	1.18404	0.31516
0.02	0.004	-0.85839	0.28753	1.07382	0.25435
0.03	0.002	-1.04183	0.13107	-0.00438	0.58697
0.03	0.003	-1.08112	0.17321	-0.01267	0.50927
0.03	0.004	-1.04543	0.21688	0.09868	0.44211
0.03	0.006	-0.66364	0.31101	0.65587	0.32278
0.04	0.002	-1.20353	0.13865	-3.47731	0.76454
0.04	0.003	-1.02267	0.16376	-1.30830	0.64438
0.04	0.004	-0.99401	0.19500	-0.73235	0.57040
0.04	0.006	-0.89057	0.26327	-0.05692	0.45585

Table 5.1: Results of the fits $R_v = a + bL$ and $\Omega = d + eL^{-1}$ to the simulation data of **Figs. 5.7** and **5.8**, for various field parameters (ω, h) .

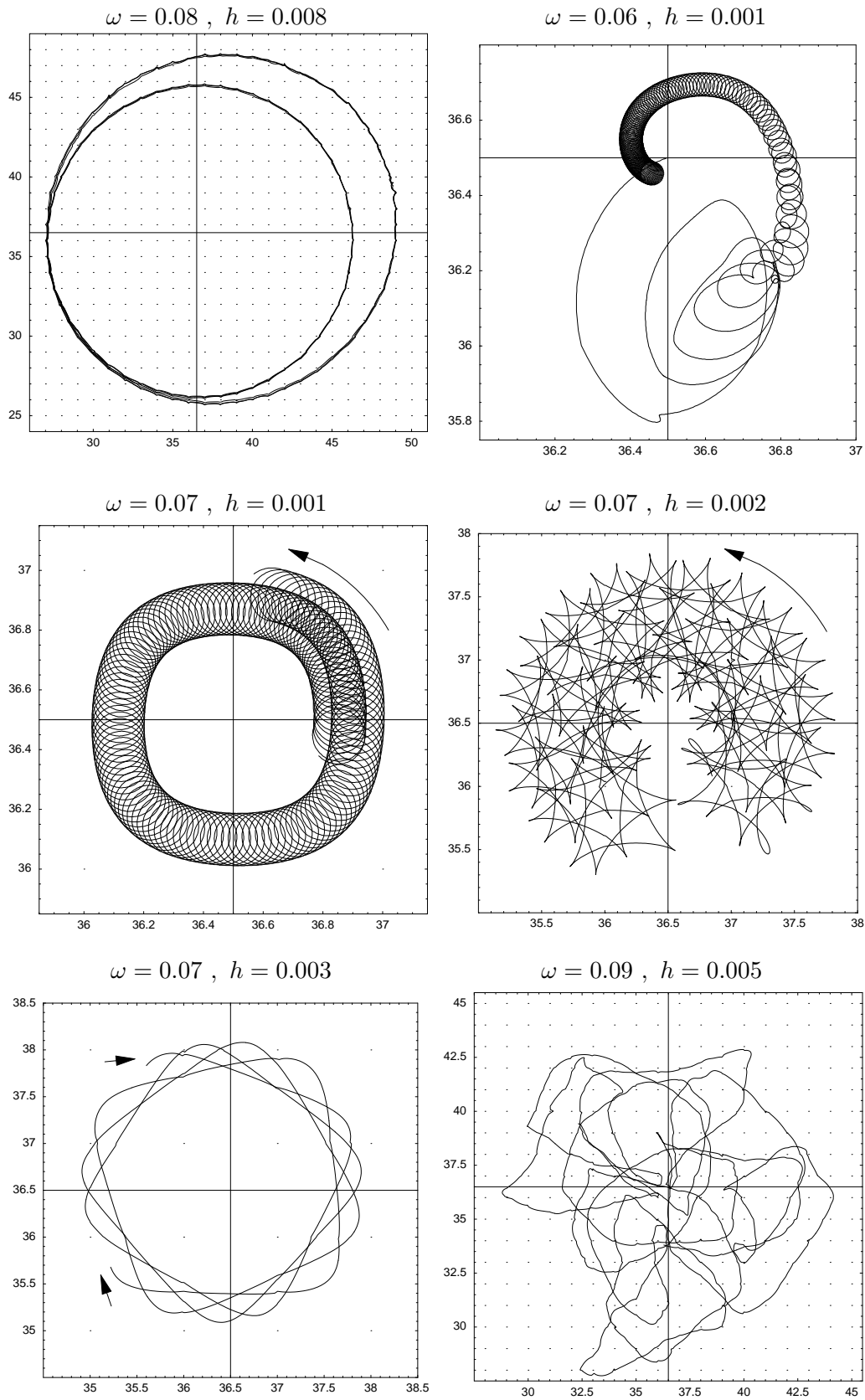


Fig. 5.6: Some other examples of trajectories. Note the different scales of movement.

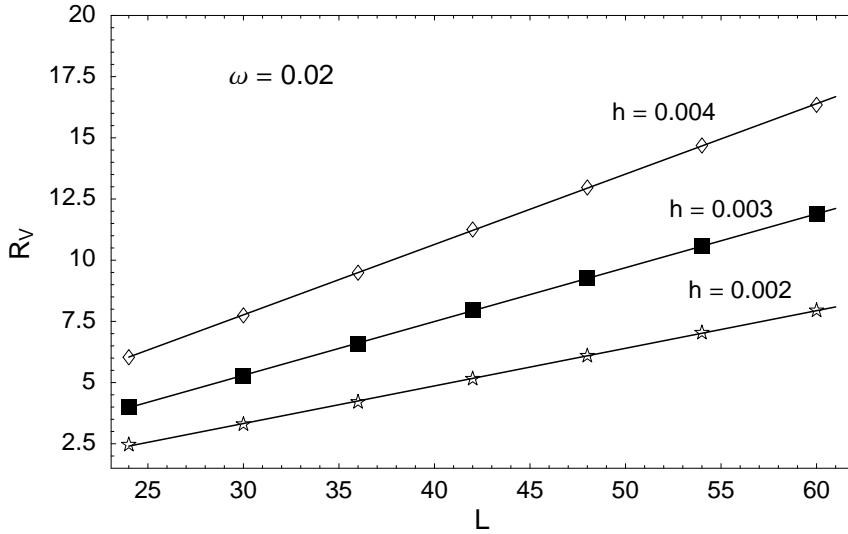


Fig. 5.7: Radius of the vortex orbit R_v vs. the system radius L , in the circular limit cycle, for a fixed field frequency ω and several amplitudes h .

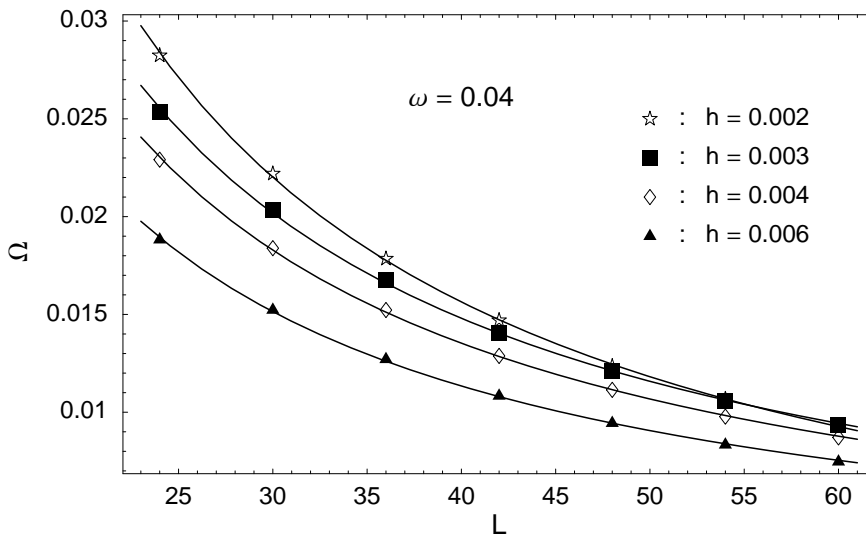


Fig. 5.8: Frequency of the vortex orbit Ω vs. the system radius L , in the circular limit cycle, for a fix field frequency ω and several amplitudes h .

from the table is seen to be of $\mathcal{O}(10^{-4})$, the average tangential velocity of the vortex $V = R_v \Omega$ must approach a constant value, which depends on the field parameters only, for increasing system size. The velocity V as a function of L is plotted in **Fig. 5.9**. We can observe that V practically saturates to a constant at the largest values of L . For completeness, we present as well some tables of simulation results of R_v and Ω , for system sizes in **Table 5.2** and different field parameters in **Table 5.3**. In the last of these tables we can see also that the frequency of oscillations of the total energy, ω_E , after the system relaxed to the circular limit cycle, is identical with that of the total magnetization ω_{M_z} . There is a case in the same table, namely for $\omega = 0.05$ and $h = 0.003$, where beats were observed in the energy and the magnetization signals, even when the vortex had reached a circular trajectory. Note that the orbit frequencies Ω are always much lower than the driving field frequencies ω .

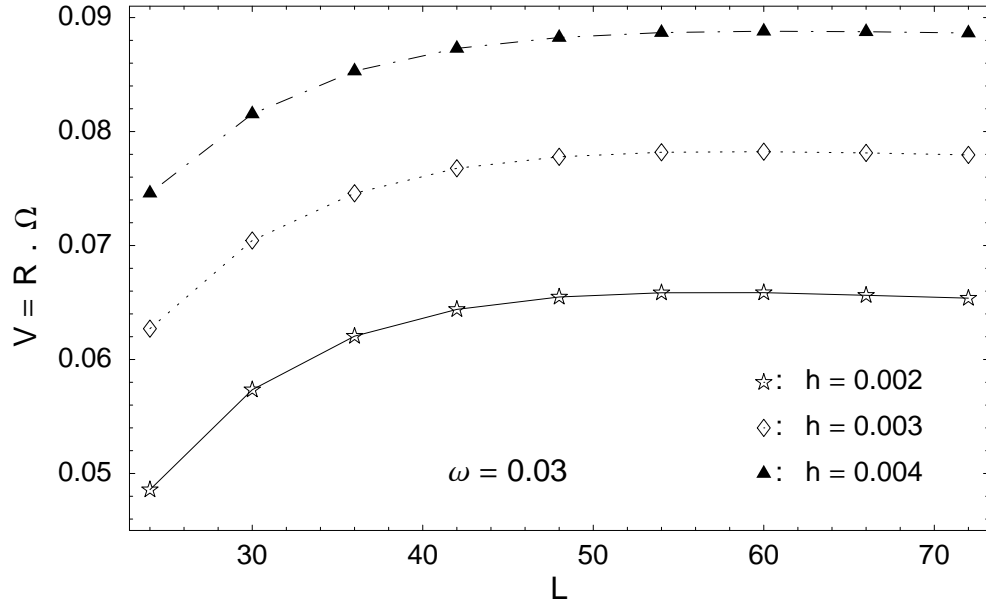


Fig. 5.9: Velocity of the vortex orbit $V = R_v \Omega$ vs. the system radius L , in the circular limit cycle, for a fixed field frequency ω and several amplitudes h .

h	L	R_v	Ω
0.002	24	2.0416	0.0237922
0.002	30	2.8711	0.0199736
0.002	36	3.6916	0.0168078
0.002	40	4.5069	0.0142885
0.002	48	5.2958	0.0123655
0.002	54	6.0794	0.0108325
0.002	60	6.8349	0.0096366
0.002	66	7.5877	0.0086498
0.002	72	8.3354	0.0078440
0.003	24	3.0112	0.0208235
0.003	30	4.0957	0.0171986
0.003	36	5.1679	0.0144321
0.003	40	6.2437	0.0122967
0.003	48	7.2808	0.0106834
0.003	54	8.3172	0.0094001
0.003	60	9.3189	0.0083951
0.003	66	10.3303	0.0075627
0.003	72	11.3301	0.0068800
0.004	24	4.0840	0.0182655
0.004	30	5.4413	0.0149865
0.004	36	6.7830	0.0125772
0.004	40	8.1197	0.0107510
0.004	48	9.4144	0.0093742
0.004	54	10.7145	0.0082771
0.004	60	11.9751	0.0074156
0.004	66	13.2465	0.0067006
0.004	72	14.5045	0.0061116
0.006	24	6.7420	0.0140090
0.006	30	8.6855	0.0115192
0.006	36	—	—
0.006	40	12.4622	0.0084252
0.006	48	14.2939	0.0074121
0.006	54	16.1405	0.0065958
0.006	60	17.9350	0.0059490

Table 5.2: Typical sets of data, as a function of the size L for the frequency $\omega = 0.03$, and several amplitudes h . There is a “window” in the middle ($h = 0.006$, $L = 36$), where the vortex escaped from the system. For the frequency $\omega = 0.02$, the amplitude $h = 0.006$ is already too high, and the vortex escapes for all the sizes.

ω	h	R_v	Ω	ω_E	ω_{M_z}
0.015	0.002	5.19112	0.009599	0.038397	0.038397
0.020	0.002	4.20599	0.012664	0.050659	0.050660
0.025	0.002	3.81915	0.015064	0.060282	0.060287
0.030	0.002	3.69158	0.016808	0.067251	0.067149
0.035	0.002	3.70005	0.017845	0.071397	0.071398
0.040	0.002	3.77435	0.017846	0.071409	0.071409
0.045	0.002	3.73297	0.018628	0.074561	0.074541
0.050	0.002	3.80943	0.019053	0.076201	0.076102
0.015	0.003	8.90246	0.007255	0.029037	0.029153
0.020	0.003	6.58863	0.010218	0.040762	0.040761
0.025	0.003	5.63241	0.012569	0.050398	0.050380
0.030	0.003	5.16784	0.014432	0.057742	0.057735
0.035	0.003	4.96004	0.015817	0.063407	0.063265
0.040	0.003	4.89776	0.016739	0.066839	0.066834
0.045	0.003	4.95381	0.017053	0.068226	0.068219
0.050	0.003	5.15066	0.016415	beats	beats
0.015	0.004	15.36210	0.004994	beats	beats
0.020	0.004	9.48774	0.008313	0.033266	0.033201
0.025	0.004	7.67228	0.010679	0.042706	0.042721
0.030	0.004	6.78301	0.012577	0.050342	0.050355
0.035	0.004	6.30807	0.014069	0.056305	0.056296
0.040	0.004	6.05712	0.015225	0.061124	0.060885
0.045	0.004	5.96078	0.016010	0.064111	0.064059
0.050	0.004	5.99702	0.016339	0.065350	0.065376
0.020	0.005	13.41890	0.006614	0.026278	0.026253
0.025	0.005	10.04670	0.009119	0.036575	0.036355
0.030	0.005	8.56006	0.011062	0.044239	0.044247
0.035	0.005	7.75803	0.012633	0.050468	0.050454
0.040	0.005	7.29353	0.013883	0.055527	0.055522
0.045	0.005	7.04250	0.014827	0.059261	0.059338
0.050	0.005	6.93676	0.015491	0.062162	0.062158
0.055	0.005	6.98495	0.015741	0.062893	0.062886

Table 5.3: Data from simulations, for some circular trajectories in a system with radius $L = 36$, anisotropy $\lambda = 0.92$, damping $\varepsilon = 0.01$.

5.2 The Thiele approach with a time-dependent magnetic force

We saw in the Chapter 3 that the Thiele equations (3.59) or (3.61), which assume that the vortex is in a stationary movement and has a rigid shape, describe with high accuracy the dissipative dynamics of vortices at zero field. As long as there is a stationary movement in the circular limit cycle with the AC rotating field (4.1), we may try to investigate this movement with the same kind of approach as in the Thiele

equations. For this we need to estimate the effective force \vec{F}_h exerted on the vortex by the magnetic field, at least within the same order of approximation as in the Thiele equation. The field (4.1) produces a Zeeman energy density

$$\mathcal{E}_h(\theta, \phi) = -\vec{S} \cdot \vec{h}(t) = -h \sin \theta \cos(\phi - \omega t - \beta_0) . \quad (5.1)$$

The expression for the force exerted by the magnetic field (see Ref. [31]), is given by

$$\vec{F}_h = \int d^2x \left(\vec{\nabla}_\theta \frac{\partial}{\partial \theta} + \vec{\nabla}_\phi \frac{\partial}{\partial \phi} \right) \mathcal{E}_h(\theta, \phi) , \quad (5.2)$$

where the integration is made over the *finite domain*, which is our circular system, and therefore it depends in general on the coordinates of the vortex center $\vec{X}(t) = R(t)(\cos \Phi(t), \sin \Phi(t))$. We calculate this effective force in the Appendix E, and the result is

$$\vec{F}_h = -h \left(c\pi + K(\rho) \right) \left(\cos(\omega t) \hat{x} + \sin(\omega t) \hat{y} \right) , \quad (5.3)$$

where $c = -0.624 r_v$ is a constant, with r_v the radius of the vortex, and

$$K(\rho) = L \left[E(2\pi - \Phi | \rho) + E(\Phi | \rho) \right]$$

where $\rho = R^2/L^2$ and $E(\Phi | \rho)$ is an elliptic function of the second kind. Note that the combination does not depend on the angle Φ .

With the two forces \vec{F}_h from eq. (5.3) and \vec{F}_I from eq. (3.51), the dynamical equations for the collective coordinates $\vec{X}(t)$, within the stationary movement and rigid-shape assumptions, take the form

$$\begin{aligned} g \dot{X} + G \dot{Y} &= C(R) X + B(R) \cos(\omega t) \\ -G \dot{X} + g \dot{Y} &= C(R) Y + B(R) \sin(\omega t) \end{aligned} \quad (5.4)$$

with $C(R) = -2\pi q q_I / (L^2 - R^2)$ and $B(R) = -h (c\pi + K(R))$. In the Appendix E, we also make some remarks about the consistence of this approach, and here we complete the discussion about why equations can *not* describe the dynamics observed in the numerical simulations with the time dependent field.

Let us come back to the Thiele eqs. (3.61)

$$g \dot{R} + G R \dot{\Phi} + \frac{\partial \mathcal{U}}{\partial R} = 0 \quad (5.5a)$$

$$-G \dot{R} + g R \dot{\Phi} + \frac{1}{R} \frac{\partial \mathcal{U}}{\partial \Phi} = 0 \quad (5.5b)$$

Can we guess something about the effective force produced by the rotating field on the

vortex, already from the structure of these equations? We can argue that in the limit cycle, *i.e.* asymptotically, the force should not depend on the angle Φ , because the balance concerns strictly the variable R . Thus, in this limit we should have an effective 1-D problem for R .

Then, in the approach of the eqs. (3.61b), it should be valid that

$$\frac{\partial \mathcal{U}}{\partial \Phi} \rightarrow 0 \quad \text{as} \quad t \rightarrow \infty \quad (5.6)$$

From the second equation (5.5b) we get

$$\dot{\Phi} \rightarrow \frac{G}{g} \frac{\dot{R}}{R} \quad (5.7)$$

and inserting in the first equation (5.5a) we have

$$\frac{G^2 + g^2}{G} \dot{R} + \frac{\partial \mathcal{U}}{\partial R} \rightarrow 0 \quad (5.8)$$

This means that in a circular motion, where $\dot{R} = 0$, there must be a balance of forces in the radial direction as well, such that

$$\frac{\partial \mathcal{U}}{\partial R} \rightarrow 0 \quad . \quad (5.9)$$

Thus, in the limit cycle, the force by the AC field must be *equal* and opposite to the force of the image alone,

$$F_h \rightarrow F_I \quad (5.10)$$

However, the r.h.s. does not depend on the field parameters, while the trajectories in our simulations clearly do. This means that a Thiele approach by itself can not describe the simplest trajectory, the circular limit cycle, in the presence of the rotating field, and, therefore, the Ansatz leading to this approach needs to be extended.

5.3 A new collective coordinate approach

According to the results of the previous Sections, we need to search for a simple extension of the stationary movement Ansatz (3.40), which could reproduce, at least qualitatively, the formation of the circular limit cycles. We start from the continuum

description of the Hamiltonian and the magnetic potential (in normalized units)

$$\mathcal{H} = \frac{1}{2} \int d^2x \left\{ \frac{(\nabla m)^2}{1 - m^2} + (1 - m^2) (\nabla \phi)^2 + K m^2 \right\} \quad (5.11a)$$

$$\mathcal{V}(t) = -h \int d^2x \sqrt{1 - m^2} \cos(\phi - \omega t) \quad . \quad (5.11b)$$

The dynamics of the system is described by the equations

$$\frac{\partial m}{\partial t} = - \frac{\delta [\mathcal{H} + \mathcal{V}(t)]}{\delta \phi} - \varepsilon (1 - m^2) \frac{\partial \phi}{\partial t} \quad (5.12a)$$

$$\frac{\partial \phi}{\partial t} = \frac{\delta [\mathcal{H} + \mathcal{V}(t)]}{\delta m} + \frac{\varepsilon}{(1 - m^2)} \frac{\partial m}{\partial t} \quad (5.12b)$$

At zero damping the eqs. (5.12) can be obtained from the variational principle $\delta \mathcal{S} = 0$ where the action \mathcal{S} is given by

$$\mathcal{S} = \int \mathcal{L} dt \quad , \quad (5.13)$$

with

$$\mathcal{L} = - \int d^2x (1 - m) \frac{\partial \phi}{\partial t} - [\mathcal{H} + \mathcal{V}(t)] \quad (5.14)$$

being the Lagrangian of the system. The uniform state $m = 1$ was subtracted from the first term. We want an Ansatz that removes the restriction to a rigid shape and constant magnetization, during the movement, as imposed in the Thiele-like approach. Therefore, we try an Ansatz with two additional collective coordinates $M(t)$ and $\Psi(t)$ as follows

$$m(\vec{x}, t) = f \left(\sqrt{\frac{M_0}{M(t)}} \frac{|\vec{x} - \vec{R}(t)|}{r_v} \right) \quad , \quad \phi(\vec{x}, t) = \Psi(t) + \Phi(\vec{x}, \vec{R}(t)) \quad (5.15)$$

where $M(t)$ is the out-of-plane magnetization of the system:

$$M(t) \equiv \int m(\vec{x}, t) d^2x \quad (5.16)$$

with the coefficient M_0 given by

$$M_0 = 2\pi \int f(\rho) \rho d\rho \quad , \quad \rho = \frac{|\vec{x}|}{r_v} \quad . \quad (5.17)$$

The function $\Psi(t)$ describes a uniform in-plane motion. The function $f(\rho)$, with $r_v \equiv 1/\sqrt{K}$ being the characteristic length of the static OP magnetization distribution, and the function $\Phi(\vec{x}, \vec{R})$, are the static solutions of eqs. (5.12) with free boundary conditions. In the case of a circular system with radius L , $\Phi(\vec{x}, \vec{R})$ is given by (3.27) and the static polar angle $\theta(r)$, given by the relation $f(r) \equiv \cos \theta(r)$, satisfies the equation

$$\frac{d^2\theta}{dr^2} + \frac{1}{r} \frac{d\theta}{dr} + \frac{1}{2} \left(1 - \frac{1}{r^2}\right) \sin 2\theta = 0. \quad (5.18)$$

together with the boundary conditions

$$\theta \rightarrow \frac{\pi}{2} \quad , \quad \text{for } r \rightarrow \infty \quad , \quad \text{and } \theta(0) = 0 \quad .$$

Inserting the Ansatz (5.15) into the eq. (5.14) we obtain an effective Lagrangian in the form

$$\mathcal{L} = T - E_0 - \mathcal{H} - \mathcal{V}(t) \quad , \quad (5.19)$$

where

$$T = M \dot{\Psi} + \pi R^2 \dot{\Phi} \quad (5.20)$$

is the effective kinetic energy (see *e.g.* Ref. [47] for a derivation of the 2nd term in T), R and Φ are the polar coordinates² of the vortex ($X = R \cos \Phi$, $Y = R \sin \Phi$),

$$\mathcal{H} = 2\pi \ln(L^2 - R^2) - \pi \ln M + \pi \frac{M}{M_0} \quad (5.21)$$

is the energy of the vortex which takes into account the interaction with the vortex image (see *e.g.* [10]), and

$$\mathcal{V}(t) = \pi h R L \cos(\Psi + \Phi - \omega t) \quad (5.22)$$

is the vortex-magnetic field interaction energy. The constant energy E_0 does not affect the dynamics of the system. The eqs. (5.19)-(5.22) were obtained using the following conditions and facts:

- The vortex is always far away from the boundary: $L \gg R$.
- Taking into account that the out-of-plane component m decays exponentially, in the integrals which contain $f(r)$ we can neglect finite-size effects, *i.e.* $L \rightarrow \infty$.
- We also took into account the relation $\int_0^\infty \cos^2 \theta(r) r dr = 1/2$, which was obtained in Ref. [42].

² we reserve the notation R_v for $R(t)$ evaluated *in* the circular limit cycle.

From Eqs. (5.19)-(5.22) we then obtain that in this collective coordinate approach the vortex dynamics is governed by the following set of equations (see Appendix E.2 for details)

$$2\pi \dot{R} - \varepsilon W R \dot{\Phi} = -\pi h L \sin(\Psi + \Phi - \omega t) \quad , \quad (5.23a)$$

$$2\pi R \dot{\Phi} + \varepsilon W \dot{R} = \frac{4\pi R}{L^2 - R^2} - \pi h L \cos(\Psi + \Phi - \omega t) \quad , \quad (5.23b)$$

$$\dot{M} + \varepsilon \pi \left((L^2 - r_v^2) \dot{\Psi} + R^2 \dot{\Phi} \right) = \pi h R L \sin(\Psi + \Phi - \omega t) \quad (5.24a)$$

$$\dot{\Psi} - \frac{\varepsilon c r_v^2}{M_0} \frac{\dot{M}}{M} = \pi \left(\frac{1}{M_0} - \frac{1}{M} \right) \quad (5.24b)$$

where

$$W \approx 2\pi \ln L \quad (5.25)$$

(see Appendix E.2) and c is a numerical coefficient given by

$$c = \frac{\pi}{2} \int_0^\infty r^3 \left(\frac{d\theta}{dr} \right)^2 dr. \quad (5.26)$$

The first two equations (5.23) are similar to the Thiele equations for the motion of the vortex center, except that they are coupled to the last two equations through the newly introduced collective coordinate $\Psi(t)$. The last two eqs. (5.24) describe an internal dynamics of the vortex, through $M(t)$ and $\Psi(t)$, and its coupling with the motion of the vortex center.

A further simplification is achieved by considering the case when the driving force (h) and the damping (ε) are weak and the deviation of the out-of-plane component from its static value is small:

$$M = M_0 + \mu, \quad \mu \ll 1. \quad (5.27)$$

Linearized with respect to μ , the eqs. (5.24a) and (5.24b) take the form

$$\dot{\mu} + \varepsilon \pi \left((L^2 - r_v^2) \dot{\Psi} + R^2 \dot{\Phi} \right) = \pi h R L \sin(\Psi + \Phi - \omega t) \quad , \quad (5.28a)$$

$$\dot{\Psi} - \frac{\varepsilon c r_v^2}{M_0^2} \dot{\mu} = \frac{\pi}{M_0} \mu \quad . \quad (5.28b)$$

Neglecting all terms of the order of ε^2 and εh , we get an equation for the spatially

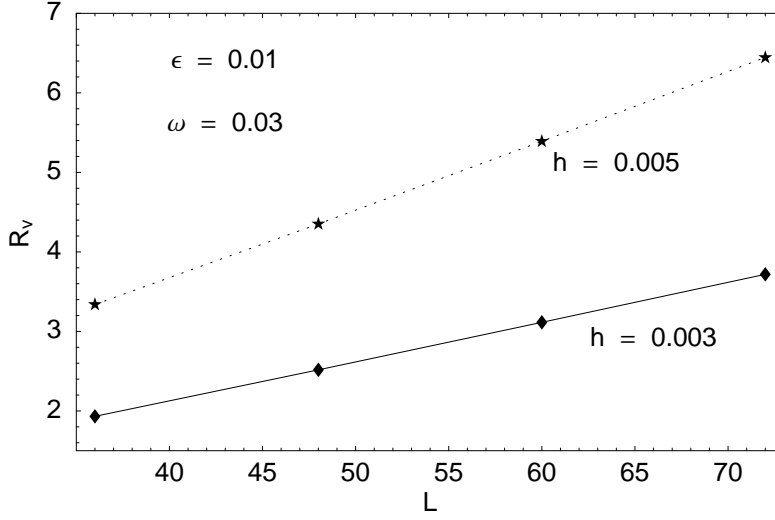


Fig. 5.10: radius R_v of the circular limit cycle from the model (5.30) vs. the system radius L , for a fixed field frequency ω and two amplitudes h .

uniform rotation angle Ψ in the form

$$\frac{M_0^2}{\pi^2} \ddot{\Psi} + \varepsilon (L^2 - r_v^2) \dot{\Psi} + \varepsilon R^2 \dot{\Phi} = h R L \sin(\Psi + \Phi - \omega t). \quad (5.29)$$

Considering that we are interested in the cases when $L \gg 1$, we can neglect also the first term on the l.h.s. of eq. (5.29) (*i.e.* neglect an inertia effect) and obtain in this approximation a vortex dynamics governed by the equations

$$\begin{aligned} \dot{R} &= \frac{1}{4\pi^2 + \varepsilon^2 W^2} \left(\varepsilon W \left(\frac{4\pi R}{L^2 - R^2} - \pi h L \cos(\psi - \omega t) \right) - 2\pi^2 h L \sin(\psi - \omega t) \right), \\ R L^2 \dot{\psi} &= \frac{L^2 - R^2}{4\pi^2 + \varepsilon^2 W^2} \left(\frac{8\pi^2 R}{L^2 - R^2} - 2\pi^2 h L \cos(\psi - \omega t) - \varepsilon W \pi h L \sin(\psi - \omega t) \right) \\ &\quad - \frac{h R^2 L}{\varepsilon} \sin(\psi - \omega t), \quad (5.30) \\ R \dot{\Phi} &= \frac{1}{4\pi^2 + \varepsilon^2 W^2} \left(\frac{8\pi^2 R}{L^2 - R^2} - 2\pi^2 h L \cos(\psi - \omega t) - \varepsilon W \pi h L \sin(\psi - \omega t) \right), \end{aligned}$$

where $\psi \equiv \Psi + \Phi$ was defined. The numerical solutions of this set of equations gives for a wide range of field parameters the circular limit cycles that we are looking for. The model exhibits qualitatively the same features that appear in our simulations, like the linear dependence of R_v on the radius L of the system. This can be seen in **Fig. 5.10** where we plot R_v for different L , from the numerical solutions of eqs. (5.30).

The stationary state of the system (5.30) can also be calculated by means of the relations

$$\dot{R}_v = 0, \quad \psi = \omega t + \alpha, \quad \dot{\alpha} = 0. \quad (5.31)$$

Inserting eq. (5.31) into the eqs. (5.30) we get

$$\sin \alpha = \frac{\epsilon W \omega}{h} \frac{\xi}{\pi(1 - \xi^2) + W \xi^2} , \quad (5.32a)$$

$$\cos \alpha = -\frac{2\pi}{h} \frac{\xi}{\pi(1 - \xi^2) + W \xi^2} \left(\omega - \frac{2}{\pi L^2} \frac{\pi(1 - \xi^2 + W \xi^2)}{1 - \xi^2} \right) , \quad (5.32b)$$

$$\Omega = \frac{\pi \omega}{\pi(1 - \xi^2) + W \xi^2} \quad (5.32c)$$

where $\xi \equiv R_v/L$ is the scaled radius of the orbit and $\Omega \equiv \dot{\Phi}$ is the frequency of the vortex rotation. Numerical estimates of these quantities using the equations (5.32), are in the order of magnitude of the corresponding results from simulations, so the agreement is at least qualitative.

To summarize, it has been shown to be useful an Ansatz which includes two additional collective variables (compared with the number of variables of the Thiele approach), allowing for internal oscillations of the shape of the vortex. This idea was motivated by our previous observations of the coupling existing between the oscillation of the OP components of the spins and the in-plane dynamics of the spins, which is another way to understand the action of the constraint $|\vec{S}|^2 = S_c^2$ on the dynamics of the spins. Concerning the values of the orbit radius and frequencies, a qualitative agreement was obtained between the collective variables model here developed and the results of simulations with the many-spins system. We believe that the whole complexity of the latter system, including the discreteness effects observed, can not be fully captured by these kinds of stationary movement approaches. It remains for future work a detailed study of the possible appearance chaos in the set of equations (5.30), since also for these equations, with three degrees of freedom, we have observed windows, self-similarity and a high sensitivity to the field parameters, like was the case in the simulations of the many-spin system.

Chapter 6

Summary

In this work, we have investigated the dynamics of a vortex in a 2D classical spin system, with anisotropic exchange interactions, under the application of driving magnetic fields and a phenomenological damping term.

In the Chapter 4 we studied the phenomenon of switching of the out-of-plane vortex magnetization, caused by the application of a rotating magnetic field. Our results may be summarized as follows:

The flipping times do not depend essentially on the size of the system, provided that the lattice is large enough (radius $L \gtrsim 36$). In other words, the switching of the vortex polarization is not much affected by the presence of boundaries.

A clear correlation is observed between the core magnetization dynamics (the oscillations of the core spins in the perpendicular-to-plane direction) and the velocity of the vortex center in the plane of the lattice.

A diagram of flipping events as a function of the field parameters, from extensive numerical simulations with an OP vortex in a rotating magnetic field, was presented. We found out that in the (ω, h) parameters space there is no well-defined curve which separates the regime where the flips do not occur from the regime where they do. For a given frequency ω and increasing amplitude h we found intervals (“windows”) of intermittent flip and non-flip events.

The switching process is unidirectional only if the anisotropy parameter λ is not too close to the critical value λ_c . The closer λ is to λ_c , the more unstable the system is against flips of the vortex polarization in a weak field, and the larger fluctuations of the vortex core magnetization are observed.

Switching of the vortex polarization can be achieved also by applying a static magnetic field with both in-plane and out-of-plane components.

The switching dynamics may be described in terms of a core model which takes into account a coupling between the vortex polarization dynamics and the motion of the

vortex center. We showed that a reduced core model, which is valid near the threshold of the IP-OP vortex instability ($\lambda \approx \lambda_c$), can be mapped to a generalized Thiele equation with an inertial term.

It is clear that the phenomenon of switching we described will not be essentially affected by the inclusion of the dipole interaction (2.10). The shape of the vortex core and the far field will be modified by this interaction, but the flipping process has to do essentially with the externally applied magnetic field. The experimental works on nanodisks mentioned in the Introduction already reported the observation of vortices in either of two polarization states, and the switching between them was forced by means of static fields perpendicular to the plane of the disks [72, 65, 68].

In Chapter 5 we turned to the study of the movement of the vortex in the XY plane, in the presence of the in-plane rotating field. Attention was directed to the existence of stable orbits, where the vortex stays inside the system in a stationary movement, forming circular limit cycles. The failure of the conventional Thiele approach was discussed, and an extended collective coordinate Ansatz was formulated, which led to a qualitative agreement with the results of the simulations.

A diagram of the different types of trajectories, as a function of the field parameters, showed the presence of non-monotonous effects and “windows”, like in the case of the switching diagram. We are led to conclude that for some regions of the field parameters space, particularly where discreteness effects are more visible, the system exhibits chaos—which is typical for many-body systems—, though no particular tool of the chaos theory was used to study our discrete and collective coordinate models, from this viewpoint. This task is proposed as a possible direction for future work.

Our theoretical work qualitatively suggests that it would be interesting to apply in the experiments weak rotating fields like those used here, to control both the mean position of a vortex in larger magnetic dots (where the vortex center could show dynamics) and at the same time the sign of the out-of-plane core magnetization.

Future directions of this work can include as well a dipolar interaction between the spins, to verify which features of the processes described here are to be modified, and which remain unchanged. Another interesting topic of expansion of this work would be the use of inhomogeneous fields, particularly with a gaussian localization in a small region of the lattice or “spot”, as a model of the field of a laser beam. In this respect, it would be interesting to observe a field-induced vortex formation, starting from random or saturated configurations. This proposal is motivated by one of our observations above, namely that new vortices are created at the boundaries, for strong enough magnetic fields. It is thus conceivable that local perturbations induce a global response of the system, whenever we deal here with the interplay of short-range (nearest-neighbor spins) and effective long-range (vortex-vortex and vortex-field) interactions.

Appendix A

Some calculations

In this Appendix, I give some details of calculations from the Chapter 2 and 3. Throughout this Thesis, the subindices indicating a lattice site, may appear in different notations, which will be clear in each case. For instance, for a 2-D lattice, I can write the spins as $\vec{S}_{\vec{n}}$ or leave out the vector arrow over “n”, and in other cases I can specify the components of $\vec{n} = (n, m)$ as in $\vec{S}_n := \vec{S}_n^m := \vec{S}_{n,m}$, when is convenient.

A.1 Classical spins from quantum spins

The quantum-mechanic spin vector-operator \vec{S} fulfills

$$[S_n^\alpha, S_m^\beta] = i \hbar \delta_{nm} \varepsilon^{\alpha\beta\gamma} S_m^\gamma \quad (\text{A.1})$$

where “n” or “m” are the indices of sites on a lattice. The sum convention for repeated cartesian components α, β , etc is assumed. To obtain the classical version of eq. (A.1) we first introduce normalized operators by

$$U_n^\alpha = \frac{1}{\hbar \sqrt{S(S+1)}} S_n^\alpha \quad . \quad (\text{A.2})$$

Replacing this in (A.1) we get

$$\hbar^2 S(S+1) [U_n^\alpha, U_m^\beta] = i \hbar \delta_{nm} \varepsilon^{\alpha\beta\gamma} \hbar \sqrt{S(S+1)} U_m^\gamma \quad (\text{A.3})$$

Applying *first* the *inversed* quantization rule¹,

$$-\frac{i}{\hbar} [,] \rightarrow \{ , \}$$

¹As if applying it in that direction were justified, which is exactly what is meant by “classical limit”, see e.g. [67].

where $\{ , \}$ stands for the Poisson brackets (2.24), i.e.,

$$\hbar^2 S(S+1) \{U_n^\alpha, U_m^\beta\} = \delta_{nm} \varepsilon^{\alpha\beta\gamma} \hbar \sqrt{S(S+1)} U_m^\gamma \quad (\text{A.4})$$

and *after* this step the classical limit

$$\hbar \rightarrow 0, \quad S \rightarrow \infty, \quad \hbar S \rightarrow S_c, \quad (\text{A.5})$$

where S_c stands for the classical value of the spin length, assuming that the operators U_n^α are replaced by unitary vectors, we get the classical relations (2.25), i.e.,

$$\{S_n^\alpha, S_m^\beta\} = \delta_{nm} \varepsilon^{\alpha\beta\gamma} S_m^\gamma \quad (\text{A.6})$$

A.2 Landau-Lifshitz equations from quantum spins

Let us “derive” the LL equations (without damping) from the Heisenberg equations for spin operators, by taking the “classical limit” (A.5) to the corresponding quantum equations in the Heisenberg picture. Let’s take the Hamiltonian of the anisotropic Heisenberg model, with local and exchange anisotropy, plus a magnetic field:

$$H = H_0 + H_1 + V(t) = -\frac{1}{2} \sum_{n,a} \vec{S}_n \cdot \hat{J} \vec{S}_{n+a} - \frac{1}{2} \sum_n \vec{S}_n \cdot \hat{D} \vec{S}_n - \vec{h}(t) \cdot \sum_n \vec{S}_n \quad (\text{A.7})$$

where \vec{S} fulfills the commutation relations (A.1). Here the Z neighbors “ a ” of n are placed symmetrically, i.e., whenever a appears in a sum, $-a$ appears as well. Exchange constants and anisotropy in the main axes are embedded in the diagonal matrix $\hat{J} = \text{diag}(J_x, J_y, J_z)$, as well as on-site anisotropy is included in $\hat{D} = \text{diag}(D_x, D_y, D_z)$. Being diagonal these matrices satisfy

$$\begin{aligned} \vec{S}_n \cdot \hat{J} \vec{S}_m &= \hat{J} \vec{S}_n \cdot \vec{S}_m \\ \vec{S}_n \cdot \hat{D} \vec{S}_m &= \hat{D} \vec{S}_n \cdot \vec{S}_m, \quad \text{for all } m, n. \end{aligned} \quad (\text{A.8})$$

First, for the exchange interaction, we have

$$\begin{aligned} [H_0, S_m^\beta] &= -\frac{1}{2} \sum_{n,a} \left([S_n^\alpha, S_m^\beta] J_\alpha S_{n+a}^\alpha + S_n^\alpha J_\alpha [S_{n+a}^\alpha, S_m^\beta] \right) \\ &= -\frac{1}{2} i \hbar \varepsilon^{\alpha\beta\gamma} \sum_{n,a} \left(\delta_{n,m} S_m^\gamma J_\alpha S_{n+a}^\alpha + \delta_{n+a,m} S_n^\alpha J_\alpha S_m^\gamma \right) \\ &= -\frac{1}{2} i \hbar \varepsilon^{\alpha\beta\gamma} J_\alpha \sum_a \left(S_m^\gamma S_{m+a}^\alpha + S_{m-a}^\alpha S_m^\gamma \right) \end{aligned} \quad (\text{A.9})$$

Now, since $\sum_a f_a \equiv \sum_a f_{-a}$ and since $[S_m^\alpha, S_{m+a}^\beta] = 0$ because $m \neq m+a$, we have

$$[H_0, S_m^\beta] = -i\hbar \varepsilon^{\alpha\beta\gamma} \sum_a S_m^\gamma J_\alpha S_{m+a}^\alpha = -i\hbar \left(\vec{S}_m \times \sum_a \hat{J} \vec{S}_{m+a} \right)^\beta \quad (\text{A.10})$$

Secondly, the autointeraction term,

$$\begin{aligned} [H_1, S_m^\beta] &= -\frac{1}{2} \sum_n \left([S_n^\alpha, S_m^\beta] D_\alpha S_n^\alpha + S_n^\alpha D_\alpha [S_n^\alpha, S_m^\beta] \right) \\ &= -\frac{1}{2} i\hbar \varepsilon^{\alpha\beta\gamma} \sum_n \left(\delta_{n,m} S_m^\gamma D_\alpha S_n^\alpha + \delta_{n,m} S_n^\alpha D_\alpha S_m^\gamma \right) \\ &= -\frac{1}{2} i\hbar \varepsilon^{\alpha\beta\gamma} \left(S_m^\gamma D_\alpha S_m^\alpha + S_m^\alpha D_\alpha S_m^\gamma \right) \end{aligned}$$

but here $[S_m^\gamma, S_m^\alpha] \neq 0$ – which makes Q.M. that rare²– and so

$$[H_1, S_m^\beta] = -\frac{1}{2} i\hbar \left(\vec{S}_m \times \hat{D} \vec{S}_m - \hat{D} \vec{S}_m \times \vec{S}_m \right)^\beta \quad (\text{A.11})$$

And finally, for the magnetic field

$$\begin{aligned} [V(t), S_m^\beta] &= -h^\alpha(t) \sum_n [S_n^\alpha, S_m^\beta] \\ &= -i\hbar \varepsilon^{\alpha\beta\gamma} S_m^\gamma h^\alpha(t) = -i\hbar \left(\vec{S}_m \times \vec{h}(t) \right)^\beta \end{aligned} \quad (\text{A.12})$$

where he have assumed that $[h^\alpha(t), S_m^\beta] = 0$.

Thus, the Heisenberg equations give:

$$\begin{aligned} \dot{S}_m^\beta &= \frac{i}{\hbar} [H_0 + H_1 + V(t), S_m^\beta] = \left(\vec{S}_m \times \sum_a \hat{J} \vec{S}_{m+a} \right)^\beta + \\ &\quad + \frac{1}{2} \left(\vec{S}_m \times \hat{D} \vec{S}_m - \hat{D} \vec{S}_m \times \vec{S}_m \right)^\beta + \left(\vec{S}_m \times \vec{h}(t) \right)^\beta . \end{aligned} \quad (\text{A.13})$$

These are the quantum equations of motion for the spin vector-operators. Since \hbar does not appear explicitly in these equations, they are valid in the classical limit (A.5), where $|\vec{S}| = S_c$ and the vectors commute, without modification. Therefore, in the classical limit we get

$$\dot{\vec{S}}_m = \vec{S}_m \times \vec{F}_m , \quad (\text{A.14})$$

² For any 2 vectors \vec{A} and \vec{B} in Q.M. is valid

$$(\vec{A} \times \vec{B})^\alpha + (\vec{B} \times \vec{A})^\alpha = \varepsilon^{\alpha\beta\gamma} [A^\beta, B^\gamma]$$

where

$$\vec{F}_m = \left\{ \sum_a \hat{J} \vec{S}_{m+a} + \hat{D} \vec{S}_m + \vec{h}(t) \right\} \quad (\text{A.15})$$

is the effective field felt by the m -esim spin \vec{S}_m . These are the Landau-Lifshitz equations for classical spins, except for the coefficients, which in this context are absorbed into the coupling constants \hat{J} , \hat{D} , and in the field $\vec{h}(t)$ (see the next subsection).

One should observe the units on both sides of Eqs (A.14). The classical spins will have units of \hbar , this is, $[S_c] = \text{energy} \cdot \text{time}$, and in any case the products $J_\alpha S_c^2$, $D_\alpha S_c^2$ and $\vec{h} \cdot \vec{S}$, will have units of energy, so the equations are well balanced.

A.2.1 The coefficients in the Landau-Lifshitz equations.

In the original paper of 1935 by Landau and Lifshitz [51], the equation with damping is presented in the form

$$\dot{\vec{s}}/\mu_0 = [\vec{f} \vec{s}] + \lambda \left(\vec{f} - \frac{(\vec{f} \vec{s}) \vec{s}}{s^2} \right) \quad (\text{A.16})$$

(this is the eq. (21) of [51]), where \vec{f} is the effective field, i.e., $\vec{f} = -\delta E/\delta \vec{s}$, and the vector operations are $[\vec{f} \vec{s}] = \vec{f} \times \vec{s}$ and $(\vec{f} \vec{s}) = \vec{f} \cdot \vec{s}$. In our notation it is

$$\dot{\vec{s}}/\mu_0 = \vec{f} \times \vec{s} - \frac{\lambda}{s^2} \vec{s} \times \vec{s} \times \vec{f} . \quad (\text{A.17})$$

Note that λ must have the same units as \vec{S} , if the equation is to be dimensionally correct. In the same paper the authors write $\mu_0 = e/mc$, and the sign of e is not indicated, though it is clear that this is the gyromagnetic factor for spins, and the vectors \vec{s} are referred to as “spin-moments”. On the other hand, in the book by the same authors [52], the eq. (A.16) without damping is written as an equation for the magnetic moment

$$\dot{\vec{M}} = \frac{g|e|}{2m_e c} \vec{H}_{\text{eff}} \times \vec{M} \quad (\text{A.18})$$

from where one concludes that in the original paper they should have beard in mind $\mu_0 > 0$, because $\vec{M} = \mu_0 \sum_i \vec{s}_i/\text{Vol.}$, in that old notation (today, $-\mu_0 \equiv \gamma < 0$). This is confirmed in the paper of Iida [35], where all the constants of his Eq. (1) are drawn in his Fig. 1 as positive. In Quantum Mechanics (see e. g. Ballentine [4]), one obtains as in the previous Section, for a Zeeman interaction with a magnetic induction $\vec{B}(t)$,

$$V = -\gamma \vec{S} \cdot \vec{B}(t) , \quad (\text{A.19})$$

the equation

$$\dot{\vec{S}} = \gamma \vec{S} \times \vec{B}(t) \quad , \quad (\text{A.20})$$

and here $\gamma = -|e|/m_e c$, which is in agreement with (A.18). We conclude that the constant γ that we have absorbed either into \hat{J} , \hat{D} , and $\vec{h}(t)$, or into the time variable, in (A.14), is negative. In any case, γH_{eff} must have units of inverse time.

In the paper by Iida [35], some aspects of the damping term in (A.17) were discussed, in comparison with the Gilbert version, which has the advantage that it can be derived from the Lagrangian formalism, and in the present units would be

$$\dot{\vec{S}} = \gamma \vec{S} \times \vec{H}_{\text{eff}} - \frac{\varepsilon}{S_c} \vec{S} \times \dot{\vec{S}} \quad . \quad (\text{A.21})$$

Here ε is adimensional. It is easy to transform this equation into the Landau-Lifshitz form, but the result will contain different coefficients:

$$(1 + \varepsilon^2) \dot{\vec{S}} = \gamma \vec{S} \times \vec{H}_{\text{eff}} - \frac{\varepsilon \gamma}{S_c} \vec{S} \times \dot{\vec{S}} \times \vec{H}_{\text{eff}} \quad , \quad (\text{A.22})$$

Now, the only way to make these eqs. coincide with the original LL eqs. (A.17), without having to define different γ 's (which would lead to different Hamilton equations at zero damping) is to rescale the time variable $t \rightarrow \tau = t/(1 + \varepsilon^2)$ in eq. (A.22), in addition to give the relation between damping parameters of both equations, $\lambda = \varepsilon S_c$, from where λ gets physical units.

A.3 Rate of change of the total energy

In this Appendix I show some simple calculations which can be done in a fully discrete manner³. We want to calculate the rate of change of the energy for Heisenberg models, whose dynamics is given by the LL eqs. (2.34),

$$(1 + \varepsilon^2) \dot{\vec{S}}_{\vec{n}} = \vec{S}_{\vec{n}} \times \vec{F}_{\vec{n}} - \frac{\varepsilon}{S_c} \vec{S}_{\vec{n}} \times (\vec{S}_{\vec{n}} \times \vec{F}_{\vec{n}})$$

where $\vec{F}_{\vec{n}} = -\partial \mathcal{H} / \partial \vec{S}_{\vec{n}}$, we redefined the time variable to $\tau := t/(1 + \varepsilon^2)$, so the dot over a variable means $d(\dots)/d\tau$, and also we absorb S_c into $\varepsilon' := \varepsilon/S_c$. We can restore all the hidden constants at the end.

³Although I got to know (from Denis Sheka) after having written this Appendix, that the whole calculation is as easy and short as I presented it in Sec. 4.1.2, which is also valid for discrete systems, I let these pages here, however, because I believe they may be useful for someone to gain some physical feeling of discrete spin systems, as it was the case for me.

Anisotropic Heisenberg chain (1-D):

To gain insight into the required calculations let's start with the 1-dimensional case. The exchange Hamiltonian with anisotropy in each of the main axes is

$$\mathcal{H} = -\frac{1}{2} \sum_n \sum_{\alpha, \beta} S_n^\alpha (\mathbf{J})^{\alpha\beta} (S_{n-1}^\beta + S_{n+1}^\beta) = -\frac{1}{2} \sum_{n=1}^N \vec{S}_n \cdot \hat{\mathbf{J}}(\vec{S}_{n-1} + \vec{S}_{n+1}) \quad ,$$

where $\alpha, \beta = \{x, y, z\}$, and $(\mathbf{J})^{\alpha\beta} = \text{diag}(J^x, J^y, J^z)$. We first note that we can in fact prove general statements about the sums implied in the Hamiltonian by shifting $n \pm 1 \rightarrow n'$ and then adjusting the limits of the sums, for we can simulate the “outside” conditions as $\vec{S}_0 = \vec{S}_{-1} = \vec{S}_{N+1} = \vec{S}_{N+2} := 0$. For example,

$$\sum_{n=1}^N \vec{S}_n \cdot \vec{f}(\vec{S}_{n-1}) = \sum_{n'=0}^{N-1} \vec{S}_{n'+1} \cdot \vec{f}(\vec{S}_{n'}) = \sum_{n=1}^N \vec{S}_{n+1} \cdot \vec{f}(\vec{S}_n) \quad , \quad (\text{A.23})$$

where the function $\vec{f}(\vec{S}_n)$ fulfills $\vec{f}(\vec{S}_0) = 0$ and is otherwise arbitrary. Being diagonal, $\hat{\mathbf{J}}$ satisfies the property

$$\vec{S}_n \cdot \hat{\mathbf{J}}\vec{S}_m = \hat{\mathbf{J}}\vec{S}_n \cdot \vec{S}_m \quad . \quad (\#a)$$

However, $\hat{\mathbf{J}}$ does not quite a cross product. Indeed, using $(\vec{A} \times \vec{B})^2 = A^2 B^2 - (\vec{A} \cdot \vec{B})^2$, it results

$$(\vec{S}_n \times \hat{\mathbf{J}}\vec{S}_m)^2 = (\hat{\mathbf{J}}\vec{S}_n \times \vec{S}_m)^2 - (\hat{\mathbf{J}}\vec{S}_n)^2 + (\hat{\mathbf{J}}\vec{S}_m)^2 \quad ,$$

providing that $\vec{S}_m \neq 0$ and $\vec{S}_n \neq 0$. The later prevents us from applying such property when one of the spins is laying on a border, i.e., \vec{S}_1 or \vec{S}_N . We therefore need to make use of (A.23). For example,

$$\sum_{n=1}^N \vec{S}_n \times \hat{\mathbf{J}}\vec{S}_{n-1} = \sum_{n=1}^N \vec{S}_{n+1} \times \hat{\mathbf{J}}\vec{S}_n = - \sum_{n=1}^N \hat{\mathbf{J}}\vec{S}_n \times \vec{S}_{n+1} \quad , \quad (\#b)$$

$$\sum_{n=1}^N \vec{S}_n \times \hat{\mathbf{J}}\vec{S}_{n+1} = \sum_{n=1}^N \vec{S}_{n-1} \times \hat{\mathbf{J}}\vec{S}_n = - \sum_{n=1}^N \hat{\mathbf{J}}\vec{S}_n \times \vec{S}_{n-1} \quad , \quad (\#c)$$

$$\sum_{n=1}^N (\hat{\mathbf{J}}\vec{S}_n \times \vec{S}_{n+1})^2 + (\hat{\mathbf{J}}\vec{S}_n \times \vec{S}_{n-1})^2 = \sum_{n=1}^N (\vec{S}_n \times \hat{\mathbf{J}}\vec{S}_{n+1})^2 + (\vec{S}_n \times \hat{\mathbf{J}}\vec{S}_{n-1})^2 \quad . \quad (\#d)$$

The LL eqs. are in the present case

$$\dot{\vec{S}}_n = \vec{S}_n \times \hat{\mathbf{J}}(\vec{S}_{n-1} + \vec{S}_{n+1}) - \varepsilon' \vec{S}_n \times \vec{S}_n \times \hat{\mathbf{J}}(\vec{S}_{n-1} + \vec{S}_{n+1}) \quad .$$

Thus, we have

$$\begin{aligned} \frac{d\mathcal{H}}{d\tau} &= -\frac{1}{2} \sum_n \left[-\varepsilon' \vec{S}_n \times \vec{S}_n \times \hat{J}(\vec{S}_{n-1} + \vec{S}_{n+1}) \right] \cdot \hat{J}(\vec{S}_{n-1} + \vec{S}_{n+1}) \\ &\quad - \frac{1}{2} \sum_n \vec{S}_n \cdot \hat{J}[\vec{S}_{n-1} \times \hat{J}(\vec{S}_n + \vec{S}_{n-2}) - \varepsilon' \vec{S}_{n-1} \times \vec{S}_{n-1} \times \hat{J}(\vec{S}_n + \vec{S}_{n-2})] \\ &\quad - \frac{1}{2} \sum_n \vec{S}_n \cdot \hat{J}[\vec{S}_{n+1} \times \hat{J}(\vec{S}_n + \vec{S}_{n+2}) - \varepsilon' \vec{S}_{n+1} \times \vec{S}_{n+1} \times \hat{J}(\vec{S}_n + \vec{S}_{n+2})] \end{aligned}$$

Using the property (#a) in the second and third sums, their first terms vanish and, after reordering,

$$\frac{d\mathcal{H}}{d\tau} = -\frac{1}{2} \varepsilon' \sum_n [\vec{S}_n \times \hat{J}(\vec{S}_{n-1} + \vec{S}_{n+1})]^2 \quad (\text{A})$$

$$- \frac{1}{2} \sum_n \vec{S}_n \cdot \hat{J}[\vec{S}_{n-1} \times \hat{J}\vec{S}_{n-2} + \vec{S}_{n+1} \times \hat{J}\vec{S}_{n+2}] \quad (\text{B})$$

$$- \frac{1}{2} \varepsilon' \sum_n [(\hat{J}\vec{S}_n \times \vec{S}_{n-1})^2 + (\hat{J}\vec{S}_n \times \vec{S}_{n+1})^2] \quad (\text{C})$$

$$+ \frac{1}{2} \varepsilon' \sum_n \vec{S}_n \cdot \hat{J}[\vec{S}_{n-1} \times \vec{S}_{n-1} \times \hat{J}\vec{S}_{n-2} + \vec{S}_{n+1} \times \vec{S}_{n+1} \times \hat{J}\vec{S}_{n+2}] \quad (\text{D})$$

By simple inspection, one sees that the sum (B) in the second line is zero, so that the energy without damping is conserved. Now (D) is

$$\begin{aligned} (\text{D}) &= +\frac{1}{2} \varepsilon' \sum_n (\vec{S}_{n-1} \times \hat{J}\vec{S}_n) \cdot (\vec{S}_{n-1} \times \hat{J}\vec{S}_{n-2}) + (\vec{S}_{n+1} \times \hat{J}\vec{S}_n) \cdot (\vec{S}_{n+1} \times \hat{J}\vec{S}_{n+2}) \\ &= -\frac{1}{2} \varepsilon' \sum_n 2 (\vec{S}_n \times \hat{J}\vec{S}_{n-1}) \cdot (\vec{S}_n \times \hat{J}\vec{S}_{n+1}) \quad . \end{aligned}$$

where we used prop.s of the kind (#b)-(#d). Using (#d) in (C), the sum (C)+(D) results a complete square and exactly the same as (A). Thus,

$$\frac{d\mathcal{H}}{d\tau} = -\varepsilon' \sum_{n=1}^N [\vec{S}_n \times \hat{J}(\vec{S}_{n-1} + \vec{S}_{n+1})]^2 = -\varepsilon' \sum_{n=1}^N [\vec{S}_n \times \vec{F}_n]^2$$

or, restoring the constants,

$$\frac{d\mathcal{H}}{dt} = -\frac{\varepsilon}{S_c(1+\varepsilon^2)} \sum_{n=1}^N [\vec{S}_n \times \vec{F}_n]^2 < 0 \quad . \quad (\text{A.24})$$

We have arrived to a definite-sign formula. Note that this result includes the case of the isotropic chain when $\hat{J} = J \hat{I}$.

Heisenberg model in 2-D and higher dimensions:

The results just obtained are not restricted to one dimension. We now show how they can be generalized to 2 dimensions. First, as a guide, we realize that the sum over bonds in the Heisenberg Hamiltonian,

$$\mathcal{H} = -\frac{1}{2} \sum_{\vec{n}} \sum_{\vec{a}} \vec{S}_{\vec{n}} \cdot \hat{J} \vec{S}_{\vec{n}+\vec{a}} \quad (\text{A.25})$$

where \vec{a} is nearest neighbor of \vec{n} , can be separated in a sum over bonds into one chain, and a sum over chains. In the 2-D case, using the notation $\vec{S}_{\vec{n}} \equiv \vec{S}_n^m$, where $n = 1, \dots, N_x$ and $m = 1, \dots, N_y$, and assuming we have a square lattice with unit lattice constant ($a_x = a_y = 1$), we have

$$\begin{aligned} \mathcal{H} &= -\frac{1}{2} \sum_n \sum_m \vec{S}_n^m \cdot \hat{J} (\vec{S}_{n-1}^m + \vec{S}_{n+1}^m + \vec{S}_n^{m-1} + \vec{S}_n^{m+1}) \\ &= \frac{1}{2} \sum_m \left[-\sum_n \vec{S}_n^m \cdot \hat{J} (\vec{S}_{n-1}^m + \vec{S}_{n+1}^m) \right] + \frac{1}{2} \sum_n \left[-\sum_m \vec{S}_n^m \cdot \hat{J} (\vec{S}_n^{m-1} + \vec{S}_n^{m+1}) \right] , \end{aligned}$$

with $\vec{S}_0^m = \vec{S}_n^0 = \vec{S}_{N_x+1}^m = \vec{S}_n^{N_y+1} := 0$. That's fine. But now the LLG equations “mix” the directions. Indeed,

$$\dot{\vec{S}}_n^m = \vec{S}_n^m \times \vec{F}_n^m - \varepsilon' \vec{S}_n^m \times \vec{S}_n^m \times \vec{F}_n^m ,$$

where the effective field is in this case $\vec{F}_n^m = \hat{J} (\vec{S}_{n-1}^m + \vec{S}_{n+1}^m + \vec{S}_n^{m-1} + \vec{S}_n^{m+1})$.

Thus,

$$\frac{d\mathcal{H}}{d\tau} = -\frac{1}{2} \sum_{n,m} \left[-\varepsilon' \vec{S}_n^m \times \vec{S}_n^m \times \vec{F}_n^m \right] \cdot \vec{F}_n^m \quad (\text{A})$$

$$-\frac{1}{2} \sum_{n,m} \vec{S}_n^m \cdot \hat{J} [\vec{S}_{n-1}^m \times \vec{F}_{n-1}^m - \varepsilon' \vec{S}_{n-1}^m \times \vec{S}_{n-1}^m \times \vec{F}_{n-1}^m] \quad (\text{B})$$

$$-\frac{1}{2} \sum_{n,m} \vec{S}_n^m \cdot \hat{J} [\vec{S}_{n+1}^m \times \vec{F}_{n+1}^m - \varepsilon' \vec{S}_{n+1}^m \times \vec{S}_{n+1}^m \times \vec{F}_{n+1}^m] \quad (\text{C})$$

$$-\frac{1}{2} \sum_{n,m} \vec{S}_n^m \cdot \hat{J} [\vec{S}_n^{m-1} \times \vec{F}_n^{m-1} - \varepsilon' \vec{S}_n^{m-1} \times \vec{S}_n^{m-1} \times \vec{F}_n^{m-1}] \quad (\text{D})$$

$$-\frac{1}{2} \sum_{n,m} \vec{S}_n^m \cdot \hat{J} [\vec{S}_n^{m+1} \times \vec{F}_n^{m+1} - \varepsilon' \vec{S}_n^{m+1} \times \vec{S}_n^{m+1} \times \vec{F}_n^{m+1}] \quad (\text{E})$$

where

$$\begin{aligned} \vec{F}_{n-1}^m &= \hat{J} (\vec{S}_n^m + \vec{S}_{n-2}^m + \vec{S}_{n-1}^{m-1} + \vec{S}_{n-1}^{m+1}) , & \vec{F}_{n+1}^m &= \hat{J} (\vec{S}_n^m + \vec{S}_{n+2}^m + \vec{S}_{n+1}^{m-1} + \vec{S}_{n+1}^{m+1}) \\ \vec{F}_n^{m-1} &= \hat{J} (\vec{S}_n^m + \vec{S}_n^{m-2} + \vec{S}_{n-1}^{m-1} + \vec{S}_{n+1}^{m-1}) , & \vec{F}_n^{m+1} &= \hat{J} (\vec{S}_n^m + \vec{S}_n^{m+2} + \vec{S}_{n-1}^{m+1} + \vec{S}_{n+1}^{m+1}) \end{aligned}$$

and $\vec{S}_{n-1}^m \equiv \vec{S}_n^{m-1} \equiv \vec{S}_{N_x+2}^m \equiv \vec{S}_n^{N_y+2} \equiv 0$. Now, for the first terms of (B) to (E) we have:

$$\begin{aligned} \sum_{n=1}^{N_x} \vec{S}_n^m \cdot \hat{J}(\vec{S}_{n-1}^m \times \vec{F}_{n-1}^m) &= \sum_{n'=0}^{N_x-1} \vec{S}_{n'+1}^m \cdot \hat{J}(\vec{S}_{n'}^m \times \vec{F}_{n'}^m) = \sum_{n=1}^{N_x} \vec{S}_{n+1}^m \cdot \hat{J}(\vec{S}_n^m \times \vec{F}_n^m) \\ \sum_{n=1}^{N_x} \vec{S}_n^m \cdot \hat{J}(\vec{S}_{n+1}^m \times \vec{F}_{n+1}^m) &= \sum_{n'=2}^{N_x+1} \vec{S}_{n'-1}^m \cdot \hat{J}(\vec{S}_{n'}^m \times \vec{F}_{n'}^m) = \sum_{n=1}^{N_x} \vec{S}_{n-1}^m \cdot \hat{J}(\vec{S}_n^m \times \vec{F}_n^m) \quad (\#2a) \end{aligned}$$

and analogously

$$\begin{aligned} \sum_{m=1}^{N_y} \vec{S}_n^m \cdot \hat{J}(\vec{S}_n^{m-1} \times \vec{F}_n^{m-1}) &= \sum_{m'=0}^{N_y-1} \vec{S}_n^{m'+1} \cdot \hat{J}(\vec{S}_n^{m'} \times \vec{F}_n^{m'}) = \sum_{m=1}^{N_y} \vec{S}_n^{m+1} \cdot \hat{J}(\vec{S}_n^m \times \vec{F}_n^m) \\ \sum_{m=1}^{N_y} \vec{S}_n^m \cdot \hat{J}(\vec{S}_n^{m+1} \times \vec{F}_n^{m+1}) &= \sum_{m'=2}^{N_y+1} \vec{S}_n^{m'-1} \cdot \hat{J}(\vec{S}_n^{m'} \times \vec{F}_n^{m'}) = \sum_{m=1}^{N_y} \vec{S}_n^{m-1} \cdot \hat{J}(\vec{S}_n^m \times \vec{F}_n^m) \quad (\#2b) \end{aligned}$$

so that the sum of this four terms, using the property (#a),

$$\sum_{n=1}^{N_x} \sum_{m=1}^{N_y} (\vec{S}_{n-1}^m + \vec{S}_{n+1}^m + \vec{S}_n^{m-1} + \vec{S}_n^{m+1}) \cdot \hat{J}(\vec{S}_n^m \times \vec{F}_n^m) = \sum_{n=1}^{N_x} \sum_{m=1}^{N_y} \vec{F}_n^m \cdot (\vec{S}_n^m \times \vec{F}_n^m) = 0.$$

It is obvious that the same treatment of the sums for the second terms of (B) to (D) will give exactly the same contribution as the term (A), so finally we get

$$\frac{d\mathcal{H}}{d\tau} = -\varepsilon' \sum_{n=1}^{N_x} \sum_{m=1}^{N_y} [\vec{S}_n^m \times \hat{J}(\vec{S}_{n-1}^m + \vec{S}_{n+1}^m + \vec{S}_n^{m-1} + \vec{S}_n^{m+1})]^2 = -\varepsilon' \sum_{n=1}^{N_x} \sum_{m=1}^{N_y} [\vec{S}_n^m \times \vec{F}_n^m]^2 .$$

The generalization for the 3-D Heisenberg model on a cubic lattice is obvious:

$$\frac{d\mathcal{H}}{d\tau} = -\varepsilon' \sum_{l=1}^{N_x} \sum_{m=1}^{n_y} \sum_{n=1}^{N_z} [\vec{S}_{l,m,n} \times \vec{F}_{l,m,n}]^2 < 0 ,$$

with $\vec{F}_{l,m,n} = \hat{J}(\vec{S}_{l-1,m,n} + \vec{S}_{l+1,m,n} + \vec{S}_{l,m-1,n} + \vec{S}_{l,m+1,n} + \vec{S}_{l,m,n-1} + \vec{S}_{l,m,n+1})$.

More generally, given the Hamiltonian (A.25) on a hypercubic lattice of some dimension, and the dynamical equations

$$\dot{\vec{S}}_{\vec{n}} = \vec{S}_{\vec{n}} \times \vec{F}_{\vec{n}} - \varepsilon' \vec{S}_{\vec{n}} \times (\vec{S}_{\vec{n}} \times \vec{F}_{\vec{n}}) ,$$

with the effective field

$$\vec{F}_{\vec{n}} = \hat{J} \sum_{\vec{a}} \vec{S}_{\vec{n}+\vec{a}} ,$$

where for each neighbor \vec{a} of \vec{n} there appears the neighbor $-\vec{a}$ as well, it is easily seen that

$$\sum_{\vec{n}} \vec{S}_{\vec{n}} \cdot \dot{\vec{F}}_{\vec{n}} = \sum_{\vec{n}, \vec{a}} \vec{S}_{\vec{n}} \cdot \hat{J} \dot{\vec{S}}_{\vec{n}+\vec{a}} = \sum_{\vec{n}, \vec{a}} \hat{J} \vec{S}_{\vec{n}-\vec{a}} \cdot \dot{\vec{S}}_{\vec{n}} = \sum_{\vec{n}} \vec{F}_{\vec{n}} \cdot \dot{\vec{S}}_{\vec{n}} \quad , \quad (\text{A.26})$$

and therefore, in general

$$\frac{d\mathcal{H}}{d\tau} = - \sum_{\vec{n}} \dot{\vec{S}}_{\vec{n}} \cdot \vec{F}_{\vec{n}} = - \sum_{\vec{n}} (- \varepsilon' \vec{S}_{\vec{n}} \times \vec{S}_{\vec{n}} \times \vec{F}_{\vec{n}}) \cdot \vec{F}_{\vec{n}} = - \varepsilon' \sum_{\vec{n}} [\vec{S}_{\vec{n}} \times \vec{F}_{\vec{n}}]^2 \quad .$$

or, restoring the constants

$$\frac{d\mathcal{H}}{dt} = - \frac{\varepsilon}{S_c(1 + \varepsilon^2)} \sum_{\vec{n}} [\vec{S}_{\vec{n}} \times \vec{F}_{\vec{n}}]^2 < 0 \quad . \quad (\text{A.27})$$

Adding on-site anisotropy and magnetic field:

Including on-site anisotropy and a general magnetic field the total energy is

$$\mathcal{H} = -\frac{1}{2} \sum_{n,a} \vec{S}_n \cdot \hat{J} \vec{S}_{n+a} - \frac{1}{2} \sum_n \vec{S}_n \cdot \hat{D} \vec{S}_n - \sum_n \vec{S}_n \cdot \vec{h}_n(t) := -\frac{1}{2} \sum_n \vec{S}_n \cdot \vec{F}_n - \sum_n \vec{S}_n \cdot \vec{h}_n(t) \quad , \quad (\text{A.28})$$

where $\hat{J} = \text{diag}(J_x, J_y, J_z)$ and $\hat{D} = \text{diag}(D_x, D_y, D_z)$ are diagonal matrices, and $\vec{h}_n(t)$ is a site- and time-dependent field. Here \vec{F}_n as the effective field from the exchange and on-site anisotropy terms (here “ n ” is actually a set of indices in any dimension). Now the total effective field is

$$\vec{B}_n = - \frac{\partial \mathcal{H}}{\partial \vec{S}_n} = \hat{J} \sum_a \vec{S}_{n+a} + \hat{D} \vec{S}_n + \vec{h}_n(t) \equiv \vec{F}_n + \vec{h}_n(t) \quad , \quad (\text{A.29})$$

and the LL equations are

$$\dot{\vec{S}}_n = \vec{S}_n \times \vec{B}_n - \varepsilon' \vec{S}_n \times \vec{S}_n \times \vec{B}_n \quad . \quad (\text{A.30})$$

The prop. (A.26) is still valid, only the dynamics has changed, so \vec{F}_n satisfies

$$\sum_n \vec{S}_n \cdot \dot{\vec{F}}_n = \sum_n \vec{F}_n \cdot \dot{\vec{S}}_n = \sum_n \vec{F}_n \cdot [\vec{S}_n \times \vec{B}_n - \varepsilon' \vec{S}_n \times \vec{S}_n \times \vec{B}_n] \quad , \quad (\text{A.31})$$

which is easy to show in the way of the previous section, and therefore,

$$\begin{aligned} \frac{d\mathcal{H}}{d\tau} &= - \sum_n \dot{\vec{S}}_n \cdot \vec{F}_n - \sum_n \dot{\vec{S}}_n \cdot \vec{h}_n - \sum_n \vec{S}_n \cdot \dot{\vec{h}}_n = - \sum_n \dot{\vec{S}}_n \cdot \vec{B}_n - \sum_n \vec{S}_n \cdot \dot{\vec{h}}_n \\ &= - \sum_n (- \varepsilon \vec{S}_n \times \vec{S}_n \times \vec{B}_n) \cdot \vec{B}_n - \sum_n \vec{S}_n \cdot \dot{\vec{h}}_n \end{aligned}$$

so finally

$$\frac{d\mathcal{H}}{d\tau} = -\varepsilon' \sum_n \left[\vec{S}_n \times \vec{B}_n \right]^2 - \sum_n \vec{S}_n \cdot \frac{d\vec{h}_n(t)}{d\tau}$$

or

$$\boxed{\frac{d\mathcal{H}}{dt} = -\frac{\varepsilon}{S_c(1+\varepsilon^2)} \sum_n \left[\vec{S}_n \times \vec{B}_n \right]^2 - \sum_n \vec{S}_n \cdot \frac{d\vec{h}_n(t)}{dt}} \quad (\text{A.32})$$

We recognize in the last term the contribution of the magnetic field at zero damping. If we separate the terms in the square:

$$\frac{d\mathcal{H}}{d\tau} = -\varepsilon' \sum_n \left\{ (\vec{S}_n \times \vec{F}_n)^2 + (\vec{S}_n \times \vec{h}_n)^2 + 2(\vec{S}_n \times \vec{F}_n) \cdot (\vec{S}_n \times \vec{h}_n) \right\} - \sum_n \vec{S}_n \cdot \frac{d\vec{h}_n}{d\tau}, \quad (\text{A.33})$$

we see that the last term (of order $\mathcal{O}(h\omega)$, where h is the amplitude and ω the frequency of an AC field), could be larger than the damped terms which contain the field (of orders $\mathcal{O}(\varepsilon h^2)$ and $\mathcal{O}(\varepsilon h)$, respectively), for small damping ε and small amplitude h , when $\varepsilon \ll h\omega$. Under these conditions, the energy may oscillate, instead of decreasing. But there is still the first term, proportional to ε . Thus, how small should be ε with respect to h and ω , to have a quasi-linear response to the field? This can be extracted from the simulations, measuring the r.h.s. of this formula. Alternatively, one can measure also the various terms of the total energy (A.28), and compare them or their numerical derivatives. A usual situation is that the energy oscillates during a transient of ‘‘accommodation’’ of the system to the field, and the amplitude of these oscillations decreases in time, as is common in relaxation of driven-damped systems. The decrease of the energy at zero or static fields is in any case a good test for the correctness of the signs of coefficients in LL and for the numerical accuracy of computer codes.

Eq. (A.32) is of course equivalent to the discrete analogous of (4.14),

$$\frac{d\mathcal{H}}{dt} = -\frac{\varepsilon}{S_c} \sum_n (\dot{\vec{S}}_n)^2 - \sum_n \vec{S}_n \cdot \frac{d\vec{h}_n}{dt}, \quad (\text{A.34})$$

since from (2.36) and (2.33) one easily derives that for each n is valid

$$(\dot{\vec{S}}_n)^2 = \dot{\vec{S}}_n \cdot (\vec{S}_n \times \vec{B}_n) = \frac{1}{(1+\varepsilon^2)} (\vec{S}_n \times \vec{B}_n)^2. \quad (\text{A.35})$$

Removing the field from the damping term:

In our simulations we often used a modified version of the LLG equations, namely

$$\dot{\vec{S}}_n = \vec{S}_n \times \vec{B}_n - \varepsilon' \vec{S}_n \times \vec{S}_n \times \vec{F}_n. \quad (\text{A.36})$$

where in the last (damping) term, the magnetic field is absent. With this dynamics, the property (A.26) reads

$$\sum_n \vec{S}_n \cdot \dot{\vec{F}}_n = \sum_n \vec{F}_n \cdot \dot{\vec{S}}_n = \sum_n \vec{F}_n \cdot [\vec{S}_n \times \vec{B}_n - \varepsilon' \vec{S}_n \times \vec{S}_n \times \vec{F}_n] , \quad (\text{A.37})$$

and we find

$$\frac{d\mathcal{H}}{d\tau} = -\varepsilon' \sum_n [\vec{S}_n \times \vec{F}_n]^2 - \varepsilon' \sum_n (\vec{S}_n \times \vec{F}_n) \cdot (\vec{S}_n \times \vec{h}_n(t)) - \sum_n \vec{S}_n \cdot \frac{d\vec{h}_n(t)}{d\tau} . \quad (\text{A.38})$$

The difference between the eqs. (A.33) and (A.38) is

$$-\varepsilon' \sum_n (\vec{S}_n \times \vec{h}_n)^2 - \varepsilon' \sum_n (\vec{S}_n \times \vec{F}_n) \cdot (\vec{S}_n \times \vec{h}_n(t)) ,$$

which are terms of $\mathcal{O}(\varepsilon'h^2)$ and $\mathcal{O}(\varepsilon'h)$, resp., and still the 1st and the last terms in (A.38), like in (A.32), are the dominant ones.

Expressions in the continuum limit

All of the above results can be expressed in the continuum limit, as an alternative way to derive the expressions in Sec. 4.1.2. For instance, in (A.28) and (A.32): we simply replace the sums by integrals, inserting the continuous versions of the effective fields,

$$\vec{B}(\vec{x}, t) = \vec{F}(\vec{x}, t) + \vec{h}(\vec{x}, t) \quad , \quad \vec{F}(\vec{x}, t) = (\tilde{\mathbf{J}} + \tilde{\mathbf{D}}) \vec{S}(\vec{x}, t) + \hat{\mathbf{J}} \nabla^2 \vec{S}(\vec{x}, t) \quad (\text{A.39})$$

where $\tilde{\mathbf{J}} = \hat{\mathbf{J}}/a^2$ and $\tilde{\mathbf{D}} = \hat{\mathbf{D}}/a^2$, with a the lattice constant, and $\nabla^2 \equiv (\partial_x^2 + \partial_y^2 + \partial_z^2 + \dots)$ is the Laplacian in the corresponding space dimensions. The resulting expressions are valid for any configuration of the spin field which solves the LLG equations⁴.

It is worthy to note, however, that should we start the whole calculation from the continuum version of the dynamical equations, namely, in the simplest case,

$$\frac{d\vec{S}(\vec{x}, t)}{d\tau} = \vec{S}(\vec{x}, t) \times \nabla^2 \vec{S}(\vec{x}, t) - \varepsilon' \vec{S}(\vec{x}, t) \times \vec{S}(\vec{x}, t) \times \nabla^2 \vec{S}(\vec{x}, t) \quad (\text{A.40})$$

would we deal with expressions which involve products of second order partial deriva-

⁴In particular, but not necessarily, solitons in 1-D allow doing exact calculations. In this case, it would be interesting to calculate the same quantity, i.e., the rate of change of the energy, but starting from the definition of the energy density, replacing there the soliton exact solution, derivating it with respect to time and integrating it in space. The result so obtained could be compared with the result of simply inserting the soliton solution into the continuum version of (A.32) with (A.39), and doing (when possible!) the integrals.

tives. In principle, integrations by parts can be done, but one has to impose conditions at spatial infinity, or, otherwise, at the border of the system, and of course, it is supposed that the objects to be integrated are continuous. That's not the case of the vortex in 2-D. But for other configurations without singularities and asymptotically well behaved, the calculation can be done. In 1-D, with the simple energy

$$H = \frac{1}{2} \int_{-\infty}^{\infty} dx \partial_x \vec{S} \cdot \partial_x \vec{S} \quad (\text{A.41})$$

results

$$\begin{aligned} \frac{dH}{d\tau} &= \int_{-\infty}^{\infty} dx \partial_x \vec{S} \cdot \partial_x [\vec{S} \times \partial_{xx} \vec{S} - \varepsilon' \vec{S} \times \vec{S} \times \partial_{xx} \vec{S}] \\ &= \int_{-\infty}^{\infty} dx \partial_x [\partial_x \vec{S} \cdot (\vec{S} \times \partial_{xx} \vec{S})] - \varepsilon' \int_{-\infty}^{\infty} dx \partial_x \vec{S} \cdot \partial_x [\vec{S} \times \vec{S} \times \partial_{xx} \vec{S}] \end{aligned}$$

The first term should be zero, under proper conditions at infinity, like $\partial_x \vec{S} \rightarrow 0$, or $\vec{S} \rightarrow \vec{S}_0$, where \vec{S}_0 is some constant unit vector, sufficiently fast. The second gives after integration by parts, again under the same conditions,

$$\frac{d\mathcal{H}}{d\tau} = -\varepsilon' \int_{-\infty}^{\infty} dx \left(\vec{S} \times \partial_{xx} \vec{S} \right)^2 . \quad (\text{A.42})$$

It is interesting to note that, in the discrete case, the calculations are carried out for systems of some finite size, without having to impose any asymptotics at all nor worrying about the geometry, but only saying that outside the system there is “nothing” ($\vec{S}_0 = \vec{S}_{N+1} = 0$, etc.).

A.4 The energy of an IP vortex in a circular domain

In this Appendix we will calculate some double integrals in the reference frame which is fix to the vortex center,

$$x - X(t) = \rho \cos \chi \quad , \quad y - Y(t) = \rho \sin \chi \quad . \quad (\text{A.43})$$

Viewed from this point, the distance to the circular border of the lattice changes as a function of the azimuthal angle χ . With the settings of the **Fig. A.1**, we have that the limits for the integral in this reference frame are: $0 \leq \chi \leq 2\pi$, $0 \leq \rho \leq \sigma(\alpha)$, where $\alpha = \chi - \Phi$, and from the cosine theorem we have

$$\sigma(\alpha) = -R \cos \alpha + \sqrt{L^2 - R^2 \sin^2 \alpha} \quad , \quad (\text{A.44})$$

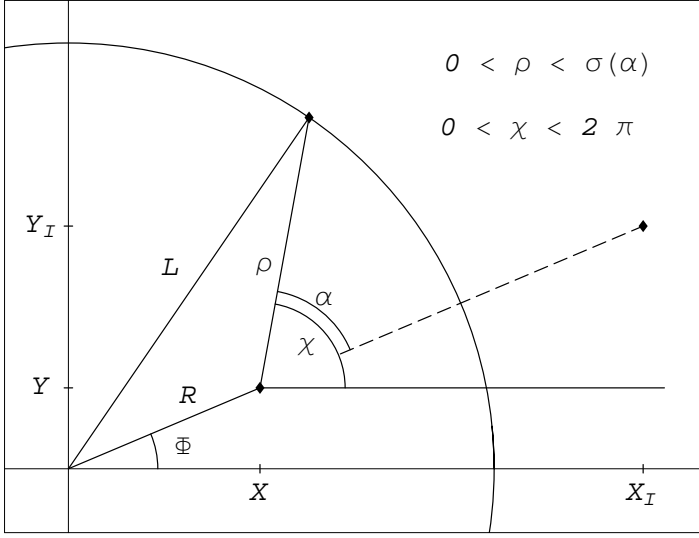


Fig. A.1: Arrangement of angles in the mobil frame centered in the vortex coordinates $\vec{X}(t) = R(t) (\cos \Phi(t), \sin \Phi(t))$

The exchange energy of a configuration with a static IP vortex (say, for simplicity, at $\vec{X} = (R, 0)$, since the energy should not depend on Φ), inside a *finite* circular domain C_L , plus its image (outside C_L) at $\vec{X}_I = (R_I, 0)$, with $R_I = \frac{L^2}{R}$,

$$\phi(x, y) := \Phi_0 + \Phi_I = q \arctan \frac{y}{(x - R)} + q_I \arctan \frac{y}{(x - R_I)}$$

with $q = -q_I = 1$, we have to calculate $E_T = E_0 + E_I + E_{0I}$ with

$$\text{(a.) } E_0 = \frac{1}{2} \int d^2x (\vec{\nabla} \Phi_0)^2 \quad , \quad \text{(b.) } E_I = \frac{1}{2} \int d^2x (\vec{\nabla} \Phi_I)^2 \quad ,$$

$$\text{(c.) } E_{0I} = -\frac{1}{2} \int d^2x \vec{\nabla} \Phi_0 \cdot \vec{\nabla} \Phi_I$$

where all the energies are in units of JS_c^2 .

(a.) E_0 :

$$(\vec{\nabla} \Phi_0)^2 = \frac{1}{(x - R)^2 + y^2} = \frac{1}{\rho^2} \tag{A.45}$$

is singular inside C_L , we calculate

$$E_0 = \frac{1}{2} \int_0^{2\pi} d\chi \int_{r_v}^{\sigma(\chi)} \rho d\rho \frac{1}{\rho^2} \tag{A.46}$$

$$\sigma(\chi) = -R \cos \chi - Z(\chi) \quad , \quad Z(\chi) = \sqrt{L^2 - R^2 \sin^2 \chi}.$$

$$\begin{aligned} E_0 &= \frac{1}{2} \int_0^{2\pi} d\chi \log \left(\frac{\sigma(\chi)}{r_v} \right) = \int_0^\pi d\chi \log \left(\frac{\sigma(\chi)}{l_0} \right) \\ &= \int_0^{\pi/2} d\chi \log \left(\frac{\sigma(\chi)}{r_v} \right) + \int_{\pi/2}^\pi d\chi \log \left(\frac{\sigma(\chi)}{r_v} \right) \end{aligned}$$

in the 2nd term we do $\eta = \pi - \chi$, then

$$E_0 = \int_0^{\pi/2} d\chi \log \left(\frac{\sigma(\chi)}{r_v} \right) + \int_0^{\pi/2} d\eta \log \left(\frac{\tilde{\sigma}(\eta)}{r_v} \right) \quad (\text{A.47})$$

where $\tilde{\sigma}(\eta) = +R \cos \eta + Z(\eta)$, $Z(\eta) = Z(\chi)$, then

$$E_0 = \int_0^{\pi/2} d\chi \log [\sigma(\chi) \tilde{\sigma}(\chi)] - \pi \log r_v$$

but $\sigma(\chi) \tilde{\sigma}(\chi) = Z^2 - R^2 \cos^2 \chi = L^2 - R^2$, so

$$E_0 = \frac{\pi}{2} \log [L^2 - R^2] - \pi \log r_v \quad . \quad (\text{A.48})$$

(b.) E_I :

$$(\vec{\nabla} \Phi_I)^2 = \frac{1}{(x - R_I)^2 + y^2} = \frac{1}{r^2 + R_I^2 - 2r R_I \cos \varphi}$$

is not singular inside C_L , with $(x, y) = r(\cos \varphi, \sin \varphi)$, we calculate

$$E_I = \frac{1}{2} \int_0^L r dr \int_0^{2\pi} \frac{d\varphi}{r^2 + R_I^2 - 2r R_I \cos \varphi}$$

which trivially gives

$$E_I = -\frac{\pi}{2} \log \left[\frac{L^2 - R^2}{L^2} \right] \quad (\text{A.49})$$

(c.) E_{0-I} :

$$\vec{\nabla} \Phi_0 \cdot \vec{\nabla} \Phi_I = \frac{(x - R)(x - R_I) + y^2}{((x - R)^2 + y^2)((x - R_I)^2 + y^2)} \equiv \frac{\rho - B \cos \chi}{\rho(\rho^2 - 2B\rho \cos \chi + B^2)}$$

where $B = R_I - R = (L^2 - R^2)/R$. The product $\rho \vec{\nabla} \Phi_0 \cdot \vec{\nabla} \Phi_I$ is not singular inside C_L , we calculate

$$\begin{aligned} E_{0-I} &= -\frac{1}{2} \int_0^{2\pi} d\chi \int_0^{\sigma(\chi)} d\rho \frac{(\rho - B \cos \chi)}{(\rho^2 - 2B\rho \cos \chi + B^2)} \\ &= -\frac{1}{2} \int_0^{2\pi} d\chi \log [\sigma(\chi)^2 - 2B\sigma(\chi) \cos \chi + B^2] + 2\pi \log B \end{aligned}$$

in the integral we repeat the steps leading to (A.47),

$$\begin{aligned} E_{0-I} &= - \int_0^{\pi/2} d\chi \log \left[\left(\sigma(\chi)^2 - 2B\sigma(\chi) \cos \chi + B^2 \right) \left(\tilde{\sigma}(\chi)^2 + 2B\tilde{\sigma}(\chi) \cos \chi + B^2 \right) \right] \\ &\quad + 2\pi \log \left[\frac{L^2 - R^2}{R} \right] \end{aligned}$$

After some algebra, using

$$\begin{aligned}\sigma\tilde{\sigma} &= Z^2 - R^2 \cos^2 \chi = L^2 - R^2 \\ \tilde{\sigma} - \sigma &= 2R \cos \chi \\ \sigma^2 + \tilde{\sigma}^2 &= 4R^2 \cos^2 \chi + 2(L^2 - R^2) \\ \sigma^2\tilde{\sigma} + \sigma\tilde{\sigma}^2 &= \sigma\tilde{\sigma}(\sigma + \tilde{\sigma}) = (L^2 - R^2)(-2R \cos \chi)\end{aligned}$$

the integrand can be much reduced, since

$$\left(\sigma(\chi)^2 - 2B\sigma(\chi) \cos \chi + B^2\right) \left(\tilde{\sigma}(\chi)^2 + 2B\tilde{\sigma}(\chi) \cos \chi + B^2\right) = \frac{L^4}{R^4} [L^2 - R^2]^2$$

and it results

$$E_{0-I} = -\pi \log \left[\frac{L^2}{R^2} (L^2 - R^2) \right] + 2\pi \log \left[\frac{L^2 - R^2}{R} \right] = \pi \log \left[\frac{L^2 - R^2}{L^2} \right] \quad (\text{A.50})$$

Adding (A.48),(A.49) and (A.50) we get the result

$$E_{\text{ex}} = \pi \log \left[\frac{L^2 - R^2}{Lr_v} \right] \quad (\text{A.51})$$

A.5 Dynamics with the original LLG equations

We repeat here the derivation, in the frame of the Lagrangian formulation, of the LLG eqs. with their original coefficients. The $2N$ freedom degrees are (ϕ_n, Π_n) , where n is a site index in a lattice of some dimensionality, and $\phi_n := \arctan(S_n^y/S_n^x)$ as before, but $\Pi_n := S_n^z/\gamma$, where $\gamma = -|e|/m_e c < 0$ is the gyromagnetic factor (see Appendix A.2.1). Now \vec{S}_n has units of magnetic moment (not simply action units, see Sec. 2.1). The Poisson brackets of two functions $F(\phi_n, S_n^z)$ and $G(\phi_n, S_n^z)$ is the operation defined by

$$\{F, G\} := \gamma \sum_n \left(\frac{\partial F}{\partial \phi_n} \frac{\partial G}{\partial S_n^z} - \frac{\partial F}{\partial S_n^z} \frac{\partial G}{\partial \phi_n} \right). \quad (\text{A.52})$$

We then get the obvious relations $\{\phi_n, \Pi_m\} = \delta_{nm}$, and the more interesting relations

$$\{S_n^\alpha, S_m^\beta\} = \gamma \delta_{nm} \varepsilon^{\alpha\beta\gamma} S_m^\gamma, \quad (\text{A.53})$$

These eqs. are *not* to be identified with the quantum commutation relations (A.1) for spins, but refer to magnetic momenta. In the sense of (A.52), the variables $(\phi_n, S_n^z/\gamma)$

are canonically conjugated. The Lagrangian is

$$\mathcal{L} = \sum_n \frac{1}{\gamma} \dot{\phi}_n S_n^z - \mathcal{H}(\{\phi_n\}, \{S_n^z/\gamma\}) \quad , \quad (\text{A.54})$$

where $\mathcal{H}(\{\phi_n\}, \{S_n^z/\gamma\})$ is the Hamiltonian, and the dot over a variable means total time derivative. The dissipation function takes the form

$$\mathcal{F} = -\frac{\varepsilon}{2\gamma S_c} \sum_n (\dot{\vec{S}}_n)^2 = -\frac{\varepsilon S_c}{2\gamma} \sum_n \left\{ \frac{1}{P_n^2} (\dot{S}_n^z)^2 + \frac{P_n^2}{S_c^2} (\dot{\phi}_n)^2 \right\} > 0 \quad , \quad (\text{A.55})$$

where again $P_n^2 = S_c^2 - (S_n^z)^2$, and $\varepsilon > 0$ is an adimensional damping constant, The Euler-Lagrange equations with dissipation (2.26), result in the equations of motion

$$\dot{\phi}_n = \gamma \frac{\partial \mathcal{H}}{\partial S_n^z} - \frac{\varepsilon S_c}{P_n^2} \dot{S}_n^z \quad (\text{A.56a})$$

$$\dot{S}_n^z = -\gamma \frac{\partial \mathcal{H}}{\partial \phi_n} + \frac{\varepsilon}{S_c} P_n^2 \dot{\phi}_n \quad (\text{A.56b})$$

Note that the signs of the damping terms are opposite to those of eqs. (2.29), reflecting precisely the presence of $\gamma < 0$. At zero damping, eqs. (A.56) coincide with the Hamilton equations for a Hamiltonian depending on the $2N$ variables $(\phi_n, S_n^z/\gamma)$, canonically conjugated in the Hamiltonian sense, since the momentum conjugated to ϕ_n is now $\Pi_n := \partial \mathcal{L} / \partial \dot{\phi}_n = S_n^z/\gamma$. The eqs. (A.56) are equivalent to the LLG form

$$\dot{\vec{S}}_n = -\gamma \vec{S}_n \times \frac{\partial \mathcal{H}}{\partial \vec{S}_n} + \frac{\varepsilon}{S_c} \vec{S}_n \times \dot{\vec{S}}_n \quad , \quad (\text{A.57})$$

and, again, the sign of the damping term is reversed with respect to the analog eq. (2.33). The LL form is obtained when replacing $\dot{\vec{S}}_n$ on the r.h.s. of (A.57) by its value, i.e., by the whole r.h.s. of the equation, and using $\vec{S}_n \times \vec{S}_n \times \dot{\vec{S}}_n = -S_c^2 \dot{\vec{S}}_n$, the result is

$$(1 + \varepsilon^2) \dot{\vec{S}}_n = -\gamma \vec{S}_n \times \frac{\partial \mathcal{H}}{\partial \vec{S}_n} - \frac{\gamma \varepsilon}{S_c} \vec{S}_n \times \vec{S}_n \times \frac{\partial \mathcal{H}}{\partial \vec{S}_n} \quad . \quad (\text{A.58})$$

(Compare with (2.34)). The last procedure is consistent with the result of replacing successively \dot{S}_n^z and $\dot{\phi}_n$ on the r.h.s. of eqs. (A.56). All these equations are again dimensionally correct.

Rate of change of the energy

As calculated in the Appendix A.3, we have for the rate of change of the Hamiltonian (specifically, the eq. (2.12) with a –generally– non-uniform time-dependent magnetic

field $\vec{h}_n(t)$, under the dynamics (A.58), the relation

$$\frac{d\mathcal{H}}{dt} = + \frac{\gamma}{S_c} \frac{\varepsilon}{(1 + \varepsilon^2)} \sum_n \left[\vec{S}_n \times \vec{B}_n \right]^2 - \sum_n \vec{S}_n \cdot \frac{d}{dt} \vec{h}_n(t) \quad (\text{A.59})$$

where the total effective field, this time really with units of magnetic induction, is defined as

$$\vec{B}_n := - \frac{\partial H}{\partial \vec{S}_n} = \hat{J} \sum_a \vec{S}_{n+a} + \hat{D} \vec{S}_n + \vec{h}_n(t) \quad (\text{A.60})$$

from which it is seen that even in presence of a static field the energy *decrease* as a consequence of damping (recall $\gamma < 0$ here), and otherwise is conserved if the damping is zero.

For the magnetization, with the dynamics (A.58), we have

$$\frac{d\vec{M}}{dt} := \sum_n \dot{\vec{S}}_n = - \frac{\gamma}{(1 + \varepsilon^2)} \sum_n \vec{S}_n \times \vec{B}_n - \frac{\gamma \varepsilon}{(1 + \varepsilon^2) S_c} \sum_n \vec{S}_n \times \vec{S}_n \times \vec{B}_n \quad . \quad (\text{A.61})$$

Appendix B

Total momenta and Thiele equation: discrete *vs.* continuum

There is an important property which is fulfilled in the continuum system but not in the discrete one, namely,

$$\vec{S} \cdot \frac{\partial \vec{S}}{\partial x_\mu} = 0 \quad , \quad \text{for } \mu = x, y. \quad (\text{B.1})$$

which follows from the uniform length of the spins. The difficulty with this property in the discrete system¹, is that we must approximate (or define) the spatial derivatives, typically with “centered differences” like

$$\partial_x \vec{S}_{n,m} \approx \Delta_x \vec{S}_{n,m} := \frac{1}{2} (\vec{S}_{n+1,m} - \vec{S}_{n-1,m}) \quad . \quad (\text{B.2})$$

It follows that, in general,

$$\vec{S}_{n,m} \cdot \Delta_{x_\mu} \vec{S}_{n,m} \neq 0 \quad , \quad \text{although} \quad \Delta_{x_\mu} (\vec{S}_{n,m})^2 = 0 \quad ! \quad (\text{B.3})$$

(something must go wrong while trying to apply the usual chain rule to the calculus in finite differences). However, in summing over the concerned index a property analogous to (B.1) is restored,

$$\sum_n \vec{S}_{n,m} \cdot \Delta_{x_\mu} \vec{S}_{n,m} = 0 \quad (\text{B.4})$$

This fact also touches properties of second space derivatives, like

$$\vec{S} \cdot \vec{\nabla}^2 \vec{S} = -(\vec{\nabla} \vec{S})^2 \quad (\text{B.5})$$

¹in contrast with $\vec{S}_n \cdot \dot{\vec{S}}_n = 0$ which follows from the peculiar “vector product” character of the discrete dynamical equations (2.33) or (2.34).

which is valid, again, for the continuum system, as a consequence of (B.1). The Laplacian is typically discretized as [11]

$$\vec{\nabla}^2 \vec{S}_{n,m} \approx \vec{S}_{n+1,m} + \vec{S}_{n-1,m} + \vec{S}_{n,m+1} + \vec{S}_{n,m-1} - 4 \vec{S}_{n,m} \quad (\text{B.6})$$

The first 4 terms are essentially the discrete effective field (apart from anisotropy) of the exchange interaction, the last term contributes a constant to the energy and does not contribute to the motion equations (2.33) or (2.34), due to the vectorial products in the latter. Thus, for the case of the LLG equations, at least in cartesian components, the discrete version coincides exactly with the discretization of the continuum model. This is not longer valid in other coordinate systems (for instance, eqs. (2.29) or (2.35)).

These discreteness details have to be taken into account also when talking about the discrete versions of the total linear and angular momenta as defined in Classical Field Theory,

$$\vec{P} = \int d^2x S^z \vec{\nabla} \phi \quad , \quad (\text{B.7})$$

$$\vec{L} = \int d^2x \vec{x} \times (S^z \vec{\nabla} \phi) \quad , \quad (\text{B.8})$$

where spatial gradients are involved. It is easy to prove the conservation of these quantities by using the Hamilton equations (zero damping), but I did not find a reason why the discrete versions should be conserved in the simulations, and, as a matter of fact, they are not (see Appendix D).

The Thiele equation:

It is interesting to derive the Thiele equation in a fully discrete manner, to see whether some difference with the usual continuum version arise. We start from the LLG eq. (2.33), in the form

$$\dot{\vec{S}}_n + \frac{\varepsilon}{S_c} \vec{S}_n \times \dot{\vec{S}}_n = - \vec{S}_n \times \frac{\partial \mathcal{H}}{\partial \vec{S}_n} \quad , \quad (\text{B.9})$$

and assume the time dependence of the vortex field can be transferred to a set of functions $\vec{X}(t)$ such that

$$\vec{S}_n(t)|_{\text{vortex}} = S_n(\vec{n} - \vec{X}(t)) \quad , \quad (\text{B.10})$$

and, therefore,

$$\dot{\vec{S}}_n(t) = - \sum_j \frac{\partial \vec{S}_n}{\partial X_j} \dot{X}_j \quad , \quad \frac{\partial \mathcal{H}}{\partial \vec{S}_n} \frac{\partial \vec{S}_n}{\partial X_i} = \frac{\partial \mathcal{H}}{\partial X_i} \quad . \quad (\text{B.11})$$

We then multiply (B.9) by $\vec{S}_n \cdot \frac{\partial \vec{S}_n}{\partial X_i} \times \dots$ and using (B.11), the fact that $\vec{S}_n \cdot \dot{\vec{S}}_n = 0$, and elemental application of $\vec{A} \times \vec{B} \times \vec{C} = \vec{B}(\vec{A} \cdot \vec{C}) - \vec{C}(\vec{A} \cdot \vec{B})$, we obtain

$$-\sum_j \vec{S}_n \cdot \left(\frac{\partial \vec{S}_n}{\partial X_i} \times \frac{\partial \vec{S}_n}{\partial X_j} \right) \dot{X}_j - \varepsilon S_c \sum_j \left(\frac{\partial \vec{S}_n}{\partial X_i} \cdot \frac{\partial \vec{S}_n}{\partial X_j} \right) \dot{X}_j = -S_c^2 \frac{\partial \mathcal{H}}{\partial X_i} + \left(\vec{S}_n \cdot \frac{\partial \mathcal{H}}{\partial \vec{S}_n} \right) \left(\vec{S}_n \cdot \frac{\partial \vec{S}_n}{\partial X_i} \right) \quad (\text{B.12})$$

The last term is zero in the continuum system, due to (B.1). In the discrete case, this last term is not obviously vanishing. After summing over all sites, we can express the equation as

$$(\hat{\mathbf{G}} + \hat{\mathbf{g}}) \frac{d\vec{X}}{dt} = \vec{F} + \vec{F}^d, \quad (\text{B.13})$$

with the usual (antisymmetric) gyromagnetic tensor

$$G_{ij} = -\sum_n \vec{S}_n \cdot \left(\frac{\partial \vec{S}_n}{\partial X_i} \times \frac{\partial \vec{S}_n}{\partial X_j} \right) \quad (\text{B.14})$$

the usual (symmetric) dissipation tensor

$$g_{ij} = -\varepsilon S_c \sum_n \frac{\partial \vec{S}_n}{\partial X_i} \cdot \frac{\partial \vec{S}_n}{\partial X_j} \quad (\text{B.15})$$

the usual force

$$F_x = -S_c^2 \sum_n \frac{\partial \mathcal{H}}{\partial X} = -\frac{1}{2} S_c^2 \sum_n \vec{B}_n \cdot (\vec{S}_{n+1,m} - \vec{S}_{n-1,m}) \quad (\text{B.16})$$

$$F_y = -S_c^2 \sum_n \frac{\partial \mathcal{H}}{\partial Y} = -\frac{1}{2} S_c^2 \sum_n \vec{B}_n \cdot (\vec{S}_{n,m+1} - \vec{S}_{n,m-1}), \quad (\text{B.17})$$

where \vec{B}_n is the effective field (A.29), and an “unusual” force

$$\vec{F}_i^d = \sum_n \left(\vec{S}_n \cdot \frac{\partial \mathcal{H}}{\partial \vec{S}_n} \right) \left(\vec{S}_n \cdot \frac{\partial \vec{S}_n}{\partial X_i} \right) \quad (\text{B.18})$$

which seems to be an effect of discreteness (therefore the superindex d). Now from (B.2), we have

$$\vec{F}_x^d = -\frac{1}{2} \sum_n (\vec{S}_n \cdot \vec{B}_n) \vec{S}_n \cdot (\vec{S}_{n+1,m} - \vec{S}_{n-1,m}) \quad (\text{B.19a})$$

$$\vec{F}_y^d = -\frac{1}{2} \sum_n (\vec{S}_n \cdot \vec{B}_n) \vec{S}_n \cdot (\vec{S}_{n,m+1} - \vec{S}_{n,m-1}) \quad (\text{B.19b})$$

which can not be shown to vanish in general. The diagonal elements of $\hat{\mathbf{G}}$ are still

obviously zero, but (another feature that appears only for the discrete system) the non-diagonal elements of $\hat{\mathbf{g}}$ are not zero.

There is no error in this algebra. The moral here is: if we are going to calculate in simulations the discrete versions (how could be otherwise?) of the gyrovector and the dissipation matrix, to be consistent, we must include in the account the “strange” term \vec{F}^d from (B.18).

This is more accurate than just taking the continuum Thiele equation and discretize it. The four terms of Eq. (B.13) can be measured, relying on the accuracy of the Ansatz (B.10), which permits to connect the gradient with respect to \vec{X} to the (discrete) gradient with respect to \vec{n} , this is, $\vec{\nabla}_{\vec{X}} = -\vec{\nabla}_{\vec{n}} \approx -\Delta_{\vec{n}}$.

It results from the simulations that the “strange” term \vec{F}^d and the non-diagonal elements of $\hat{\mathbf{g}}$ become negligible when the size of the lattice is very large.

Appendix C

Vorticity & winding number: 2D vs. 3D

The definition of the topological density $\gamma(x, y)$ in (3.17) suggests to consider it indeed as the third component γ_z of a vector quantity,

$$\gamma_i = -\frac{1}{2} \varepsilon_{ijk} (\partial_j \vec{S} \times \partial_k \vec{S}) \cdot \vec{S} \quad , \quad (\text{C.1})$$

where $i, j, k = x, y, z$, the volume integral of which was named “gyrovector” (\vec{G}), by Thiele [76]. In components,

$$\gamma_x = -(\partial_y \vec{S} \times \partial_z \vec{S}) \cdot \vec{S} \quad , \quad \gamma_y = -(\partial_z \vec{S} \times \partial_x \vec{S}) \cdot \vec{S} \quad , \quad \gamma_z = -(\partial_x \vec{S} \times \partial_y \vec{S}) \cdot \vec{S} \quad ,$$

The 2D case has to be considered as formally embedded into the 3D space, as in the case of a thin film which extends over the XY plane with a small thickness d , and is limited by two plane surfaces at, say $z = \pm d/2$, such that the spin field does not depend on the coordinate z . In this case the only non-null component of the gyrovector is the integral of γ_z .

From its definition in eq. (C.1) it is clear that the vector $\vec{\gamma}$ represents a solenoidal field,

$$\vec{\nabla} \cdot \vec{\gamma} = 0 \quad , \quad (\text{C.2})$$

which implies that the “vortex lines” –those lines whose tangent vector is parallel to $\vec{\gamma}$ everywhere– in a 3D magnetic medium cannot end inside the medium but only at the surfaces (if a vortex line terminates at a point in the medium, this would mean that the divergence of $\vec{\gamma}$ would not be zero at that point). Therefore, in an infinite 3D medium vortices can only be realized as closed paths, or “vortex rings”. In contrast, the surfaces limiting the 2D medium remove naturally this constraint.

In terms of the canonical variables (S_z, ϕ) we have

$$\vec{\gamma} = \vec{\nabla} S_z \times \vec{\nabla} \phi \quad (\text{C.3})$$

from where we see the analogy between the fields (S_z, ϕ) and the Clebsch potentials familiar in hydrodynamics [6, 48]. Thus, Eq. (C.3) says that “vortex lines” (formed by all points where $\vec{\gamma} \neq 0$) are defined as the intersections of the two equipotential surfaces $S_z(\vec{x}) = C_1$ and $\phi(\vec{x}) = C_2$ with arbitrary constants C_1 and C_2 . This is, vortex lines are curves (reduced to a single point in 2-D) along which the magnetization (the spin field \vec{S} in our case) remains constant. In the 2D case, this feature translates into the condition that $S_z \rightarrow \pm S_c$ at the center of a vortex ($\vec{x} \rightarrow \vec{X}$), or that the polarization p of the vortex is a constant.

The fact that the field $\vec{\gamma}$ from (C.1) is solenoidal implies that it can be written as the curl of a vector potential $\vec{a}(\vec{x})$,

$$\vec{\gamma} = \vec{\nabla} \times \vec{a} \quad , \quad (\text{C.4})$$

and a preserved value, the Hopf index,

$$N = \frac{1}{4\pi} \int (\vec{a} \cdot \vec{\gamma}) d^3x \quad , \quad (\text{C.5})$$

can be defined, in the same way as in hydrodynamics [48]. Although the vector potential is defined up to a gauge transformation ($\vec{a} \rightarrow \vec{a} + \vec{\nabla} \lambda$, for some scalar function $\lambda(\vec{x})$), the integral (C.5) is obviously gauge invariant. Considering $\vec{\gamma}$ as a given vorticity distribution which enters as a source in the Poisson equation for \vec{a} (derived from (C.4), supplemented with a gauge condition $\vec{\nabla} \cdot \vec{a} = 0$, see [6]) we have the solution

$$\vec{a}(\vec{x}) = -\frac{1}{4\pi} \int \frac{\vec{R} \times \vec{\gamma}(\vec{x}')}{R^3} d^3x' \quad , \quad \vec{R} = \vec{x} - \vec{x}' \quad . \quad (\text{C.6})$$

and the Hopf index is expressed as

$$N = \frac{1}{(4\pi)^2} \int \vec{\gamma}(\vec{x}) \cdot \left(\frac{\vec{R} \times \vec{\gamma}(\vec{x}')}{R^3} \right) d^3x d^3x' \quad . \quad (\text{C.7})$$

It is remarkable that this integral gives always an integer number [16]. From eq. (C.3) we can derive a local expression for the vector potential

$$\vec{a} = S_z \vec{\nabla} \phi \quad . \quad (\text{C.8})$$

However, inserting (C.3) and (C.8) into (C.5) results in a zero Hopf index, providing that both S_z and ϕ are differentiable functions. This means that the canonical variables

S_z and ϕ cannot be both differentiable for field for configurations with $N \neq 0$. In fact, we know that the spin field reaches the north as well as the south pole $\vec{S}^2 = S_c^2$ along a vortex line, where the variable ϕ becomes multivalued. We note also that the expression (C.8) coincides with the definition of the linear momentum density associated to the Hamilton equations

$$\dot{S}_z = \frac{\delta H}{\delta \phi} \quad , \quad \dot{\phi}_z = -\frac{\delta H}{\delta S_z} \quad , \quad (\text{C.9})$$

from which we can observe the close relationship between the dynamics of the spin field and its topological properties. The differentiability issues connected with (C.8) make ambiguous the usual definition of linear momentum in ferromagnets with topologically non-trivial configurations.

The expression for the Hopf index is no longer meaningful in presence of the boundary surfaces in the case the quasi-2D film. Instead, the flux of the vorticity density

$$\Gamma = \frac{1}{4\pi} \int_S \vec{\gamma} \cdot d\vec{s} = \frac{1}{4\pi} \oint_c S_z \vec{\nabla} \phi \cdot d\vec{l} \quad (\text{C.10})$$

through an arbitrary surface contained within the film, is usually considered. The choice of the surface is arbitrary in view of (C.2) and the divergence theorem. In particular this surface can be any region R_{xy} of the XY plane, and

$$\Gamma = \frac{1}{4\pi} \int_{R_{xy}} \gamma_z dx dy \quad (\text{C.11})$$

agrees with our previous definition of the modulus of the gyrovector; it is also known as “winding number” [16], and is also integer-valued. Again, with $\Gamma \neq 0$ the fields S_z and ϕ cannot be both differentiable and the linear momentum becomes ambiguous.

Note the difference between (C.11) and our definition (3.20) of total vorticity as the circulation of $\vec{\nabla} \phi$,

$$Q = \frac{1}{2\pi} \oint_c \vec{\nabla} \phi \cdot d\vec{l} \quad , \quad (\text{C.12})$$

which is also seen to be integer-valued. While Γ can be zero for in-plane vortices ($S_z = 0$), the total vorticity Q still is non-null. The choice of the curve is also arbitrary, even when $\vec{\nabla} \phi$ is singular at the vortex center, as can be proven by application of the Green theorem

$$\int_{R_{xy}} \left(\frac{\partial Q}{\partial x} - \frac{\partial P}{\partial y} \right) dx dy = \oint_{\partial R_{xy}} (P dx + Q dy) \quad , \quad (P, Q) = \vec{\nabla} \phi \quad (\text{C.13})$$

to the region R_{xy} between two any closed and disjunct curves c_1 and c_2 surrounding the singularity, with the total border ∂R_{xy} being the union of c_1 and c_2 oriented such that the region is kept at the left of both curves. In addition, even in the discrete version

of our simulations, (C.12) remains constant and integer valued, in contrast to (C.11), of course, as long as the vortex stays inside the path of integration.

Appendix D

Numerical procedures

Since we have been using parts of a program code which has already a good 15 years or more, with contributions and modifications of many colleagues, I would like to describe here the main features I have used, and the modifications I have done. Some old procedures of the code are also described here, since the only documentation available is in German in the Ph.D. thesis of my predecessors [69, 39].

D.1 Integration in time in the simulations

The current version (Dec. 2003) of the code `vmd`, integrates in time the equation:

$$\dot{\vec{S}}_{\vec{n}} = \frac{1}{(1 + \varepsilon^2 S^2)} \left\{ \vec{S}_{\vec{n}} \times \frac{\partial}{\partial \vec{S}_{\vec{n}}} [H + V(t)] - \varepsilon \vec{S}_{\vec{n}} \times \left(\vec{S}_{\vec{n}} \times \frac{\partial}{\partial \vec{S}_{\vec{n}}} [H + V(t)] \right) \right\} \quad (\text{D.1})$$

using a 4th-order Runge-Kutta scheme [11]. By default, it is set $S^2 = 1$, and setting in addition the denominator $(1 + \varepsilon^2 S^2)$ to unity makes a practically negligible difference. Here $\vec{n} = (n, m)$ are the two indices of the square lattice. The integration is done by the subroutine `<difeq>` inside `<tstep.F>`. Details of the building of the effective field and the differential equation are given below.

D.2 Boundary conditions, image vortices

For the boundary conditions (BC) used in this work, Neumann BC (free BC) or Dirichlet BC (fix BC), for a circular system, only one image vortex or anti-vortex is placed at the position

$$\vec{X}_I = \frac{L^2}{|\vec{X}|^2} \vec{X} \quad (\text{D.2})$$

BC	q	p	G	q_I	p_I	G_I
Neumann	+1	+1	+2 π	-1	+1	-2 π
	+1	-1	-2 π	-1	-1	+2 π
	-1	+1	-2 π	+1	+1	+2 π
	-1	-1	+2 π	+1	-1	-2 π
Dirichlet	+1	+1	+2 π	+1	-1	-2 π
	+1	-1	-2 π	+1	+1	+2 π
	-1	+1	-2 π	-1	-1	+2 π
	-1	-1	+2 π	-1	+1	-2 π

Table D.1: Charges and modulus of the gyrovector for the image vortex

where \vec{X} is the position of the vortex inside the system. The following table summarizes the corresponding image vortex charges.

For a rectangular geometry, not used in this work, details are to be found in the Appendix D of Schnitzer's Ph.D. thesis [69] (in German).

D.3 Numerical relaxation of an initial condition

Static solutions of the discrete LL equations satisfy the algebraic equations

$$\vec{S}_{\vec{n}} \times \vec{B}_{\vec{n}} = 0 \quad , \quad \vec{B}_{\vec{n}} = - \frac{\partial H}{\partial \vec{S}_{\vec{n}}} \quad , \quad (\text{D.3})$$

so that each spin must align itself parallel to its effective field, given by the action of its neighbors and possible anisotropy and/or magnetic fields. Thus, in order to solve (D.3) we can apply an iterative procedure which, starting from an approximate solution (often given by the continuum limit), in each step will turn the spins in the direction of the local effective field. This means, the spin in the $(i + 1)$ -esim step is obtained from the spin in the i -esim step as

$$\vec{S}_{\vec{n}}^{(i+1)} := \omega \frac{|\vec{S}_{\vec{n}}^{(i)}|}{|\vec{B}_{\vec{n}}^{(i)}|} \vec{B}_{\vec{n}}^{(i)} + (1 - \omega) \vec{S}_{\vec{n}}^{(i)} \quad . \quad (\text{D.4})$$

where $\vec{B}_{\vec{n}}^{(i)}$ is the effective field of the spin $\vec{S}_{\vec{n}}^{(i)}$ at the i -esim step, and a relaxation parameter ω was introduced, which determines a relative weight of $\vec{B}_{\vec{n}}^{(i)}$ in each iteration. For $0 < \omega < 1$ we speak about "underrelaxation" , for $\omega > 1$ we speak about

“overrelaxation” [71]. The convergence rate, and whether convergence is reached at all, strongly depend on the choice of ω . For relaxing vortex solutions, we have used in all the cases a value $\omega = 1$, which gives a good convergence in few decens of steps. Note that for $\omega \neq 1$, the Eq.(D.4) does not longer preserve the length of the spins, so that in this case one has to renormalize the spins to the desired length after each iteration step.

D.4 Measurement/definition of the center of the vortex in the simulations

Method 1:

This method is implemented in the routine `<vpos.F>` and is based in the static IP structure of a single vortex (3.19), assuming it is valid in the innermost plaquette of the vortex core, which is the only that contains non-null vorticity, without essential perturbation under a broad range of situations (e.g., even when *weak* magnetic fields are present). It is described in the Sec. 4.6 of [39].

Method 2:

Also implemented in `<vpos.F>` and based in static IP structure, it uses a fitting procedure, to fit (3.19) over squares of 3 x 3 plaquettes around the one which contains vorticity (the innermost), and if it does not succeed, over larger squares. It is also described in the Sec. 4.6 of [39].

Let us refer to the positions given by either of these two methods as $(X^{\text{IP}}, Y^{\text{IP}})$.

Method 3:

This method is implemented in a new routine, `<vposjp.F>`, and calculates the center of mass of the OP structure of the vortex, i.e., of the z-component S^z of the spins, over a **disk** of few lattice constants radius, a “spot” which follows the vortex movement. This disk matches better the quasi-circular symmetry of the vortex structure, and at the same time it is quasi-local, i.e. it is not so local as method **1**, and not so global that could take into account non desired contributions to S^z coming from the field far from the vortex, which, in addition, saves computing time.

The method proves to be smoother than the previous two methods for some situations, in particular in presence of a magnetic field, but, unfortunately, not in all situations.

In order to follow the vortex, this method takes as initial input the position given by the **Method 1** or **Method 2** (from `<vpos.F>`), to define the vortex position for the

first time, and afterwards, the previous position calculated by itself. The positions are thus defined by

$$X_v^{\text{CM}} = \frac{\sum_{n,m} n S^z(n, m)}{\sum_{n,m} S^z(n, m)} \quad , \quad Y_v^{\text{CM}} = \frac{\sum_{n,m} m S^z(n, m)}{\sum_{n,m} S^z(n, m)} \quad . \quad (\text{D.5})$$

where the sums run over (n, m) inside a disk of a radius $\text{rv}0$, small compared with the lattice size, but larger than the vortex radius. Typically, in our simulations, $\text{rv}0=4.1$ (lattice spacings) produce smooth results. We have measured also the ‘‘polarization’’ into this spot, i.e., the average of $S^z(n, m)$ as

$$p^{\text{CM}} = \frac{1}{N_d} \sum_{n,m} S^z(n, m) \quad (\text{D.6})$$

where N_d is the number of spins into the disk, which varies in time. The value of this p^{CM} is thus arbitrary, but its fluctuations are to be compared with those of the polarization obtained by other methods.

D.5 Gyrodensity and its momenta

The program calculates in the routine `<gyrodensity.F>` for each spin the ‘‘topological density’’ defined in papers by Papanicolaou, Komineas, etc. [59, 61, 60, 62, 41], but in a discrete form, as

$$\gamma(n, m) \approx \frac{1}{4} \vec{S}(n, m) \cdot \left\{ \left[\vec{S}(n+1, m) - \vec{S}(n-1, m) \right] \times \left[\vec{S}(n, m+1) - \vec{S}(n, m-1) \right] \right\} \quad (\text{D.7})$$

which uses centered-differences to replace the spacial derivatives. Because of this, care has to be taken when the spin is laying on the lattice border. Notice also that there must be some denominator 4π in (D.7), for this equation to define the ‘‘winding number’’ or ‘‘flux of vorticity’’ [41], factor that will dissappear in some quotients of interest (see eq. (D.10) below).

The program calculates also the integral of γ , or ‘‘degree of mapping’’ (or the modulus of the Gyro-vector of Thiele), as

$$\Gamma \approx \sum_{n,m} \gamma(n, m) \quad (\text{D.8})$$

and the linear and angular momenta defined in the way of Papanicolaou, as first mo-

menta of this density:

$$\begin{aligned} P_{\text{Pap}}^x &\approx - \sum_{n,m} m \gamma(n, m) \quad , \quad P_{\text{Pap}}^y \approx \sum_{n,m} n \gamma(n, m) \\ L_{\text{Pap}} &\approx \frac{1}{2} \sum_{n,m} (n^2 + m^2) \gamma(n, m) \end{aligned} \quad (\text{D.9})$$

Note that these definitions depend on where the origin of coordinates for (n, m) is located, while (D.8) do not. The shifting of the origin from $\vec{O} = (0, 0)$ to, say, $\vec{C} = (c_x, c_y)$ can be done by simple data manipulation after running the program, since

$$\begin{aligned} (P_{\text{Pap}}^x)' &= - \sum_{n,m} (m - c_y) \gamma = P_{\text{Pap}}^x + c_y \Gamma \quad , \\ (P_{\text{Pap}}^y)' &= \sum_{n,m} (n - c_x) \gamma = P_{\text{Pap}}^y - c_x \Gamma \quad , \\ L'_{\text{Pap}} &= \frac{1}{2} \sum_{n,m} (\vec{n} - \vec{C})^2 \gamma(n, m) = L_{\text{Pap}} - (c_x P_{\text{Pap}}^y - c_y P_{\text{Pap}}^x) + \frac{1}{2} \vec{C}^2 \Gamma \quad . \end{aligned}$$

From the measurement of $\gamma(n, m)$ we also obtain another method to “define” the vortex center position, as that of the “guiding center” (GC), or center of mass of the topological density:

Method 4:

$$\begin{aligned} X_v^{\text{GC}} &= \sum_{n,m} n \gamma(n, m) / \Gamma = P_{\text{Pap}}^y / \Gamma \\ Y_v^{\text{GC}} &= \sum_{n,m} m \gamma(n, m) / \Gamma = - P_{\text{Pap}}^x / \Gamma \quad . \end{aligned} \quad (\text{D.10})$$

Thus, together with the methods described before, we have three methods (the first two, both based in the IP structure, give very similar results, and are to be considered here as one) which I will compare briefly in the next sections.

Finally, the routine also calculates the lineal momentum density, in the way of Classical Field Theory, in a discrete form,

$$\begin{aligned} P_x &\approx \frac{1}{2} S^z(n, m) \left[\phi(n+1, m) - \phi(n-1, m) \right] \\ P_y &\approx \frac{1}{2} S^z(n, m) \left[\phi(n, m+1) - \phi(n, m-1) \right] \end{aligned} \quad (\text{D.11})$$

This definition does not depend on the the location of the origin of coordinates. Here also care has to be taken for spins on the border of the lattice.

D.6 Results of simulations

Methods for measuring/defining vortex positions:

As an illustration, let us see the result for a simple system of diameter $D = 40$, with anisotropy $\lambda = 0.92$, at zero damping and zero magnetic field. A vortex is launched from the initial position $(n, m) = (20.5, 32.5)$. Trajectories are measured by either of the IP methods **1** or **2**, if not otherwise explicitly said. The trajectory, up to a time $t = 2300$, is shown in **Fig. 3.3** (initially without image-vortex) and **Fig. 3.4** (initially with image-vortex).

In the **Fig. D.1** we zoom-in a piece of the trajectory of **Fig. 3.3**, and compare it with the results of methods **3** and **4**.

In the **Fig. D.2** we compare the signals of the components of the vortex velocity for the trajectory without image of **Fig. 3.3**, calculated as discrete time derivatives (“centered differences”) of the position signals obtained with: methods **1-2** in the 1st and 3th panels from above, (V_x, V_y) , and method **4** in the 2nd and 4th panels, (V_x^{GC}, V_y^{GC}) . We show an enhancement of a small part of this figure in **Fig. D.3**. The **Fig. D.4** shows also velocity signals, but for the trajectory with the image vortex, corresponding to **Fig. 3.4**.

We can see that the method **4**, based on a *simultaneous* measurement of IP *and* OP properties which are strongly localized in the region of the vortex core, produces the smoothest trajectory and velocity signals. Now we can conclude that the fluctuations seen in **Fig. D.2** are due to 3 causes: **(1.)** the locality/globality of the method (the narrow vertical lines in the 1st and 3rd panels), **(2.)** the underlying Peierls-Nabarro potential of the lattice (oscillations which are present also in the 2nd and 4th panels, and even in the **Fig. D.4**), and **(3.)** the interaction with spin waves giving cycloidal oscillations (much smaller in **Fig. D.4** when the vortex is initially in presence of its image). The enhancement in **Fig. D.3** makes this points more clear.

Gyrovector and momentum signals

In **Fig. D.6** it is shown the results of (a) $\gamma(t)$ from (D.8) (Above) and (b) the modulus of the momentum from (D.11) (Below), as a function of time. The same is shown in **Fig. D.6** but for the trajectory with the image.

We can appreciate a clear correlation between these two signals. Note that they are global quantities, not depending on any particular choice of the method to define the vortex position. Both components of the linear momentum are shown in the **Fig. D.8** for longer times.

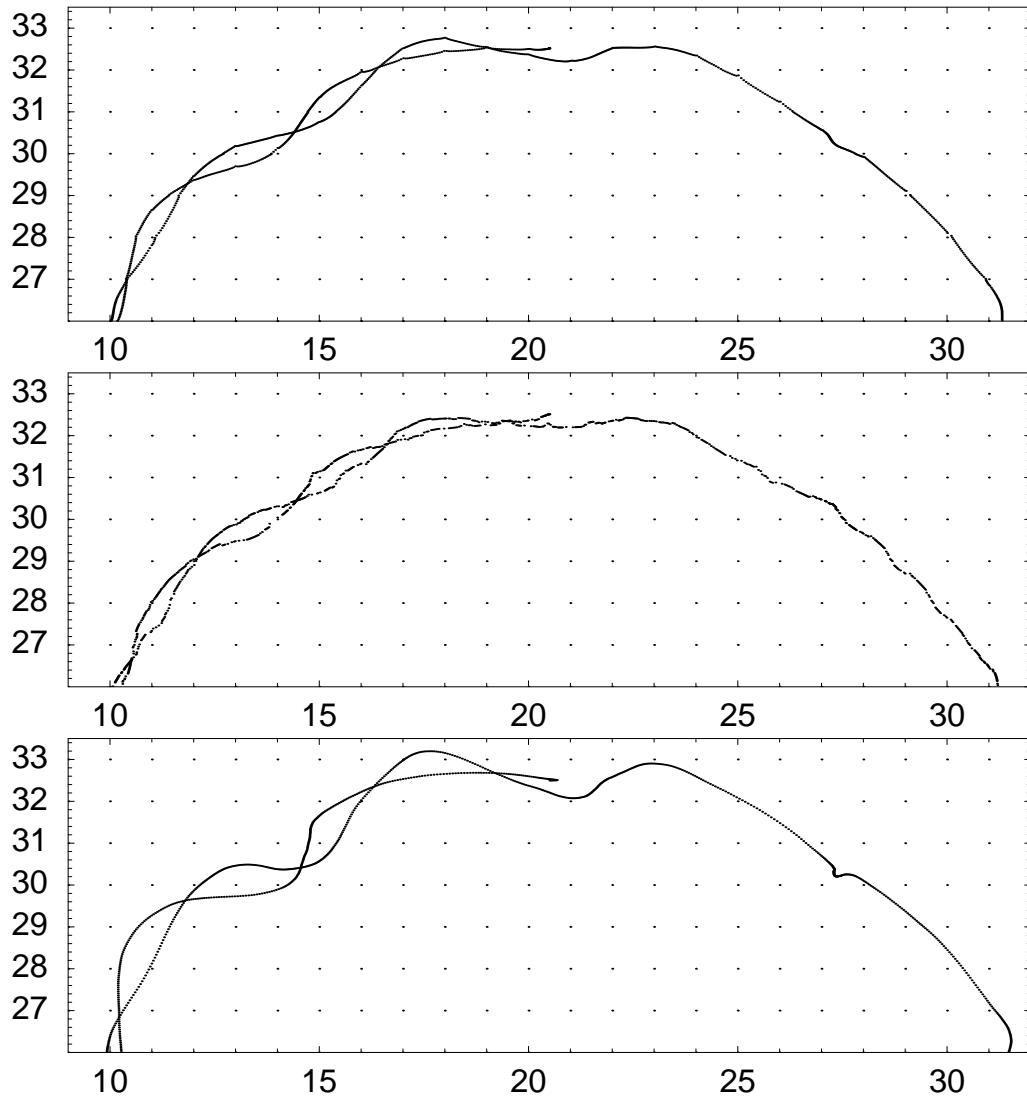


Fig. D.1: Zoom-in of **Fig. 3.3**, measured by **Method 1-2** (Top), **Method 3:** eq. (D.5) (Middle), and **Method 4** eq. (D.10) (Bottom), up to $t = 2300$: a sector of the 2nd turn is also shown. The method for the (Top) picture is the most local (involves only the 4 innermost spins), for the (Middle) one is “quasi” local (some 20-40 spins), and for the (Bottom) one is global (all the spins).

Both **Fig. D.6** and **Fig. D.8** show non-conservation of quantities which in the continuum limit are theoretically conserved.

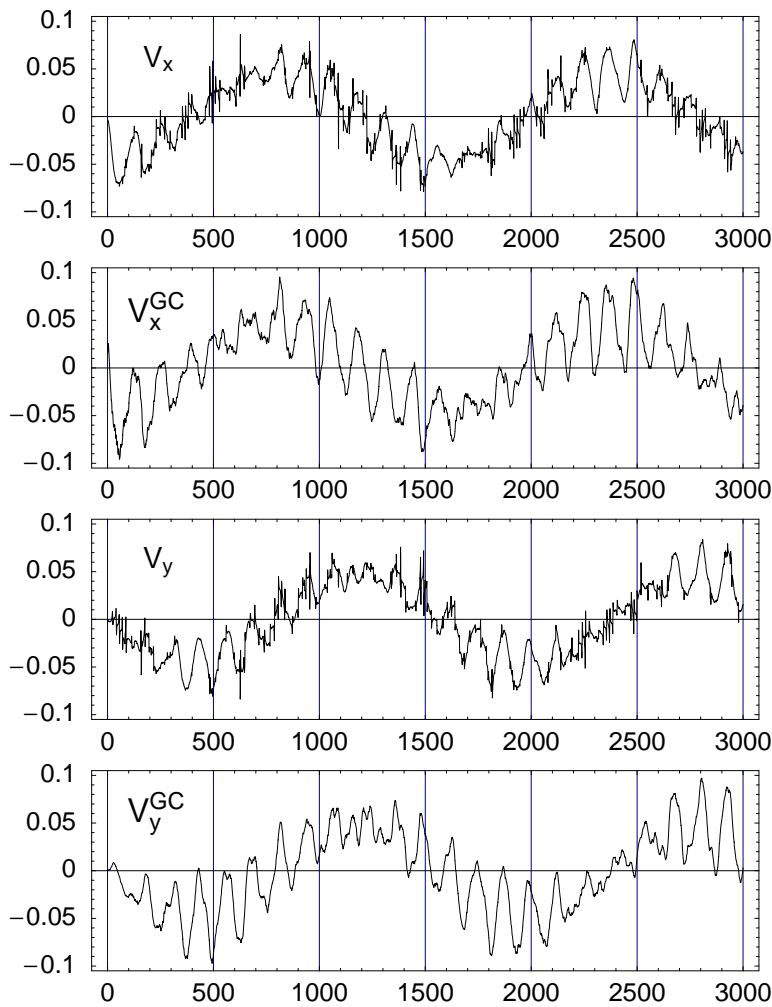


Fig. D.2: Components of the vortex velocity, corresponding to **Fig. 3.3**, measured by **Method 1-2** (1st and 3th panels from above: V_x , V_y) and **Method 4** (2nd and 4th panels: V_x^{GC} , V_y^{GC}), while the vortex is describing cycloidal osc. around a circular trajectory

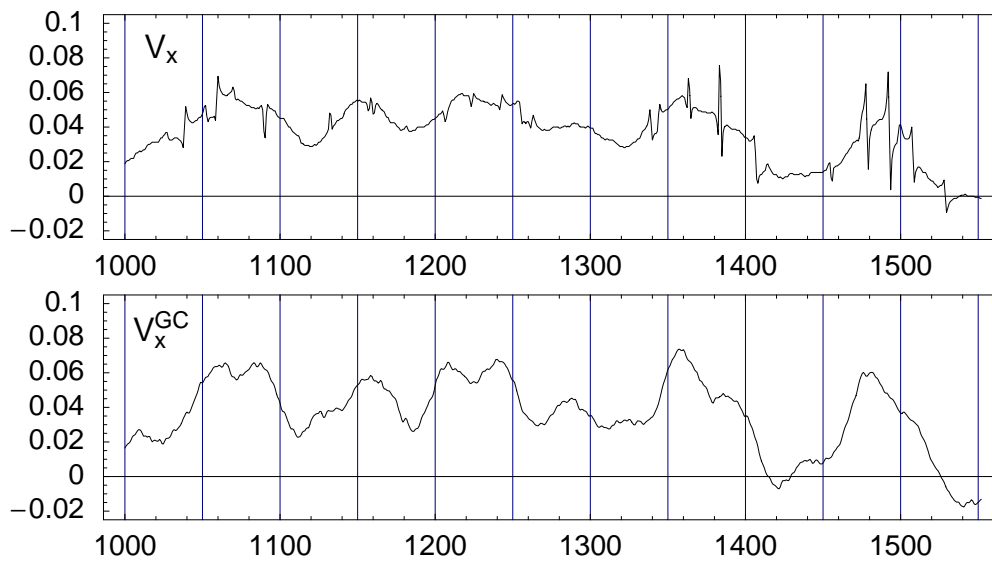


Fig. D.3: Enhancement of a part of **Fig. D.2**, 1st and 2nd panels from above.

Fig. D.4: Same as in the **Fig. D.2**, but corresponding to **Fig. 3.4**: the vortex initialized with the image vortex.

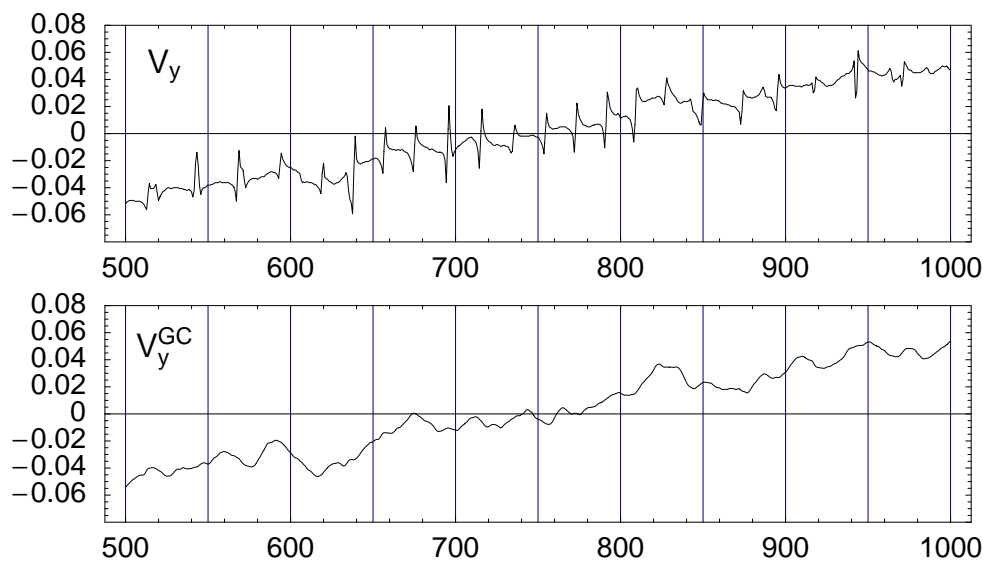
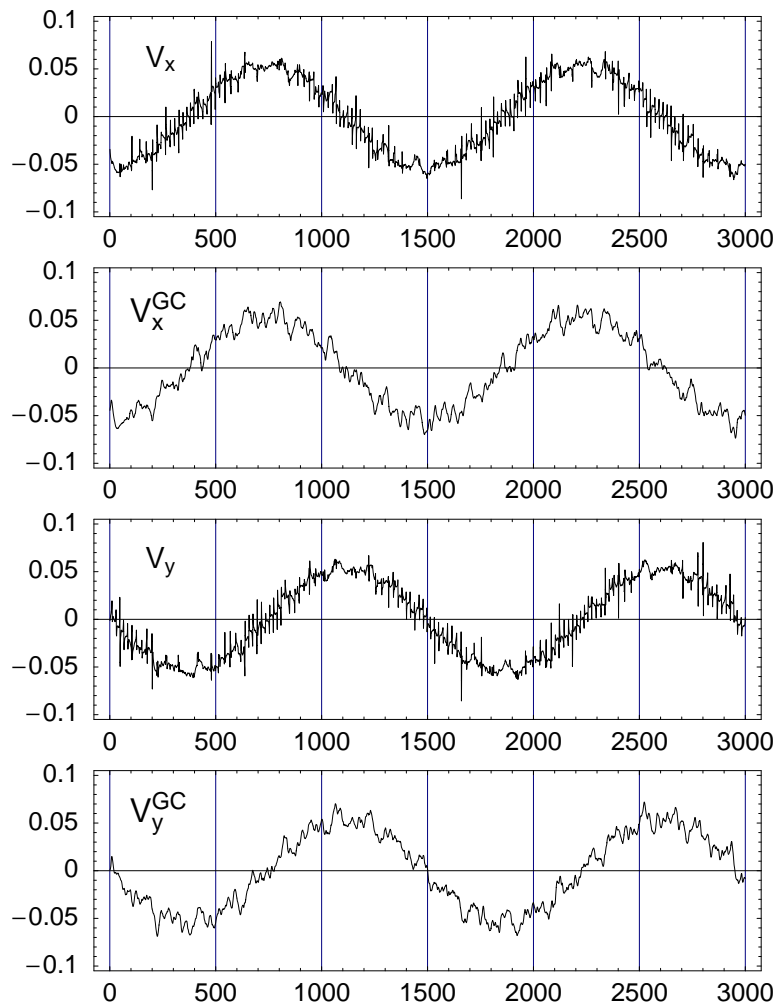


Fig. D.5: Enhancement of a part of **Fig. D.4**, 3rd and 4th panels from above.

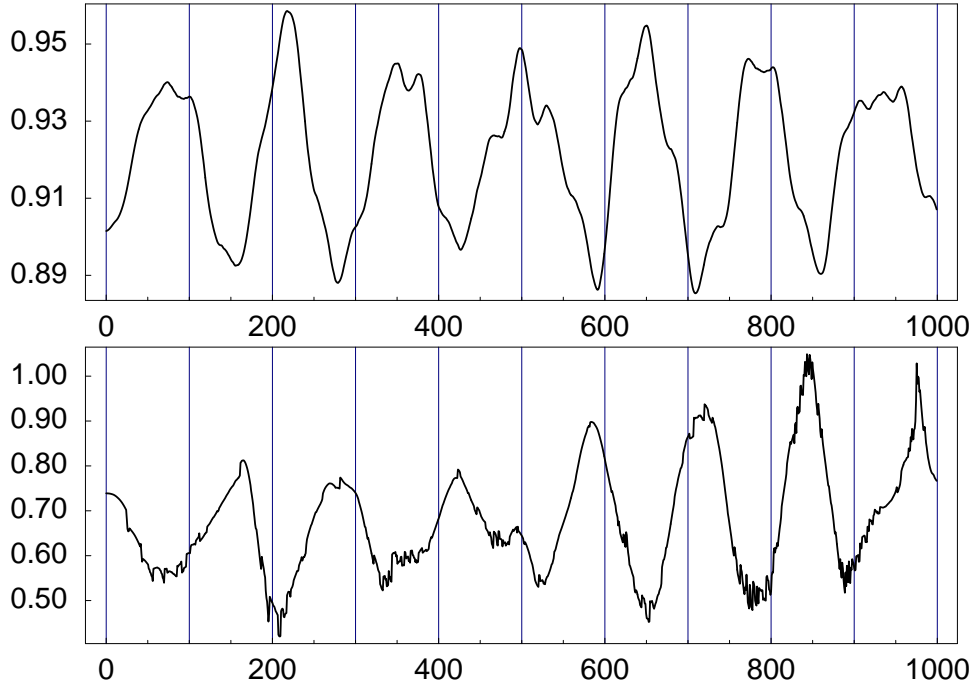


Fig. D.6: Corresponding to **Fig. 3.3**: (Above) Integrated gyrodensity Γ from (D.8) (divided by 2π). (Below) Modulus of total linear momentum $\sqrt{P_x^2 + P_y^2}$ from (D.11) (divided by the maximum value = 18). Both signals vs. time.

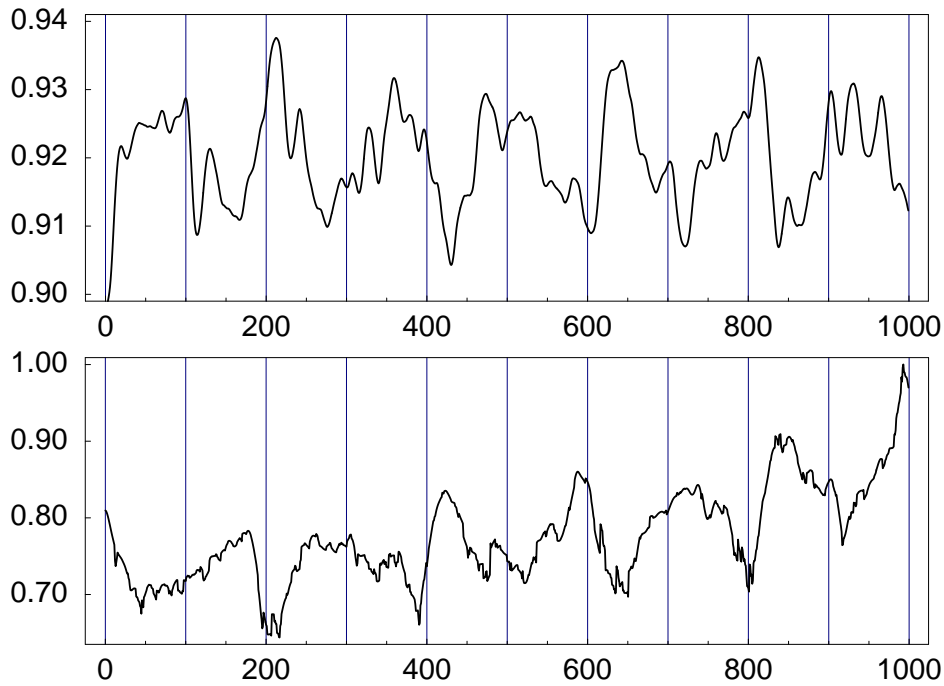


Fig. D.7: The same as in **Fig. D.6**: Corresponding to **Fig. 3.4**: the trajectory with the image vortex. Momentum modulus rescaled by its maximum value = 15.6. Note the reduced amplitude of the oscillations.

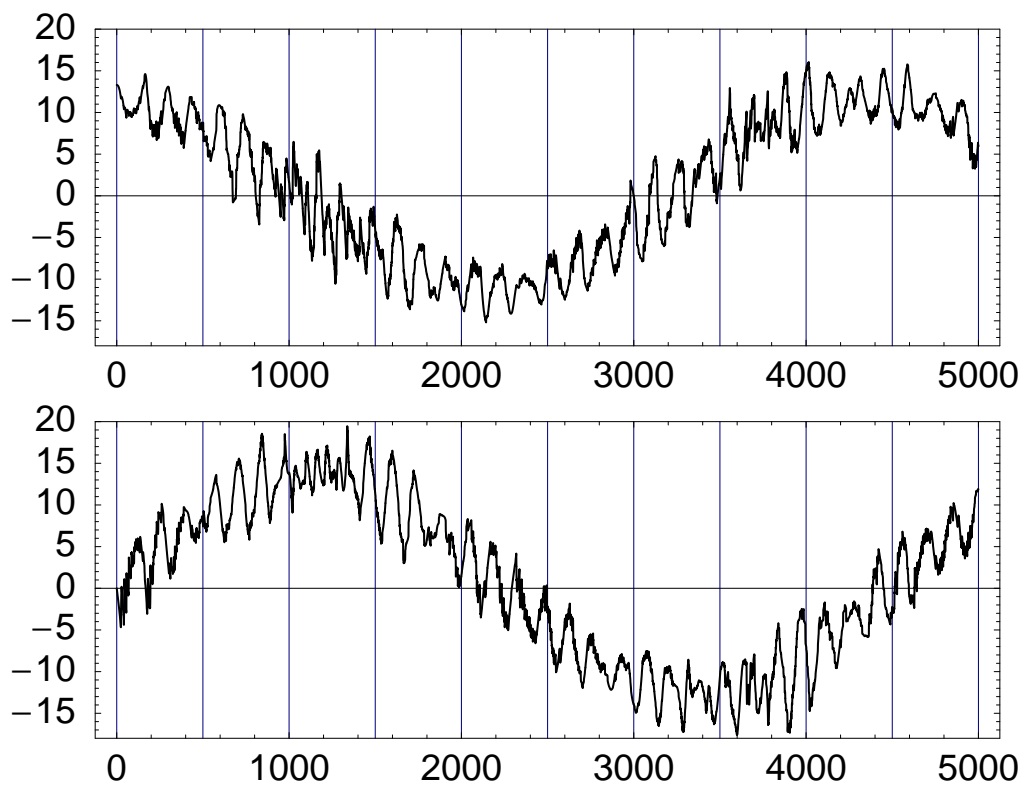


Fig. D.8: Corresponding to **Fig. 3.3:** (Above) x-component P_x and (Below) y-component P_y of the total linear momentum from (D.11). Both signals vs. time.

Appendix E

Force due to the rotating field

The idea here is to calculate the double integral (5.2) in the reference frame which is fix to the vortex center. Viewed from this point, the distance to the circular border of the lattice changes as a function of the azimuthal angle χ . With the settings of the **Fig. A.1**, we have that the limits of the integral, in this reference frame, are: $0 \leq \chi \leq 2\pi$, $0 \leq \rho \leq \sigma(\alpha)$, where, from the cosine themem,

$$\sigma(\alpha) = R \cos \alpha + \sqrt{R^2 \cos^2 \alpha + L^2 - R^2} \quad , \quad \cos \alpha = - \cos(\chi - \Phi) \quad . \quad (\text{E.1})$$

In this frame we assume a static vortex structure (removing the primes)

$$\begin{aligned} \theta &= \theta(\rho) \quad , \quad \vec{\nabla} \theta = \theta'(\rho) \hat{\rho} \\ \phi &\equiv \Phi = q\chi \quad , \quad \vec{\nabla} \Phi = \frac{q}{\rho} \hat{\chi} \quad , \quad q = \pm 1. \end{aligned}$$

with $\hat{\rho} = \cos \chi \hat{x} + \sin \chi \hat{y}$, $\hat{\chi} = -\sin \chi \hat{x} + \cos \chi \hat{y}$, and for $q = 1$, we have to calculate the integral

$$\vec{F}_h(R, \Phi, t) = -h \int_0^{2\pi} d\chi \int_0^{\sigma(\alpha)} \rho d\rho \left\{ \theta'(\rho) \cos \theta \cos(\chi - \omega t) \hat{\rho} - \frac{1}{\rho} \sin \theta \sin(\chi - \omega t) \hat{\chi} \right\} \quad (\text{E.2})$$

where we have set $\beta_0 = 0$. Defining

$$\begin{aligned} T(\alpha) &= \int_0^{\sigma(\alpha)} d\rho \sin \theta(\rho) \quad , \\ P(\alpha) &= \int_0^{\sigma(\alpha)} d\rho r \theta'(\rho) \cos \theta(\rho) = r \sin \theta(\rho) \Big|_0^{\sigma(\alpha)} - T(\alpha) \quad , \end{aligned} \quad (\text{E.3})$$

and using the asymptotic values $\sin \theta(\rho = 0) = 0$, $\sin \theta(\rho = \sigma(\alpha)) = 1$, we see that actually $P(\alpha) = \sigma(\alpha) - T(\alpha)$. Now for $T(\alpha)$ we can split the integral into an inner and

an outer part

$$\int_0^{\sigma(\alpha)} d\rho \sin \theta(\rho) = \int_0^{r_v} d\rho \sin \theta(\rho) + \int_{r_v}^{\sigma(\alpha)} d\rho \sin \theta(\rho)$$

and use then in each part the asymptotics

$$\cos(\theta(\rho)) = \begin{cases} \left(1 - \frac{3}{7}\rho^2/r_v^2\right) , & \text{for } \rho \rightarrow 0, \\ \frac{4e^1}{7} \sqrt{\frac{r_v}{\rho}} \exp[-\rho/r_v] , & \text{for } \rho \rightarrow \sigma(\alpha), \end{cases}$$

which match at $\rho = r_v$. The first integral is a constant $(\frac{2\sqrt{14}}{3\sqrt{3}} - \frac{11\sqrt{11}}{21\sqrt{3}})r_v \approx 0.437r_v$, and the second integral, observing the exponential behaviour of the integrand, can in turn be separated as

$$\int_{r_v}^{\sigma(\alpha)} = \int_{r_v}^{a_c} + \int_{a_c}^{\sigma(\alpha)}$$

where $a_c \approx 6r_v$ (in any case is $a_c \ll \sigma(\alpha)$), such that for $\rho < a_c$ the integral can be numerically calculated ($\approx 4.938 r_v$), while for $\rho > a_c$ the integrand is to a high order of approximation equal to 1, and the corresponding integral results $(\sigma(\alpha) - 6r_v)$. Finally, we have

$$T(\alpha) \approx 0.437 r_v + 4.938 r_v - 6 r_v + \sigma(\alpha) \equiv c + \sigma(\alpha) \quad (\text{E.4})$$

with $c = -0.624 r_v$. Introducing this result in (E.2) we get

$$\begin{aligned} \vec{F}_h(R, t) = & - h \int_0^{2\pi} d\chi \cos(\chi - \omega t) \sigma(\alpha) (\cos \chi \hat{x} + \sin \chi \hat{y}) \\ & - h \int_0^{2\pi} d\chi \sin(\chi - \omega t) (c + \sigma(\alpha)) (\sin \chi \hat{x} - \cos \chi \hat{y}) \end{aligned} \quad (\text{E.5})$$

Fortunately,

$$\begin{aligned} \cos(\chi - \omega t) \cos \chi + \sin(\chi - \omega t) \sin \chi &= \cos(\omega t) , \\ \cos(\chi - \omega t) \sin \chi - \sin(\chi - \omega t) \cos \chi &= \sin(\omega t) , \end{aligned}$$

and the integrals in the terms proportional to the constant c are easy, so we have

$$\begin{aligned} \vec{F}_h(R, t) = & - h c \pi (\cos(\omega t) \hat{x} + \sin(\omega t) \hat{y}) \\ & - h K(R) (\cos(\omega t) \hat{x} + \sin(\omega t) \hat{y}) \end{aligned} \quad (\text{E.6})$$

where

$$\begin{aligned}
K(R) &= \int_0^{2\pi} d\chi \sigma(\alpha) = \int_0^{2\pi} d\chi \sqrt{L^2 - R^2 \sin^2(\chi - \Phi)} \\
&= L [E(2\pi - \Phi | \rho) + E(\Phi | \rho)]
\end{aligned} \tag{E.7}$$

is a decreasing function of $\rho = R^2/L^2$. This is the result (5.3). Interestingly, the combination of elliptical functions (E.7) does not depend on the angle Φ . The intensity of the force $|\vec{F}| = h(c\pi + K(R))$ is thus only dependent on R . The function $K(R)$ is strictly decreasing, and it has its maximum value $2\pi L$ at the origin $R = 0$ and its minimum value $4L$ at the border $R = L$.

It is interesting as well to express the force in polar coordinates of the vortex, in the original frame fixed at the center of the system. Restoring the primes, we have

$$\begin{aligned}
\hat{x}' &= \hat{X} = \cos \Phi \hat{R} - \sin \Phi \hat{\Phi} \\
\hat{y}' &= \hat{Y} = \sin \Phi \hat{R} + \cos \Phi \hat{\Phi}
\end{aligned}$$

and introducing these in (E.6) we get

$$\vec{F}_h(R, \Phi, t) = B(R) \left[\cos(\omega t - \Phi) \hat{R} + \sin(\omega t - \Phi) \hat{\Phi} \right] \tag{E.8}$$

where $B(R) = -h(c\pi + K(R))$. In the same frame

$$\vec{F}_h(R, \Phi, t) = -\nabla_{R,\Phi} \mathcal{V} = -\left(\frac{\partial \mathcal{V}}{\partial R} \hat{R} + \frac{1}{R} \frac{\partial \mathcal{V}}{\partial \Phi} \hat{\Phi} \right) \tag{E.9}$$

and, therefore, we should have

$$\begin{aligned}
-\frac{\partial \mathcal{V}}{\partial R} &= B(R) \cos(\omega t - \Phi) \\
-\frac{1}{R} \frac{\partial \mathcal{V}}{\partial \Phi} &= B(R) \sin(\omega t - \Phi)
\end{aligned} \tag{E.10}$$

On the other hand, when taking the gradient to a general expression $\mathcal{V} = g(R) \cos(\omega t - \Phi)$, we see that the conditions $g'(R) = -B(R)$ and $g(R) = -R B(R)$ are to be fulfilled, which can only be compatible with $B(R) = \text{const}$. This implies that the force we have just calculated is not compatible with the potential energy that arises directly with the same method of calculation, as we see in the next Section.

E.1 The energy of a vortex in the AC magnetic field

With the same method of the last Section, it is even easier to calculate the energy

$$\mathcal{V}(R, \Phi, t) = -h \int_0^{2\pi} d\chi \int_0^{\sigma(\alpha)} d\rho \sin \theta(\rho) \cos(\chi - \omega t) \quad (\text{E.11})$$

Using the previous result

$$T(\alpha) = \int_0^{\sigma(\alpha)} d\rho \sin \theta(\rho) \equiv c + \sigma(\alpha) \quad (\text{E.12})$$

we see that the constant is not important: it drops out of the calculation since

$$\int_0^{2\pi} d\chi \cos(\chi - \omega t) = 0$$

and then

$$\mathcal{V}(R, \Phi, t) = -h \int_0^{2\pi} d\chi \cos(\chi - \omega t) \sigma(\alpha) \quad (\text{E.13})$$

For this integral, recalling that $\sigma(\alpha) = R \cos \alpha + \sqrt{R^2 \cos^2 \alpha + L^2 - R^2}$ and $\cos \alpha = -\cos(\chi - \Phi)$, we need

$$\begin{aligned} \int_0^{2\pi} d\chi \cos(\chi - \omega t) \cos(\chi - \Phi) &= \pi \cos(\omega t - \Phi) \\ \int_0^{2\pi} d\chi \cos(\chi - \omega t) \sqrt{R^2 \cos^2(\chi - \Phi) + L^2 - R^2} &= 0 \end{aligned} \quad (\text{E.14})$$

and finally

$$\mathcal{V}(R, \Phi, t) = -h \pi R \cos(\omega t - \Phi) \quad (\text{E.15})$$

We see that this calculation give us, in an easier way, almost the same result as the one obtained by Yu. Gaididei (private comm.), who introduces, instead, the coordinates of the vortex center into the ϕ field,

$$\phi(R, \Phi) = \arctan \left(\frac{r \sin \chi - R \sin \Phi}{r \cos \chi - R \cos \Phi} \right)$$

and integrates over r in the range $0 \leq r \leq L$. The only difference is that the coefficient in front of $R \cos(\omega t - \Phi)$ in (E.15) is in this case $-h(8/3)L$.

However, the gradient of the expression (E.15) for the effective magnetic potential, does not coincide with our previous result (E.6) for the effective magnetic force.

We note also that in our simulations we have measured every term of the energy including the magnetic Zeeman contribution. When the stationary circular movement

is reached, we observe that all the terms in the energy, as well as the z-component of the total magnetization, show a sinusoidal signal with a well defined frequency ω_E (a sharp peak in the Fourier transforms is found). This allows for a check of the formula (E.15), because we know that in the circular limit cycle $\Phi = \Omega t + \alpha_0$, where Ω is measured in the simulations too. Therefore, the prediction of this model would be

$$\omega - \Omega = \omega_E \quad . \quad (\text{E.16})$$

However, this estimate is not consistent with the results of our simulations (see **Table 5.2**).

E.2 Equations of motion for collective coordinates

We derive here the equations of motion for the collective coordinates Ansatz (5.15) of the Sec. 5.3 in the case with damping. The equations of motion (5.12a) and (5.12b) can be written as follows

$$\frac{\delta L}{\delta \phi} = \varepsilon(1 - m^2) \frac{\partial \phi}{\partial t}, \quad (\text{E.17})$$

$$\frac{\delta L}{\delta m} = \varepsilon \frac{1}{(1 - m^2)} \frac{\partial m}{\partial t} \quad (\text{E.18})$$

Assuming that the solution of these equations has the form of the Ansatz ((5.15)), one can write

$$\frac{\delta \mathcal{L}}{\delta M} = \frac{\partial \mathcal{L}}{\partial M} = \int \left(\frac{\delta L}{\delta \phi} \frac{\partial \phi}{\partial M} + \frac{\delta L}{\delta m} \frac{\partial m}{\partial M} \right) d^2x \quad (\text{E.19})$$

$$= \int \frac{\delta L}{\delta m} \frac{\partial m}{\partial M} d^2x = \varepsilon \int \frac{1}{(1 - m^2)} \frac{\partial m}{\partial t} \frac{\partial m}{\partial M} d^2x \quad (\text{E.20})$$

where Eq. (E.18) was invoked. Taking now into account the explicit form of the effective Lagrangian \mathcal{L} and the Ansatz (5.15) we get

$$\dot{\Psi} = \pi \left(\frac{1}{M_0} - \frac{1}{M} \right) + \varepsilon \frac{\dot{M}}{MM_0} \frac{\pi r_v^2}{2} \int_0^\infty r^3 \left(\frac{d\theta}{dr} \right)^2 d\rho. \quad (\text{E.21})$$

In the same way

$$\frac{\delta \mathcal{L}}{\delta \Psi} = \frac{\partial \mathcal{L}}{\partial \Psi} - \frac{d}{dt} \frac{\partial \mathcal{L}}{\partial \dot{\Psi}} = \int \left(\frac{\delta L}{\delta \phi} \frac{\partial \phi}{\partial \Psi} + \frac{\delta L}{\delta m} \frac{\partial m}{\partial \Psi} \right) d^2 x \quad (\text{E.22})$$

$$= \int \frac{\delta L}{\delta \Psi} \frac{\partial \phi}{\partial \Psi} d^2 x = \varepsilon \int (1 - m^2) \frac{\partial \phi}{\partial t} \frac{\partial \phi}{\partial \Psi} d^2 x \quad (\text{E.23})$$

and consequently

$$- \dot{M} - \frac{\partial \mathcal{V}}{\partial \Psi} = \varepsilon \pi \left((L^2 - r_v^2) \dot{\Psi} + R^2 \dot{\Phi} \right). \quad (\text{E.24})$$

The equations for the center of vortex motion may be derived in the similar manner. They have the form

$$\begin{aligned} \frac{\partial \mathcal{L}}{\partial X} - \frac{d}{dt} \frac{\partial \mathcal{L}}{\partial \dot{X}} &= \varepsilon W \dot{X}, \\ \frac{\partial \mathcal{L}}{\partial Y} - \frac{d}{dt} \frac{\partial \mathcal{L}}{\partial \dot{Y}} &= \varepsilon W \dot{Y} \end{aligned} \quad (\text{E.25})$$

where

$$W = \frac{1}{2} \int d^2 x \left\{ \frac{(\nabla m)^2}{1 - m^2} + (1 - m^2) (\nabla \phi)^2 \right\}$$

and in the limit $L \gg 1$, $L \gg R$

$$W \approx 2\pi \ln \left(\sqrt{\frac{M_0}{M}} \frac{L^2 - R^2}{L} \right) \approx 2\pi \ln L$$

Bibliography

- [1] M. J. Ablowitz and P. A. Clarkson, *Solitons, Nonlinear Evolution Equations and Inverse Scattering*, Cambridge Univ.Press, (1991). 25
- [2] A. Aharoni, *Introduction to the Theory of Ferromagnetism*, International Series of Monographs on Physics **93**, Oxford Science Publications, Oxford (1996). 7, 8, 9, 21
- [3] R. Balakrishnan and A. R. Bishop, Phys. Rev. B **40**, 9194 (1989). 19
- [4] L. E. Ballentine *Quantum Mechanics, a modern development*, World Scientific, (1998). 7, 108
- [5] V. G. Bar'yakhtar and B. A. Ivanov, Sov. Sci. Rev. A. Phys. **16**, 1 (1992). 7
- [6] G. K. Batchelor, *An introduction to Fluid Dynamics*, Cambridge Univ. Press, Cambridge (2000) 128
- [7] A. A. Belavin and A. M. Polyakov, JETP Lett. **22**, 245 (1975). 3, 25
- [8] V. L. Berezinskii, Sov. Phys. JETP **32**, 493 (1970) and **34**, 610 (1972). 3
- [9] W. F. Brown, Jr. , *Micromagnetics*, Krieger, New York, (1978). 2
- [10] J-G. Caputo, J. P. Zagorodny, Yu. B. Gaididei and F.G. Mertens, J. Phys. A: Math. Gen. **36**, 4259 (2003). 99
- [11] W. Cheney and D. Kincaid, *Numerical Mathematics and Computing*, Brooks/Cole Publishing Company, (1999). 124, 131
- [12] R. P. Cowburn, D. K. Koltsov, A. O. Adeyeye, M. E. Welland and D. M. Tricker, Phys. Rev. Lett. **83**, 1042 (1999). 2, 44
- [13] *Magnetic Properties of Layered Transition Metal Compounds*, ed. by J. de Jongh, Kluwer Academic Publishers, Dordrecht (1990). 3
- [14] A. Fernandez and C. J. Cerjjan, J. Appl. Phys. **87**, 1395 (2000). 2, 44
- [15] H. C. Fogedby, J. Phys. A: Math. Gen. **13**, 1467 (1980). 25
- [16] W. Fulton, *Algebraic topology, a first course*, Graduate Texts in Mathematics, Springer-Verlag, (1995). 128, 129

-
- [17] Yu. Gaididei, T. Kampetter, F. Mertens and A. R. Bishop, Phys. Rev. B **59**, 7010 (1999). 67
- [18] Yu. Gaididei, T. Kampetter, F. Mertens and A. R. Bishop, Phys. Rev. B **61**, 9449 (2000). 4, 5, 58, 64, 65, 67, 69, 70, 71, 74, 76
- [19] J. L. García-Palacios, Eur. Phys. J. B **11**, 293, (1999). 3
- [20] E. Yu. Vedmedenko, A. Ghazali, and J.-C. S. Lévy, Phys. Rev. **B 59**, 3329, (1999). 11
- [21] H. Goldstein, *Classical Mechanics*, 2nd. Ed., Addison-Wesley (1980). 15
- [22] M. E. Gouvêa, G. M. Wysin, A. R. Bishop, and F. G. Mertens, Phys. Rev. B **39**, 11840 (1989). 3, 4, 30, 31, 75
- [23] M. E. Gouvêa, F. G. Mertens, A. R. Bishop, and G. M. Wysin, J. Phys.: Cond. Matt. **2**, 1853 (1990). 45, 46
- [24] M. E. Gouvêa, G. M. Wysin and A. S. T. Pires, Phys. Rev. B **55**, 14144 (1997). 4, 45
- [25] M. E. Gouvêa, G. M. Wysin, S. A. Leonel, A. S. T. Pires, T. Kampeter and F. G. Mertens, Phys. Rev. B **59**, 6229 (1999). 3
- [26] F. D. M. Haldane, Phys. Rev. Lett. **57**, 1488 (1986). 19
- [27] W. Heisenberg, Z. Phys. **49**, 619 (1928). 9
- [28] S. Hikami and T. Tsuneto, Prog. Theor. Phys. **63**, 387 (1980). 2, 3, 31
- [29] B. Hillebrands and K. Ounadjela (Eds.), “*Spin Dynamics in Confined Magnetic Structures*” I, Topics in Applied Physics **83**, Springer (2002). 2, 7, 44
- [30] A. R. Völkel, A. R. Bishop, F. G. Mertens and G. M. Wysin, J. Phys. B: Cond. Matt. **4**, 9411 (1992); K. Hirakawa, H. Yoshizawa and K. Ubukoshi, J. Phys. Soc. Jpn. **51**, 2151 (1982). 11, 58
- [31] D. L. Huber, J. Appl. Phys. **53**, 1899 (1982). 35, 38, 96
- [32] D. L. Huber, Phys. Rev. B **26**, 3758 (1982). 35, 47
- [33] A. Hubert and R. Schäfer, *Magnetic Domains*, Springer-Verlag, Berlin (1998). 2, 7, 44
- [34] O. Hudák, Phys. Lett. **89 A**, 245 (1982). 44
- [35] S. Iida, J. Phys. Chem. Solids **24**, 625 (1963). 108, 109
- [36] B. A. Ivanov and D. Sheka, Low Temp. Phys. **21**, 881 (1995). 3, 4, 13, 49, 52, 75
- [37] B. A. Ivanov, H. J. Schnitzer, F. G. Mertens, and G. M. Wysin, Phys. Rev. B **58**, 8464 (1998). 67

-
- [38] B. A. Ivanov and G. M. Wysin, Phys. Rev. B **65**, 134434 (2002). 4, 13, 32, 49, 52, 54, 55, 58, 63, 75
- [39] T. Kamppeter, *Dynamic von Wirbeln im klassischen zweidimensionalen Heisenbergmodell bei endlichen Temperaturen*, Ph. D. Thesis, Universität Bayreuth (1999). 7, 33, 38, 131, 133
- [40] T. Kamppeter, F. G. Mertens, A. Sánchez, A. R. Bishop, F. Domínguez-Adame, and N. Grombech-Jensen, Eur. Phys. J. B **7**, 607, (1999). 3
- [41] S. Komineas and N. Papanicolaou, Physica **D 99**, 81 (1996). 26, 134
- [42] S. Komineas and N. Papanicolaou, Nonlinearity, **11**, 265 (1998). 99
- [43] A. M. Kosevich, B. A. Ivanov and A. S. Kovalev, Phys. Rep. **194**, 117 (1990). 7, 25, 26
- [44] J. M. Kosterlitz and D. J. Thouless, J. Phys. **C6**, 1181 (1973). J. M. Kosterlitz, J. Phys. **C7**, 1046 (1974). 2, 3, 39
- [45] A. S. Kovalev, F. G. Mertens and H. J. Schnitzer, Eur. Phys. J. B **33**, 133 (2003). 29, 34, 82
- [46] R. Kuhn, *Dynamik von Wirbelpaaren in zweidimensionalen easy-plane Ferromagneten*, Diploma Thesis, Universität Bayreuth (2003). 29
- [47] H. Kuratsuji and H. Yabut, J. Phys. A: Math. Gen, **29**, 6505 (1996). 99
- [48] E. A. Kuznetsov and A. V. Mikhailov, Phys. Lett. A **77**, 37 (1980). 128
- [49] M. Lakshmanan and M. Daniel, Physica **107 A**, 533 (1981). 25
- [50] M. Lakshmanan, TH. W. Ruijgrok and C. J. Thompson, Physica **84 A**, 577 (1976). 25
- [51] L. Landau and E. Lifshitz, Phys. Z. Sowjetunion **8**, 153 (1935). 108
- [52] L. Landau and L. P. Pitaevskii, *Statistical Physics*, Vol 9 Part 2 of the “Course of Theoretical Physics” by L. Landau and E. Lifshitz. 108
- [53] N. D. Mermin and H. Wagner, Phys. Rev. Lett. **28**, 1133 (1966). 3
- [54] N. D. Mermin, Rev. Mod. **51**, 591 (1979). 3
- [55] F. G. Mertens, A. R. Bishop, G. M. Wysin, and C. Kawabata, Phys. Rev. Lett. **59**, 117 (1987); Phys. Rev. B **39**, 591 (1989). 4
- [56] F. G. Mertens and A. R. Bishop, in *Nonlinear Science at the dawn of the 21st century*, Ed. by P. L. Christiansen, M. P. Soerensen and A. C. Scott, Lecture Notes in Physics, Springer, Berlin (2000). 3, 7

- [57] F. G. Mertens, H. J. Schnitzer and A. R. Bishop, Phys. Rev. B **56**, 2510 (1997). 34, 35
- [58] A. V. Nikiforov and É. B. Sonin, Sov. Phys. JETP **58**, 373 (1983). 3, 28, 31, 32
- [59] N. Papanicolaou Physica **D 74**, 107 (1994). 134
- [60] N. Papanicolaou and T. N. Tomaras, Nuc. Phys. **B 360**, 425 (1991). 19, 26, 134
- [61] N. Papanicolaou Physica **D 80**, 225 (1995). 134
- [62] N. Papanicolaou and P. N. Spathis, Nonlinearity **12**, 285 (1999). 19, 134
- [63] M. L. Plumer J. van Ek and D. Weller (Eds.) *The Physics of Ultra-High-Density Magnetic Recording*, Springer-Verlag (2001). 44
- [64] V. L. Pokrovskiĭ and G. V. Uĭmin, JETP Lett. **41**, 128 (1985). 4
- [65] J. Raabe, R. Pulwey, R. Sattler, T. Schweinböck, J. Zweck and D. Weiss, J. Appl. Phys. **88**, 4437 (2000). 2, 44, 104
- [66] R. M. Rosenberg, *Analytical Dynamics of Discrete Systems*, Plenum, New York (1977). 15
- [67] T. Schneider and E. Stoll, in [73] 105
- [68] M. Schneider, H. Hoffmann and J. Zweck, Appl. Phys. Lett. **77**, 2909 (2000). 2, 44, 104
- [69] H. J. Schnitzer, *Zur Dynamik kollektiver Anregungen in Hamiltonschen Systemen*, Ph. D. Thesis, Universität Bayreuth (1996). 7, 33, 35, 131, 132
- [70] H. J. Schnitzer, F. G. Mertens and A. R. Bishop, Physica **D 141**, 261 (2000). 35
- [71] H. R. Schwartz, *Numerische Mathematik* B. G. Teubner, Suttgart (1993). 133
- [72] T. Shinjo, T. Okuno, R. Hassdorf, K. Shigeto and T. Ono, Science, **289**, 930 (2000). 2, 44, 104
- [73] *Solitons*, Vol. 17 of *Modern Problems in Condensed Matter Sciences*, Ed. by V. M. Agranovich and A. A. Maradudin, North-Holland, (1986). 7, 152
- [74] S. Takeno and S. Homma, Prog. Theor. Phys. **64**, 1193 (1980). 2
- [75] A. A. Thiele, Phys. Rev. Lett. **30**, 230 (1973). 2, 35
- [76] A. A. Thiele, J. Appl. Phys. **45**, 377 (1974). 35, 38, 127
- [77] S. Trimper, Phys. Lett. **70 A**, 114 (1979). 25, 26
- [78] A. Völkel, *Spindynamik im klassischen zweidimensionalen Heisenberg Antiferromagneten mit planarer Anisotropie*, Ph. D. Thesis, Universität Bayreuth (1992). 7

- [79] A. Völkel, F. G. Mertens, A. R. Bishop and G. M. Wysin , Phys. Rev. B **43**, 5992 (1991). 35
- [80] A. Völkel, G. M. Wysin, F. G. Mertens, A. R. Bishop and H. J. Schnitzer. Phys. Rev. B **50**, 12711 (1994). 34, 35
- [81] G. E. Volovik, Jour. Phys. C: Solid State Phys. **20**, L83 (1987). 19
- [82] G. M. Wysin, M. E. Gouvêa, A. R. Bishop and F. G. Mertens, in *Computer Simulation Studies in Condensed Matter Physics*, ed. by D. P. Landau, K. K. Mon, and H.-B. Schüttler, Springer-Verlag, Berlin (1988). 31
- [83] G. M. Wysin, Phys. Rev. B **49**, 8780 (1994). 4, 31, 67, 69, 75, 77, 78, 79
- [84] G. M. Wysin, F. G. Mertens, A. R. Völkel, and A. R. Bishop in *Nonlinear Coherent Structures in Physics and Biology*, ed. by K. H. Spatschek and F. G. Mertens (Plenum, New York, 1994). 5
- [85] G. M. Wysin, A. R. Völkel, Phys. Rev. B **52**, 7412 (1995). 67, 79
- [86] G. M. Wysin, Phys. Rev. B **54**, 15156 (1996). 5, 35, 82
- [87] J. P. Zagorodny, Yu. Gaididei, F. G. Mertens and A. R. Bishop, Eur. Phy. J. **B 31**, 471 (2003). 4, 5, 58, 65, 66, 67, 69, 71, 82

Note: the years of publication are the numbers inside parenthesis. *Before* the year, in the case of journal-like publications, it is indicated the number of page into the journal where the article is. *After* the year it follows the number(s) of page(s) *inside this Thesis* where that reference was cited.

Thank you! Vielen Dank! Muchas gracias!

To my wife Mariana, who has supported and tolerated me in uncountable ways and manners, just for love, te agradezco tanto!

To my parents Susy and Oscar, who always encouraged and stimulated me with the necessary freedom, and to my brother and my sisters, because along the time they all have taught me that everything can be accomplished if one really has a strong wish to do it (just do it!), to my new parents Ana María and Luis, for the loving support to me and to the daughter that I've borrowed forever, and to my new brother and sisters, for being so nice people... Gracias a todos!

To Prof. Dr. Franz George Mertens, for all the teachings and rich discussions, for all the support and supervision of my research work, and for all the effort in the administration of projects which gave me the possibility to come to Bayreuth. Also for the nice bike tours around the Fränkische Schweiz in the summers. Ich danke Ihnen sehr viel!

To all the people behind the European Graduate School, because of the truly good organization of Seminars and Congresses in Avila-Gredos (2002) and Benasque (2003). Specially to Prof. Dr. Ingo Rehberg and Prof. Dr. Angel Sánchez, for all that efforts of organization, and to Mrs Lindser, and to the secretary of our Chair, Mrs. Glas, for the patience with lots of paper junk concerning the foreigners. Thank you all!

To Till Kamppeter, who probably will not read this as he is already lost in the Free-Software jungle, for having introduced me in the world of the spin-dynamics simulations and getting me giving the first steps with the simulator code "vmd". The CDs that you've prepared were really helpful! Ich danke dir!

To Yuri Gaididei for the intense collaboration in all the work done along these years. Thank you for sharing with me your enormous professional experience.

To Jean Guy Caputo, hard worker, good teacher and nice friend, who was always teaching me something good. To Denis Sheka, idem. Both of you guys, have made my days of physics in Bayreuth –and in Rouen and in Kiev– a very interesting and pleasant experience, Merci beaucoup! Дуже дякую (Duzhe dyakuyu)

To Boris Ivanov and Gary Wysin, for helpful discussions at the distance, Дуже дякую, thank you!

Also to Landau and Lifshitz, why not, for having discovered such beautiful equations that none could solve, Спасибо (spasibo)

To my coworkers in the network system-managing, who contributed to a nice work atmosphere, Bernd Schlesier, vielen Dank! and Alexei Krekhov, who by the way helped me to say and type "thanks" in Cyrillic, Большое спасибо (bolshoe spasibo).

To the former system-managers who have trained me, specially Bernd Dreßel, lots of thanks! Also to Gabor Demeter and Friedrich Schmögner, thank you very much!

To Matthias Meister, my former office mate, and Alexander Weiße, for nice talks and useful tips, vielen Dank!

To Martin Petry, Robert Kuhn, Cord Müller and Martin Endres, für die nette Freundschaft and the hard work in getting me talking German (Wir schaffen es!), vielen Dank!

To the white-russian and russian “factions” of my friends in Bayreuth, Dmitry Krimer and Pavel Akimov, repectively, just –which is a lot– for the nice friendship, Большое спасибо

Lots of thanks to all the rest of friends, professors, colleagues and coworkers of the Physics Institut of Bayreuth, for all the good time I’ve spent with you.

Thank you all very much!